Dissertation

CRACking the Riddle

Inquiring the role of the cholesterol binding motif of the HIV-1 glycoprotein gp41

zur Erlangung des akademischen Grades
doctor rerum naturalium (Dr. rer. nat.)
im Fach Biophysik

eingereicht an der
Mathematisch-Naturwissenschaftlichen Fakultät I
der Humboldt-Universität zu Berlin

von
Diplom Biophysiker Roland Schwarzer

Präsident der Humboldt-Universität zu Berlin
Prof. Dr. Jan-Hendrik Olbertz

Dekan der Mathematisch-Naturwissenschaftlichen Fakultät I
Prof. Dr. Stefan Hecht

Gutachter: 1. Prof. Dr. Andreas Herrmann

2. Prof. Dr. Martin Hof

3. PD Dr. Michael Veit

eingereicht: 18.12.2013

Datum der Promotion: 16.06.2014

Zusammenfassung

In den vergangenen Jahren sind Lipide, Membranen und deren Organisationsformen mehr und mehr in den Fokus der biologischen Forschung gerückt. Es wurde vorgeschlagen, dass in zellulären Membranen selbstassemblierende, submikroskopische Aggregate aus Sphingolipiden, Cholesterol und bestimmten Proteinen existieren und man vermutet, dass insbesondere Viren diese “Lipid Rafts” für ihren Zusammenbau nutzen und auf diese Art ihre Proliferationseffizienz erhöhen. Gleichwohl sind die genaue biologische Funktion und auch die molekulare Basis der Assoziation bestimmter Protein mit Lipid Rafts auch weiterhin unbekannt. In der vorliegenden Arbeit wurde Fluoreszenz-Lebenszeit-Mikroskopie genutzt, um die Lipid-Raft-Anreicherung des HIV-1 Glycoproteins gp41 zu untersuchen. Förster-Resonanz-Energietransfer zwischen fluoreszenzmarkierten viralen und Raft-Marker-Proteinen wurde gemessen, um deren gemeinsame, lokale Aufkonzentrierung in Lipid Rafts nachzuweisen. Durch Verwendung verschiedener Deletions- und Mutationsvarianten des Proteins konnte nicht nur seine Lipid-Raft-Präferenz demonstriert, sondern auch das Cholesterol-Bindemotiv (CRAC) als entscheidender Faktor der lateralen Sortierung identifiziert werden. Wir haben in diesem Kontext auch eine systematische Zell-zu-Zell-Variabilität in unseren Daten bemerkt, die einen zugrundeliegenden zellbiologischen Mechanismus der Membranorganisation nahelegt. Mithilfe von Fluoreszenz-Polarisations-Mikroskopie konnte zudem eine klare CRAC-Abhängigkeit der gp41-Oligomerisierung aufgezeigt werden. Um darüber hinaus noch eine wichtige biologische Funktion des HIV Envelope-Komplexes, die Membranfusion, zu untersuchen, wurde einer der Nebeneffekte dieser Funktion, die membranlytische Wirkung verschiedener Teile von gp41verfolgt. Diese Eigenschaft der externen Elemente von gp41 wurde mithilfe einer durchflusszytometrischen Methode nachgewiesen, wobei sich abermals eine signifikante CRAC-Abhängigkeit feststellen liess. Die von uns gewonnenen Daten erlauben einen tieferen Einblick in die molekulare Basis und die biologischen Folgen der cholesterol-abhängigen lateralen Proteinorganisation für Virusassemblierungsprozesse an biologischen Membranen.

Schlagwörter: Human Immundefizienz-Virus

Gp41

Lipid Rafts

Fluoreszenz-Lebenszeit-Mikroskopie

Abstract

In recent years, there has been a considerable interest in the molecular organization of biological membranes. It has been hypothesized that self-assembling, freely diffusing, submicroscopic domains consisting of sphingolipids, cholesterol and certain proteins exist and the prevailing view is that those lipid rafts serve as platforms for specific molecular interactions by the preferential exclusion and inclusion of proteins. It was presumed, that in particular viruses make use of plasma membrane lipid rafts to augment the infection process and spread efficiently. However, the exact biological function and physical basis of protein partitioning into microdomains remains an outstanding question in virus biology. In the present study, fluorescence lifetime imaging microscopy was used to study lipid raft partitioning of the HIV-1 glycoprotein gp41 by detecting Foerster Resonance Energy Transfer between fluorescently labeled viral and raft marker proteins in living cells. Plasma membrane microdomain association of gp41 was demonstrated and by introducing systematic mutations and truncations in different gp41 motifs, the cholesterol recognition amino acid consensus (CRAC) was identified as the crucial determinant of the lateral sorting. Interestingly, we observed a systematic cell-to-cell variability in our raft related data that suggests underlying cell-biological mechanisms of membrane organization. Moreover, fluorescence polarization microscopy revealed a distinct CRAC requirement for gp41 oligomerization whereas other properties, such as intracellular distribution and expression efficiency were clearly demonstrated to be CRAC independent. Based on those findings a biological function of gp41, namely the membrane perturbation exerted by the protein's membrane proximal external region was investigated using flow cytometry. Again, a significant CRAC dependence of that property was found underlining the importance of a functional cholesterol binding motif. Our data provide further insight into the molecular basis and biological implications of the cholesterol dependent lateral protein sorting for virus assembly processes at cellular plasma membranes.

Keywords: Human immunodeficiency virus

Gp41

Lipid rafts

Fluorescence lifetime imaging microscopy

Abbreviations

Å	Ångstrom
aa	Amino acid
AFM	Atomic force microscopy
AIDS	Acquired immune deficiency syndrome
C-	Carboxy-
C6-NBD-PC	1-Palmitoyl-2-[6-[(7-nitro-2-1,3-benzoxadiazol-4-yl)amino]hexanoyl]-sn-Glycero-3-
CA	Capsid
cDNA	Complementary DNA
CFP, mCFP	Cyan fluorescent protein, monomeric cyan fluorescent protein
Chol	Cholesterol
CRAC	Cholesterol recognition amino acid consensus
CT	Cytoplasmic tail
DMSO	Dimethylsulfoxide
DNA	Deoxyribonucleic acid
DRM	Detergent resistant membrane
DSM	Detergent soluble membrane
Env	Envelope protein
ER	Endoplasmic reticulum
FACS	Fluorescence activated cell sorting
FAIM	Fluorescence anisotropy imaging microscopy
FLIM	Fluorescence lifetime imaging microscopy
FP	Fusion peptide
FRET	Foerster resonance energy transfer
GalCer	Galactosyl ceramide
Gp120	Glycoprotein 120
Gp41	Glycoprotein 41
GPI	Glycoslylphosphatidylinositol
GPMV	Giant plasma membrane vesicles
GUV	Giant unilamellar vesicles

HA	Hemagglutinin
HIV	Human immunodeficiency virus
HR	Heptad repeats
IN	Integrase
L_d	Liquid disordered
LLP	Lentivirus lytic peptide
L_o	Liquid ordered
MA	Matrix protein
MPER	Membrane proximal external region
mRNA	Messenger RNA
MβCD	Methyl-β-Cyclodextrin
NC	Nucleocapsid protein
Nef	Negative regulatory factor
PAGE	Polyacrylamide gel electrophoresis
PALM	Photoactivated localization microscopy
PBS	Phosphate buffered saline
PC	Phosphatidylcholine
PM	Plasma membrane
PMS	Plasma membrane spheres
PR	Protease
RER	Rough endoplasmic reticulum
Rev	Regulator of expression
RNA	Ribonucleic acid
RT	Room temperature
RTr	Reverse transcriptase
SD	Standard deviation
SDS-PAGE	SDS polyacrylamide gel electrophoresis
SEM	Standard error of the mean
SIV	Simian immunodeficiency virus
SU	Surface subunit

Tat	Transactivator of transcription
TCR	T-cell receptor
TCSPC	Time-correlated single photon counting
TM	Transmembrane subunit
TMD	Transmembrane domain
Trp	Tryptophan
Vif	Viral infectivity factor
Vpr	Viral protein r
Vpu	Viral protein u
vRNA	Viral RNA
WT	Wild type
YFP, mYFP	Yellow fluorescent protein, monomeric yellow fluorescent protein

Table of content

Zusammenfassung ..... **IV**

Abstract ..... **V**

Abbreviations ..... **VI**

1. Introduction **1**

1.1 AIDS and the HI virus 1

1.1.1 History 1

1.1.2 Classification 2

1.1.3 Epidemiology 2

1.1.4 Origin and evolution of HIV 4

1.1.5 HIV transmission 4

1.1.6 Pathogenesis 4

1.1.7 Immune response 5

1.1.8 Tropism 6

1.1.9 HIV structure and components 6

1.1.10 HIV replication 9

1.1.11 Structure and function of the HIV envelope complex 11

1.2 The transmembrane protein gp41 12

1.2.1 Structure of the glycoprotein gp41 13

1.2.2 Gp41 domains 14

1.2.3 Alternative structures of gp41 and functional consequences 21

1.2.4 Gp41 intracellular trafficking and transport 22

1.2.5 Interactions of gp41 with other viral components 23

1.2.6 Diversity of the envelope complex 25

1.3 Lateral membrane organization 26

1.3.1 Lipid rafts in the virus context 28

1.3.2 Methods used to study membrane microdomains 29

1.3.3 Protein factors of lateral membrane sorting 30

1.3.4 Molecular background of a potential gp41 raft partitioning 30

1.4 The toolbox: fluorescence spectroscopy and microscopy 31

1.4.1 Foerster resonance energy transfer 33

1.4.2 Fluorescence lifetime imaging microscopy and FLIM-FRET 34

1.4.3 Fluorescence polarization microscopy 36

1.4.4 Total internal reflection fluorescence microscopy 38

1.4.5 Fluorescence activated cell sorting (FACS) 39

2. Aim of the study **40**

3. Material and Methods 43
3.1 Materials 43
3.1.1 Chemicals 43
3.1.2 Equipment and instruments 44
3.1.3 Consumables 46
3.1.4 Cell culture media and reagents 47
3.1.5 Enzymes, molecular biology reagents 48
3.1.6 Kits for DNA preparation 49
3.1.7 Antibodies 49
3.1.8 Plasmids 50
3.1.9 Buffers and solutions 50
3.1.10 Biological material 53
3.1.11 Software 54
3.2 Methods 56
3.2.1 Molecular biology 56
3.2.2 Cell biology 64
3.2.3 Microscopy 71
3.2.4 Flow cytometry 77
3.2.5 Biochemical methods 79
4. Results 82
4.1 Generating tools to study gp41 lipid raft partitioning 82
4.1.1 Construction of the raft marker 82
4.1.2 Construction of the chimeric gp41 fusion protein gp41-YFP 82
4.2 Characterizing the chimeric gp41 83
4.2.1 Intracellular distribution and trafficking 84
4.2.2 Incorporation of the construct in virus-like particles 88
4.3 Investigating plasma membrane raft partitioning of gp41 89
4.4 Perspectives - gp41 trafficking 91
4.4.1 Particle tracking of fluorescently labeled fusion proteins 91
4.4.2 Timing of gp41 intracellular distribution 92
4.5 Chasing the molecular basis of gp41 raft partitioning 94
4.5.1 Construction of gp41-truncation and mutation variants 94
4.5.2 Characterization of gp41 fusion proteins 95
4.5.3 Plasma membrane raft partitioning of gp41 variants 99
4.6 Verifying plasma membrane raft clustering 101
4.7 Insertion: Investigating population heterogeneities in membrane organization 103
4.7.1 Perspective: Cell-to-Cell variability in plasma membrane order 105
4.8 Elucidating raft partitioning of gp41 variants in the Golgi apparatus 108
4.9 Detecting palmitoylation of gp41 variants 109

4.10 Analyzing lipid raft partitioning using giant plasma membrane vesicles 109
4.10.1 GPMV preparation types 110
4.10.2 Cell type dependence of GPMV preparation 112
4.10.3 Domain partitioning of fluorescent proteins in GPMVs 113
4.11 Inquiring oligomerization of chimeric proteins 116
4.11.1 FAIM as a tool to study gp41 oligomerization 116
4.12 Analyzing membrane perturbation caused by the MPER of gp41 120
4.12.1 Flow cytometric study of gp41 membrane perturbation 120
4.12.2 Perspective: Patch clamp to sense gp41 plasma membrane perturbation...123
5. Discussion 125
5.1 Raft partitioning of the glycoprotein gp41 125
5.1.1 Critical evaluation of FLIM-FRET data 125
5.1.2 Giant plasma membrane vesicles as a tool to study raft partitioning 132
5.1.3 Biological relevance of the gp41 raft partitioning 133
5.2 Population heterogeneity in plasma membrane lipid rafts 135
5.3 Oligomerization of gp41 variants 136
5.4 Membrane perturbation by gp41 139
5.5 Integration of the results into the prevailing understanding of gp41 142
6. Summary and conclusions 145
Addendum 149
Bibliography 149
Acknowledgements 165
Publications 166
Collaborations 168
Curriculum vitae 169
Eidesstattliche Erklärung 170

1. Introduction

1.1 AIDS and the HI virus

The acquired immune deficiency syndrome (AIDS) with its causative agent the human immunodeficiency virus (HIV) ranks amongst the most devastating pandemics ever observed. Since the discovery of HIV in the early eighties of the last century[1–4] around sixty-million people have been infected and nearly half of them have died[5–7]. In recent years, billions of dollars have been spent on HIV research and innumerable studies were published dealing with HIV and AIDS (PubMed hits for HIV: 250000) making HIV the most intensively investigated and best characterized pathogen in human history. As a result of that effort disease, virus lifecycle and viral components have been described accurately and different therapeutic strategies were developed. For instance, the application of protease inhibitors that prevent virus maturation and thus lower the infectivity of newly synthesized particles, AIDS death rates could be lowered by more than two-thirds within the first two years of their licensing in the US[8]. However, the pandemic still spreads uncontrolled in wide parts of the world and the number of new infections rose unconfined from below 0,002 ‰ of the global population in 1960 up to around 0,5 % in 2010[6,9].

1.1.1 History

AIDS resulting from HIV infection, was first described in 1981 when a common pattern of symptoms was observed among a small number of homosexual men in the US[1]. The most prevalent causative pathogen, HIV type 1 (HIV-1) was discovered in 1983 in the group of Luc Montagnier and in the following years, several related members of the lentivirus genus were identified. The Simian immunodeficiency virus (SIV) was discovered in 1985 and HIV type 2 (HIV-2) shortly afterwards in 1986[10]. In spite of decades of research, to date, the AIDS pandemic still continues to spread globally with more than 34 million individuals currently infected with HIV[6].

1.1.2 Classification

HIV is an enveloped, single stranded RNA virus. As a member of the lentiviruses it is furthermore assigned to the family of retroviridae. Two different forms of HIV are known, type 1 and type 2. Although the general progression of the respective diseases and the virus lifecycles are very similar, both types share a sequence homology of only 50 %[11] and possess significant differences in their molecular structure[12]. While most infections worldwide are due to type 1 strains, HIV-2 is of significant relevance in some countries, such as Guinea-Bissau or Portugal[10]. Based on genetic similarities, HIV-1 is classified in groups and subtypes. It is divided in four subgroups, designated M, N, O and P but more than 90 % of new-infections are from group M, which is again subdivided in the nine subtypes A, B, C, D, F, G, H, I, J and K (Figure 1-1). Co-infection with different subtypes leads to hybrids termed circulating recombinant forms (CRF)[6].

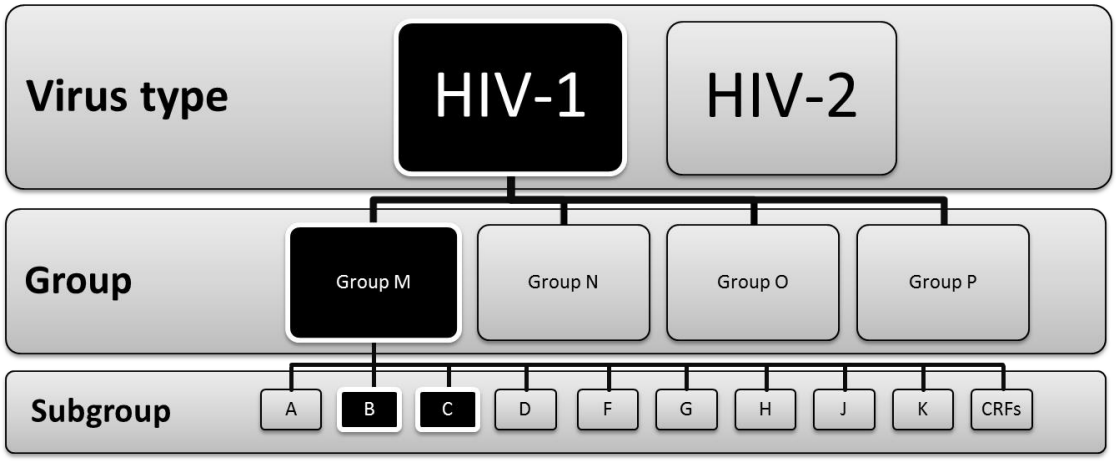

Figure 1-1: HIV classification. Based on genetic similarities, the numerous virus strains may be classified into types, groups and subtypes or subgroups. Adapted from [6]. The most prevalent forms of HIV, namely the subtypes B and C from group M of HIV-1 are highlighted in black.

1.1.3 Epidemiology

Although the number of HIV infected people is only slightly rising in the last ten years (Figure 1-2) and both the number of new HIV-infections and the number of AIDS related deaths are regressive (Figure 1-2), HIV and AIDS remain highly relevant. Statistics for the end of 2010 reported that over 30 million people were infected with HIV and every year 1.8 million people die of AIDS (Figure 1-2). In some countries, in particular in sub-Saharan

Africa more than one fifth of the adults is already infected with HIV and in Eastern Europe as well as Central Asia the epidemic is nowadays spreading rapidly with an increase of infected people to 250 % between 2001 and 2010[6].

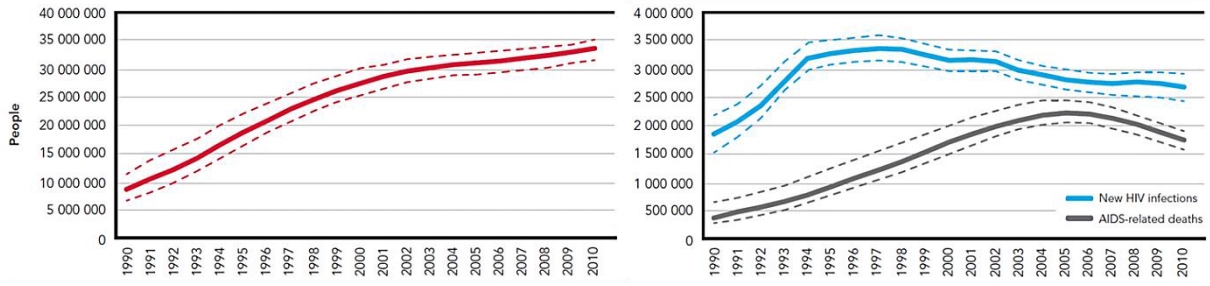

Figure 1-2: Recent AIDS related statistics. Development of the total number of infected people (red), new infections (blue) and AIDS-related deaths (grey) in the last 20 years. The dashed lines reflect uncertainties and deviations in statistical investigations. Adapted from [13].

Interestingly, there is a high geographic correlation between HIV new infections and the causative virus type (Figure 1-3). Whereas worldwide the subtype C of the HIV-1 major group M is responsible for around 50 % of new infections[7], the subtype B is the most prevalent form in Western Europe and in the US (Figure 1-3).

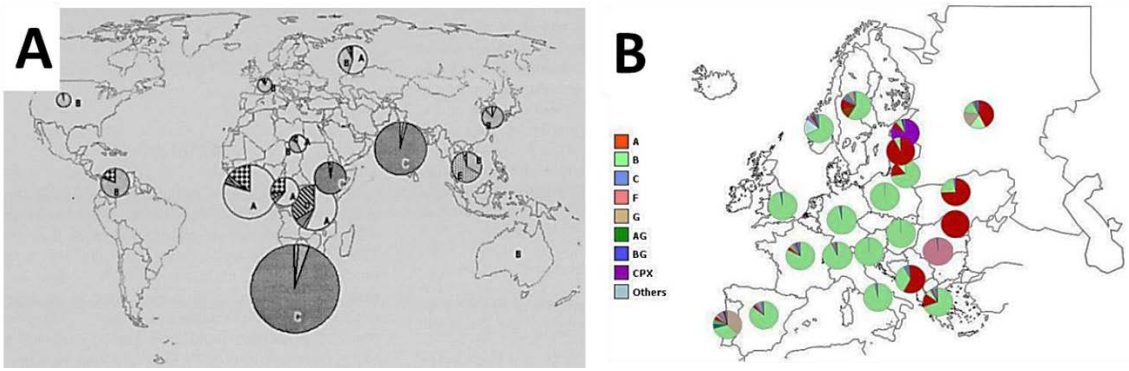

Figure 1-3: Global and local distribution of HIV-1 subtypes and recombinants. (A) The pie charts represent the distribution of HIV-1 subtypes and recombinants from the year 2000 worldwide. The relative surface areas of the pie charts correspond to the relative numbers of people living with HIV in the regions. The grey shades reflect the different HIV-1 subtypes. Adapted from [7]. (B) HIV-1 subtype distribution in central Europe adapted from a publication from 2007[14].

1.1.4 Origin and evolution of HIV

These days, it is largely accepted that HIV is a descendant of a simian immunodeficiency virus. Phylogenetically, HIV-1 clusters with chimpanzee SIV[15] whereas HIV-2 descends from a sooty mangabey ancestor virus[15]. Interestingly, it was found that at least seven independent transmissions occurred from sooty mangabey resulting in the 7 known HIV-2 subtypes[10] and it was hypothesized, that all HIV-1 groups represent separate crossover events from chimps to humans. The first zoonotic transmission from chimpanzees was dated back to, most likely 1908 whereas HIV-2 crossed the species barrier in the 30ies of the last century[9].

1.1.5 HIV transmission

Typical ways of HIV infection are sexual intercourse without condoms, the use of unsterilized syringes by drug users, blood transfusion and mother-to-child transmissions[6]. Most infections occur by sexual exposure, where HIV is transmitted from one individual to another by body fluids like for instance blood, sperm or vaginal secretion. It enters the human body via open wounds or vulnerable and thin areas of the skin and through mucous membranes and usually, multiple sexual exposures are needed for infection to occur. Interestingly, it has been shown, most of the mucosally transmitted HIV-1 infections are initiated by a single virus particle[16].

1.1.6 Pathogenesis

Acute primary infection[5,6]**.** After entering the body and if necessary crossing mucosal barriers, viruses first infect a large number of CD4 positive cells (Figure 1-4). It replicates rapidly and spreads throughout the whole body, in particular infecting the lymphoid organs thymus, spleen and the lymph nodes. In this phase up to 70 % of the infected people suffer flu-like symptoms. The virus can integrate in the host's genome and might lie dormant, shielded from the immune system, for an extended period of time up to many years.

Clinically asymptomatic stage[5,6]**.** In this phase, lasting for an average of ten years, the immune system fights the infection with killer T-cells (CD8 positive T-cells) and B-cell produced antibodies. As a result of that, this phase is free of symptoms and the virus load in the peripheral blood is very low (Figure 1-4). Still, the patient remains infective and

indications were found that HIV is not dormant on a systemic level in this phase of infection but rather is very active in the lymph nodes.

Symptomatic HIV infection[5,6]**.** Over time, the immune system is severely damaged by the infection. The lymph nodes loose activity as a result of years of continues challenging, the virus evolves and becomes more pathogenic and less immunogenic allowing eluding and hampering the immune system (see also 1.1.8) and moreover, the organism fails to replace destroyed T-helper cells. Opportunistic infections emerge and often multi-system disease and infections occur in all parts of the body.

Progression to AIDS[5,6]**.** As the immune system becomes more and more damaged, the organism faces progressively severe opportunistic infections and cancer. The HIV viral load in the blood dramatically increases while the number of CD4 positive cells drops to dangerously low levels. AIDS is diagnosed when the patient has one or more opportunistic infections and less than 200 CD4 positive cells per ml (1000 cells/ml for a healthy person)[6].

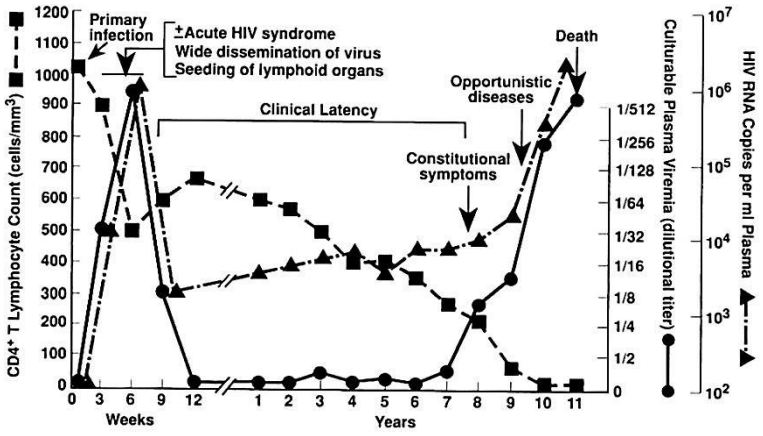

Figure 1-4: Typical course of HIV infections. The relationship between virus load and the number of T-cells in the context of disease progression in case of untreated HIV infection is plotted. Adapted from [17].

1.1.7 Immune response

During the first months of infection, an effective immune response to the virus is established. CD8 T-cells act against HIV by directly killing HIV-infected cells and by secreting anti-viral chemokines[16,18]. Whereas CD4 positive cells are quickly depleted after infection, the number of CD8 positive cells increases up to 20-fold[18]. Moreover, a humoral response is developed after 4 to 8 weeks with antibodies mainly targeting cell-free virions and to a lower extend

infected cells[18]. A detailed description of the immune response to acute infections of HIV-1 can be obtained from the literature[19].

1.1.8 Tropism

All HIV isolates are able to infect CD4 positive primary T-cells[10]. However, differences were found in the relative tropism for macrophages and human T-cell lines. Therefore, isolates were historically divided into three groups with respect to their replication rate and syncytium-induction *in vitro*. The first group are the R5 tropic viruses that infect macrophage cell lines *in vitro* and use CCR5 as a coreceptor[10]. The second group are the CXCR4 or X4 tropic viruses that use CXCR4 as a coreceptor and viruses from this group replicate to high titers in CD4 positive cell lines[10]. The third group uses both coreceptors and thus are designated dual-tropic or R5/X4 viruses[10]. It has been reported, that R5 viruses are predominantly transmitted and thus macrophages and CD4 positive memory cells are the first target of a HIV-1 infection. R5/X4 viruses precede the evolution to X4 tropism and a broader T-cell targeting[20]. Presumably, this evolution from R5 to X4 tropism in an infected individual is related to the individual disease progression and development[10,20,21] from the milder and specific proliferation in macrophages and memory T-cells in the early phase of infection to an aggressive and invasive replication with an expanded T-cell tropism in the late phase[22].

1.1.9 HIV structure and components

A typical HI virus particle is composed of two strands of RNA, 15 different viral and some host cell proteins, all surrounded by a lipid bilayer membrane (Figure 1-5). The genetic organization of HIV is complex. HIV-1 codes for 9 genes, the canonical genes Gag, Pol and Env but also several regulatory and accessory genes, designated Tat, Vif, Vpu, Vpr and Nef. The Pol gene encodes three crucial enzymes: the reverse transcriptase (RTr), which converts the viral RNA genome into DNA; the integrase (IN), which mediates the insertion of that DNA into the genome of the host cell and finally the protease, which is essential for the maturation of virions into their infective form. Whereas the genes Tat and Rev are important for virus replication, Vif, Vpr, Vpu and Nef modulate immune functions *in vivo*. Env and Gag code for the surface receptor and major structural components, respectively. The envelope protein is cleaved into the surface subunit gp120 and the transmembrane subunit gp41 upon maturation in the host cell.

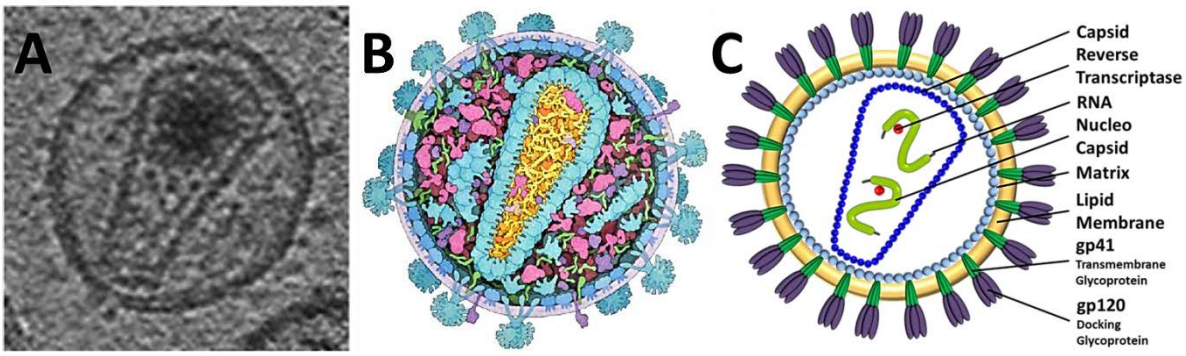

Figure 1-5: Structure of a mature HIV virion. (A) Electron micrograph of a released and maturated virus particle[23]. (B) Virtual model of a virus particle including all viral and some incorporated cellular proteins under consideration of ava ilable protein structures with atomic resolution[24]. (C) Highly simplified schematic textbook representation with a focus on the major components of the virion.

Gag maturation occurs later. This polyprotein precursor is incorporated in the virus particle and processed by the viral protease concomitant with or after virion release to finally yield the matrix protein (MA or p17), the capsid protein (CA or p24), the nucleocapsid (NC or p7) and p6. The specific functions of the individual viral proteins will be described briefly below. The proteins structures were gathered from the protein data bank[24].

1.1.9.1 Enzymes

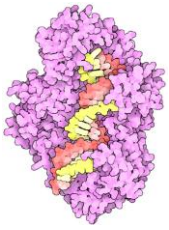

RTr: The reverse transcriptase (pink) generates a double stranded DNA copy of the viral genome by producing a complementary DNA strand to the single stranded RNA, a subsequent digestion of the RNA and the generation of a second DNA (red and yellow) strand. (250 copies/virion)[24,25].

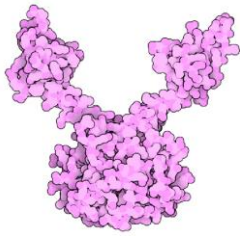

IN: The integrase inserts the DNA copy of the viral genome into active regions of the cellular genome, generating the provirus and thus establishing a persistent infection. (250 copies/virion)[24,25].

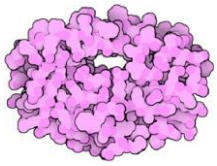

PR: The protease is crucial for maturation of released HIV particles. Since HIV proteins are synthesized as long polyprotein precursors, the HIV protease is necessary to cleave them into mature, functional pieces. (250 copies/virion)[24,25].

1.1.9.2 Structural proteins

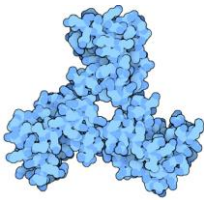

MA: The matrix protein forms a coat on the inner leaflet of the viral membrane. It plays a central role during budding of nascent viruses from the surface of infected cells by mediating the Gag interaction with the plasma membrane (PM). (5000 copies/virion)[24,25].

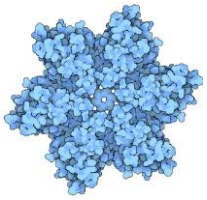

CA: The capsid protein forms a cone-shaped coat around the viral RNA[26]. Stable hexamers of this protein assemble to geodesic capsids that deliver the viral genome in the host cell. (5000 copies/virion)[24,25].

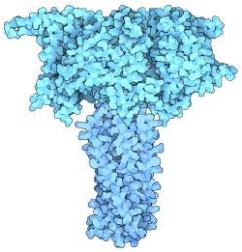

SU and TM: The envelope proteins gp120 (SU) and gp41 (TM) bind to receptors on the surface of the target cell and penetrate the plasma membrane to finally induce fusion. Only low numbers of those trimeric, gp120/gp41 heterodimers were found in viral particles and the spikes formed by these proteins were demonstrated to be highly decorated with carbohydrates. (4 to 35 trimers/virion)[24,25].

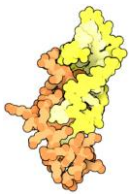

NC: The nucleocapsid protein (orange) forms a stable complex with the viral RNA (yellow). It works as a primer for the reverse transcription and mediates packaging and folding of genomic RNA. Moreover, it was reported to assist during virion assembly. (5000 copies/virion)[24,25].

1.1.9.3 Accessory proteins

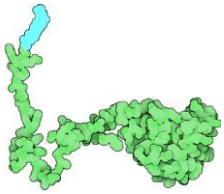

Nef: The negative regulatory factor inhibits the expression of cellular defensive proteins. It blocks apoptosis, enhances viral replication and infectivity and connects cellular proteins to sorting pathways thus regulating trafficking, degradation and immune recognition. (extent of incorporation unknown)[24,25].

Rev: The regulator of expression of virion proteins (orange) binds hairpins of the viral RNA (yellow) and regulates its splicing and transport from the nucleus to the cytoplasm. (not incorporated into the virion)[24,25].

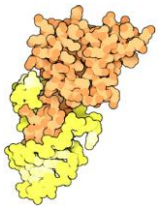

Tat: The transactivator of transcription (orange) binds to viral RNA (yellow) and greatly enhances transcription elongation. (not incorporated into the virion)[24,25].

no high resolution available yet

P6: This protein promotes virion budding by recruiting the cellular endosomal sorting complex required for transport (ESCRT) machinery and is involved in the incorporation of vpr in the nascent virus. (5000 copies/virion)[24,25].

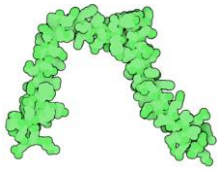

Vpr: The viral protein r targets the viral genome to the nucleus after infection. Moreover, it arrests the host cell in the G2/M cell cycle phase. (700 copies/virion)[24,25].

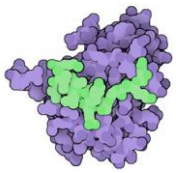

Vif: The viral infectivity factor efficiently suppresses the host cell infection inhibition by APOBEC3G/APOBEC3F. Vif recruits cellular ubiquitin ligases to subject both proteins to degradation. (1 to 150 copies/virion)[24,25].

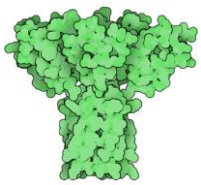

Vpu: The viral protein u forms an ion channel in the viral membrane and causes degradation of CD4. Moreover, by binding cellular tetherin and causing internalization, it prevents tethering of nascent viral particles at the host cell surface and thus inhibition of virus release. (not incorporated into the virion)[24,25].

1.1.10 HIV replication

The HIV replications cycle is very complex and requires a highly regulated interplay of the viral components and interactions with cellular proteins. For a better understanding it is schematically displayed in Figure 1-6. The first step of HIV infection is the attachment of the

virus particle to the target cell. For this purpose, the glycoprotein gp120 interacts with the CD4 antigen receptor and subsequently with a coreceptor (see 1.1.8) on the surface of the host cell. After this initial binding, the envelope transmembrane subunit gp41 mediates fusion of the membranes (see 1.1.11), which results in the entry of HIV into the cell[27,28]. In the cytoplasm, the viral capsid initially remains intact but upon binding of more and more cellular cypA proteins this shell is disassembled and the viral RNA and various enzymes are released into the cytoplasm[29].

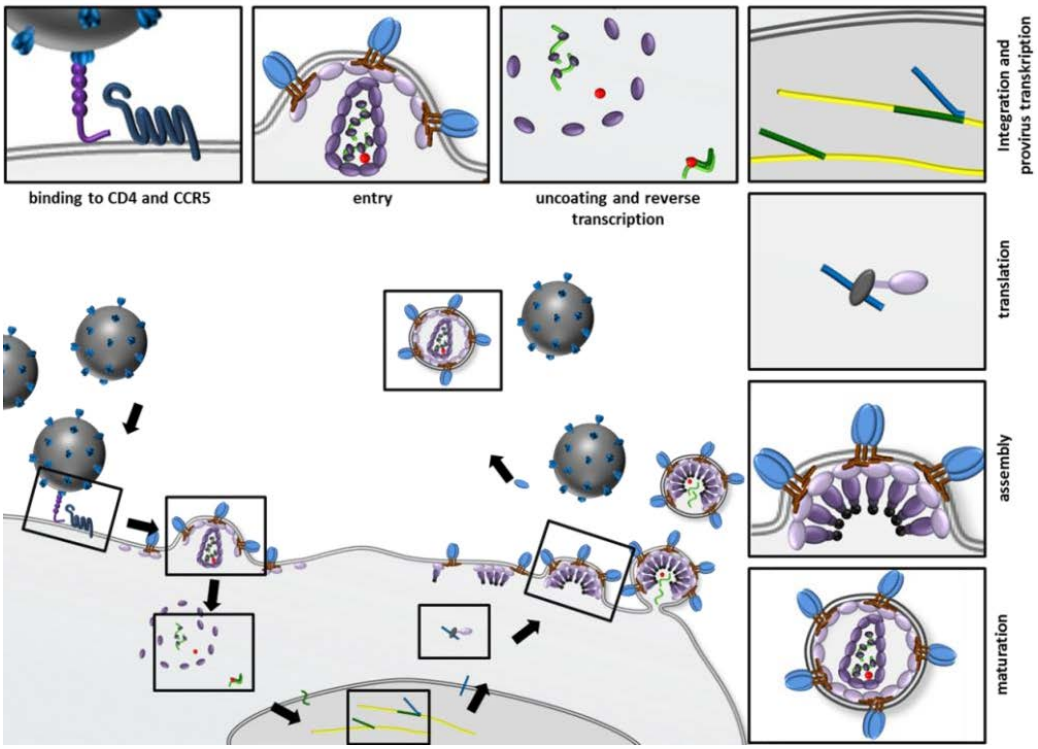

Figure 1-6: HIV replication cycle. After binding to the surface of the host cell, viral proteins mediate the fusion between the viral lipid envelope and the plasma membrane. RNA, reverse transcriptase, integrase and other viral proteins enter the host cell and double stranded viral DNA is generated by the reverse transcriptase. Subsequently, this DNA is transported through the nuclear membrane and integrated into the host cell genome. Upon cell activation, viral RNA can be generated, encoded by integrated DNA and viral proteins are synthesized on host ribosomes. These new viral RNA and proteins move to the cell surface and immature HIV particles form. Concomitant with or subsequent to the release, viral protease causes virus maturation to finally yield infective virions.

The viral enzyme reverse transcriptase removes attached viral proteins from the single stranded positive strand RNA genome and produces a complementary DNA (cDNA) strand[30]. As the first DNA strand is formed, the enzyme degrades the RNA and complements the single stranded cDNA. This process is accompanied by a microtubule-based transport to the nucleus.

Then, the ends of the double stranded viral DNA are joined non-covalently and the resulting circular DNA is moved into the nucleus for further insertion in the host cell chromosome by the viral integrase enzyme[30]. The integrated viral DNA, called proviral DNA can remain dormant or, upon activation by cellular transcription factors, RNA may be synthesized yielding messenger RNA and viral genomic RNA. For protein synthesis, the integrated provirus is first transcribed into mRNA which in turn is spliced and exported to the cytosol[30]. Translation to the regulatory proteins tat and rev occurs and rev begins to accumulate in the nucleus, where it eventually binds viral mRNA and mediates the nucleus-exit of unspliced transcripts. As a result of that, the structural proteins Gag and Env are translated from the full-length mRNA which also represents the actual virus genome. As many viral proteins the envelope protein gp160 requires cleavage by cellular proteases to process the long polyprotein precursors to functional proteins. The viral components assemble at the host cell plasma membrane and finally the virion is released by budding. Maturation of the virus particles occurs either in the forming bud or in the immature virion after release from the cell. To this purpose, the Gag polyprotein has to be cleaved into individual functional proteins by the work of the viral protease so that finally the virion rearranges to yield a mature, infective particle[31].

1.1.11 Structure and function of the HIV envelope complex

As described before, the HIV replication cycle is initiated by adhesion of extracellular virions to the target cells and fusion of the virus envelope with cellular membranes, a process that is mediated by the viral envelope glycoprotein complex. The prevailing model describes a three step mechanism of conformational changes in the envelope complex that cause virus binding and membrane fusion (Figure 1-7). At first, the envelope complex exists in the native state with the hydrophobic gp41 ectodomain efficiently shielded from the environment[32]. Upon binding of envelope surface subunit gp120 to the receptor protein CD4, the variable regions V1, V2, V3 of gp120 are rearranged and the so called bridging sheet which is comprised of two double-stranded beta-sheets is formed[33]. Both, bridging sheet and variable region V3 are required for the subsequent gp120 coreceptor binding. Besides rare exceptions, binding of primary receptor and coreceptor, usually the chemokine receptors CXCR4 or CCR5, is necessary to allow a further progression of the fusion reaction. But, it has been proposed that also other cellular proteins like the protein disulfide isomerase (PDI)[34], dendritic cell-specific intercellular adhesion molecule-3-grabbing non-integrin (DC-SIGN)[33], a4b7 integrins[33] or syndecans[35] might be involved in the gp120 rearrangement or in the formation of the

immunological synapse, respectively. Nevertheless, this fusogenic conformational change leading to the pre-hairpin intermediate, triggers exposure of the gp41 hydrophobic fusion peptide and its insertion in the host cell membrane[32]. The final step of the virus entry is then the folding of gp41 into a low energy trimeric hairpin conformation. This formation of a six-helix bundle, consisting of three N-terminal and three antiparallel C-terminal heptad repeats, provides the energy to bring viral and cell membrane in a proximity that is close enough to permit fusion[32]. Interestingly, HIV was reported to "surf" after receptor binding and prior to the fusion process on the cell surface to reach specific destinations that are needed for the infection or facilitate the entry[33,36].

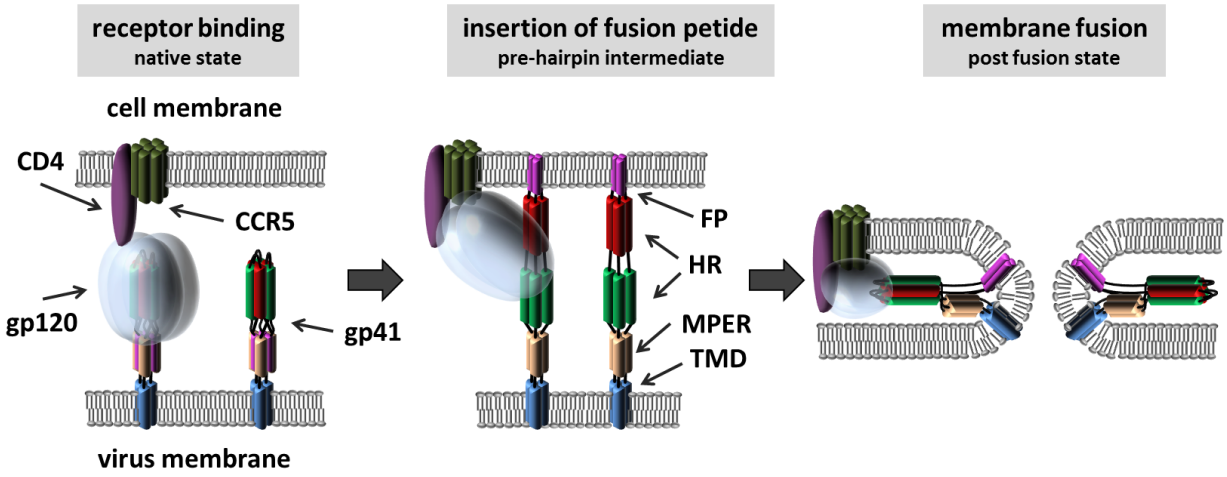

Figure 1-7: Model of the envelope-mediated membrane fusion. In the native, non-fusogenic state the transmembrane subunit gp41 is shielded by the gp120 subunit. Upon binding of gp120 to the receptor CD4 and the coreceptor, gp120 is rearranged concomitantly with a refolding of gp41. N and C-heptad repeats (HR) of gp41 are exposed and the fusion peptide (FP) penetrates the target membrane. This conformation is termed per-hairpin intermediate. Subsequently, another refolding occurs in gp41 leading to the compact six-helix bundle of the post-fusion state. This rearrangement causes a merger of viral and cellular membranes, followed by the formation of a fusion pore and finally membrane fusion. For better visualization of gp41 conformational changes, the right complex is displayed without gp120 and cellular receptors. Adapted from [32].

1.2 The transmembrane protein gp41

The HIV-1 glycoprotein gp41 is a typical class I fusion protein[37]. It is trimeric in its pre- and post-fusion state and it possesses a central N-terminal trimeric α-helical coiled coil that is covered with three C-terminal helices, thereby forming the six-helix bundle. Furthermore, the

protein was classified as a type I transmembrane protein, meaning that is anchored to the membrane with a stop-transfer sequence that is removed after synthesis and exposes its N-terminus on the extracellular side of the membrane.

1.2.1 Structure of the glycoprotein gp41

The structure of the HIV-1 glycoprotein gp41 and the precise arrangement of its domains are crucial for the function and fate of the whole protein (Figure 1-8).

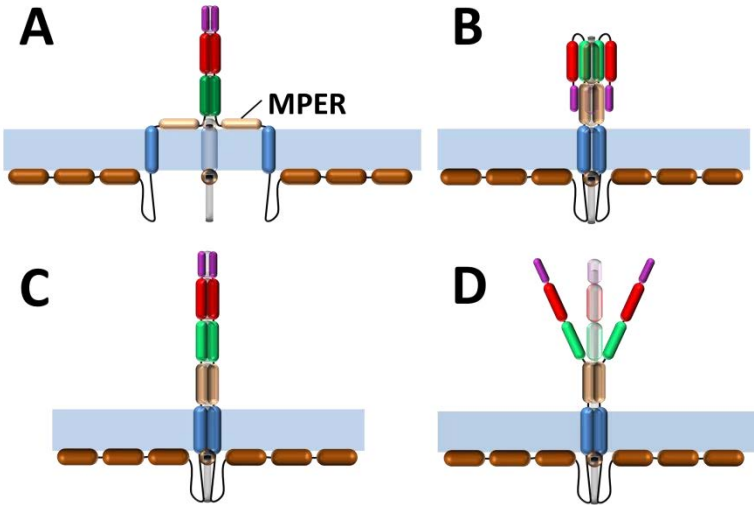

Figure 1-8: Schematic representations of hypothetical trimeric gp41 complexes. Gp41 is mainly α-helical (brown tubes) and was often described to comprise only one single membrane spanning domain. Possible conformations are: (A) Tripod-like oligomeric structure with a membrane associated membrane proximal external region (MPER) as proposed by [38,39]. (B) Oligomerization of the transmembrane domain (TMD) with MPER associated fusion peptide[40]. (C) Trimerization of TMD and all external α-helical domains[38,41,42]. (D) Oligomerization of TMD and MPER as the base of gp41 trimeric structure[31]. Hypothetical structures were designed based on the publications cited.

Many important intramolecular-interactions[41,43,44] require particular conformations and the interplay with cellular or other viral components is tightly connected to the specific positioning of the responsible motif[45,46] with respect to the membrane gp41 is embedded in. Although the overall folding of gp41 is not known, for the most part it could be demonstrated to have a complex, mainly α-helical secondary structure that is necessary to exactly position important residues at their site of action. The HIV-1 envelope complex is known to be composed of trimers of gp41/gp120 heterodimers but still the exact arrangement of the structural elements and in particular the interplay between gp41 and gp120 is widely unclear.

Four hypothetical native state conformations of gp41 are displayed here, based on suggested structures from different publications (Figure 1-8).

1.2.2 Gp41 domains

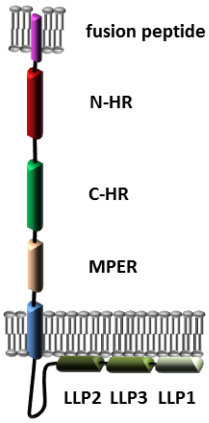

Figure 1-9: Schematic representation of the structural elements of Gp41. For a better visualization the protein is displayed in the stretched pre-hairpin conformation.

Gp41 can be roughly divided in several structural and functional elements. The arrangement of the different, for the most part α-helical domains is, especially in the context of the prefusion gp41-gp120 complex not known (see 1.2.1). Nevertheless, most of them were massively studied and functionally characterized in recent years so that nowadays their role and relevance in many steps of the virus lifecycle has been revealed. In the following section the current knowledge will be briefly summarized. Thereby, the individual domains are described from the N-terminal fusion peptide to the C-terminal end (Figure 1-9).

1.2.2.1 External Domain

1.2.2.1.1 Fusion peptide

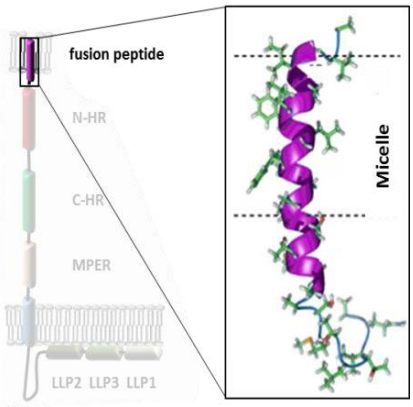

Figure 1-10: Ribbon representation of the gp41 fusion peptide structure. Adapted from [220].

The first gp41 component that is invading the host cell is the gp41 fusion peptide (Figure 1-10). This 23-residue, hydrophobic, glycine rich domain is critical for viral infectivity[47–50] and is, even in absence of other parts of the envelope complex or viral components able to induce membrane fusion[51–53]. It penetrates the hydrocarbon region of the host cell bilayer, dehydrates the outer bilayer and causes a membrane thinning and reduction of the bending modulus[54,55]. Interestingly, recent experimental data insinuate an interaction between fusion peptide and gp41 transmembrane domain (TMD) in context of the membrane

fusion[41]. Another recent finding is that a specific binding between a conserved FP motif (AxxxG) with the T-cell receptor (TCR) α transmembrane domain results in an inhibition of the assembly of functional TCR complexes[43].

1.2.2.1.2 Heptad repeats/six-helix bundles

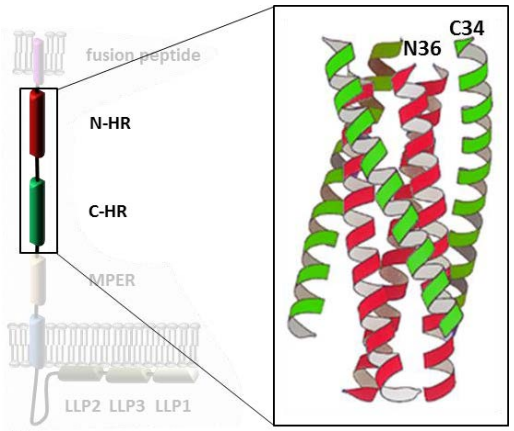

Figure 1-11: Six-helix bundle, composed of NHRs in blue and CHRs in pink. Adapted from [57].

Adjacent to the Fusion Peptide Proximal Region (FPPR, not shown) lays the heptad repeat region (Figure 1-11). It consists of the N-terminal heptad repeat (NHR) that is linked by a hydrophilic loop with the C-terminal heptad repeat (CHR). The HR motifs possess a characteristic repeating pattern with a typical packaging of bulky, hydrophobic side chains in a coiled-coil structure[34]. During membrane fusion the HR-region self-assembles into an extremely thermostable six-helix bundle[56]. Crystal structures of that low energy conformation revealed the six-helical bundle being composed of three NHRs that form a parallel coiled-coil with three CHRs packed in the grooves of the NHR structure in an antiparallel fashion[57,58]. Since the formation of that trimer-of-hairpins is an indispensable step of the infection process, highly active fusion inhibitory peptides could be developed. The underlying principle is simple. The peptides basically mimic the NHR and thus specifically and tightly bind the protein's CHR. As a result of that, this motif is blocked, the formation of the six-helix bundle is prevented and thus membrane fusion and virus entry do not occur[59,60]. This mechanism is very efficient and some of those inhibitors already reached clinical trials (reviewed in [61]). Additionally, neutralizing antibodies were often found to target heptad repeats[62] which further underlines the significance of the domains for virus progression. The hydrophobic motif that links the heptad repeats contains a conserved disulfide loop. It mediates interactions with gp120 cysteines that are a prerequisite for gp160 processing by cellular furin proteases[63] but is not required for the formation of the six-helix bundle[64].

1.2.2.1.3 Membrane proximal external region

Another important structural element of the gp41 ectodomain is the membrane proximal external region (Figure 1-12). In membrane contact it was demonstrated to have a basically α-

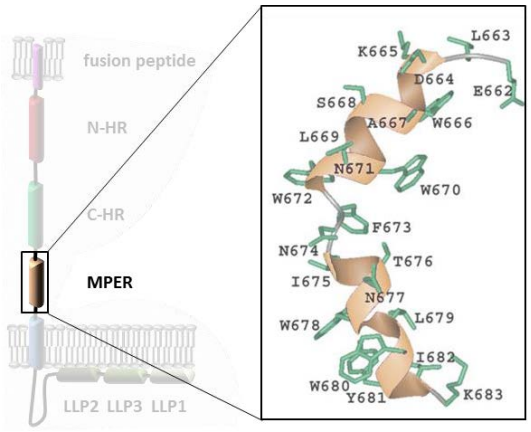

Figure 1-12: Ribbon diagram of the gp41 MPER in a lipid micelle. Adapted from [65].

helical conformation with a sequence of aromatic residues oriented along the axial length[40]. Most likely, those amino acids are arranged at the membrane-water interface of the bilayer[65]. In presence of a membrane-water interface MPER peptides consist of a tilted N-terminal α-helix that is connected via a short hinge to a flat C-terminal segment[65] (Figure 1-14). In the mature trimer, this configuration might result in a tripod-like structure[39] of MPERs protruding from the exoplasmic trimer stalk (Figure 1-8). Moreover, the MPER was not only reported to hamper the integrity of membranes but also to possess a higher bilayer disruption potential than the N-terminal fusion peptide[66]. The region alone has furthermore the potential to induce trimerization[67,68] and accordingly, the oligomeric MPER has been suggested to be involved in the formation of the prefusion conformation of gp41[69]. Moreover, a direct interaction has been reported between FP and MPER N-terminus[70] suggesting a structural mechanism of fusion peptide inhibition and protection in the non-fusogenic state. Importantly, two highly relevant motifs are located in the MPER domain of gp41, the GalCer binding site and the CRAC domain.

1.2.2.1.3.1 GalCer binding site

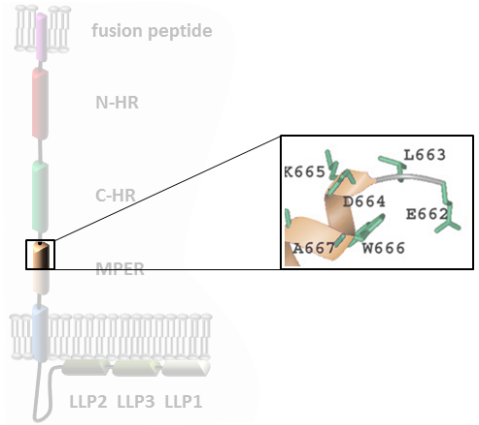

Figure 1-13: GalCer binding site. Relevant section of the gp41 MPER. Adapted from [65].

Since the major sites for the initial HIV-1 infection are epithelial cells in mucosal surfaces[71], the virus has to bind and enter those cells efficiently. A prerequisite of mucosal transmission is the interaction of gp120 and gp41 with the glycosphingolipid galactosyl ceramide (GalCer) that is localized in basolateral plasma membrane lipid rafts on the mucosal cell surface[71,72]. Upon transcytosis, HIV-1 is then able to cross the epithelial barrier to finally target CD4 positive host cells. At the N-terminus of the MPER, the peptide ELDKWA

was identified that is responsible for a specific interaction between gp41 and the GalCer[71] (Figure 1-13). Since GalCer represents an alternative receptor for HIV-1 that is crucial for an efficient entering of the organism, this gp41 epitope is highly conserved[71].

1.2.2.1.3.2 CRAC motif

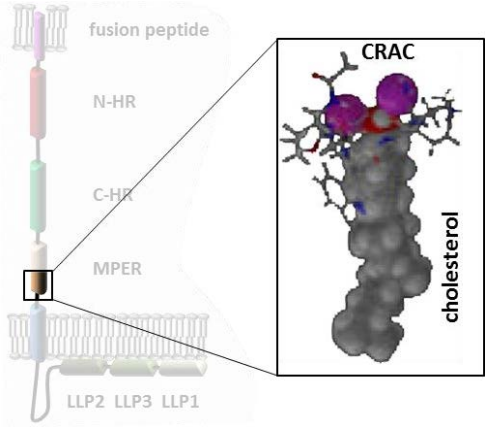

Figure 1-14: Simulation-based model of interaction between the gp41 CRAC and cholesterol. Adapted from [78].

The glycoprotein gp41 comprises a cholesterol binding motif (CRAC)[73,74] adjacent to the transmembrane domain (Figure 1-14). This conserved gp41 sequence LWYIK fulfills all requirements of a cholesterol recognition amino acid consensus[75]. It conforms to the pattern -L/V-(X)(1-5)-Y-(X)(1-5)-R/K-, in which (X)(1-5) represents one to five residues of any amino acid and the domain is in a high proximity of the protein's membrane spanning domain. In fact, it has been demonstrated, that gp41 CRAC-derived peptides bind cholesterol specifically[76]. Most likely, the motif's leucin is crucial for the conformational flexibility that is a prerequisite for the stacking of CRAC aromatic groups with the cholesterol A-ring[77] and thus it has often been targeted in mutation studies[74,78,79]. In micelles a high cholesterol sequestering action[78] could be found for gp41 wildtype peptides whereas CRAC mutants of gp41 caused a reduced one-cycle replication, a loss of the membrane fusion ability[78,80,81] and even a reduced Env incorporation[82] in virus particles in several independent studies. In contrast to that, gp41 CRAC mutations were elsewhere shown not to affect the protein's incorporation in rafts, gp41 maturation and intracellular transport[81].

1.2.2.2 Transmembrane domain

The definition of a protein's transmembrane domain is not always trivial. Although hydrophobicity and other theoretical considerations allow predicting sequences that have a high probability of being membrane spanning domains, reliable statements can be made only on the basis of NMR data. For gp41, different conformations have been suggested with various domains of the protein traversing the membrane (see 1.2.3). Nevertheless, it is widely

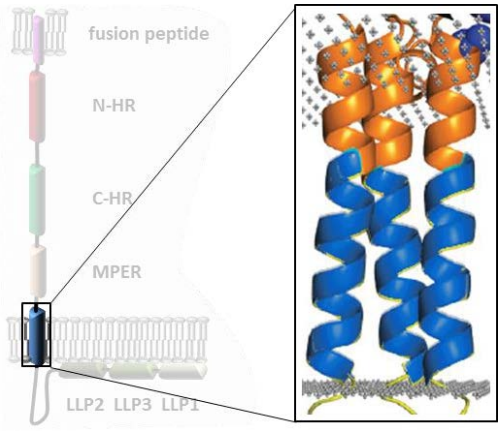

Figure 1-15: Ribbon diagram of a gp41 transmembrane trimer.
Adapted from [221].

accepted that the transmembrane domain, at least in the prefusion-state of gp41 comprises the amino acids 685-705 (Figure 1-15). Whereas only a few residues, amino acids 684-695, are sufficient to anchor the protein in the membrane, the full TMD is required for other functions of the domain[82]. Indications were found, that the membrane spanning α-helices possess an oligomerization potential[83,84] and are involved in the gp41 induced fusion process[41,85,86]. A highly conserved GXXXG motif seems to be a crucial factor of both properties[41,83], but to date, experimental data are contradictory. However, it has been reported in that context, that interactions between the gp41 fusion peptide and the transmembrane domain promote the membrane fusion process[41] (compare 1.2.2.1.1).

1.2.2.3 Cytosolic domain

Most lentiviral envelope proteins possess a very long cytoplasmic tail (CT) compared to other retroviruses[87]. In case of HIV-1, HIV-2 and SIV it is about 150 amino acids in length whereas for instance in case of Rous sarcoma virus (RSV) or Murine leukemia virus it comprises only 20-40 residues. Although isolates of HIV-1 were found with significant truncations of the transmembrane subunit's cytoplasmic tail[88], in general it is highly conserved and truncation mutants were reported to be impaired in efficient virus progression[88]. So far, no high resolution data are available for the gp41 CT, but it was reported to comprise three individual α-helical regions[89]. The gp41 internal region is involved in several important processes and influences many of the glycoprotein properties[90,91]. Env incorporation into virus particles, virus infectivity, cell surface expression and membrane fusion depend on the functionality of conserved cytoplasmic motifs[90,91].

1.2.2.3.1 Lentivirus lytic peptides

Three α-helical regions were identified in the intracellular domain of gp41, designated lentivirus lytic peptides (LLP). The exact structure and function of the LLPs have not been

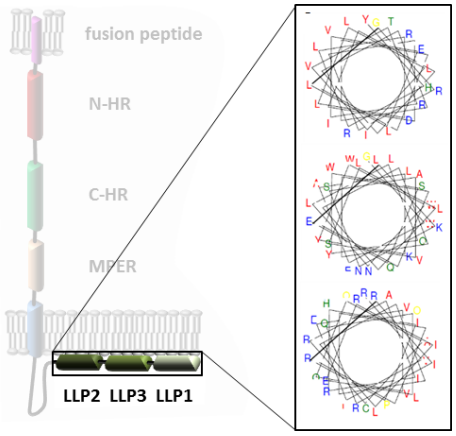

Figure 1-16 : Helical wheel diagrams showing the amphipathic nature of each LLP domain. Hydrophobic residues are displayed in red whereas polar amino acids are blue. Adapted from [92].

sufficiently elucidated, but they are known to adopt their α-helical folding upon partition into lipid membranes and to increase the permeability of model membranes[90,92] (Figure 1-16). LLP-1 seems to be involved in Env oligomerization, stability, membrane binding and Env incorporation into nascent virus particles[93]. Interestingly, it has been reported that the gp41 cytoplasmic tail is involved in virus maturation on one hand and gp41-gp120 heterodimer stability on the other hand[44]. It was surmised that the interaction of the LLP-1 segment with the viral Gag protein in immature virions (CT interaction inside the virion) inhibits the receptor-induced conformational changes in Env that are a prerequisite for the membrane fusion[44] by preventing a crucial interactions of the gp41 cytoplasmic tail with gp120 (CT interaction outside the virion)[44]. This regulatory mechanism would permit to concert particle maturation with infectivity. However, it requires interactions of the cytoplasmic tail on either sides of the bilayer and again points to a dynamic folding of the complete protein that might evoke different conformational arrangements of the Env domains.

1.2.2.3.2 Protein interaction sites

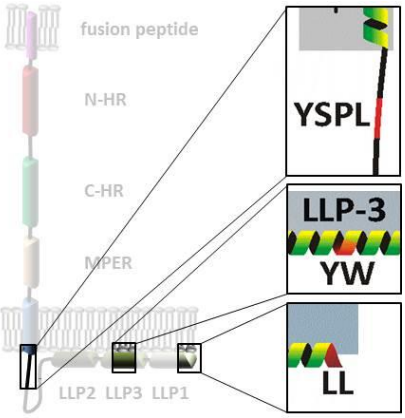

Figure 1-17 : Schematic representation of gp41 motifs that interact with cellular adaptor proteins.

During the virus assembly, the gp41 CT is exposed to the cytosol of the infected cell. Numerous, gp41 interaction sites for host proteins or other viral components have been reported in recent years (Figure 1-17). Nevertheless, the identity and significance of certain motifs is still under debate. A tyrosine-based YXXL motif, starting at residue 712 was reported to be responsible for the association of Env with the μ2-chain of the clathrin-associated adaptor complex AP-2[27,94,95] and possibly with μ1 of AP-1[96]. Both adaptor complexes are involved in intracellular vesicle formation and trafficking regulation. Whereas AP-2 mediates clathrin-associated endocytosis, the AP-1 complex is

involved in the opposing direction, the transport from trans-Golgi-network to the plasma membrane. It has been reported, that this latter trafficking route requires a conserved c-terminal dileucine motif of gp41[94] and it is not yet clear, whether YXXL also participates in the AP-1 interaction[94,96] since contradicting experimental observations were published. However, it is known that the C-terminal dileucine also assists the Y712 motif in restricting the cell surface localization of env[94]. Finally, another tyrosine-based motif, Y802W803 was demonstrated to specifically bind TIP47[46] (tail-interacting protein of 47kDa), a protein that is necessary for the retrograde transport from late endosomes to the TGN[95]. This interaction was reported to moderate the formation of a ternary complex between env, Gag and TIP47 and therefore influence Gag-Env colocalization, virion infectivity and Env incorporation. From the previous, partly contradictory observations it seems that several gp41 motifs are involved in host protein interactions and regulation of its intracellular transport and that the interactions with cellular trafficking proteins are interdependent, presumably at least partly redundant, and perhaps cooperatively.

1.2.2.3.3 Protein palmitoylations

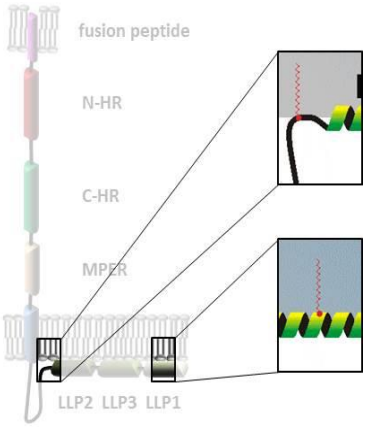

Figure 1-18: Schematic representation of HXB2 gp41 palmitoylations.

The cytoplasmic tail of the HIV-1 Env protein carries palmitoylated cysteine residues (Figure 1-18). This protein modification was reported to promote association with ordered domains in giant unilamellar vesicles (GUVs), giant plasma membrane vesicles (GPMVs)[97,98] and lipid rafts in cellular membranes. Depending on the virus isolate, two, one (the N-terminal, left) or even no palmitoylation (Figure 1-22) were found indicating a minor importance of that protein modification for an efficient virus progression. However, experimental results regarding the function of gp41 palmitoylation are very contradictory. Some publications report a palmitoylation-dependence of gp41 raft partitioning[99,100] and virus incorporation[100] whereas others demonstrated that microdomain sorting and virus incorporation are completely independent of palmitoylation[101] and rather require different, yet to be identified factors in the C-terminal part of the gp41 cytoplasmic tail[90].

1.2.3 Alternative structures of gp41 and functional consequences

It has been proposed that gp41 can adopt at least two different conformations with one or three individual membrane spanning domains (Figure 1-19). This hypothesis is based on the observation that antibodies against the Kennedy sequence, a motif located in the cytoplasmic tail of the protein and thus supposed to be shielded from the environment, bind to the protein on expressing cells as well as on virus particles[45]. Structural analyses yielded a model suggesting that the putative transmembrane domain is spanning the membrane twice, which allows surface exposure of the Kennedy sequence but also requires a third membrane crossing to permit intracellular interactions of the remaining cytosolic domain (Figure 1-19 B, right). Interestingly, this model would impede interactions of the YXXL endocytosis signal with cellular adaptor proteins and thus prevent reinternalization of the protein. As a consequence, Env adopting this conformation should be preferentially retained at the plasma membrane. Considering the fact that the gp41 CT has also been reported to influence the stability of the gp41-gp120 heterodimer this might suggest a CT-dependent mechanism to achieve a preferential surface exposure of those complexes that possess a more stable overall folding and structure.

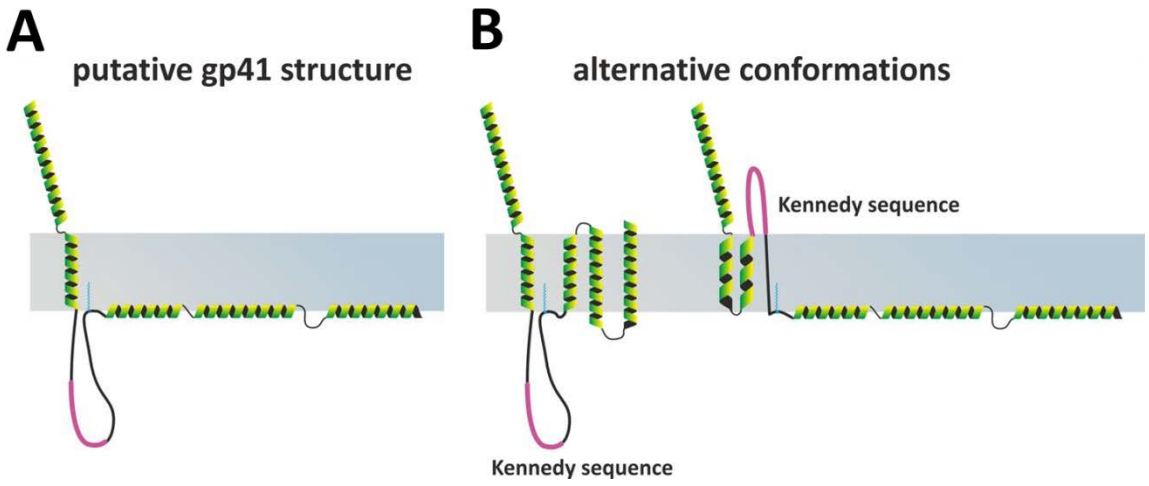

Figure 1-19: Alternative gp41 conformations. The displayed models of the cytosolic domain organization with respect to experimental results reporting gp41-induced pore-formation[92] and surface exposure of the putative internal Kennedy-sequence[102]. Schemes showing the conventional, putative conformation (A) and alternative structures (B) based on the pore model (left) or the model emphasizing the exposure of Kennedy sequence (right). The Kennedy sequence is highlighted in pink.

Another possibility, proposed by Costin et al.[92] favors a membrane spanning of the lentivirus lytic peptides (Figure 1-19 B left). In this model, the putative TMD as well as the three LLPs

cross the membrane and upon trimerization of monomers to the oligomeric complex this organization might allow the formation of a pore with the hydrophilic residues of the amphipathic LLPs exposed to the lumen of that pore.

1.2.4 Gp41 intracellular trafficking and transport

The HIV-1 envelope complex is synthesized as a polyprotein precursor from a spliced bicistronic vpu/Env mRNA. The unprocessed precursor gp160 contains an N-terminal endoplasmic reticulum signal sequence which targets the protein to the membrane of the rough endoplasmic reticulum and is post-translationally removed by cellular signal peptidases[103] (Figure 1-20). A hydrophobic stop-transfer signal in the transmembrane domain retains the protein in the ER membrane, leaving the intracellular domain in the cytoplasm and later in the interior of the virion[27]. Concomitant with its translation, gp160 is glycosylated and assembles into oligomers as a prerequisite of its trafficking to the Golgi apparatus[27]. Here, gp160 is proteolytically cleaved by cellular furin or furin-like proteases at a conserved motif to generate the mature receptor protein gp120 and the transmembrane subunit gp41[27]. Both proteins remain associated by non-covalent interactions, resulting in heterotrimeric complexes composed of three individual gp41 and gp120 molecules each[27]. This process is followed by complex high-mannose oligosaccharide-modifications in the trans-Golgi network[27].

Further transport to the plasma membrane in the cell is very complex and highly regulated. Although many cellular interaction partners of the envelope proteins have been described, the exact progression and significance of different cellular transport routes is under debate. At least three different motifs were identified in the gp41 cytoplasmic tail (see Figure 1-17) and each of those sequences is able to interact with several adaptor complexes in different cellular environments[27]. It is known that the majority of Env molecules is transported to the plasma membrane and rapidly reinternalized via AP-2 driven clathrin-mediated endocytosis[27]. However, the function of this constrained surface localization and also the fate of internalized glycoproteins is unknown, but most likely it contributes to the relatively low cell- and virion-surface levels of Env (~10-30 spikes/virion). Furthermore, it might help the virus to evade the host immune response and decrease virus-induced cytopathicity[27].

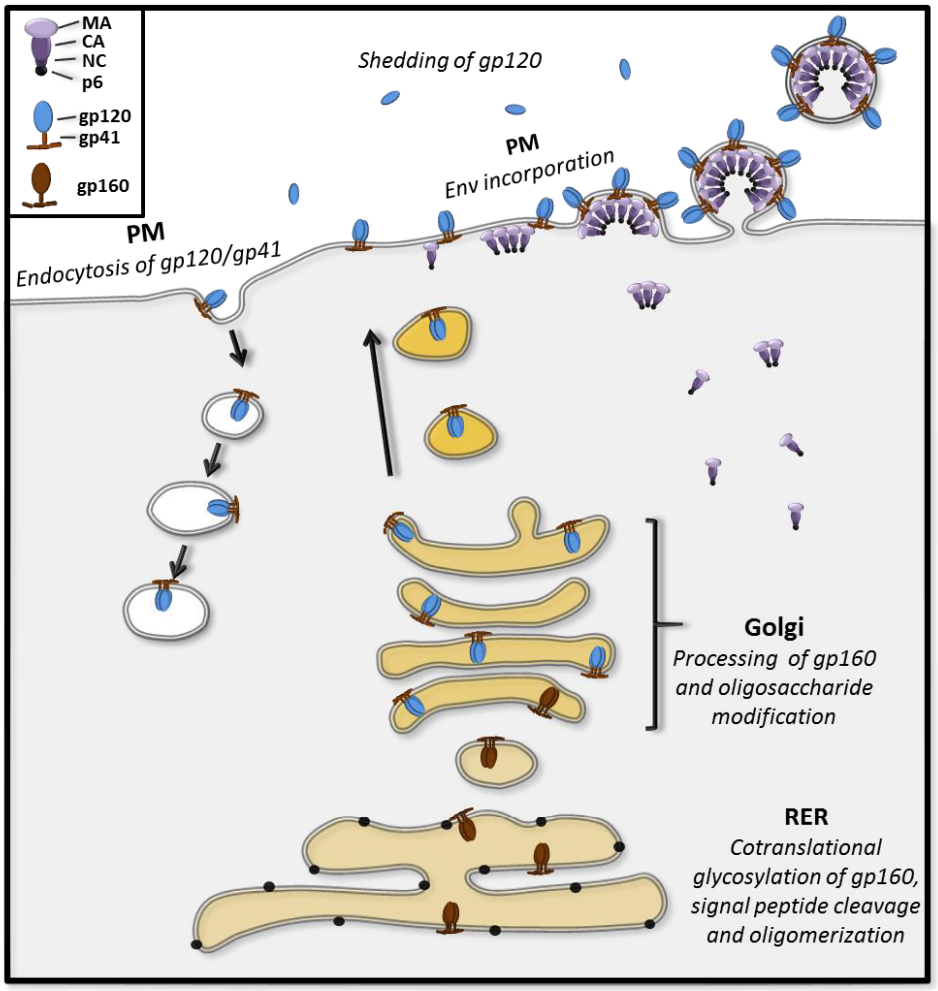

Figure 1-20: Trafficking of gp41. The HIV-1 envelope complex is synthesized as a precursor in the rough endoplasmic reticulum (RER). Following oligomerization, it is transported to the Golgi apparatus where cleavage into gp41 and gp120 is conducted by cellular proteases. Subsequently, the trimeric heteroduplexes interact with cellular trafficking associated adaptor complexes to mediate transport to the plasma membrane where it is incorporated into nascent virus particles. After surface exposure, clathrin-mediated endocytosis is induced by intrinsic internalization signals. Adapted from [27].

1.2.5 Interactions of gp41 with other viral components

The unusual length of the gp41 CT suggests important functions to be comprised in this domain. Different motifs were identified being responsible for communications with cellular proteins (see 1.2.2.3.2) but it has also been reported that the CT mediates interactions with other viral components[95,104]. Both properties, active incorporation of Env in nascent virus particles and infectivity of virus particles, depend on interactions between gp41 and the Gag protein[95] (Figure 1-21).

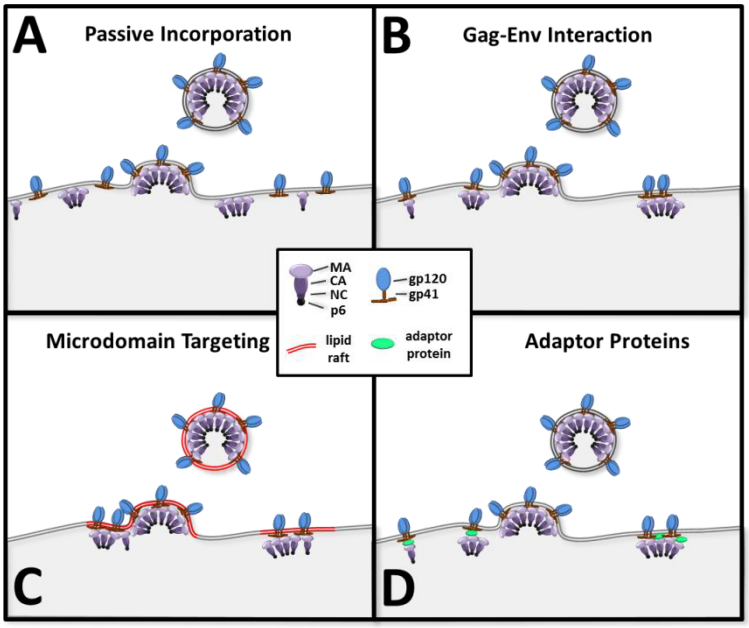

Figure 1-21: Models for Env incorporation in nascent viral particles. (A) *The passive incorporation* model assumes that there is no interaction between Gag and Env in the assembly process. Plasma membrane exposed gp41 is packed together with other viral components without further regulation. (B) *The active incorporation* model takes interactions between gp41 and Gag into account. As a result of that Env is specifically targeted to viral budding sites. (C) Considering experimental findings that report a clustering of Env and Gag in lipid rafts and t he deduced model of a HIV-budding from plasma membrane microdomains it was hypothesized that this *Gag-Env cotargeting* facilitates virus assembly. (D) The *indirect Gag-Env interaction* models based on publications demonstrating, that interactions of Gag and Env with cellular adaptor proteins are necessary to ensure efficient virus assembly. Taken from [27].

To appraise the relevance of that cooperative mechanism it is important to have a closer look on the function and properties of Gag. This viral polyprotein is synthesized on cytosolic polysomes and subsequently transported to the plasma membrane[95]. Gag alone is necessary and sufficient to form non-infectious virus-like particles[95] and its N-terminal myristate in combination with a cluster of highly basic residues in its matrix (MA) subunit targets this process mainly to the plasma membrane[105]. Gag-multimerization, a prerequisite of budding and release, depends on interactions between the p6 subunit and the host cell endosomal sorting complex required for transport (ESCRT)[12]. Interactions have also been reported with the cellular proteins AP-1, AP-2, AP-3 and rab 9[95] and the cellular lipid PI(4,5)P2 at the plasma membrane[105]. However, the role of Gag in the gp41 progression has not been completely elucidated. It was reported, that association of Env with DRM[106] and Env surface exposure might be influenced by Gag[107]. Moreover, the cellular protein TIP47 was shown to

be required to bridge both proteins[46]. However, still several models of Env incorporation in virus particles exist (Figure 1-21) and further experiments are required to enlighten the interplay of viral proteins in the assembly process. Interestingly, interactions between the gp41 CT and Gag also seem to influence virus maturation and rigidity after budding and release and, as a result of that, also the infectivity of virus particles[95] (see also 1.2.2.3.2).

1.2.6 Diversity of the envelope complex

HIV is a dynamic and highly divers virus. A distinction is made between two types of the virus with completely different phylogenetic origins. As described before (see 1.1.4), type 1, which causes most of the infections worldwide, most likely descents form chimpanzee SIV, whereas HIV-2 was supposed to be a zoonosis from the sooty mangabey. Since HIV-2 is regionally very restricted it only causes a significant minority of all occurring HIV infections[10]. Therefore, most of the present knowledge has been derived from type 1 virus isolates.

Since the envelope complex is the only virus protein that is exposed to the cell surface, a high variability in this protein is mandatory for the pathogen to escape host immune reactions. Thus, changes in the gp120 variable region do not only promote the escape of HIV-1 from the humoral immune response but also control the coreceptor specificity[27]. Interestingly, it has been suggested that the envelope complex regularly evolves during disease progression in a single organism regarding receptor usage and host cell target (from R5 to X4 tropism). The switch from the during infection easy-accessible macrophages and memory T-cells (R5) to basically all T-cells (X4) was proposed to allow more efficient virus production in later phases of the etiopathology[22] (see also 1.1.8). A consequence of this variability and mutability is a high genetic diversity of the HIV-1 pandemia. Most of the HIV-1 cases can be classified into the two main groups, M and O. Group M comprises the majority of HIV-1 isolates and can be subdivided into at least nine sequence subtypes or clades, designated A to K. The sequence diversity between different isolates is high (see also 1.1.2). The Env amino acid sequence varies up to 47 % between the groups and the variation ranges from 25 to 35 % between different M group members[88]. But even within one subtype the variation ranges from 3 to 23 %[88]. Most lab-adapted virus isolates used for non-clinical studies in recent years belong to the subtype B. The glycoprotein gp41 of the prevalent isolates HXB2 and JRFL

share around 86 % of the amino acids (uniprot alignment) but nevertheless show some significant differences (Figure 1-22).

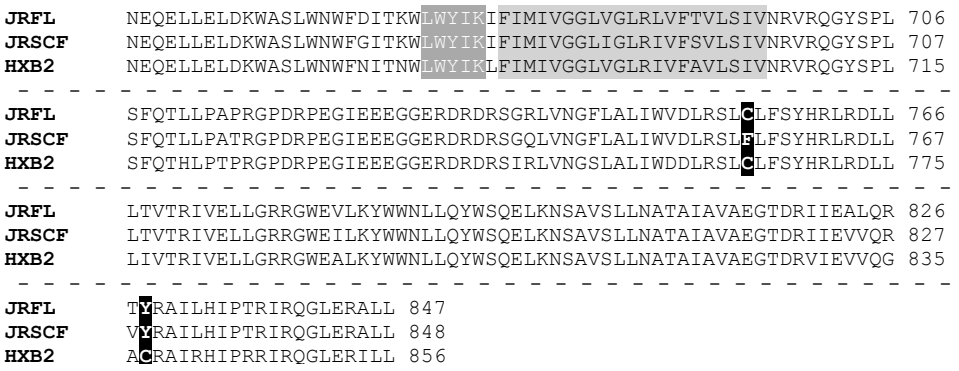

Figure 1-22: Partial gp41 sequence alignment of the common HIV-1 virus isolates JRFL (Uniprot-entry: Q75760), JRSCF (P20871) and HXB2 (P04578). The conserved CRAC domain highlighted in dark grey and transmembrane domain in light grey are highly conserved, whereas for instance the palmitoylated cysteines C764 and C837 (numeration from HXB2) labeled in black are variable.

The isolate JRSCF, another important lab strain, although isolated from the same patient as JRFL was demonstrated to have a deviating phenotype and also differences in the amino acid sequence. One particular difference between the three isolates is the cytoplasmic cysteines that are targets of palmitoylation. Whereas HXB2 harbors two palmitoylation sites, JRFL comprises only one and JRSCF completely lacks targets of post-translational lipidation (Figure 1-22). It should be pointed out here, that usually the HIV-1 literature refers to the HXB2 isolate regarding residue numbering, amino acid sequences and structures.

1.3 Lateral membrane organization

Cellular membranes are formed by hundreds of different lipid species[108], interacting with a tremendous amount of membrane proteins in various conformational states. As a result of that complexity, eukaryotic bilayers are believed to exist not only in various ordering states with respect to their environmental context and lipid composition[109] but also to be laterally heterogeneous[110] (schematically displayed in Figure 1-23A). It is therefore widely accepted that biological membranes and in particular plasma membranes have a subcompartmentation due to self-organizing properties of the molecules they are consisting of. Ordered domains with a higher lipid packaging than the surrounding membrane have been reported to spontaneously form in artificial membrane systems of a suited composition[111,112]

(Figure 1-23B). It has been proposed that cellular analogues of those lateral microdomains exist, termed lipid rafts. They are enriched in typical lipids such as cholesterol and sphingolipids and are supposed to facilitate protein assembly, signal transduction processes as well as different steps of viral lifecycles by ensuring efficient protein-protein interactions[98,113–115].

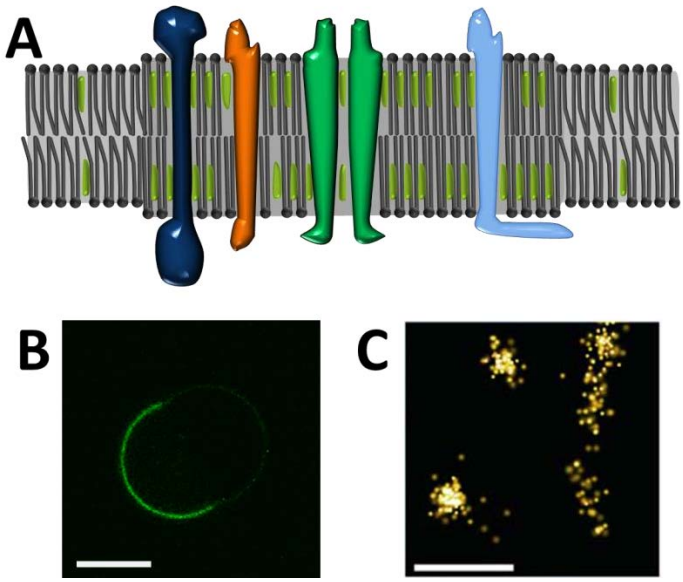

Figure 1-23: Lateral organization of biological and artificial membranes. Biological membranes have been proposed to possess a lateral subcompartmentation due to self-organizing properties of their heterogeneous components. (A) S chematic representation of plasma membrane lipid rafts. Microdomains were proposed to comprise high amounts of cholesterol and saturated lipids resulting in a thickening of the bilayer. Moreover, protein composition and local concentration were reported to be distinct to other parts of the surrounding membrane. (B) Confocal image of phase separating GUVs labeled with C6-NBD-PC. Microscopic domain formation is visible in vesicles of a simple, multicomponent lipid-mixture (Cholesterol, POPC, SM 1:1:1) due to the preferentially incorporation of the lipid analogue in the liquid disordered domain. The scale bar refers to 10 µm. (C) Cholesterol-enriched domains on the plasma membrane of HeLa cells. In biological membranes phase separation is usually restricted to very small scales. Optical observation is impossible with conventional microscopy and just achievable using superresolution methods[116]. The scale bar refers to 500 nm.

While an intramembranous phase separation is easy to visualize using fluorescence microscopy in artificial bilayer systems like GUVs, obtaining direct evidences in a cellular context is sophisticated. Most likely, physiological rafts are too small (<200nm)[74,117] and too unstable (<1s)[118] to be detected with conventional microscopic methods (compare Figure 1-23C). Obviously, the general concept of lipid rafts is highly plausible. Nevertheless,

many doubts remain regarding the lateral subcompartmentation model in general but more importantly regarding the hitherto experimental approaches[119,120] (also addressed in 1.3.2).

1.3.1 Lipid rafts in the virus context

Proteins supposed to be associated with membrane microdomains cover the whole spectrum of life. Rafts and raft associated proteins were found in viruses[98], bacteria[121,122] and all kinds of eukaryotic cells[118,123]. Nevertheless, a reasonable focus of research in the field lies on viruses and phages since especially virus assembly and budding dictates a high spatial and temporal control of molecular interactions. Correspondingly, virus proteins were found in raft preparations of infected cells[90,98,123–126] pointing to an important function of lipid microdomains in virus lifecycles. Furthermore, for several viruses the role of microdomains and cholesterol in both infection and assembly was demonstrated by observing the severe effects of raft disrupting agents like methyl-beta-cyclodextrin[125,127,128] or nystatin[127] on different virus functions.

1.3.1.1 The relevance of rafts in the HIV-1 lifecycle

Depletion of cholesterol from HIV-1 virions, was shown by Campbell and coworkers[128], to cause a significant reduction of infectivity and this effect was abrogated after restoring cholesterol. Moreover, HIV-1 particles produced from cholesterol-depleted cells were proven to be less infectious and virus entry could be inhibited by cholesterol-binding compounds[129]. Furthermore, it is known that both HIV-1 receptors on a T-cell surface, CD4 and CCR5, are associated with lipid rafts and CD4 mutants defective in raft partitioning are unable to support HIV-1 infections[130] pointing to an important role of lipid rafts in the first infection steps. Vpu, another HIV-1 protein, counteracts the function of cellular tetherin, which fixes assembled virions at the plasma membrane and prevents virus spread[131]. Both proteins, tetherin and vpu were found to be raft associated and it is reasonable that their interaction depends on the common clustering in lipid microdomains[132,133]. Finally, it is well documented that the assembly of Gag oligomers occurs in lipid rafts at the plasma membrane and a mechanism based on the myristoylation of the p17 subunit could be proposed, explaining the molecular background of the polyprotein's lateral sorting into ordered microdomains[105].

1.3.1.2 Function of a potential gp41 raft partitioning

The general relevance and in particular the function and of a protein's raft partitioning is still under debate. For virus proteins the most obvious guess would be a role in virus assembly and budding. Although it could be shown that cholesterol depletion of HIV-1 infected cells is significantly impairing virus production and virus infectivity[115] the question whether gp41 raft partitioning is influencing its incorporation in virus particles, or virus infectivity has yet not been elucidated definitely. Publications regarding that question are not always consistent and sometimes contradictory[90,100,101]. Further studies are necessary to deepen our understanding of the biological background of protein enrichment in membrane microdomains and specific lipid binding motifs.

1.3.2 Methods used to study membrane microdomains

In recent years, different techniques have been applied to study cellular lipid rafts. Often detergent resistant membranes (DRM) were investigated assuming that those preparations are representative for plasma membrane microdomains[90,106,119,134]. In those experiments a remarkable compositional discrepancy was found between DRM and the membranes they are derived off regarding both purified lipids and proteins[135]. This finding points to a lateral subcompartmentation of the plasma membrane, a hypothesis that was further supported by cholesterol depletion assays. For those experiments cells were treated with cholesterol depleting agents like cyclodextrins or statins since cholesterol is supposed to be a major component of plasma membrane microdomains and it was demonstrated that raft related properties are significantly influenced by the cholesterol depletion[135]. But, both methods are controversial and obtained results should be judged carefully[136]. Although DRM preparations are generally supposed to selectively purify lipids and proteins comprising plasma membrane microdomains, often contradictory results were obtained in different attempts and findings were found to be prone to slight changes in the experimental setups[117]. Cholesterol depletion assays on the other hand generate reproducible and reliable results, but since cholesterol is a crucial factor of cellular metabolism, side-effects of a depleting treatment are hard to survey and might influence observed properties in an unpredictable manner[117].

Recently, several new techniques were applied to circumvent those drawbacks and observe lipid rafts within the native environment of an undisturbed cell. FRET approaches,

fluorescence polarization anisotropy and FCS (fluorescence correlation spectroscopy) as well as super resolution microscopic methods like STED (stimulated emission depletion), STORM (stochastical optical reconstruction), PALM (photoactivated localization microscopy) or SIM (structured illumination) confirmed cholesterol-dependent clustering of proteins in nanoscale microdomains with diameters of 100 nm and less in living cells[117,137,138].

1.3.3 Protein factors of lateral membrane sorting

In recent years, several determinants for a targeting of proteins to lipid rafts have been proposed or even identified. GPI anchors[98,113,139–143] and protein acylation[97,98,100,144] were found to cause a lipid phase preference. Acylation is conducted with myristic acid on the N-terminal amino group or with palmitic acid on cysteine residues[145] and in their final form, GPI anchored proteins are linked with a stearoyl group[146]. Considering that, in general saturated acyl chains of phospholipids and cholesterol moieties induce partition into the highly ordered lipid rafts due to their smooth surface, all the aforementioned modifications are usually believed to support a lateral sorting of the protein they are bound to. Another indirect mechanism depends on other bilayer components that are themselves part of a particular domain. Proteins to be targeted to lipid rafts might bind those scaffolding molecules like caveolin or raft enriched lipids like cholesterol to associate with lipid rafts. Finally, the influence of membrane thickness and the smoothness of transmembrane domains are physical factors the might also contribute to protein sorting and preferential lateral sorting. In theory, the thick and ordered lipid rafts should facilitate incorporation of unruffled and longer membrane spanning domains due to energetic reasons and to avoid hydrophobic mismatch[147].

1.3.4 Molecular background of a potential gp41 raft partitioning

Since several viral proteins were shown to be directly associated with DRM and HIV-1 in general turned out to be highly influenced by cholesterol[114,115,129,130,148] it is very likely that the envelope glycoprotein complex is associated with plasma membrane lipid rafts. It is the only HIV-1 transmembrane protein and as described before it contains several determinants supposed or known to drive proteins into ordered lipid microdomains.

Interestingly, over the years all of the aforementioned raft partitioning mechanisms have been proposed to play a role in the lateral sorting of env. The gp41 cholesterol recognition amino

acid consensus, for instance, was reported to specifically bind cholesterol, suggesting an important function of this sequence for microdomain sorting. Contradictory results were obtained regarding gp41 palmitoylation sites. In 2000, Rousso et al. reported that gp41 DRM partitioning and virus infectivity depends on palmitoylated cysteins[100], whereas Chan et al. demonstrated a wild type like behavior, including unaffected raft partitioning, of gp41 palmitoylation mutants[101]. The fact that isolated virus clones were found to contain one, two or even completely lack palmitoylated cysteines also points against an important function of this modification for the induction of raft partitioning. Taking a more holistic point of view Yang showed in 2010 that α-helical and amphipathic motifs within the cytosolic domain of gp41, the so called lentivirus lytic peptides, affect gp41 localization in lipid rafts[90]. Insertion of proline in the hydrophobic face of those helices turned out to significantly reduce gp41 association with lipid rafts without influencing intracellular localization, cell surface expression, virion incorporation or viral replication capacity. An extrinsic factor of gp41 raft partitioning might be the interaction with other viral components. Indications were found for example, that the microdomain sorting of the envelope complex is a result of its interaction with the Gag polyprotein, which is itself widely accepted to be a raft protein[106].

In summary, gp41 was repeatedly shown to be enriched in DRM by several groups in the last ten years. However, evidence based on more reliable methods than DRM preparation are still missing and moreover, the molecular background of the preference for ordered domains remains insufficiently elucidated.

1.4 The toolbox: fluorescence spectroscopy and microscopy

Fluorescence-based methods are indispensable tools of modern biological research. They offer a high versatility, specificity and sensitivity and allow visualization and analysis of complex and dynamic events in a wide range of systems from completely artificial structures like for instance GUVs to the physiological context of a living animal[149]. Processes can be studied over several orders of magnitude in time (from picoseconds to days)[150] and space (from nm to cm)[137,149]. Although many assays just assess fluorescence intensities and wavelength, a wide spectrum of methods has emerged utilizing different aspects of the fluorescence process to collect as many information as possible.

The physical basis of fluorescence lies in the electronic states of fluorochromic molecules, typically π-electron systems that combine several aromatic groups. The process of fluorescence can be divided in several steps that are often depicted in a schematic Jablonski diagram (Figure 1-24).

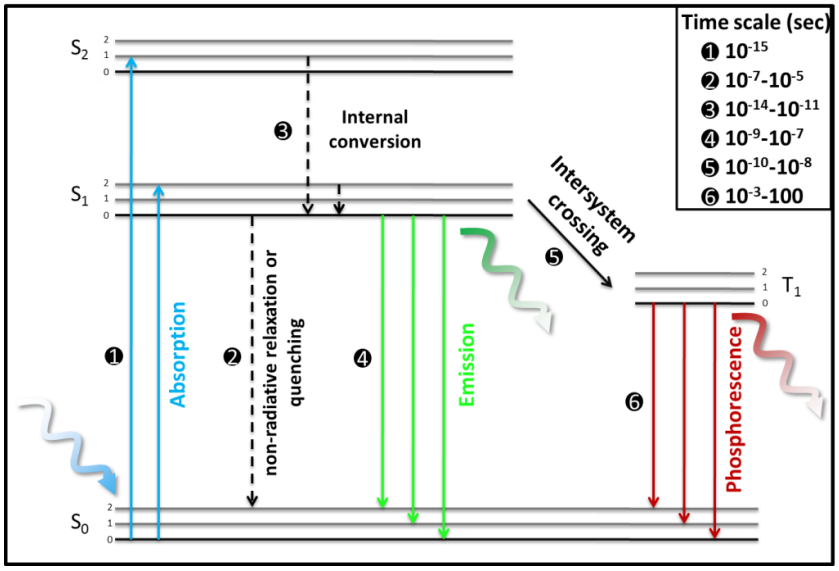

Figure 1-24: Jablonski diagram. In this diagram different electronic states of a chromophore are represented schematically as horizontal lines with ascending energies. S_0, S_1 and S_2 reflect the ground, the first excited and the second excited singlet electronic states of the fluorophore. Vibrational energy levels of each of these states are labeled with the numbers 0, 1 and 2. As the thermal energy is too low to populate the higher vibrational level at room temperature, absorption and emission mainly occur from molecules with the lowest vibrational energy.

Upon exposure to light of a wavelength suited to exceed the energy barrier between ground state and excited state, a valence electron of the fluorophore is lifted to a higher energy orbital. This process occurs in the femtosecond range and typical energies are in the range of 1-5 eV which, according to Planck's law

$$\boldsymbol{E = h \times f = h \times \frac{c}{\lambda}} \qquad (1)$$

corresponds to wavelength of 300-1000 nm. In the formula h is the Planck's constant, f is the frequency, c is the velocity of light and λ is the wavelength. Excitation from the high energy level can occur to several excited state sublevels, but electrons quickly relax to the lowest possible excited energy level in the order of a few picoseconds through non-radiative conversion of the energy via collisions of the excited fluorophore with solvent molecules.

Usually, emission spectra are independent of the excitation wavelength because of this rapid relaxation process. External conversion, which is an energy transfer to the solvent or a solute, depletes the excited state by molecular collision. This kind of quenching depends on contact between analyte and quencher and therefore is a function of temperature, solution viscosity and quencher concentration. Intersystem crossing is another energy dissipation pathway. The excited electron has to change its spin multiplicity from singlet to triplet state and since this process is essentially quantum-mechanically forbidden, it is very unlikely and thus occurs in a time range of ms to minutes. The most prominent process, fluorescence is the returning of the electron to the lower energy level it originated from that is accompanied by an emission of light. Since internal conversion causes a significant energy loss, the wavelength of the emitted photons is reduced compared to the excitation light, resulting in red-shift or Stokes shift of the emission.

1.4.1 Foerster resonance energy transfer

Among the huge variety of applied fluorescence-based methodologies, Foerster resonance energy transfer (FRET) assays remained unique for decades as the only techniques that allow investigation of processes with a nanometer resolution. FRET is a process in which the energy of the excited state of a fluorophores (donor) is non-radiatively transferred to another fluorophore (acceptor) via a dipole-dipole coupling mechanism. The rate constant of FRET depends on the distance and relative orientation of the participating fluorophores, the overlap between the donor emission and acceptor excitation spectra, the quantum yield and the fluorescence lifetime of the donor[151]. Since FRET is proportional to the sixth power of the distance between the two contributing fluorophores, FRET typically spans distances of 2 to 10 nm and therefore is often used as a reporter of direct molecular interactions or a specific clustering. The following formula describes the rate of energy transfer

$$\boldsymbol{k_T(r) = \frac{1}{\tau_D}\left(\frac{R_0}{r}\right)^6} \qquad (2)$$

Where τ_D is the decay time of the donor in absence of the acceptor, R_0 is the specific Forester distance and r is the donor-acceptor distance[150].

Hitherto, FRET was already often used to study subresolution protein-protein interactions[98,124,151] but concomitant with recent improvements in the detector technology an

experimental precision could be achieved that enables investigations even in the Ångström range with resolutions advancing in the atomistic regime[152]. Those approaches can help to complement static high resolution methods like nuclear magnetic resonance (NMR) and electron microscopy (EM) with dynamic data and for the first time allow to follow molecular processes instead of just observing static conformations[152,153].

Several experimental approaches are available to measure FRET based on different properties of the energy transfer. As described before, for FRET to occur the donor fluorophore has to be in the excited state. Instead of relaxing upon emission of fluorescence, excited states undergoing FRET transfer the excitation energy radiationless to another fluorophore. This causes a decrease of the number of emitting donor fluorophores and thus a reduced fluorescence intensity. In parallel, acceptor emission emerges without a specific excitation. Both values, emission intensity of the donor and emission intensity of the acceptor can be used to estimate steady-state FRET. Another property of fluorophores that can be used to study energy transfer is the lifetime of the excited state. The likelihood of an energy transfer is the higher the longer an electron is in the excited state and as a result of that, long-living excited states undergo energy migration with a higher probability. As a consequence, the overall lifetime of the excited state is significantly reduced.

1.4.2 Fluorescence lifetime imaging microscopy and FLIM-FRET

Several techniques can be applied to assess fluorescence lifetime data using a microscopic setup. Fluorescence lifetime imaging microscopy (FLIM) is a method that maps the spatial distribution of fluorescence lifetimes within microscopic images. In general, the lifetime of an excited state is the average time individual molecules spend in the excited state prior to relaxation to the ground state[150]. Since fluorescence emission is a random process, molecules will not emit their photons at a distinct timepoint. Therefore, in the ensemble description the emission of a certain fluorophore will decay according to:

$$\boldsymbol{I(t) = I_0 \exp\left(\frac{-t}{\tau}\right)} \qquad (3)$$

In this mathematical description, the fluorescence lifetime τ is the characteristic time needed for the fluorescence intensity I to decrease to 1/e of its initial value I_o[150].

Technically, a distinction is made between lifetime measurements in the frequency and in the time domain. In time domain fluorometry, the sample is excited with a pulse of light and the emission photons are detected with high temporal resolution. The decay time is then calculated from the slope of a histogram of the individual photon arrival times. Alternatively, in frequency domain measurements the excitation intensity is modulated, forcing the emission to respond at the same modulation frequency. The lifetime of the fluorophore causes a shift of the emission in time and this phase shift can be used to calculate the decay time. Different microscopic setups are available such as the time-correlated single photon counting (TCSPC) with confocal microscopes or fast gated intensifier CCD cameras in wide field microscopy. TCSPC has a very good signal-to-noise ratio and a high temporal resolution in terms of single photon events but suffer of long acquisition times and thus a low temporal resolution in terms of the imaging process. For fast processes, wide-field detection is preferable[150].

FLIM-FRET experiments are based on the fluorescence lifetime of the FRET donor. Since FRET offers an additional possibility for the FRET donor to relax to the ground state, upon energy transfer the probability of relaxation is significantly increased. As a result of that, the fluorescence lifetime of a FRET donor decreases in presence of a suitable FRET acceptor. Taking this phenomenon into account, the FRET efficiency can be calculated according to:

$$\boldsymbol{E_{FRET} = 1 - \left(\frac{\tau_{DA}}{\tau_D}\right)} \qquad (4)$$

Where τ_{DA} and τ_D are the fluorescence lifetimes of the donor in presence and absence of the acceptor, respectively and E_{FRET} is the FRET efficiency[150].

1.4.2.1 TCSPC

For time correlated single photon counting (TCSPC) measurements, the sample is excited with pulsed laser light. It is crucial that laser intensity and pulse frequency are precisely adjusted in a way that at maximum one photon is detected per repetition cycle. This setting allows assigning every emission photon to its respective excitation pulse. The time delay between every individual excitation pulse and the arrival of the emission photon is then determined and ‘stored’ in a histogram (Figure 1-25). Upon detection of sufficient single events the histogram is representative of the lifetime decay and can be analyzed to obtain the average lifetime of the fluorophore’s excited state[150].

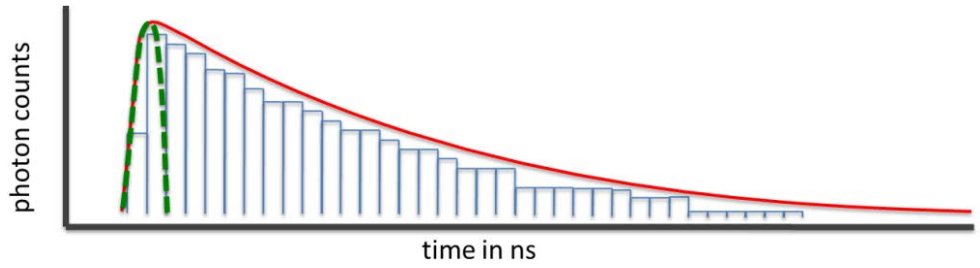

Figure 1-25: TCSPC histogram. The time delay between the excitation pulse (dashed green line) and the arrival of the emission photon of many individual fluorescence events is stored in a histogram (blue columns). Fluorescent lifetimes are calculated upon fitting an exponential decay curve (red) to the obtained time distribution. Adapted from [150]

TCSPC experiments require sophisticated instrumentation. Only detectors such as photomultiplier tubes (PMTs), multi-channel plates (MCPs) or single photon avalanche photodiodes (SPAD) are sensitive enough to detect single photons. Moreover, precise picosecond or femtosecond laser light sources are required to provide high repetition frequencies and sharp laser pulses[150].

1.4.3 Fluorescence polarization microscopy

Another important property of fluorescence is the anisotropy or polarization; both terms describe the same physical phenomenon, of the emission. The cause of anisotropy is that the transition moments, i.e. their dipole moments for absorption and emission of fluorophores possess distinct orientations. As a result of that, upon excitation with polarized light the emission from many samples is also polarized. Anisotropy measurements can be used to detect the average angular displacement of the fluorophore that occurs between absorption and subsequent emission of a photon. This depolarization can be caused by different processes (Figure 1-26). Rotational diffusion for instance can change the direction of the transition moments while the fluorophore is in the excited state and hence influences the polarization of the emission. It depends on the viscosity of the solvent and the size and shape of the rotating molecule. Since the timescale of rotational diffusion of proteins is in a similar range as the fluorescence lifetime of many fluorophores, anisotropy measurements are suited to study protein motility and were often used in biological research[150]. However, another important source of depolarization is homo-FRET. Since homo-FRET transfers the excitation energy to another fluorophore with a different orientation, the specific directional selection of the polarized laser pulse is partly lost. This energy transfer, in contrast to hetero-FRET, requires

only one single fluorophore species and it is often used to measure molecular self-assembly processes in cells. An important prerequisite of homo-FRET is a fluorophore with a small Stokes-shift to permit an appreciable overlap between the emission and absorption spectra[154]. Since donor and acceptor are spectroscopically indistinguishable, intensity ratios cannot be used and lifetime measurements are impossible or in the best case difficult[155]. Thus, anisotropy measureme nts are the only established method of detecting homo-FRET.

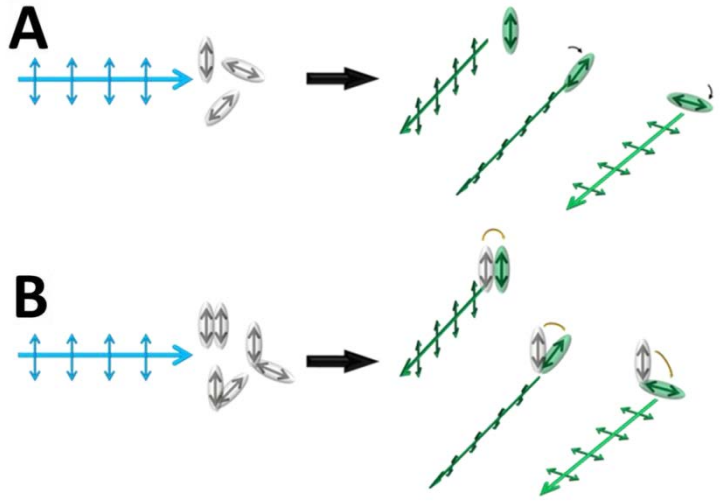

Figure 1-26: Origins of fluorescence depolarization. For fluorescence anisotropy experiments, the excitation light (blue) has to be linearly polarized. The fluorophores (grey) absorb the energy and can undergo two different processes causing an angular displacement of their dipole moment (small arrows) while being in the excited state. (A) Fast rotational diffusion in or below the time scale of the excited state lifetime randomize the orientation of the fluorescence light. (B) Energy migration from the excited fluorophore to another adjacent, identical fluorophore (homo-FRET) with a different orientation causes immediate depolarization.

1.4.3.1 Fluorescence anisotropy imaging microscopy (FAIM)

A simple implementation of a microscopic setup to assess fluorescence anisotropy can be achieved adding several polarizers in the light path of the microscope. Since the laser light used for confocal imaging is usually linearly polarized, here only the detection has to be adapted for anisotropy experiments. Briefly, the setup is realized as follows. The excitation laser beam is guided through objective on the sample. Then, after transit through objective, pinhole and sample, the fluorescence light is split into parallel and perpendicular component. Subsequently, both signals are detected independently. The anisotropy is then determined by the equation:

$$r(t) = \frac{I_{\parallel}(t) - G \times I_{\perp}(t)}{I_{\parallel}(t) - 2 \times G \times I_{\perp}(t)} \qquad (5)$$

Since, monochromators, dichroic mirrors and even detectors can have different sensitivities for vertically and horizontally polarized light the measured intensities do not directly reflect polarization parameters of the sample but are rather influenced by those factors as well. To take this into account, the G-factor has to be estimated as an instrumentation specific correction factor:

$$G = \frac{I_{\parallel}}{I_{\perp}} \qquad (6)$$

with $I_{\parallel}$ being the intensity of the parallel and $I_{\perp}$ the intensity of the perpendicular channel.

1.4.4 Total internal reflection fluorescence microscopy

In fluorescence microscopy, the physical limits of optics define the maximal achievable resolution. Recently, new super resolution methods like STED, STORM, PALM or SIM pushed light microscopy below the limits of Abbe's criterion (recently reviewed in [156,157]). However, even some of those superresolution microscopes suffer of a very low optical resolution in the z-direction. Total internal reflection fluorescence microscopy (TIRFM) makes use of an evanescent illumination to exclusively excite fluorophores in a restricted region adjacent to the glass-water interface[158] thus achieving a high z-resolution. To this aim, in TIRF microscopy the angle of the incident laser beam is tilted with respect to the normal of the glass surface of a coverslip or a glass-bottom dish for instance. When the light strikes the surface at a sufficient high angle, it is entirely reflected. Nevertheless, the reflected light generates a highly restricted electromagnetic field that decays exponentially with distance. As a result of that, the field extents at the utmost around 100 nm or less into the specimen in the z-direction[158]. This approach significantly improves signal-to-noise and allows single-molecule detection in areas close to the glass surface of the object slide[158]. Thus, TIRF microscopy is often used to observe and study plasma membrane fluorophores and processes at the cell surface although the penetration depth of this technique does not allow distinguishing between fluorophores at or in the plasma membrane and molecules that are only adjacent.

1.4.5 Fluorescence activated cell sorting (FACS)

Flow cytometry is a technology that simultaneously measures multiple physical parameters of single particles in a fluid stream as it passes through a beam of light[159]. Obtainable data include the relative size, granularity or rather internal complexity of the observed particles and the fluorescence intensity of as many fluorophore species one is able to distinguish in parallel. Any object from 0.2 to 150 μm in size is suitable for analysis and all available data will be collected for every individual particle in the fluid stream. Fluorescence activated cells sorting is a specialized type of flow cytometry. It provides a method for sorting the analyzed particles based on their specific light scattering and fluorescence properties. For fluorescence activated cell sorting (FACS), the stream of particles is dissected into individual droplets by a vibrating mechanism[159]. The system and the particle solution are adjusted to have a high probability of just on cell per droplet so that upon selective collecting of single droplets, specific cells can be sorted. To this aim, every individual droplet has to be provided with an electric charge and an electrostatic deflection system diverts single particles into containers based upon their charge[159].

2. Aim of the study

Assembly and the subsequent budding of enveloped viruses are complex and highly regulated processes. At the site of assembly, all necessary components have to be enriched and arranged with an outstanding local and temporal precision. Most likely, this accurate orchestration is achieved not only by specific molecular interactions between the participating molecules but also by a systematic use of the subcompartmentation that is provided by cellular lipid rafts. Both structural HIV proteins, gp41 and Gag have been found in detergent resistant membrane fractions[100,115,160–162] and the viral envelope was found to resemble DRMs in composition and physical properties[163,164]. However, since DRMs were lately considered as a poor model of plasma membrane lipid rafts and the experimental procedure is supposed to harbor a high risk of inducing artifacts[136], other methods have to be preferentially applied to study the lateral sorting of membrane proteins. Correspondingly, Gag and Env were shown to cluster with cellular raft components[123,161,165] in microscopy experiments and cholesterol depletion was demonstrated to impair HIV-1 particle production[115,132,161,166,167]. Nevertheless, live cell experiments are lacking in that context and studies regarding the lateral sorting mechanism and the protein domains responsible for the association of the HIV-1 Env glycoprotein complex with lipid rafts are controversial or even contradictory. In general, observing the lateral organization of proteins in the plasma membrane is hindered by the fact, that lipid domains in biological membranes are very small, in the submicroscopic region, and highly dynamic[168,169].

In the present study, a FRET-based assay was applied to elucidate the raft partitioning of the HIV-1 glycoprotein gp41 in plasma membranes of mammalian cells[98,144]. Fluorescence lifetime imaging microscopy was used to detect the energy transfer between a glycoslylphosphatidylinositol (GPI) anchored cyan fluorescent protein (CFP) and the protein under study tagged with a yellow fluorescent protein. Since GPI anchors are generally believed to drive proteins into plasma membrane microdomains, GPI-CFP was employed as a putative raft marker protein. Assuming average microdomain diameters below 100 nm, two labeled proteins associated with lipid rafts should encounter each other with a high probability resulting in an efficient FRET (Figure 2-1).

Different variants of the fluorescently labeled gp41 were generated by truncation and site-directed mutagenesis to pinpoint the molecular background of the potential raft partitioning of

the protein. In particular this works aims on the role of the cholesterol recognition amino acid consensus of gp41. This motif has been reported to specifically bind and sequester[74,76] cholesterol, which is a crucial component of plasma membrane lipid rafts and the virus envelope. Therefore, the sequence is an obvious and self-evident candidate for the gp41 raft targeting. Surprisingly, altho ugh it is highly conserved in different virus isolates and subtypes, the physiological function has not yet been elucidated.

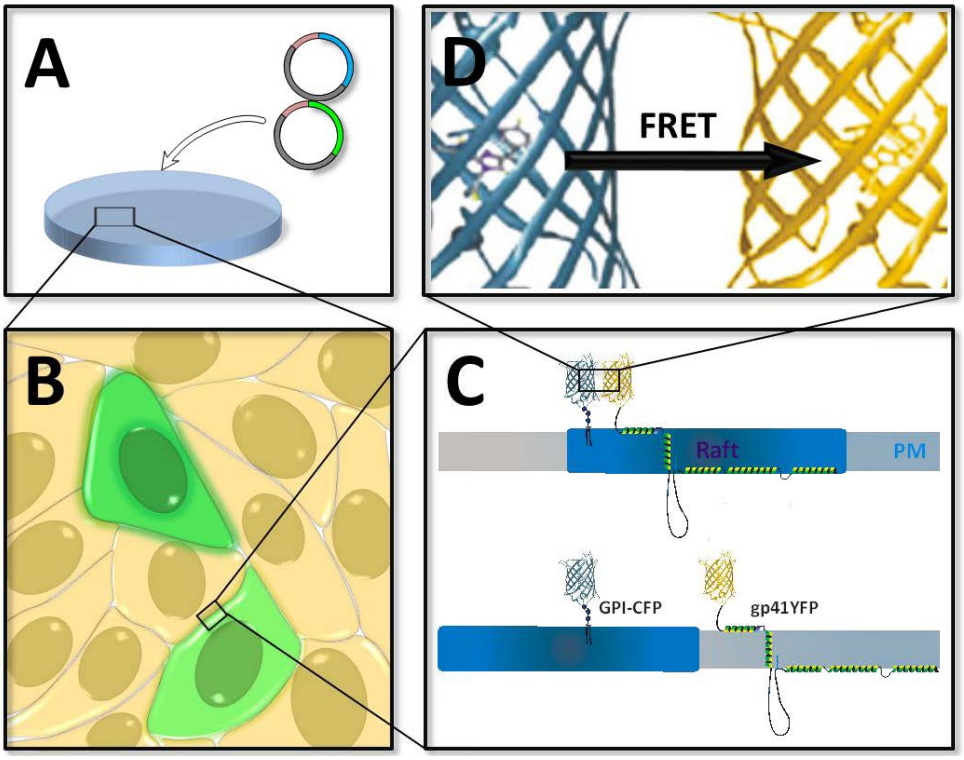

Figure 2-1: Studying lipid raft partitioning using FRET. For the assay conducted in the framework of this thesis, (A) cells were transfected with GPI-CFP as a raft marker protein and the YFP-labeled protein under study. Then, (B) the plasma membranes of expressing cells were investigated with a FLIM setup to detect FRET between raft partitioning fluorescently-labeled fusion proteins. (C and D) This assay is based on the assumption that energy between the raft residing GPI-CFP and the protein under study only occurs if both proteins are localized in lipid rafts.

Moreover, as a complementary approach, oligomerization was studied by fluorescence anisotropy imaging microscopy as described below. This assay allows to detect and localize assembled oligomers in living cells due to the depolarization of fluorescence that is a consequence of occurring homo-FRET between the fluorescently labeled proteins under study (Figure 2-2).

The question arises whether the introduced mutations also have consequences on biological functions of the protein. In recent years it has been often reported that gp41 has a perturbing influence on membranes it resides in. To study the relevance of certain gp41 domains and motifs for the lytic properties of the protein, flow cytometer experiments were performed. To this aim, cells transfected with gp41 fusion proteins harboring different truncation or mutation were treated with propidium iodide as a reporter of plasma membrane integrity and cell viability.

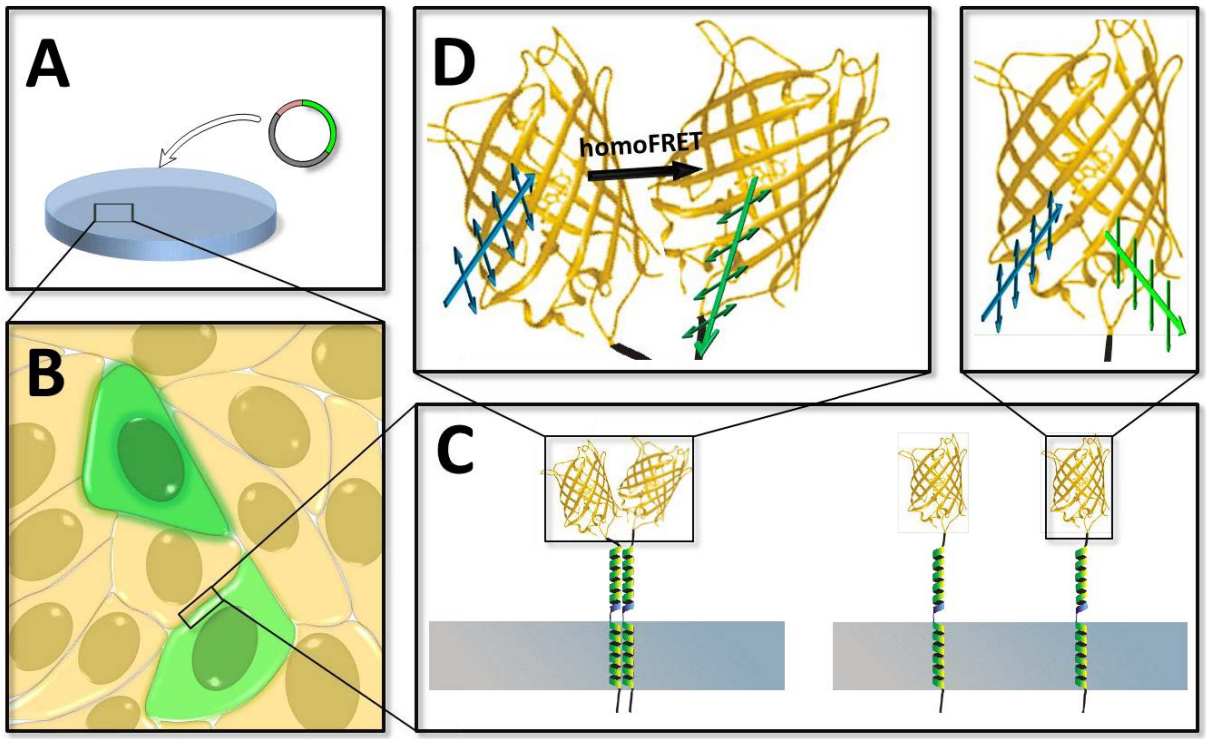

Figure 2-2: Studying protein oligomerization using fluorescence anisotropy. Firstly, (A) cells have to be transfected with the YFP-labeled protein under study. Then, (B) expressing cells were investigated utilizing FAIM. (C and D) Only fluorescently labeled proteins that form oligomeric complexes cause an approaching of the fluorophores to a proximity that is small enough for homo-FRET to occur. This arising energy migration can be then detected by means of a decrease in the fluorescence anisotropy.

3. Material and Methods

3.1 Materials

3.1.1 Chemicals

Chemicals that are not included in the following list were purchased either from Sigma-Aldrich (Taufkirchen, Germany) or Carl Roth (Karlsruhe, Germany) in analytical standard quality. Phospholipids and fluorescent phospholipid analogues were obtained from Avanti Polar Lipids (Alabaster, AL, USA).

Table 1: Chemicals used for molecular biology, biochemical and biophysical assays.

Compound	Manufacturer
3,3'-Diaminobenzidine tetrahydrochloride (DAB)	Sigma-Aldrich, Taufkirchen, Germany
3-Amino-1,2,4-triazole (Aminotriazole)	Sigma-Aldrich, Taufkirchen, Germany
Acetic acid, 100 %	Carl Roth, Karlsruhe, Germany
Acrylamide/bisacrylamide (37.5:1), 30 %,	Carl Roth, Karlsruhe, Germany
"Rotiphorese® Gel 30"	Carl Roth, Karlsruhe, Germany
Ammonium persulfate (APS)	Sigma-Aldrich, Taufkirchen, Germany
Bacto™agar	BD Biosciences, Heidelberg, Germany
Bacto™tryptone	BD Biosciences, Heidelberg, Germany
Bacto™ yeast extract	BD Biosciences, Heidelberg, Germany
Chloroform Uvasol® for spectroscopy	Merck, Darmstadt, Germany
Cholesterol	Sigma-Aldrich, Taufkirchen, Germany
Coomassie Brilliant Blue R-250	Carl Roth, Karlsruhe, Germany
4',6-diamidino-2-phenylindole (DAPI)	Invitrogen, Karlsruhe, Germany
Dithiothreitol (DTT)	Sigma-Aldrich, Taufkirchen, Germany
ER-Tracker™	Invitrogen, Karlsruhe, Germany

Ethanol for spectroscopy, >99.5 % Ph. Eur.	Carl Roth, Karlsruhe, Germany
Ethylenediaminetetraacetic acid (EDTA)	SERVA, Heidelberg, Germany
Formaldehyde 37 % (w/v)	Fluka/Sigma-Aldrich, Taufkirchen, Germany
Formalin solution, 10 %, neutral buffered	Sigma-Aldrich, Taufkirchen, Germany
Glycine	Sigma-Aldrich, Taufkirchen, Germany
Methanol Uvasol® for spectroscopy	Merck, Darmstadt, Germany
N,N,N',N'-Tetramethyl-ethane-1,2-diamine (TEMED)	Sigma-Aldrich, Taufkirchen, Germany
N-Ethylmaleimid (NEM)	Sigma-Aldrich, Taufkirchen, Germany
Octyl β-D-glucopyranoside	Sigma-Aldrich, Taufkirchen, Germany
Potassium cyanide (KCN)	Sigma-Aldrich, Taufkirchen, Germany
Sodium dodecyl sulfate (SDS)	Carl Roth, Karlsruhe, Germany
Sucrose	AppliChem, Darmstadt, Germany

3.1.2 Equipment and instruments

Basic laboratory equipment is not included in this list.

Table 2: Equipment and instruments used in this work. The list comprises centrifuges, microscopes and thermocyclers.

Compound	Manufacturer
Biophotometer *plus*	Eppendorf, Hamburg, Germany
Centrifuge *Avanti J-20XP (Rotor JLA10.500)*	Beckman Coulter, Krefeld, Germany
Centrifuge *Heraeus Biofuge Stratos*	Thermo Scientific, Langenselbold, Germany
Confocal laser scanning microscope *FluoView™ FV1000*	Olympus, Hamburg, Germany
Electrophoresis equipment *(agarose gel electrophoresis)*	Bio-Rad, München, Germany

Electrophoresis equipment *(SDS-PAGE) Mini-PROTEAN 3 electrophoresis system with accessories*	Bio-Rad, München, Germany
Gel documentation system *DESAGA Digital CabUVIS with CCD camera HV-C20A (Hitachi)*	Sarstedt, Nümbrecht, Germany
Incubators *Heraeus*	Thermo Scientific, Langenselbold, Germany
Infrared imaging system *Odyssey®*	LI-COR Bioscience, Bad Homburg, Germany
Inverted epifluorescence microscope *IX-81*	Olympus, Hamburg, Germany
Laminar flow hood *Heraeus*	Thermo Scientific, Langenselbold, Germany
Nucleofection *system Lonza 4D*	Lonza, Basel, Switzerland
Phase contrast inverted microscope *(cell culture) Telaval 31*	Zeiss, Göttingen, Germany
Phosphorimager*: Fluorescent image analyzer FLA-3000*	Fujifilm, Düsseldorf, Germany
Power supply for electrophoresis and Western blotting*: PowerPac 1000 and Amersham EPS 601*	Bio-Rad, München, Germany GE Healthcare, Freiburg, Germany
Rotary evaporator*: Rotavapor R-200*	Büchi Labortechnik, Essen, Germany
Shaker*: Mini-rocker MR-1 and rocking shaker*	Bioscan, Paris, France GFL, Burgwedel, Germany
Spectrofluorometer *AMINCO-Bowman™ Series 2*	Thermo Electron Corporation, Germany
Thermal Cycler *MyCycler™*	Bio-Rad, München, Germany
Thermomixer *comfort*	Eppendorf, Hamburg, Germany

Trans-Blot® *SD semi-dry electrophoretic transfer cell*	Bio-Rad, München, Germany
Ultra-pure water purification system *Milli-Q*	Millipore, Schwalbach, Germany
Ultracentrifuge *Optima L-100K* ***Rotors****: 45Ti, 70.1Ti, SW40Ti, SW60Ti*	Beckmann Coulter, Krefeld, Germany
Ultracentrifuge TL-100*, tabletop, rotor TLA 100.3*	Beckman Coulter, Krefeld, Germany
Ultracentrifuge *XL-70 and Optima L-100K*	Beckman Coulter, Krefeld, Germany
UV transilluminator	Vilber Lourmat, Eberhardzell, Germany
UV-Vis spectrophotometer *UV1*	Thermo Electron Corporation, Germany

3.1.3 Consumables

Basic laboratory consumables are not included in this list.

Table 3: Consumables used in this work. List includes cell culture vessels and other laboratory plasticware.

Device	Manufacturer
Microfuge Tube *Beckman, 1.5 ml, polyallomer*	Beckman Coulter, Krefeld, Germany
blot paper*, extra thick*	Bio-Rad, München, Germany
Cell culture flasks *T25, T75, T175*	Nunc, Langenselbold, Germany
Cell culture plate*s 6-well and 12-well*	Nunc, Langenselbold, Germany
Cuvettes*, acrylic, and semi-micro cuvettes, polystyrene*	Sarstedt, Nümbrecht, Germany
Glass bottom culture dishes *for microscopy, 35 mm, uncoated*	MatTek, Ashland, U.S.A, # P35G-1,5-14C

Glass cover slips *for microscopy* *24×60 mm* *24x32 mm*	Carl Roth, Karlsruhe, Germany
Nitrocellulose membrane*: Amersham Hybond ECL*	GE Healthcare, Freiburg, Germany

3.1.4 Cell culture media and reagents

Table 4: Reagents used in this work. Including cell culture media, antibiotics and transfection reagents.

Reagent	Manufacturer
BSA *(Bovine serum albumin, 35 % in DPBS)*	Sigma-Aldrich, Taufkirchen, Germany
DMSO *(Dimethylsulfoxid) for cell culture*	Sigma-Aldrich, Taufkirchen, Germany
DMEM *(Dulbeccos Medium Essential Medium) without phenol red, high glucose*	PAA Laboratories GmbH, Pasching, Austria
PBS (+/+) *(Phosphate Buffered Saline with Ca^{2+} and Mg^{2+})*	PAA Laboratories GmbH, Pasching, Austria
PBS (-/-) *(Phosphate Buffered Saline without Ca^{2+} and Mg^{2+})*	PAA Laboratories GmbH, Pasching, Austria
FBS *(Fetal bovine serum)*	PAA Laboratories GmbH, Pasching, Austria
L-Glutamine *(200 mM)*	PAA Laboratories GmbH, Pasching, Austria
Lipofectamine^{TM} *2000 Transfection Reagent*	Invitrogen, Karlsruhe, Germany
Geneticin solution *(50 mg/ml), sterile filtered*	Sigma-Aldrich, Taufkirchen, Germany
Penicillin/Streptomycin *(100×: 10,000 U/ml, 10 mg/ml)*	PAA Laboratories GmbH, Pasching, Austria
Trypsin/EDTA	PAA Laboratories GmbH, Pasching, Austria

TurboFect^{TM} *Transfection Reagent*	Fermentas, St. Leon-Rot, Germany

3.1.5 Enzymes, molecular biology reagents

Table 5: Enzymes and substances for molecular biology. Including Cloning enzymes and reagetns and buffers for agarose gel electrophoresis.

Substance	Manufacturer
Agarose	Biozym Scientific, Hessisch Oldendorf, Germany
DNA Loading Dye *(6×)*	Fermentas, St. Leon-Rot, Germany
dNTP-Mix*, 10 mM each*	Fermentas, St. Leon-Rot, Germany
DNA Ladder*, GeneRuler*^{TM} *1kb*	Fermentas, St. Leon-Rot, Germany
T4 DNA Ligase	New England Biolabs, Frankfurt/Main, Germany
CIP *(Calf Intestinal Alkaline Phosphatase)*	New England Biolabs, Frankfurt/Main, Germany
Polymerases	
Phusion™ High-Fidelity DNA Polymerase	Finnzymes, Espoo, Finland
Taq DNA Polymerase	peqlab, Erlangen, Germany
Restriction enzymes	New England Biolabs, Frankfurt/Main, Germany
AgeI, BamHI, BsaI HF, BsrGI, SacII, XhoI	
TBE buffer*, Rotiphorese*® *10×, running buffer for agarose gel electrophoresis*	Carl Roth, Karlsruhe Germany
DNA Gel Stain *SYBR*® *Safe (1000×)*	Invitrogen, Karlsruhe, Germany

3.1.6 Kits for DNA preparation

Table 6: Kits used for molecular biology.

Kit	Manufacturer
QIAquick ***Gel Extraction Kit***	Qiagen, Hilden, Germany
QIAprep Spin ***Miniprep Kit***	Qiagen, Hilden, Germany
QIAGEN Plasmid ***Maxi Kit***	Qiagen, Hilden, Germany

3.1.7 Antibodies

3.1.7.1 Primary antibodies

Table 7: Primary antibodies. Used for immunofluorescence and Western Blot.

Antibody	Provider
anti-GFP antibody*, monoclonal (mouse IgG) #11[814460 001]*	Roche, Mannheim, Germany

3.1.7.2 Secondary antibodies

Table 8: Secondary antibodies. Used for immunofluorescence and Western Blot.

Antibody	Provider
AlexaFluor 568 anti-mouse *(goat IgG), #11004*	Invitrogen, Karlsruhe, Germany
IRDye-680 anti-mouse *(goat IgG), #926-32220*	LI-COR Bioscience, Bad Homburg, Germany,

3.1.7.3 Labeled antibodies

Table 9: Labeled antibodies. Used for immunofluorescence.

Antibody	Provider
***AlexaFluor555 anti–GFP**, #A31851*	Invitrogen, Carlsbad, CA

3.1.8 Plasmids

Table 10: Plasmids. Used for cloning.

Antibody	Provider
pECFP-N1	Invitrogen, Karlsruhe, Germany
pEYFP-N1	Invitrogen, Karlsruhe, Germany
pCAGGS JR-FL gp160WT	Scolari, Humboldt University, Berlin, Germany
pfastFT-N1	Verkusha[170], New York, USA

3.1.9 Buffers and solutions

Table 11: Cell culture media and solutions. Used for biochemistry, cell staining and molecular biology.

Cell culture media	
Complete medium	DMEM with 10 % (v/v) FBS, 2 mM L-Glutamine and Penicillin/Streptomycin (100 U/ml, 100 µg/ml)
Freezing medium	70 % (v/v) DMEM, 20 % (v/v) FBS, 10 % (v/v) DMSO
Coomassie staining solutions	
Coomassie staining solution	45 % (v/v) ethanol, 10 % (v/v) acetic acid, 2.5 g/l Coomassie Brilliant Blue R-250

Coomassie destaining solution	40 % (v/v) ethanol, 7.5 % (v/v) acetic acid
Immunofluorescence solutions	
Fixative	4 % formalin in DPBS with Ca^{2+} and Mg^{2+} (made from a 10 % formalin stock solution)
Blocking buffer	3 % (w/v) BSA in DPBS (for cell culture)
Permeabilization buffer	0.5 % (v/v) Triton X-100 in DPBS
PBST	3.2 mM Na_2HPO_4, 0.5 mM KH_2PO_4, 1.3 mM KCl, 135 mM NaCl, 0.05 % Tween 20, pH 7.4
Fluorescent cell labeling dyes	
DiO (lipiphilic carbocyanine)	Invitrogen, Karlsruhe, Germany
R18 (Octacedyl rhodamine B)	Invitrogen, Karlsruhe, Germany
LysoTracker Red	Invitrogen, Karlsruhe, Germany
ER-Tracker Red	Invitrogen, Karlsruhe, Germany
Propidium iodide	Invitrogen, Karlsruhe, Germany
DAPI (4',6-diamidino-2-phenylindole)	Invitrogen, Karlsruhe, Germany
C6-NBD-PC (1-palmitoyl-2-{6-[(7-nitro-2-1,3-benzoxadiazol-4-yl)amino]hexanoyl}-sn-glycero-3-phosphocholine)	Avanti Polar Lipids, Alabaster, USA
Isolation of Virus Like Particles	
TNE buffer	10 mM Tris-HCl, 100 mM NaCl, 1 mM EDTA, pH 7.4
TNE sucrose gradient	linear gradient formed from 20 % and 60 % (w/v) sucrose in TNE buffer
Isolation of GPMVs	
GPMV buffer	2 mM $CaCl_2$, 10 mM Hepes, 0.15 M NaCl
Protein palmitoylation assay	
lysis buffer	25 mM HEPES, 25 mM NaCl, 1 mM EDTA, Proteinase Inhibitor Cocktail, pH7.5)

blocking buffer	100mM HEPES, 1mM EDTA, 2.5 % SDS, 0.1 % MMTS, pH7.5
binding buffer	100mM HEPES, 1mM EDTA, 1 % SDS, pH 7.5
Media for propagation of *E.coli*	
LB medium	10 g/l Bacto™ tryptone, 5 g/l Bacto™ yeast extract, 5 g/l NaCl with 50 µg/ml kanamycin or 100 µg/ml ampicillin
LB agar	LB medium with 15 g/l agar, 50 µg/ml kanamycin or 100 µg/ml ampicillin
Antibiotic stocks	50 mg/ml ampicillin; 100 mg/ml kanamycin (in ddH_2O, sterile filtered)
PBS	137 mM NaCl, 2.7 mM KCl, 8.1 mM Na_2HPO_4, 1.5 mM KH_2PO_4, pH 7.2
SDS-PAGE buffers	
Stacking gel (5 %)	5 % (w/v) acrylamide/bisacrylamide (37.5:1; 30 % stock solution "Rotiphorese® Gel 30", Carl Roth, Karlsruhe, Germany), 125 mM Tris-HCl pH 6.8, 0.1 % (w/v) SDS, 0.1 % (w/v) APS, 0.1 % (v/v) TEMED
Resolving gel (10% or 12%)	10 % or 12 % (w/v) acrylamide/bisacrylamide, 375 mM Tris-HCl pH 8.8, 0.1 % (w/v) SDS, 0.1 % (w/v) APS, 0.04 % (v/v) TEMED
SDS sample buffer, non-reducing (4×)	5 % (w/v) SDS, 0.5 g/l bromophenol blue, 25 % (v/v) glycerol, 500 mM Tris-HCl pH 6.8
SDS sample buffer, reducing (4×)	5 % (w/v) SDS, 0.5 g/l bromophenol blue, 25 % (v/v) β-mercaptoethanol, 25 % (v/v) glycerol, 500 mM Tris-HCl pH 6.8

Protein standards	Precision Plus Protein All Blue Standards [Bio-Rad, München, Germany]; PageRuler™ Prestained Protein Ladder [Fermentas, St. Leon-Rot, Germany]
Running buffer	3 g/l Tris-HCl, 1 g/l SDS, 14.4 g/l glycine; pH 8.3
Western blotting solutions	
Transfer buffer	40 % (v/v) running buffer, 20 % (v/v) methanol, 0.06 % (w/v) SDS
Blocking buffer (for IR-dye coupled secondary antibodies and fluorescence detection)	Odyssey® Blocking Buffer 1:2 in PBS
Washing buffer	PBS with 0.1 % (v/v) Tween®-20 (PBST)

3.1.10 Biological material

3.1.10.1 Eukaryotic cells lines

Table 12: Cell lines used in this work. The cell type is indicated in brackets.

	Cell line	Cat. no.
CHO-K1	*Chinese hamster ovary cells (epithelial-like)*	ATCC CCL-61
HeLa	*Human cervical cells (epithelial)*	ATCC CCL-2
MDCK II	*Madin-Darby canine kidney cells (epithelial)*	ATCC CCL-34
HEK293T	*Human embryonic kidney cells (epithelial)*	ATCC CCL-1573
RBL	*Rat basophil leukemia (epithelial)*	ATCC CRL-1378

3.1.10.2 Prokaryotic cells

Table 13: Bacteria used in this work. Cells were used for transformation.

Cell line	Description
E.coli DH5α	genotype: F^- *endA1 recA1 hsdR17*(rk^- mk^+) *supE44* λ^- *thi-1 gyrA*(Na1) *relA1* Φ80 *lacZ*ΔM15Δ *(lacZY* A-*argF),* chemically competent, provided by Christine Klaus (Humboldt-University)

3.1.11 Software

Table 14: Software applied in this work. Provider or source and the specific application of the programs or plugins are stated in the list.

Software	Provider	Application
A plasmid Editor (ApE)	M. Wayne Davis, Utah, USA	*cloning simulation; DNA sequence viewing, alignment, editing and ORF analysis*
FV 10-ASW FluoView1000	Olympus, Hamburg, Germany	*device control, image viewing and data analysis software for confocal microscope FV1000*
ImageJ *Version 1.46e*	Wayne Rasband, National Institute of Health, Bethesda, MD, USA (http://imagej.nih.gov/ij/)	*signal quantification, particle tracking, image processing*
MtrackJ *ImageJ plugin*	Erik Meijering, Biomedical Imaging Group, Erasmus MC, Rotterdam, Netherlands	*particle tracking*
Spot Tracker *ImageJ plugin*	Daniel Sage, Biomedical Imaging Group, Ecole Polytechnique Féd. de Lausanne , Switzerland	*particle recognition*

***Symphotime**, Version 3.2.4*	PicoQuant, Berlin, Germany	*analysis of FLIM and polarization microscopy*
MetaMorph	Olympus, Hamburg, Germany	*device control, image viewing and data analysis software for IX-81 epifluorescence microscope*

3.2 Methods

3.2.1 Molecular biology

To reveal the localization or function of a certain protein it is often necessary to specifically change its amino acid sequence. For this purpose the sequence of the encoding DNA has to be controlled and adapted. The easiest way to study a protein in a cellular context is to clone the respective DNA sequence into an expression vector and deliver it into target cells by a suited method. Expression is than purchased by the cellular machinery and the designed protein can then be investigated in the physiological environment of the selected cellular system.

For mammalian expression, purified DNA under the control of a suited promotor is required. Thus, a prerequisite of an experimental examination is often a cloning of the DNA sequence under study. Subsequently, the obtained plasmid is transformed and amplified in bacteria followed by purification and transfer into the mammalian cells. A typical strategy consists of the following steps:

1. Generation of the gene of interest with flanking restriction sites using PCR
2. Enzymatic digestion to target the gene insertion to a specific vector position
3. Enzymatic ligation of vector and insert
4. Transformation into competent bacteria and antibiotic selection
5. Amplification of positive bacterial clones
6. Plasmid DNA purification
7. Transfection via lipofection

3.2.1.1 Molecular biology methods

3.2.1.1.1 Polymerase chain reaction (PCR)

Since the first description of the polymerase chain reaction in 1985[171] this method was improved and extended so that it nowadays is an indispensable tool of molecular biology. The fundamental principle of a PCR is simple. Basically it combines all sufficient and necessary components of native DNA replication under the controlled conditions of an *in vitro*-assay.

PCRs are carried out in a thermocycler machine that allows the fast temperature change which is needed to control the progression of that cyclic reaction. Firstly, the template, containing the DNA sequence to be amplified is denaturated at 94°C. Subsequently, upon lowering of the

temperature to 45-70°C, the primers, available in high excess, hybridize with the template open strands. Finally, the temperature is raised to the optimum of the thermophile DNA polymerase to allow extension of the primer and thus formation of template complementary DNA strands. In every cycle the number of DNA fragments is doubled and as a result of that, upon many repetitions amplified exponentially. A typical PCR protocol used to amplify DNA of HIV-1 envelope fragments is reported in the table below (Table 15).

Table 15: Standard PCR. PCR scheme used for the amplification of gp41 DNA fragments.

PCR mix		PCR scheme			
50 ng	*DNA template*		**Cycle step**	**T (°C)**	**Time (min)**
0.5 mM	*dNTPs*	Initial denaturation		94	5
1 µM	*Forward primer*		Denaturation	94	1
1 µM	*Reverse primer*	30x	Annealing	50	1
10x	*PCR Buffer*		Extension	72	1
5 U	*Taq-polymerase*	Final extension		72	10
final V=50µl	*ddH_2O*	Cooling		12	∞

3.2.1.1.2 Colony PCR

Colony PCR was performed to verify successful insertion of DNA into a plasmid. For this PCR the same protocol as described above was used with the only exception that the initial denaturation time was extended to 10 min. Instead of template DNA parts of an *E.coli* colony were picked with a pipette tip and resuspended in the reaction mixture. Although colony PCR primers do not have to contain restriction sites and can be chosen freely to amplify any arbitrary fragment of the target gene, in this study usually the original cloning primers were used for the colony PCRs.

3.2.1.1.3 AB-PCR

To introduce small mutations in the range of one or just a few amino acids, a special form of site-directed mutagenesis can be used, the AB-PCR or overlap-extension PCR[172]. Hereby, primers are designed to bind in the region of the desired mutation. DNA amplification is performed in two steps (Figure 3-1).

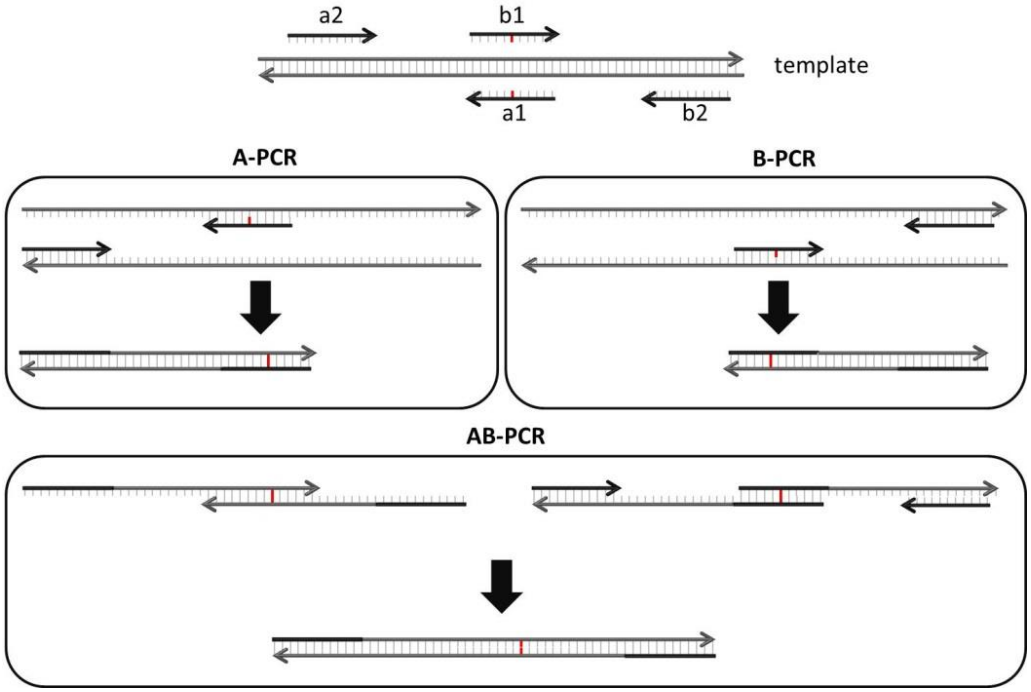

Figure 3-1: AB-PCR principle. This site directed mutagenesis procedure allows the introduction of small mutations in two independent PCR steps. Required are the two conventional flanking primers a2 and b2 (black) with restriction sites for the subsequent cloning of the PCR product, two overlapping primers (black) a1 and b1 that carry the mutation (red) in the middle, and the wild type template (dark grey). In the first step, two PCRs are run in parallel, one using the primer pair a1/a2 and another one using pair b1/b2. Those PCRs yield two overlapping fragments of the final gene, both including the restriction sites on one end and the mutation adjacent to the other end. In a second PCR steps the fragments serve as templates and, in combination with the flanking primers, as second set of primers for the amplification of the complete gene, containing the desired mutation.

First, two fragments of the gene are amplified independently, ranging from either sides of the gene to the mutation site. Here, primers are binding that contain the nucleic base changes surrounded by bases being complementary to the original DNA sequence. The first two PCRs yield two fragments of the native gene with overlapping sequences and the selected mutation. In the second part of the assay, both PCR-products are mixed to serve as templates and primers for the synthesis of the complete, mutated gene. Additional primers binding on both sides of the gene are added to increase the yield of the amplification. A typical PCR protocol used to introduce the CRAC mutation in HIV-1 envelope fragments is reported in the table below (Table 16).

Table 16: AB-PCR. PCR scheme and reagents used for site-directed mutagenesis using AB-PCRs.

PCR mix			PCR scheme			
	A-PCR	**B-PCR**		**Cycle step**	**T (°C)**	**Time (min)**
50 ng	*DNA template*	*DNA template*	Initial denaturation		94	3
0.5 mM	*dNTPs*	*dNTPs*		Denaturation	94	30
1 µM	*Fw-Primer (a2)*	*Fw-Primer (b2)*	30x	Annealing	50	30
1 µM	*Rv-Primer (a1)*	*Rv-Primer (b1)*		Extension	68	1
10x	*PCR Buffer*	*PCR Buffer*	Final Extension		68	10
5 U	*Taq-polymerase*	*Taq-polymerase*	Cooling		4	∞
V=50µl	*ddH_2O*	*ddH_2O*				
	AB-PCR			**Cycle step**	**T (°C)**	**Time (min)**
50 ng	*A-PCR product*		Initial denaturation		94	3
50 ng	*B-PCR product*			Denaturation	94	30
0.5 mM	*dNTPs*		30x	Annealing	50	30
1 µM	*Fw-Primer (a2)*			Extension	68	1
1 µM	*Rv-Primer (b2)*		Final Extension		68	10
10x	*PCR Buffer*		Cooling		4	∞
5 U	*Taq-polymerase*					
V=50µl	*ddH_2O*					

3.2.1.1.4 Agarose gel electrophoresis

In order to verify size and to purify the obtained DNA, PCR products were examined using agarose gels produced with 1 % (w/v) agarose in TBE buffer supplemented with the DNA stain SYBR Safe. Electrophoresis was run at 90-120 V to separate negatively charged DNA fragments according to their size. For further applications, DNA bands were cut from the gel and the DNA was extracted using the QIAquick Gel Extraction Kit according to the manufacturer's protocol. This procedure is necessary to eliminate reagents and enzymes from previous steps. Especially digestion enzymes need to be removed by gel electrophoresis since they might stick to the restriction sites and hamper the following ligation due to sterical prevention of sticky end hybridization and the ligase binding.

3.2.1.1.5 Enzymatic cleavage and dephosphorylation

Both, PCR products and target vector were subjected to enzymatic cleavage. Restriction endonucleases cut the DNA within enzyme specific sequences yielding two or more double-stranded DNA fragments with, depending on the enzyme used, sticky (single stranded overhangs) or blunt (both backbones cutted at the same base pair) ends. In general, cloning strategies are chosen with insert and vector being digested with the same two enzymes that produce sticky ends to achieve a directional control of the insert incorporation in the cleaved vector. A typical protocol for a double digestion of a PCR product or purified vector DNA is reported in the following (Table 17).

Table 17: Digestion protocol. Reagents mix for a typical enzymatic cleavage of vector and insert.

Digestion Mix	
1 µg	*DNA*
10 – 20 U	*1st Enzyme*
10 – 20 U	*2nd Enzyme*
10x	*Cleavage Buffer*

1-2 hours of cleavage at 37° C are followed by dephosphorylation of the vector to avoid self-ligation. To this aim, the reaction mixture of the plasmid-digestion was supplemented with calf intestinal alkaline phosphatase (1 µl) which removes the reactive 5′ phosphate. The reaction products were further analyzed and purified by agarose gel electrophoresis (3.2.1.1.4), and DNA fragments were extracted using the QIAquick Gel Extraction kit for subsequent ligation.

3.2.1.1.6 Ligation

As a result of the enzymatic digestion insert and plasmid possess complementary sticky ends. Thus, the DNA fragments spontaneously associate with each other. The enzyme T4 DNA ligase catalyzes the formation of phosphodiester bonds between the juxtapositioned 3′ hydroxyl and 5’ phosphate groups of the different DNA strands. It joints blunt or cohesive ends, leading to DNA molecules with the desired insert incorporated in the target vector. The linearized plasmid was incubated with an excess of DNA insert (molar ratio around 1:3-1:5)

and the T4 DNA ligase in the corresponding ligase buffer at 16°C for at least 1 h or better overnight (Table 18).

Table 18: Ligation protocol. Reagents mix for a typical ligation reaction of vector and insert.

Ligation Mix	
0.2 µg	*vector DNA*
0.8 µg	*insert DNA*
400 cohesive end U	*T4 DNA-Ligase*
10x	*T4-Ligation Buffer*

3.2.1.1.7 Transformation of *E.coli*

Amplification of plasmids was performed by transformation into chemically competent *E.coli* DH5α. 100 µl aliquots of bacteria were carefully thawed on ice and mixed with a few nanograms to 1µg plasmid DNA. The solution was incubated on ice for 10 min, treated by heat shock at 42°C for 45 s and placed back on ice for 5 min. The transformation proceeded by addition of 500 µl LB medium and an incubation of 1 hour at 37°C before plating the mix on agar plates containing the appropriate antibiotic (usually 50 µg/ml) for selection of bacteria carrying the plasmid. The plates were incubated overnight at 37° C and single colonies were picked for colony PCR or plasmid purification. Clones were stored in 30 % glycerol in LB medium at –80° C.

3.2.1.1.8 Plasmid purification

For plasmid purification, single colonies were picked from agar plates for inoculation in 2-300 ml LB-medium with appropriate antibiotics (50 µg/ml) for selection. After propagation at 37° C for 16 h in a shaking incubator, bacteria were pelleted, and plasmids were isolated using the QIAprep Spin Miniprep Kit (for below 10 ml culture) or QIAGEN Plasmid Maxi Kit (for 300 ml culture) according to the manufacturer's manual. DNA concentrations were determined photometrically by measuring the absorbance at 260 nm (Biophotometer plus), and the plasmids were used for sequencing, transfection of eukaryotic cells or molecular biology.

3.2.1.2 Cloning strategy for viral fusion protein variants

In this section, the general cloning strategy that was followed to obtain the fusion proteins described in the thesis at hand is briefly described.

The cloning vectors pECFP-N1, pEYFP-N1 were used to generate plasmids for overexpression of fluorescent fusion proteins. They all encode a fluorescent protein under control of a constitutive cytomegalovirus (CMV) immediate early promoter for expression in mammalian cells and possess a multiple cloning site upstream of the fluorescent protein ORF for insertion of the sequence of interest. As all cloning plasmids, both harbor a bacterial origin of replication and a gene encoding an antibiotic resistance for prokaryotic selection. Moreover, eukaryotic selection is permitted by a neomycin resistance gen. GFP-derived fusion proteins possess dimerizing properties[144]. To prevent unwanted self-aggregation of fluorescently tagged proteins, monomeric variants were used provided by Silvia Scolari[173] (HU Berlin, Germany). The corresponding single amino acid exchange was generated using AB-PCR and was described in detail in the thesis of Silvia Scolari[173]. All fluorescent proteins utilized in this work, if not otherwise mentioned, are the monomeric forms of the original enhanced fluorescent proteins.

The vector containing the HIV-1 envelope sequence (Uniprot ID: Q75760) originating from the JRFL isolate of HIV-1 was kindly provided by Silvia Scolari (HU Berlin, Germany). Fluorescent virus protein chimeras were generated based on the plasmids described above. Relevant sections of the complete gp160 precursor protein plasmid, JRFL gp160wt were amplified by polymerase chain reaction using the following primer (Table 19).

Table 19: Cloning primers. Forward and reverse primers of clonings for the protein variants gp41-YFP, Δ1 and Δ2. The restrictions sites for NotI and BsrgI digestions in forward and reverse primers, respectively are underlined.

Primer	Sequence
*Forward **gp41-YFP&Δ1***	CGAGC **TGTACA** AGGAAATTGACAATTACACAAG
*Forward **Δ2***	GAGC **TGTACA** AGCTGTGGTATATAAAAATATT
*Reverse **gp41-YFP***	AGAGCT **GCGGCCGC** TTATAGCAAAGCCCTTTCCA
*Reverse **Δ1&Δ2***	AGTC **GCGGCCGC** TTAGTATCCCTGCCTAACTCTAT

All forward primer contain the restriction site BsrGI whereas reverse primer comprise NotI. Cloning vectors and PCR products were digested using both enzymes, subsequently gel purified and ligated with a 1:5-1:10 molar excess of the insert. Successful clonings yielded virus protein variants directly linked to the C-terminus of the fluorescent protein.

The rabbit lactase phlorizin hydrolase (LPH) signal peptide (SP) DNA sequence derived from the GPI-XFP vector provided by Mark Keller was cut from the plasmid and ligated to the n-terminus of the fluorescent protein to ensure physiological targeting of the virus protein chimeras. In eukaryotes, signal sequences are n-terminal extensions of nascent polypeptide chains. They direct the insertion of the protein into the membrane of the endoplasmic reticulum and are usually cleaved off by signal peptidases. Since sometimes, cleaved signal peptides are supposed to fulfill yet-to-define post-targeting functions[174], this GPI-SP strategy was chosen to express the same signal peptide in both donor-only and cells expressing donor and acceptor protein to avoid any SP-induced side effects.

Presumptively successful cloned vectors were verified by colony PCR and sequencing (Invitek, Berlin, Germany) using the following primers (Table 20).

Table 20: Sequencing primers. Sequencing primer binding either in the fluorophore directing towards the protein or within the vector directing towards the fluorophore.

Primer	Sequence
*Forward **XFP***	CTG CTG CCC GAC AAC CAC TAC CTG A
*Forward **pre Protein***	CGT GTA CGG TGG GAG GTC TAT ATA AG

Mutations were introduced in the cholesterol recognition amino acid consensus by site-directed mutagenesis as described later. The following primers were used for the corresponding AB-PCRs (Table 21).

Table 21: AB-PCR primer. Site-directed mutagenesis using the two primers reported here was applied to introduce single amino acid changes from leucine to isoleucine (underlined) in the CRAC motif.

Primer	Sequence
*Forward **mCRAC***	ACA AAA TGG ATT TGG TAT ATA AAA ATA TTC ATA
*Reverse **mCRAC***	TAT GAA TAT TTT TAT ATA CCA AAT CCA TTT TGT

3.2.2 Cell biology

3.2.2.1 Cell culture and propagation

CHO-K1, Cos7, HEK293T, HeLa and MDCKII cells were grown in complete DMEM (DMEM with 10 % FBS, 5 % L-Glutamine, 5 % Penicillin against gram-positive and 5 % Streptomycin against gram-negative bacteria), RBL-2H3 cells in RBL medium (MEM medium with 30 % RPMI 1640, 10 % FBS, 5 % L-Glutamine, 5 % Penicillin and 5 % Streptomycin) under mammalian cell culture conditions in a humified atmosphere at 37°C with 5 % CO_2. All working steps were performed in the sterile environment of a laminar flow hood. If not otherwise mentioned, the cells were grown in 75 cm^2 (T75) culture flasks supplied with in 10-12 ml medium. All cells were splitted 1:10 or 1:12 when ~90 % confluence was reached (2-3 times per week). For this purpose, adherent cells were washed with 10 ml PBS without Ca^{2+} and Mg^{2+} and incubated with 2 ml Trypsin/EDTA for three up to several minutes depending on the cell type at 37°C. After detachment of the cells, the trypsin reaction is blocked with 10 ml complete DMEM and 1 ml of the cell suspension is transferred to a new flask supplied with 9-11 ml of fresh complete medium.

3.2.2.2 Cell storage and thawing

For longtime storage mammalian cells had to be detached using Trypsin/EDTA as described above. Subsequently, floating cells were centrifuged with <300 g for 10 min at RT. After resuspension of the cell pellet in freezing medium (3.5 ml complete DMEM, 1 ml FBS, 0.5 ml DMSO) suited aliquots, containing high densities of cells ($1x10^6$-$5x10^6$ cells per ml) were distributed in cryotubes and frozen slowly (-1° C per minute) in a -80°C refrigerator using an

isopropanol freezing container. Finally the tubes were transferred into a liquid nitrogen tank for virtually unlimited storage.

To reactivate stored cells, complete DMEM was prewarmed to 37° C. Cell suspensions from the nitrogen tank were unfrozen in water bath and mixed with the warm medium. After centrifugation (<300 g, 10 min at RT) the cell pellet was resuspended in warm medium and transferred to a culture flask for further propagation. Freshly thawn cells were only grown until 70 % density and should not be directly used for experiments since passage 0 is supposed to contain freezing/thawing artifacts.

3.2.2.3 Transient and stable transfection

Typically, transfection of plasmid DNA into eukaryotic cells was conducted using the cationic lipid-based Lipofectamine 2000 or the Turbofect reagent according to the manufacturer's instructions. Usually, transfections were performed in a 35 mm glass-bottom dish or single wells of a 6 well for microscopy or FACS experiments, respectively.

Lipofectamin 2000 transfection. A total of 4 µg DNA and 10 µl Lipofectamine 2000 were used for transfection of cells grown to 90 % confluency in 35 mm dishes. Both, DNA and transfection reagent were mixed independently with pure DMEM to final volumes of 250 µl. The solutions were incubated for 5 min at RT, combined, thoroughly mixed and incubated for another 20 min at RT. In the meanwhile, the cells were washed with prewarmed PBS with Ca^{2+} and Mg^{2+} and covered with 1.5ml of warm DMEM without additives. Then, the transfection mixture was added dropwise to the cells and the dishes were gently swirled. The transfection medium was replaced by DMEM with additives after 4 h of incubation at 37°C to avoid cytotoxic effects of the transfection reagent.

Turbofect transfection. 4 µg DNA are required to transfect a 35 mm dishes of mammalian cells grown to 90 % confluency. 6 µl of pre-vortexed turbofect were mixed with the DNA in 200 ml of complete DMEM and after another vortexing, incubated for 20 min. Meanwhile, the cells were washed with pre-warmed PBS with Ca^{2+} and Mg^{2+} and covered with 1.8 ml of warm, DMEM without additives. Then, the transfection mixture was added to the cells; the dishes were gently swirled and incubated at 37°C. The transfection medium could be replaced by complete DMEM after 4 h but the cytotoxicity of turbofect is so low that even incubations overnight are possible.

Nucleofection. This specialized type of electroporation-based DNA delivery was conducted with an Amaxa Nucleofector 4D device. Since for this procedure, suspended cells are required, cells were firstly trypsinized and resuspended in PBS without Ca^{2+} and Mg^{2}. Subsequently, the cell concentration was assessed using a hemocytometer, $1x10^{6}$ cells were resuspended in a mix of 82 µl transfection reagent and 18 µl supplement with 2 µg of DNA and finally filled in the nucleofection cuvette. Then, a suited electroporation program was used according to the manufacturer's protocol to deliver the DNA (for instance T03 for CHO-K1). Finally, cells were allowed to relax for 10 minutes at room temperature in the cuvettes and added to glass bottom dishes or 6 wells with 2 ml prewarmed DMEM with additives.

Stable transfection. Different protocols are available to achieve a permanent expression of genetically modified genes. Stable transfections are extensions of transient transfections. Thus, to produce stable transfected cells, firstly a lipofection as described before was performed. Both aforementioned reagents, but also other transfection methods such as $CaCl_2$ based DNA delivery or electroporation are suited for the initial step.

Cells with a confluency of 40-70 % were usually transfected as described before in 35 mm dishes or 6 wells. After transfection and protein expression for 1 to 2 days in complete DMEM, the medium was exchanged against selection medium (DMEM supplemented with 500 µg/ml Geneticin). This concentration of the Geneticin (or shortly G418) was pretested to kill non-transfected cells completely within two weeks of exposure. Thus, the cells were propagated in the selective medium for at least one week. In that period, confluent cultures were splitted 1:5 to avoid losing transfected cells by hard splitting. After one to three weeks of selection, cells expressing fluorescent proteins were further enriched by FACS. To this purpose, cultures were detached using 0.5 ml of a mild reagent, 2 mM EDTA in PBS without Ca^{2+} and Mg^{2+}. 2 ml PBS without Ca^{2+} and Mg^{2+} was then added to the suspended cells prior to centrifugation (<300g, 10 min at RT). The cell pellet was resuspended in PBS without Ca^{2+} and Mg^{2+} and subjected to FACS. Cells were analyzed and 2 to 3 populations were selected for sorting: a high fluorescent population, a medium plus the high fluorescent population and all fluorescent cells. 100-5000 events of every population were sorted in 4 different wells of a 12 well, prepared with 1 ml of complete, prewarmed selection medium. Subsequently, the cells were quickly transferred to an incubator and propagated further for some days. From the 12 well, populations were chosen for further cell culture, freezing or experiments depending on the transfection efficiency, protein expression level, population homogeneity and cell

condition. If the transfection efficiency was still too low for stable transfected cells, further selection using G418-supplemented medium or another round of the FACS assay was performed. Propagation of sufficiently selected cells required utilization of complete DMEM containing 250 µg/ml G418 to maintain the selective pressure and avoid a spontaneous loss of the protein expression. We observed that the feasibility of a stable expression does not only depend on cell type, selection conditions and transfection efficiency but also to a great extent on the protein which is overexpressed. Whereas some proteins were stably expressed very easily just by the use of selection medium, other proteins could not be obtained in a stable expression system even upon application of different selection condition, FACS sorting or manual selection of single cell colonies.

3.2.2.4 Giant plasma membrane vesicles formation

Two different preparation methods were used to produce GPMVs, also called blebs. Cells form GPMVs spontaneously upon treatment with buffer containing N-Ethylmaleimid or a mixture of paraformaldehyde and DTT as previously described [97,175] (Figure 3-2).

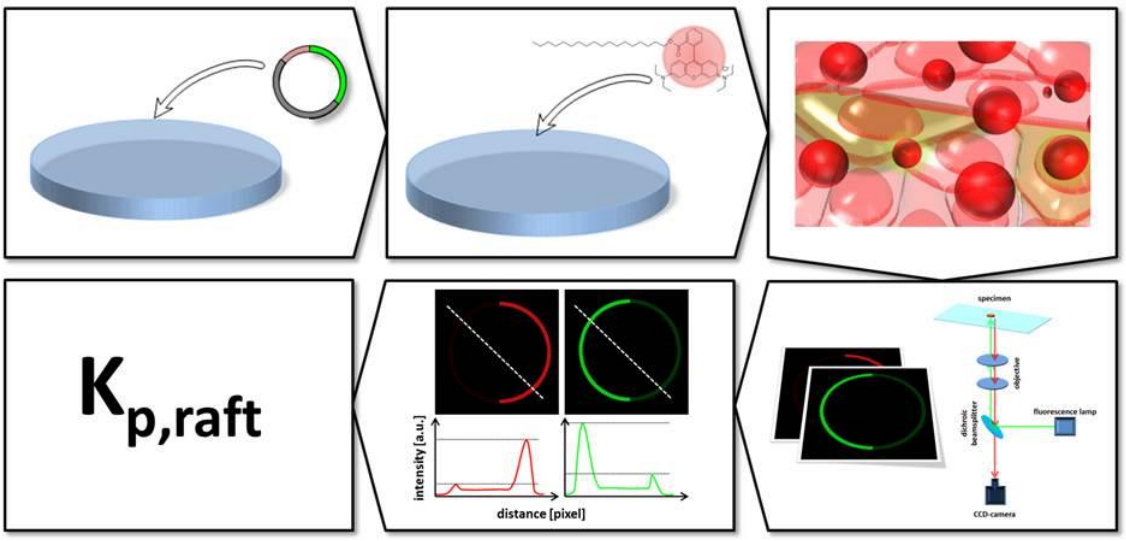

Figure 3-2: GPMV assay workflow. Cells were transfected with the GFP or YFP labeled proteins and prior to the experiment, labeled with a marker possessing a preference of disordered domains. Then, cells were treated with the blebbing mixture to induce the formation of GPMVs. After collection of the cell supernatant, sedimented bleb solutions were investigated using epifluorescence microscopy utilizing a temperature controlled setup that will be described later (Figure 3-3). Obtained images were analyzed regarding intensity in the ordered and in the disordered domain of the phase separated GPMVs by applying the plot profile function of ImageJ to finally calculate the raft partitioning parameter $K_{p,raft}$.

Briefly, confluent cells seeded in 6 wells or 35 mm dishes are washed twice with PBS with Ca^{2+} and Mg^{2+}. Subsequently, cellular plasma membrane were prestained using 20 µM solutions of DiO or octadecylrhodamine (R18) in PBS (+/+) for 10 min at 4° C. After removal of the labeling solution and another two washing steps with GPMV-buffer, the blebbing solutions were added to the cells either containing 2 mM NEM or 2 mM DTT and 25 mM paraformaldehyde in GPMV buffer. The cells were incubated for one to two hours at 37° C and the supernatant was collected in a conical glass or eppendorf tube where the vesicles were allowed to sediment for about 30 min at 4° C. GPMVs are stable for at least some hours up to several days. To study phase separation, bleb solutions needed to be cooled down to temperatures below 4° C. Conventional cooling devices and glass slides were not sufficient to provide those conditions. Thus, a special setup of cooling device and a user-assembled glass-slide-chamber had to be prepared for every sample (Figure 3-3).

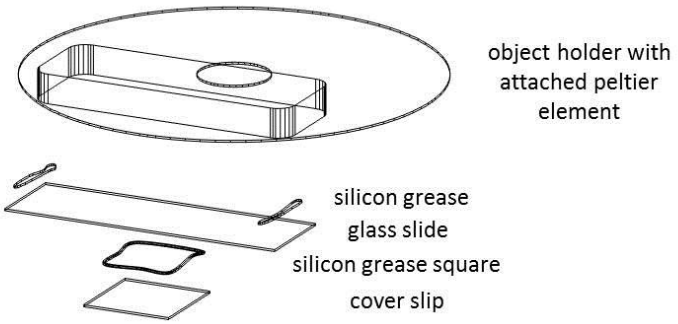

Figure 3-3: Sample chamber and cooling device setup for GPMV microscopy. Firstly, a silicon grease square was drawn on a glass slide. Then, a small drop of the sample was pipetted in the middle of that square which was subsequently covered with a cover slip. Using again silicon grease, the whole chamber was directly attached to the bottom of the peltier element on the object holder.

To this aim, a squared chamber of at about 1.5x1.5 cm was prepared, by drawing thin lines of silicon grease on a conventional, rectangular glass slide (24x60 mm). A drop of 10-30 µl of the GPMV solution, taken from the bottom (to get the sedimented GPMVs), but not the ground of the tube (to avoid cell debris), was placed in the middle of that square. Then, a cover slip (24x32 mm) was pushed softly on the silicon grease to flatten the GPMV-solution drop and seal the chamber. This arrangement was then, with the bigger glass slide facing towards the cooling device, attached to the bottom of a precooled peltier-element, again using a small film of silicon grease. To avoid fogging of the cooled cover slip with condensed water, compressed air was blown at the sample. The whole setup was then ready for fluorescence

microscopy. Images of the equatorial plane of the blebs were taken at different temperatures using an epifluorescence microscope (Olmypus IX81). The images were analyzed using the plot profile function of ImageJ and the raft partitioning parameter $K_{p,raft}$ was calculated according to:

$$K_{p,raft} = \frac{I_{raft}}{I_{nonraft}} \qquad (7)$$

3.2.2.5 Fluorescence labeling of fixed and living cells

For different fluorescence microscopy approaches cells were labeled with fluorescent antibodies, compartment specific fluorescent probes or fluorescent lipid analogs. To this aim, cells were grown in 35 mm glass-bottom dishes and labeled prior to the microscopic experiments.

3.2.2.5.1 Immunofluorescence (IF)

Antibody staining experiments were conducted to prove the identity of specific cellular regions or label viral proteins. Briefly, the different primary and the secondary antibodies (typically Alexa568 anti-mouse antibodies from Invitrogen, Carlsbad, CA) were diluted to 1 mg/ml in 1 % BSA/PBST. Mammalian cells were washed twice with PBS (+/+) and fixed with 4 % paraformaldehyde for 10 min at room temperature. Then, the cells were permeabilized and blocked with 0.3 % Triton X-100, 0.2 % Tween 20, 3 % BSA in PBS (+/+) for 30 min at RT. The cells were stained with the primary antibody solution for 1 h at room temperature, washed three times, labeled with the secondary antibody for another 1 h at RT and washed again three times. Without further mounting, the samples were imaged within some hours or latest at the next day.

Antibody staining experiments were also performed to quantify the amount of surface-exposed GFP-labeled proteins. Here, fusion proteins were transfected utilizing turbofect and expressed for at least 24 h as described before. Afterwards, cells were washed twice with PBS (+/+) incubated with the AlexaFluor555 anti–GFP for 60 min at 4° C and then washed thoroughly again. To ensure a complete saturation of accessible YFP molecules with antibodies, different antibody concentrations were pretested. A concentration of 1 µg/ml

turned out to be sufficient to achieve complete labeling of external fluorescent proteins, since higher antibody concentrations did not cause a further increase of the antibody fluorescence.

3.2.2.5.2 Labeling of subcellular structures

Viral fusion proteins were co-expressed with different fluorescently labeled, cellular proteins or specific commercially available compartment marker dyes to study their intracellular distribution and localization. Viral fusion chimeras labeled with cherry were co-transfected with rab5-GFP, rab7-GFP, rab11-YFP and Tau-YFP for 24 h using turbofect according to the manufacturer protocol. Moreover, live cell staining experiments were conducted using ER-Tracker blue (Invitrogen, Carlsbad, CA) or lysotracker (Invitrogen, Carlsbad, CA) according to the manufacturer's protocol 24 h post-transfection with YFP-labeled viral fusion proteins.

For visualization of DNA or cellular actin filaments, fixed and permeabilized cells were stained with DAPI, propidium iodide (PI) or rhodamine phalloidin respectively. This was generally done following immunostaining.

Staining of the cell nuclei was performed by incubation of the cells with 100 nM DAPI in PBS (+/+) at RT for three minutes, by labeling with 500 nM PI in PBS (+/+) for five minutes or with 100nM rhodamine phalloidin in PBS (+/+) for 30 minutes. Staining procedures were followed by three washing steps with PBS (+/+) prior to imaging.

3.2.2.5.3 Labeling of cellular membranes with C6-NBD-PC

NBD-PC was used as a reporter of the rigidity and order of cellular membranes. To this aim, CHO-K1 cells were seeded in different concentrations one day prior to the experiment. At the day of microscopy, an aliquot of 5 nmol dried C6-NBD-PC was redissolved in 10 µl ethanol which were subsequently filled up to 100 µl with PBS (+/+). To obtain the final labeling solution, 20 µl of this mixture were vortexted with 1 ml of PBS (+/+) yielding a final concentration of 1 µM. Then, the cells were washed twice with PBS (+/+) and incubated with the final labeling solution for 10 min at 4° C. After two final washing steps with PBS (+/+) and the addition of medium without additives and phenolred, the cells were used for microscopy at 37° C.

3.2.2.6 Production of virus-like particles

To produce HI virus-like particles, expression of the Gag polyprotein is necessary and sufficient. A fluorescently labeled variant of this protein was used, which was obtained through the NIH AIDS Research and Reference Reagent Program, Division of AIDS, NIAID, NIH: pGag-EGFP (Cat#11468) originally generated by Dr. Marilyn Resh. To study incorporation of fusion proteins, HEK293T cells were transfected with pGag-EGFP and the protein under study. All transfections were performed in 9 cm dishes using turbofect according to the manufacturer's protocol. 48 h post-transfection cell supernatants were collected and filtered through a 0.2 µm pore-size filter. The VLPs were then separated from remaining cell debris by centrifugation for 1.5 h at 160000 g in an SW40 rotor. Subsequently, the pellet was resuspended in 100 µl TNE buffer and further purified by another centrifugation through a 20 % sucrose cushion for 2 h at 160000 g. Finally, the pellet was resuspended in 50 µl TNE buffer and analyzed using SDS-PAGE and Western Blot. Here, both virus-derived fusion proteins were detected utilizing GFP-antibodies.

3.2.3 Microscopy

3.2.3.1 Confocal fluorescence microscopy (CLSM)

An inverted FluoView 1000 microscope was modified for FLIM measurements with a time-resolved LSM Upgrade kit (PicoQuant, Berlin, Germany). Differential Interference Contrast (DIC), fluorescence intensity and FLIM images were obtained with a 60x UplanSApo oil immersion objective (numerical aperture 1.35) at 25° C with a frame size of 512x512 pixels and a pixel dwell time of 4 µs per pixel. For different combinations of fluorophores, different excitations sources, filter sets and dichroic mirrors were used. If not otherwise state the following microscope settings were applied (Table 22). As excitation source, the microscope was equipped with a multi-line argon laser, providing 458 nm, 488 nm and 515 nm wavelength, and two laser diodes providing 405 nm and 561 nm. Emission was detected with two independent confocal photon multiplier tubes. Signals of double labeled cells were recorded sequentially and, if necessary, obtained intensities were analyzed with the ImageJ analysis program.

Table 22: Applied CLSM settings. Dichroic mirrors (DM), excitation sources with typically used power in brackets and detection ranges are reported for the most important fluorophore combinations used in this study. Excitation sources were either laser diodes (LD) or an argon laser (AL).

Fluorophore combination	1st channel Excitation source	1st channel Detection range	Dichroic mirror	2nd channel Excitation source	2nd channel Detection range
CFP & YFP	458 AL (10 %)	475-490	*DM458/515*	515 AL (4 %)	535-575
GFP & Alexa568/ Alexa594/Cherry	488 AL (10 %)	495-545	*DM405/488/ 559/635*	559 LD (5 %)	570-670

3.2.3.2 Fluorescence lifetime imaging microscopy

A typical FLIM-FRET workflow that was used to study plasma membrane raft partitioning of YFP-labeled fusion protein is depicted in Figure 3-4. For raft partitioning experiments, CFP was excited using a pulsed 440 nm laser diode with a 20 MHz pulse frequency. Emission was detected with a single photon avalanche photodiode (τ-SPAD, PicoQuant) equipped with a 470/30 bandpass filter. SPAD signals were processed with the TimeHarp 300 photon counting board and analyzed with the SymPhoTime software (PicoQuant) taking into account the instrument response function (IRF) to allow consideration of short lifetime components with a high accuracy. The IRF was obtained by detecting the scatterlight (using a 440/10 bandpass) of the 440 nm laser diode from a drop of water on an object slide. FLIM images were acquired as described previously [98].

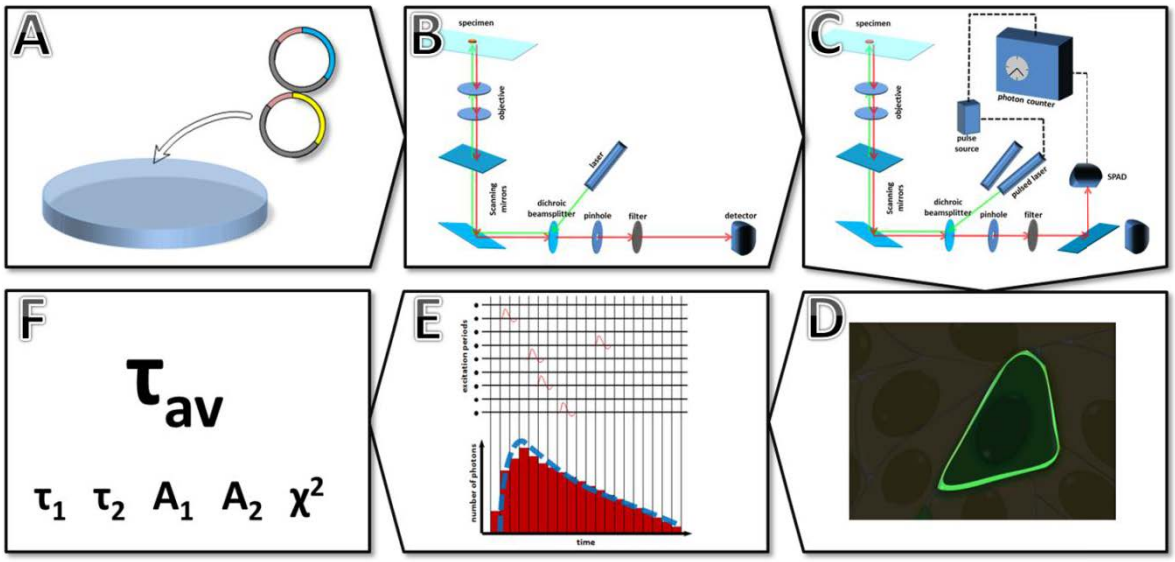

Figure 3-4: Raft partitioning assay workflow. This experimental approach can be roughly divided in three practical and three analytical steps. Firstly, (A) cells were transfected with GPI-CFP and the YFP labeled protein under study or, for the calculation of the FRET efficiency, with GPI-CFP alone. (B) Expressing cells were imaged using conventional confocal microscopy for subsequent intensity analysis and afterwards (C) investigated with the FLIM setup. For the calculation of a relevant average fluorophore lifetime and FRET efficiency suited areas of interest (D), usually plasma membranes or Golgi apparatus were selected. (E) Histograms of the detected photons in the selected area were generated by using the Symphotime software (red columns) and a decay curve was calculated (blue dashed line). (F) The fitting yielded individual fluorescent lifetimes and the respective amplitudes according to the fitting model selected. For CFP, usually a biexponential decay was assumed and the amplitude-weighted average lifetime τ_{av} in absence and presence of acceptor fluorophores was used to calculate the FRET efficiency (see FLIM analysis).

Briefly, images were accumulated for 98 s with an average photon count rate of 40000-60000 counts per second. Regions of interest (usually plasma membrane or Golgi apparatus) were selected from FLIM images and the corresponding photon counts were summed up into a lifetime histogram, according to their arrival time by the SymPhoTime software.

3.2.3.2.1 FLIM analysis

The intensity distribution decay that is represented by the lifetime histogram was further analyzed by fitting, using a nonlinear least squares iterative procedure which is included in the SymPhoTime software. As other fluorescent protein variants, CFP adopts different conformational states[176,177] with different fluorescence properties that have to be considered in fluorescence lifetime fits. Therefore, a decay that is a sum of 2 exponential terms was assumed. For every single cell the amplitude-weighted average lifetime was calculated according to

$$\boldsymbol{\tau_{Av}} = \frac{\sum_i \boldsymbol{\alpha_i \tau_i}}{\sum_i \boldsymbol{\alpha_i}} \qquad (8)$$

Where τ_{av} is the amplitude-weighted average lifetime, α is the amplitude of a lifetime component and τ is the corresponding lifetime. FLIM images were generated by the Symphotime software by displaying pixelwise average lifetimes in pseudocolors.

The calculated decays were judged by the χ^2 values and the residuals of the fit. Cells expressing donor protein alone or coexpressing FRET-donor and acceptor protein were measured and the FRET efficiency was calculated as follows.

$$\boldsymbol{E}(\%) = \left(\mathbf{1} - \frac{\boldsymbol{\tau_{DA}}}{\boldsymbol{\tau_D}}\right) \times \mathbf{100} \qquad (9)$$

Here, E(%) represents the FRET efficiency in percent, τ_{DA} the average weighted lifetime of donor in presence and τ_D in absence of the acceptor.

3.2.3.2.2 FRET clustering analysis

To elucidate whether obtained FRET values are a result of co-clustering or respectively direct protein interactions, or otherwise just reflect concentration dependent random collisions, the relation between acceptor concentration and FRET efficiency was examined. Confocal images were analyzed using ImageJ to obtain the fluorescence intensity of YFP at the plasma membrane assuming a direct proportion between acceptor concentration and fluorescence signal. Normalized and background corrected YFP fluorescence values of specific regions of single cells were plotted against the corresponding FRET efficiency and fitted to a binding kinetic model according to the following equation[144].

$$\boldsymbol{E}(\%) = \frac{\boldsymbol{E_{max}}(\%) \times \boldsymbol{F_{YFP}}}{\boldsymbol{F_{YFP}} + \boldsymbol{K_d}} \qquad (10)$$

Clustering in lipid rafts was assumed if obtained K_d values were significantly lower than the average acceptor fluorescence values F_{YFP} within the experiments. Readers should refer to previous publications in this context [98,144] for more details.

3.2.3.3 Fluorescence anisotropy imaging microscopy

The workflow of a typical FAIM assay to study protein oligomerization is depicted in Figure 3-5. The experimental setup for time resolved single photon detection was described previously (see 1.4.2). An expanded setup, explicitly described on the manufacturer's website[178] was used for fluorescence anisotropy imaging. After removal of DIC depolarization filters, images were obtained using a 60x water objective (numerical aperture 1.2) with a frame size of 512x512 pixel. A pulsed 470 nm laser diode with a repetition frequency of 20 MHz was applied to excite YFP. The polarized emission light was separated with a polarization beam splitter and detected using a 540/40 emission filter for the perpendicular polarized light and a 540/30 emission filter for the parallel polarized light prior to a τ-SPAD and Perkin/Elmer SPAD respectively. The polarization characteristics of the different

microscopical elements have important consequences in the measurement of fluorescence anisotropy. Therefore, anisotropy measurements must be corrected for the varying efficiencies of each optical component such as for example monochromators or detectors and this correction is expressed in the G-factor. The G-factor for the used microscopical arrangement was calculated from point scans of the emission signals on both channels with an Alexa488 solution. Since the rotational correlation time of this dye is significantly higher than its average fluorescence lifetime, the G-factor can be approximated by the quotient of parallel and perpendicular fluorescence intensity.

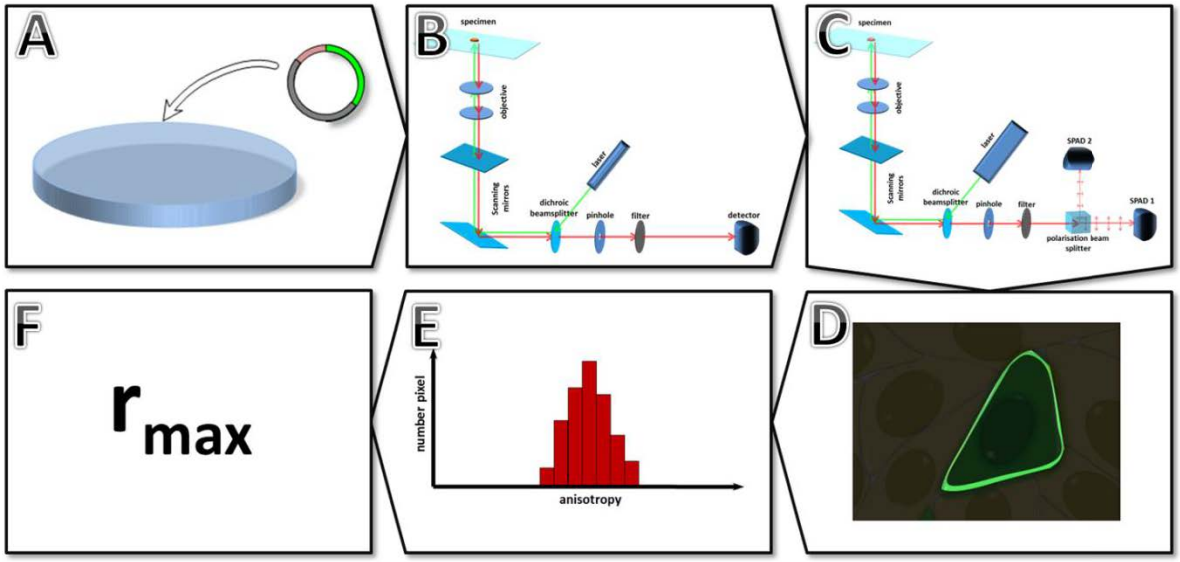

Figure 3-5: Oligomerization assay workflow. Initially, (A) cells were transfected with the YFP labeled protein of interest. Then, (B) expressing cells were imaged using conventional confocal microscopy for subsequent intensity analysis and afterwards (C) investigated with the FAIM setup. (D) Regions of interest were selected and (E) histograms of the respective pixel were generated by the Symphotime software (red columns). (F) Maximum anisotropies of Gauss-distributed histograms were then assessed to quantify oligomerization of the protein under study.

A value of 0.73 was found for the setup described above. Fluorescence steady state anisotropy pictures were accumulated for 90 s with an average p hoton count rate of 50000-100000 counts per second. Images were analyzed using the Symphotime software after selection of suited regions of interest and obtained pixel weighted values were summed up into anisotropy histograms. The anisotropy was calculated according to the following equation by the analysis software.

$$r = \frac{G \cdot I_{\parallel} - I_{\perp}}{2 \cdot I_{\perp} + G \cdot I_{\parallel}} \qquad (11)$$

Where r is the anisotropy, $I_{\parallel}$ and $I_{\perp}$ are the intensities of the parallel and perpendicular light and G is the instrument specific G-factor. To quantify the extent of the measured depolarization, maximum values of Gauss-distributed anisotropy histograms of different proteins were compared. Typically, if the distribution did not commensurate to the requirements of a simple Gaussian distribution, other regions of interest were selected in the FAIM images to spatially separate different species which then can be used to obtain individual anisotropy maxima.

3.2.3.4 Single particle tracking (SPT)

Single particle tracking of cells expressing fluorescently labeled viral proteins were conducted with the confocal setup described previously (3.2.3.1). Equatorial sections of the cells were imaged with a resolution of 256x256 pixel and a pixel dwell time of 4 µs resulting in an image acquisition time of at about 1 sec per image. Obtained t-stacks were analyzed following a protocol developed by Chris-Tina Höfer (Humboldt University, Berlin). Briefly, particles were identified using the SpotTracker ImageJ plugin and tracked with the plugin MtrackJ. With the known image acquisition parameter, the trajectories or more precisely the particle displacement can be utilized to estimate physical meaningful data such as particle velocity or covered distance.

3.2.3.5 Epifluorescence microscopy

Epifluorescence microscopy was used to study phase separation in GPMVs. Although, equatorial sections were obtained for the analysis of domain partitioning and phase separation, epifluorescence microscopy was preferred to confocal microscopy because it allows easier identification of phase separating vesicles in inhomogeneous solutions and in general, permits faster image acquisition, which is a huge advantage for the observation of the freely diffusing blebs. Epifluorescence microscopy was conducted utilizing an inverted Olympus IX-81 microscope equipped with a cooled monochrome CCD-camera. Images were obtained with a 40x UPlanFL air objective (numerical aperture 0.75) using U-MWNiba filters (BP470-495, BA520IF, DM510-550) for green fluorescence such as GFP, YFP or FITC and a U-MWG2 filter set (BP510-550, BA590, DM570) for red fluorescence, like DiO or R18. Depending on the individual protein concentration and labeling efficiency, images were obtained with

exposure times from 0.5 s to several seconds for the green channel and below 0.5 s for the red channel.

3.2.3.6 Total internal reflection fluorescence microscopy (TIRFM)

TIRFM was used to study the plasma membrane localization of expressed virus protein-derived fluorescent chimeras. An inverted FluoView 1000MPE microscope (Olympus, Tokyo, Japan) was modified with a beam expander to allow illumination of the whole field of view using laser excitation sources and a highly sensitive, cooled Hamamatsu Orca ER CCD-camera for epifluorescence observation. The tilting of the angle of the incidenting light beam was achieved by a displacement of the beam, away from the center of the observation objective[179] (60x UplanSApo oil objective with a numerical aperture 1.45). In a typical TIRFM experiment, the glass attached parts of the cells under study were focused and imaged in the epifluorescence mode applying beam expander and CCD-camera. Then, the TIRFM angle was tilted until the out-of-focus light from intracellular structures disappeared and plasma membrane structures dominated the image. As a rule of thumb, if the angle is right, changes of the focus should not change the structures displayed but only the sharpness of the plasma membrane components. Since only an evanescent field of the excitation light was used to illuminate the fluorophores, high laser intensities of around 50 % and image acquisition times of at about 1 sec were used.

3.2.4 Flow cytometry

Flow cytometric experiments were performed with a BD FACS Aria II. Initially, adherent cells were detached using either trypsin, 2mM EDTA in PBS (-/-) or a cell scraper. Afterwards the cells were pelleted with a tabletop centrifuge (<300g, 10 min at RT) and resuspended in PBS (-/-). Typical cell cytometry experiments were conducted with a 100 µm nozzle and a ND2 laser attenuation filter. The drop formation was induced with an amplitude of 12 and a frequency of 30. The exact arrangement of the optical elements and the exact filter configuration can be obtained from the BD website or the manufacturers manual (page 37). As excitation sources served a 405 nm, a 488 nm and a 633 nm laser that allowed, in combination with the provided filter setup, simultaneous observation of blue (DAPI), green (GFP) and red (Propidium Iodide, Alexa 568) fluorescence.

3.2.4.1 Flow cytometric membrane perturbation assay

The workflow of a typical FACS assay to study the membrane violation of transfected proteins is depicted in Figure 3-6.

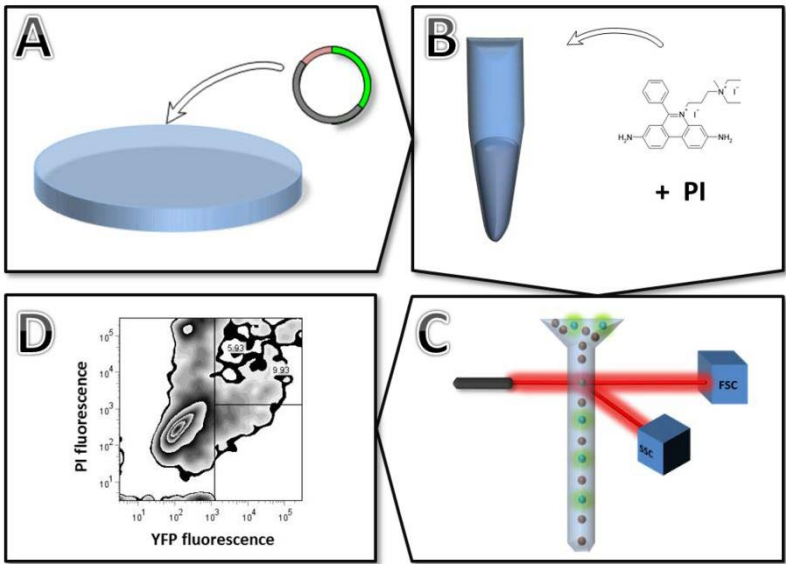

Figure 3-6: Membrane perturbation assay workflow. (A) Cells were transfected with the fluorescently labeled protein under study 24 h prior to the experiment. A detachment with a cell scraper of PBS/EDTA is followed by a brief centrifugation and a subsequent resuspension in PBS. (B) For the flow cytometric analysis, propidium iodide is added as a reported of the cells membrane integrity and general cell viability. (C) After sample observation utilizing a BD FACS, (D) the fraction of PI positive from all fluorescent cells was considered as a measure of the transfected protein's membrane perturbing influence.

In order to investigate the bilayer perturbing influence of different fluorescently labeled fusion proteins, cells were first transfected with the protein under study. After at least 24 hours of expression, adherent cells were detached by using a cell scraper or by treatment with PBS (+/+) supplemented with 2 mM EDTA for 5 min at 37°C and centrifuged at <300g for 10 min at RT. The obtained cell pellet was resuspended in PBS (+/+) and hold on ice until flow cytometric analysis. The cells were then labeled with propidium iodide (final concentration 1µg/ml) and directly used for flow cytometry. In a typical experiment, viral fusion proteins were compared with controls: a mock-transfected negative control and GPI-YFP transfected cells as a non-perturbing negative control. As a measure of the membrane violating influence of the expressed protein, the absolute number of propidium iodide (PI) positive cells (upper right quadrant of PI versus YFP dot plots) of all fluorescent cells was quantified (both right quadrants).

3.2.5 Biochemical methods

3.2.5.1 Protein palmitoylation assay (acyl-biotinyl exchange)

Acyl-biotinyl exchange was performed as described by Wan et al. [180]to prove qualitatively gp41 palmitoylation. For this purpose, 90 % confluent cells were transfected in 35 mm dishes. After one to two days of expression, the medium was changed and the cells were incubated for another hour. After two washing steps with cold PBS (+/+), 200 µl lysis buffer were applied, the cells were scraped from the bottom of the culture dish and subjected to 20 strokes of homogenization on ice utilizing a dounce homogenizer. Afterwards, nuclei were removed by centrifugation for five minutes at 800 g. The supernatant was mixed with four volumes of ice cold acetone to precipitate proteins and incubated for at least 30 min at 4° C. After a first centrifugation at 13000 g for 10 min the pellet was washed with ice cold acetone and centrifuged again. The obtained pellet was then dissolved in 50 µl blocking buffer to saturate accessible cysteines in the protein solution and incubated for at least ten minutes at 40° C while vigorously shaking. Subsequently, the proteins were acetone precipitated, acetone washed twice and redissolved in 50 µl binding buffer. Thiopropylsepharose beads were washed three times with binding buffer and redissolved in binding buffer to a final concentration of two to 3 mg of dry powder per 15µl. This volume was then added to the protein solution followed by 10 µl of freshly prepared 2 M hydroxylamine hydrochloride solution with a pH adjusted to 7-8 using NaOH and HCl and incubated for at least two hours at RT to allow binding of the beads with the depalmitoylated cysteines. The supernatant of this binding represents non-palmitoylated proteins. Bead-bound proteins were pelleted by applying 1000 g for one min and washed five times with binding buffer. The final pellet was redissolved in 50 µl binding buffer supplemented with 50 mM DTT and incubated at RT for 20 min. After a final centrifugation with 1000 g for one min the supernatant, containing originally palmitoylated protein, and the supernatant of the bead-binding step were subjected to SDS-PAGE and Western blot to estimate the fraction and identity of palmitoylated and non-palmitoylated proteins in the cell lysate.

3.2.5.2 SDS polyacrylamide gel electrophoresis

Proteins were separated according to their molecular weight by SDS-PAGE. For this purpose, gels were prepared by casting resolving gels of 10 or 12 % acrylamide/bisacrylamide at pH

8.8 and overlaying them with a 5 % collecting gel at pH 6.8. Then, the samples were incubated with a reducing SDS sample buffer at 95° C for 5 min and loaded onto the gel. For the weight determination of isolated proteins, a molecular weight marker was loaded as well and afterwards, electrophoresis was run at constant voltage of 100 V for at about 5 minutes to allow a homogenous alignment of the samples in the collection gel and then raised to 180 V in the resolving gel. For detection of the proteins after electrophoresis, the gel was processed by Coomassie blue staining or Western blotting.

3.2.5.3 Coomassie blue staining

For the detection of total protein in a SDS polyacrylamide gel, the gel was incubated for 1-2 h in Coomassie staining solution. Subsequently, the gel was washed twice with ddH_2O and destained for at least two hours or better overnight. The amount of proteins was detected (detection limit is about 0.1 µg of protein) at 700 nm with the Odyssey Infrared Imaging System (LI-COR).

3.2.5.4 Western blotting

Western blotting was performed after electrophoretic separation of proteins to identify specific protein bands by antibody recognition. A prerequisite of that detection is a transfer of the proteins under study from the gel onto a nitrocellulose membrane (‘blotting’). To this aim, the membrane and two pieces of thick blotting paper (Whatman paper) were soaked in transfer buffer. Then, a stack consisting of blocking paper, membrane, gel and another piece of blocking paper was placed in a Trans-Blot Semi-Dry Transfer Cell (Bio-Rad). An electric field was applied perpendicular to the stack with 20 V for 30-60 min. The efficiency of the transfer was estimated by the molecular weight marker. Since the membrane binds all proteins unspecifically, it needed to be blocked after the transfer to prevent unspecific binding of antibodies in the following steps by incubation for 1 h at RT with blocking buffer (LI-COR Odyssey Blocking buffer 1:1 diluted with PBST). The membrane was gently agitated during all incubation steps. Primary antibodies, which are specific for the protein of interest, were typically used in a 1:3,000 and secondary antibodies in a 1:10,000 dilution in blocking buffer. The membrane was incubated with the primary antibody for at least 1 h or better overnight at 4°C, followed by three times washing for 10 min with PBST and incubation with the secondary antibody for another one to two hours at RT. Finally, the membrane was washed as

before and stored in PBS. Secondary antibodies labeled with an IRDye were detected with the LI-COR Odyssey scanner by excitation at 700 nm.

4. Results

4.1 Generating tools to study gp41 lipid raft partitioning

The main objective of this work was to characterize the lateral segregation of the HIV-1 glycoprotein gp41 in the plasma membrane of mammalian cells. To this aim, virus protein chimeras were produced by tagging fragments of gp41 with a yellow fluorescent protein. Upon cotransfection with a GPI-anchored CFP as a raft marker emerging FRET reports raft association of the protein under study.

4.1.1 Construction of the raft marker

In order to have a genetically encoded, fluorescent raft marker, a GPI-anchored cyan fluorescent protein (CFP) was produced. The original cDNAs of GPI-CFP and GPI-YFP was provided by Patrick Keller [181] and modified by Silvia Scolari[173]. Briefly, a GPI-anchor signal was C-terminally linked with CFP and N-terminally with a plasma membrane targeting signal. Due to the properties of the membrane anchor, the resulting protein is not only efficiently transported to the plasma membrane but also preferentially incorporated in cholesterol enriched microdomains[98,144].

Native GFP and GFP-derived proteins have the propensity to spontaneously form homodimers. The aim of our approach was to study FRET between CFP- and YFP-linked proteins as a result of their putative enrichment in plasma membrane lipid rafts. Hence, a direct interaction between CFP and YFP had to be prevented. For this reason, the single amino acid mutation A206K, reported to completely abolish the oligomerization potential of GFP[144] and its derivatives, has been introduced in both fluorophores by AB-PCR.

4.1.2 Construction of the chimeric gp41 fusion protein gp41-YFP

When designing fluorescently tagged fusion proteins, several requirements have to be taken into account. Since behavior, structure and function of the chimeric proteins should resemble their native equivalent as much as possible, the position of the fluorophore has to be chosen carefully. In the present study, the focus lies on the assembly related processes. Therefore,

from the full envelope complex we removed the full external subunit gp120 and most of the gp41 external domain based on the assumption that those parts are too distal from transmembrane domain and bilayer to influence membrane-related properties. An initial construct was designed with an N-terminal signal peptide and a yellow fluorescent protein linked to the external domain of gp41 (Figure 4-1). The glycoprotein's membrane proximal external region and the complete cytoplasmic domain was included to preserve the external cholesterol binding motif and several internal motifs known to mediate intracellular, host protein or membrane interactions. In order to allow various fluorophore combinations in co-expression and staining experiments, different gp41 fusion proteins were produced by replacing YFP with CFP, GFP or Cherry.

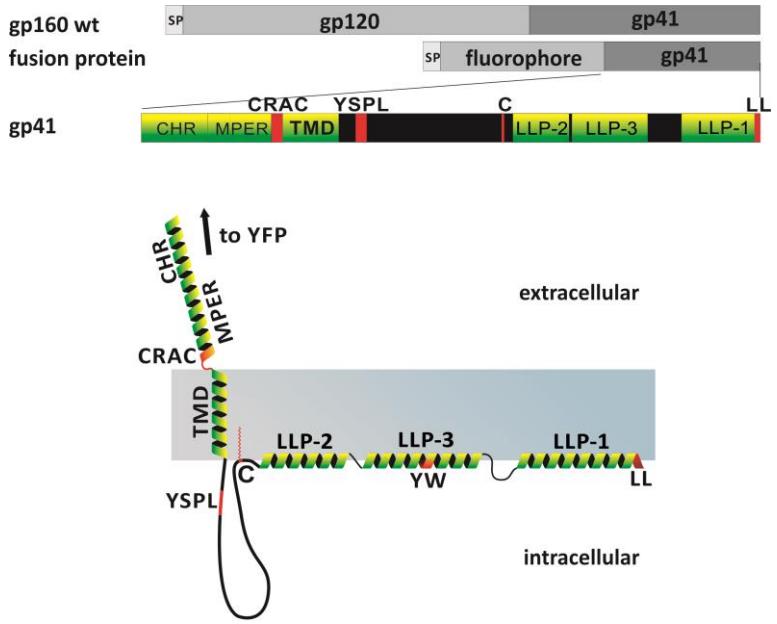

Figure 4-1: Schematic illustration of the gp41 chimeric protein. From the wild type glycoprotein precursor complex gp160, irrelevant parts of gp41 and the surface subunit gp120 were replaced by a fluorescent protein yielding the fusion protein gp41-YFP. In this variant, CRAC domain, YXXL endocytosis motif, palmitoylation site, YW tyrosine based sorting signal and C-terminal dileucine motif (highlighted in red) are maintained to ensure a physiological membrane interaction. A cartoon representation of a predicted gp41 structure is displayed in the lower panel.

4.2 Characterizing the chimeric gp41

Several experiments were performed to elucidate whether the fluorescent tagging of gp41 affected properties of the protein in the context of post-translational trafficking, assembly and

budding. To this end, we scrutinized intracellular localization, palmitoylation and incorporation in virus-like particles.

4.2.1 Intracellular distribution and trafficking

Upon expression in different mammalian cell lines, gp41-YFP was always found to be similarly distributed. In all tested cell lines, namely Cos7, HeLa, CHO-K1 and HEK293T, expression and localization showed significant deviations within the cell population. Nevertheless, all expressing cells displayed an inhomogeneous distribution of the protein over the complete cell body and a strong accumulation in the perinuclear region (Figure 4-2, white arrows).

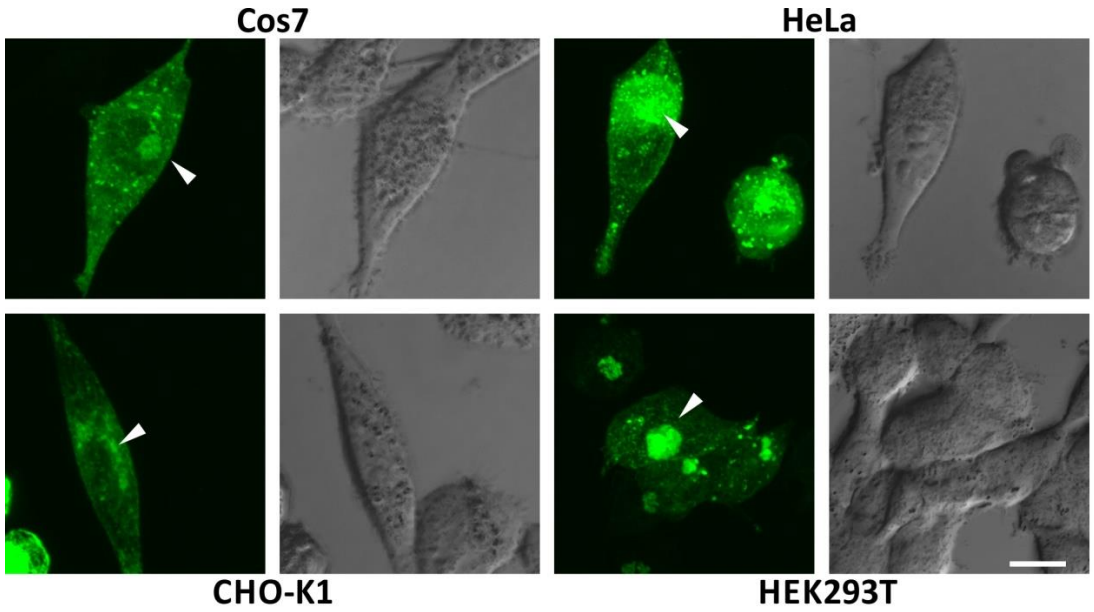

Figure 4-2: Gp41-YFP localization in different mammalian cell lines. Projections of z-stacks assessed by confocal microscopy of Cos7, HeLa, CHO-K1 and HEK293T-cells, expressing chimeric gp41-YFP are displayed. The white arrows indicate the gp41 accumulation in the perinuclear region. Scale bar, 10µm.

This accumulation in the perinuclear region is highly cell type dependent and in particular in HeLa and HEK293T cells it was found to be very pronounced. Since this local enrichment comes with a decrease of the plasma membrane localization, lipid raft partitioning experiments are rendered difficult in those cell types. Thus, CHO-K1 cells were used for further experiments. Antibody staining, nucleus staining and coexpression with different

fluorescent proteins were performed to identify the intracellular compartments and organelles and characterize the vesicles the protein was incorporated in.

Gp41-YFP is highly enriched in the Golgi apparatus. First of all, gp41-YFP expressing cells were stained with a commercially available fluorescent ER marker. Colocalization was found only in the perinuclear region but not, or only to a minor extend in other parts of the cell (Figure 4-3). Considering that ER-Tracker is labeling both, Golgi apparatus and endoplasmic reticulum (personal communication with Invitrogen application specialists) this finding suggests an only insignificant detention of gp41-YFP proteins in the ER and thus a physiological folding. However, to undoubtedly identify the perinuclear region gp41-YFP was found to be accumulated in, two independent antibody stainings were performed.

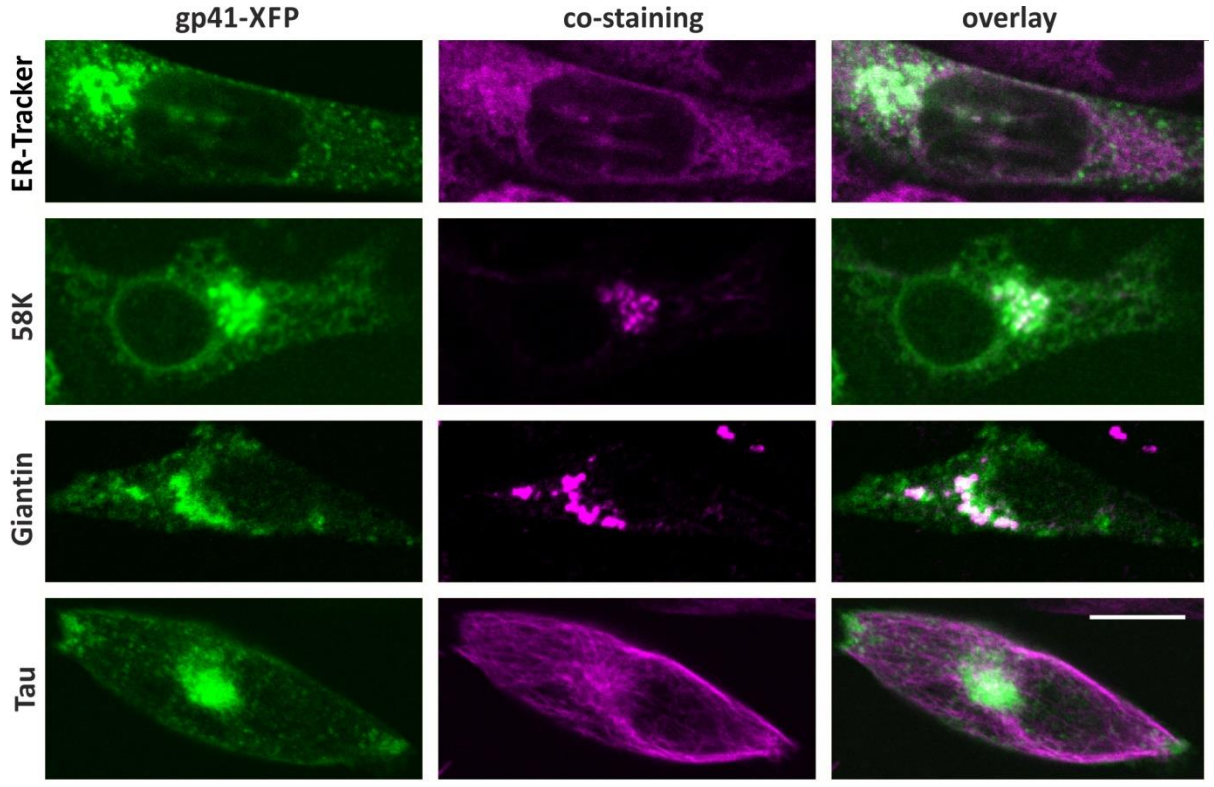

Figure 4-3: Intracellular localization of gp41 in CHO-K1 cells. Gp41-YFP or gp41-Cherry (displayed in green) expressing cells were labeled with ER-tracker, antibodies specific for the Golgi-apparatus proteins giantin[182] (cis/media) and 58K[183] (trans/late) or co-transfected with Tau-YFP as a specific microtubule marker (displayed in violet). Scale bar, 10µm.

Both cellular Golgi proteins, Giantin and 58K were found to colocalize with the intracellular accumulation site of gp41-YFP (Figure 4-3). Whereas giantin mainly resides in cis and medial parts of the Golgi apparatus[182], 58K should be concentrated in the later compartments and

Trans-Golgi network[183]. Gp41-YFP was found to colocalize with both, reporting a homogenous distribution of the protein in all subcompartments of this organelle. This results is in agreement with previous studies that already reported high concentrations of the HIV-1 envelope complex in the Golgi apparatus[184] and moreover, indicate a native folding of the fusion proteins in the ER since only correctly folded proteins are able to reach the Golgi apparatus whereas missfolded proteins accumulate in the ER and are subjected to degradation. Finally, a fluorescently tagged tau protein (Tau-YFP) was co-expressed with gp41-Cherry. Tau is a cytoskeleton binding protein[185] and thus, Tau-YFP can be used to visualize cellular microtubules in live cell experiments. Upon co-expression, the accumulation of gp41 was traced in the central crossing point of the microtubular network, presumably representing the microtubule organization center (MTOC) which is known to be associated with the Golgi apparatus[186] (Figure 4-3).

Gp41-YFP intracellular progression is associated with cellular transport vesicles and the chimeric protein is efficiently endocytosed. In order to elucidate gp41-YFP trafficking pathways, colocalization with fluorescently labeled rab proteins or a specific lysosomal marker was studied using confocal microscopy. Rab-GTPases are proteins that regulate trafficking between cellular organelles[187] (Figure 4-4). Since different rab proteins are associated with specific intracellular routes, labeled rab proteins can be used to identify cellular vesicles in live cell experiments.

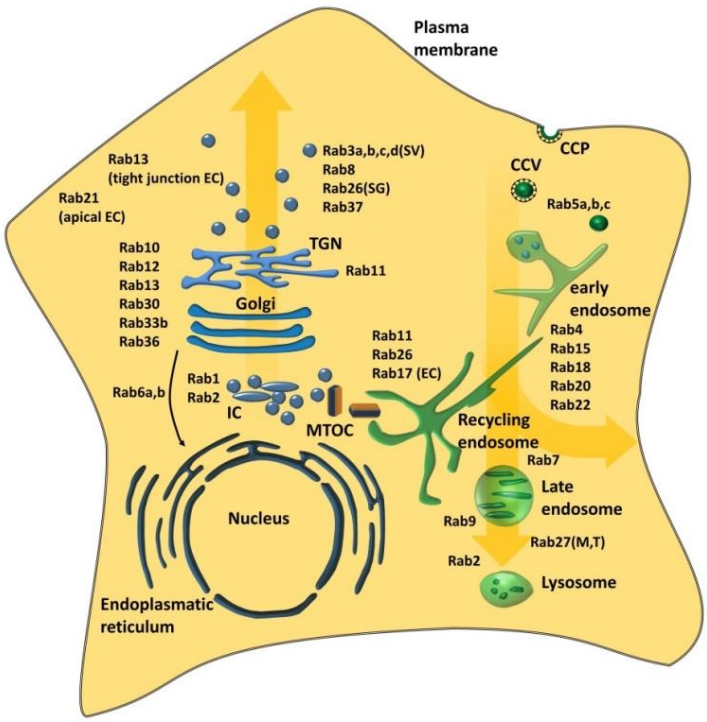

Figure 4-4: Intracellular localization of rab proteins. Whereas most of the known rab protein are ubiquitous in all mammalian cells and bind many cellular membrane compartments from clathrin coated pits and vesicles (CCV) over early, late and recycling endosomes to lysosomes and ER-Golgi intermediate compartments (IC), Golgi apparatus, trans-Golgi network (TGN) and plasma membrane, some rab protein are cell or tissue specific (M=Melanosomes, SG=secretory granules, T=T-cell granules). Adapted from [187].

Four different rab proteins were coexpressed with gp41-YFP to study transport and in particular endocytosis of the viral chimeric proteins. In addition, cells expressing gp41-YFP were stained with a lysosome-specific dye to cover a wide spectrum of cellular membranous compartments. Again, a correct folding and only minor degradation of gp41-YFP were pointed out by the finding of a negligible localization in lysosomal vesicles (Figure 4-5). Clear colocalization on the other hand was found with the endocytosis- and recycling-associated rab proteins rab5, rab7, rab11 (Figure 4-5). This is indicative of the efficient reinternalization of gp41-YFP that is caused by interactions between specific motifs within the protein's cytoplasmic domain and cellular trafficking proteins, namely the adaptor proteins AP-1 and AP-2[27].

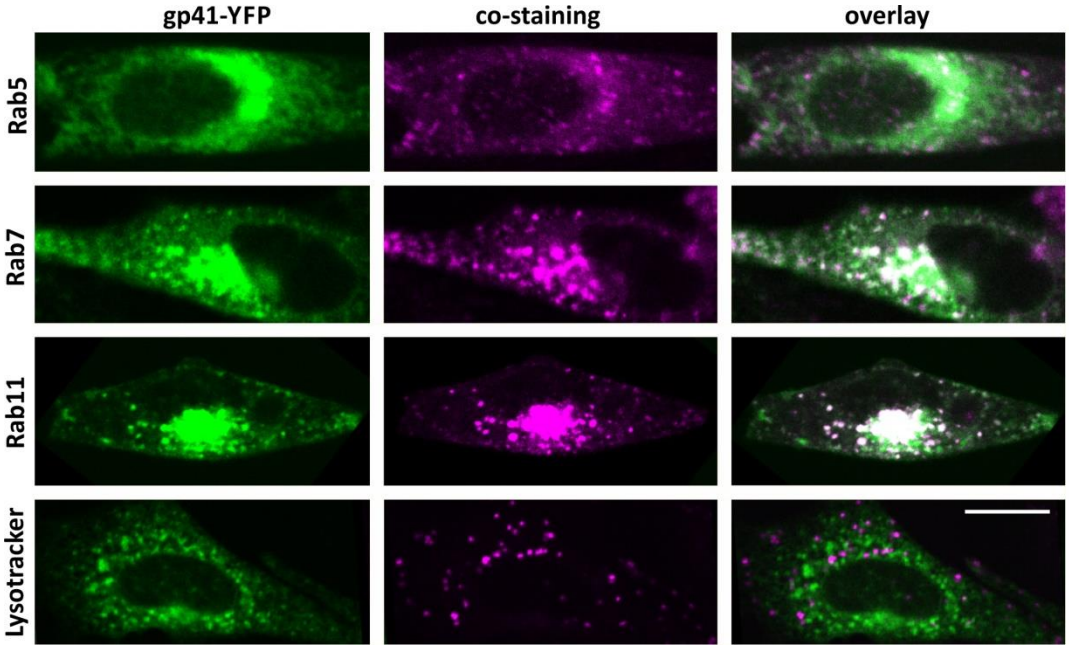

Figure 4-5: Intracellular transport of viral fusion proteins. Colocalization study of gp41-YFP with a lysosomal marker and different rab proteins indicative of early endosomes and clathrin-coated vesicles (rab5), late endosomes and lysosomes (rab7) and early and recycling endosomes (rab11). White areas indicate co-localization in the overlay images. Scale bar, 10µm.

4.2.2 Incorporation of the construct in virus-like particles

Fluorescent gp41-YFP is incorporated into virus-like particles (VLPs). During the assembly process enveloped viruses not only have to target their components to the site of assembly but they also have to efficiently bend cellular membranes and induce curvature to finally form infective particles. In case of HIV the Gag polyprotein alone is necessary and sufficient to bend bilayers and even cause virion release. In absence of other viral components, Gag expression causes formation of virus-like particles that resemble their pathogenic equivalents in size and shape. Since in released virus particles Gag forms a polymeric layer of proteins, it is the only viral component able to interact with the HIV envelope complex. Therefore, gp41 incorporation in VLPs strongly resembles the physiological equivalent in the infection context.

The protocol for this method was established and improved before with HEK293T cells (personal communication, Andrea Gramatica, Humboldt University). The cells were transfected with gp41-YFP and Gag-GFP separately or co-transfected with both proteins and after 48 h emerged VLPs in the supernatant were scrutinized using SDS-PAGE and Western blot. As expected, solely expression of Gag-GFP yielded high amounts of VLPs indicated by a strong band of the protein whereas gp41 transfected alone could not be detected in the respective supernatants (Figure 4-6). On the other hand, clear bands of both virus-derived proteins, were found in the supernatant of co-transfected cells (Figure 4-6). This result proves incorporation of gp41-YFP in nascent virus-like particles and points to a wild type like behavior in the assembly and budding context.

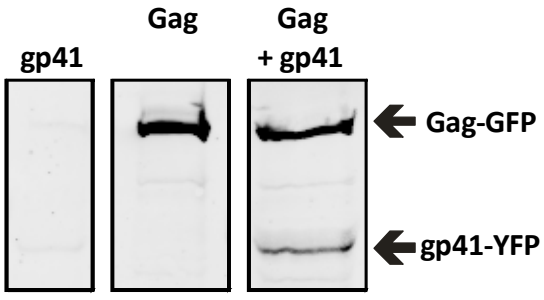

Figure 4-6: Characterization of virus-like particles. HEK293T cells were transfected with the indicated proteins labeled with YFP (gp41-YFP) or GFP (Gag-GFP). 48 h post-transfection the cell supernatant was harvested and a sucrose cushion purification was conducted. Obtained virus-like particle preparations were subjected to electrophoresis separation in a 10 % SDS-polyacrylamide gel and detected on Western blots using anti-GFP antibodies.

4.3 Investigating plasma membrane raft partitioning of gp41

In the preceding sections gp41-YFP could be demonstrated to mimic and resemble the behavior of the wild type envelope complex regarding intracellular trafficking and interactions with other viral proteins. For the remainder of the study the partitioning in plasma membrane lipid rafts should be in the focus. To this end, gp41-YFP was co-expressed with the raft marker GPI-CFP in CHO-K1 cells and examined with the confocal FLIM-FRET setup as described above (3.2.3.2). The results of *one* typical experiment are displayed in Figure 4-7. As previously shown [98,139], the raft marker clearly localized at the plasma membrane (Figure 4-7A) and amplitude-weighted CFP fluorescence lifetimes of around 2.5 ns were obtained (Figure 4-7C). To prove the reliability of the method, different positive controls were performed. Firstly, GPI-CFP was co-transfected with GPI-YFP as a raft clustering positive control. Both proteins were colocalized (Figure 4-7A), mainly at the plasma membrane and to a lower extent also in the Golgi apparatus. A reduced average CFP lifetime was measured, corresponding to a FRET efficiency of around 8 % (Figure 4-7B). For comparison, a GPI-anchored construct double-labeled with a linked CFP and YFP tag was investigated. This protein produced lifetimes below 2 ns, reporting a FRET efficiency of around 20 % (Figure 4-7B). The intracellular distribution of the chimeric gp41-YFP strikingly differed from that of GPI-anchored fluorescent proteins (Figure 4-7A). As described before, the glycoprotein was enriched in Golgi apparatus and intracellular vesicles while only a smaller fraction was found at the plasma membrane (Figure 4-7A, compare also 4.5.2). Nevertheless, upon co-expression with gp41-YFP the lifetime of GPI-CFP was significantly reduced, corresponding to a FRET efficiency of around 5-6 % (Figure 4-7B). To exclude that this decrease of the CFP lifetime results from cellular changes induced by the overexpression of the viral protein, GPI-CFP co-transfected with gp41-cherry instead of gp41-YFP was investigated. Since the spectral overlap of cherry with CFP is rather small compared with that of YFP and CFP, the reduction of donor lifetime in presence of this acceptor protein should be less pronounced. Indeed, essentially no decrease in the CFP fluorescence lifetime (Figure 4-7B) was found, confirming that the drop in presence of YFP labeled fusion proteins is a result of occurring FRET.

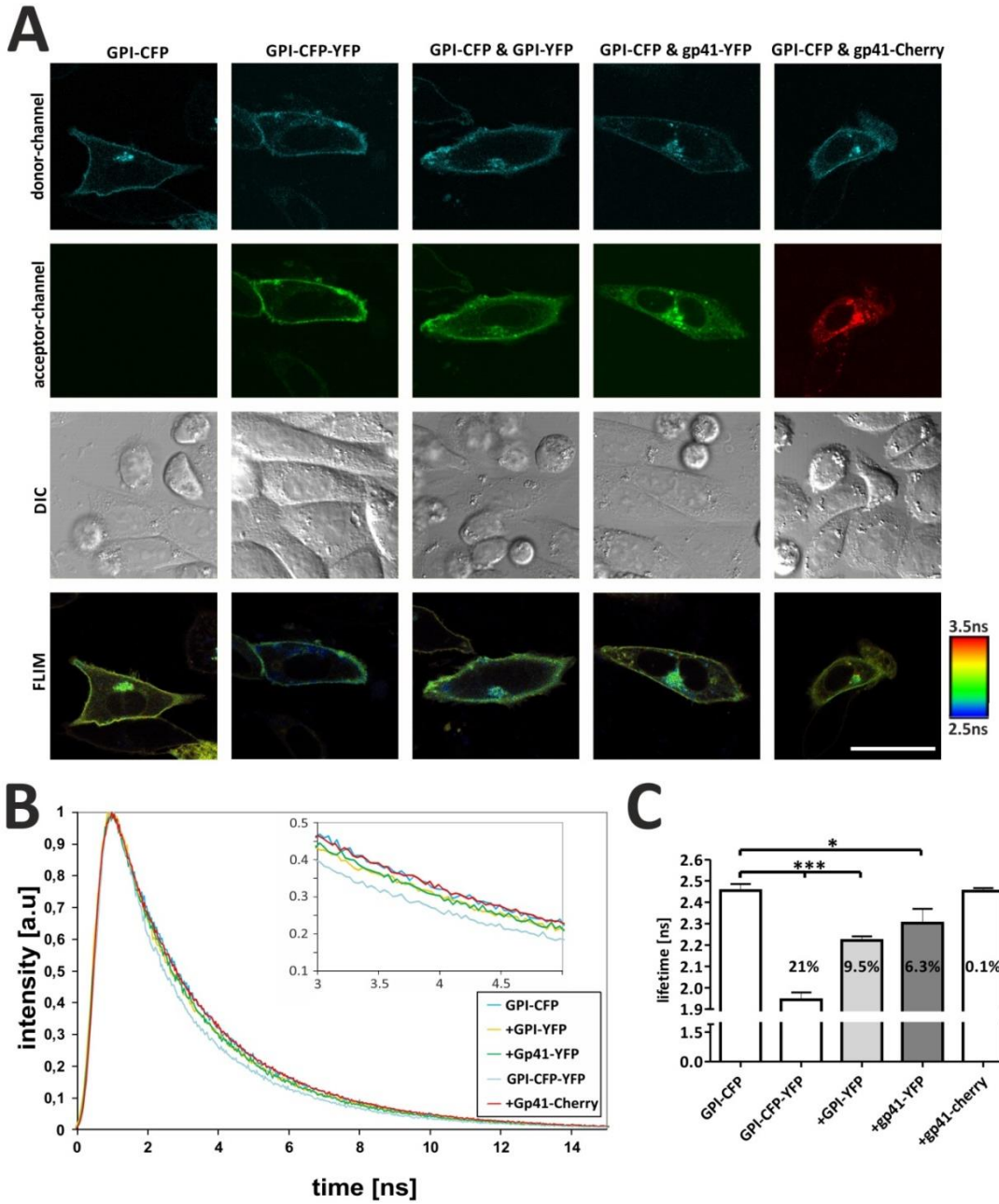

Figure 4-7: FLIM-FRET analysis of fluorescently labeled gp41 and GPI-constructs from one experiment. (A) Confocal and FLIM images o f CHO-K1 cells expressing the FRET donor GPI-CFP and different proteins labeled with YFP or Cherry as FRET acceptors. FLIM images are shown in pseudocolors displaying long lifetimes in red and yellow (i.e. first column) and shorter lifetimes in green and blue (i.e. second column). Scale bar, 20µm. (B) CFP fluorescence lifetime histograms of plasma membranes from cells containing GPI-CFP and YFP-labeled fusion proteins. A magnification of the decays is depicted in the inset (C) Examples of amplitude-weighted average CFP lifetimes at the plasma membranes of 10-15 cells per sample analyzed from one individual experiment. The corresponding FRET efficiency is indicated in the columns. The asterisks denote *** $p<0.001$, * $p<0.05$ by Student's test for unpaired data.

4.4 Perspectives - gp41 trafficking

In the "Perspectives" sections, experiments are described that were conducted to target some of the comprehensive questions that emerged from the observations circumstantiated so far. The results have been exerted from just a few, not sufficiently verified trials and should be contemplated with caution. However, although continuative and repeated experiments are necessary to proof the observations they allow glimpses on possible upcoming findings.

The trafficking of gp41 is a typical example for a biological process that has significant consequences for many, not directly connected experimental questions. For example, studying raft partitioning of a protein, independent of the method applied, requires an, at least to a certain extent, stable localization at the plasma membrane. As described before (1.2.4) the HIV-1 glycoprotein is known to contain several motifs mediating interactions with cellular components and causing an efficient reinternalization from the cell surface. This has to be taken into account when designing raft partitioning experiments and interpreting obtained results. There is a huge variety of methods available to elucidate the role of host cell proteins in infection progression and virus assembly. Direct interactions between the molecular components can be studied biochemically using crosslinking and co-immunoprecipitation assays, yeast two hybrid systems or by techniques like surface plasmon resonance and FRET approaches. Nevertheless, much additional information can be gathered by more indirect approaches. Particle tracking for instance can generate data allowing to specifically identify cellular routes utilized by a protein under study. Time correlated localization studies, usually via pulse chase assays, do report on the exact lifecycle and fate of newly synthesized proteins in expressing cells. Both kind of approaches were exerted to study gp41 constructs in a cellular context.

4.4.1 Particle tracking of fluorescently labeled fusion proteins

In recent years many cellular factors of the envelope complex' intracellular trafficking have been discovered. Nevertheless, the exact progression of the protein transport and the significance of many of the pathogen-host interactions are not completely understood.

The gp41-YFP fusion protein seems to be transported in kinesin associated vesicles. To shed further light on precise progression of gp41 trafficking in expressing cells, particle

tracking experiments were conducted. Cells transfected with gp41-YFP were observed using confocal microscopy with a high temporal resolution. Obtained t-stacks were then semi-automatically analyzed to generate single particle trajectories and thus motility data. Peak velocities of 200-800 nm/s were obtained and the trajectories (Figure 4-8) indicated movement in many different directions (towards the nucleus, directing to the periphery of the cell). The velocities point to a basically kinesin driven transport[188]. Considering that gp41 has been reported t o interact with the adaptor proteins AP-1 and AP-2, which are known to link cargo with kinesin proteins[189] this finding is in agreement with literature-based expectations.

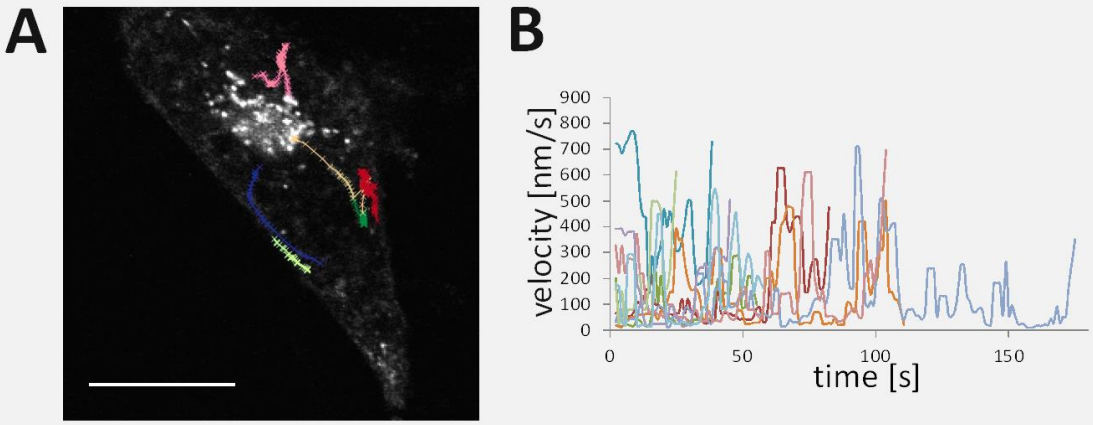

Figure 4-8: Particle tracking of gp41-YFP containing vesicles in CHO-K1 cells. (A) Confocal image of a cell expressing gp41-YFP with different independent trajectories displayed as colored lines. (B) Particle velocities of single vesicles calculated from time stacks of 180 seconds in length. Scale bar, 10µm.

4.4.2 Timing of gp41 intracellular distribution

An open question regarding the gp41 live cycle is how exactly the protein's progression is in infected cells. Although it is well understood what cellular trafficking proteins it interacts with and thus what routes it follows, the order and context of different transport steps need to be further elucidated.

By replacing the YFP fluorescent tag with a newly developed fluorescent timer protein, we addressed this question in live cell experiments. Fluorescent timer (FT) proteins were designed to change their excitation and emission upon aging[170]. The molecular basis of that transformation is the protein's maturation process. In its final conformational state, a FT protein shows a red fluorescence, but shortly after synthesis its nascent conformation causes a

transient emission of blue light (Figure 4-9B). As a result of that, individual proteins linked with a timer fluorophore can be classified with respect to their specific age just by assessing their fluorescence properties. Three different variants of the timer fluorophore were developed with deviating maturation kinetics, fastFT, mediumFT, and slowFT. For the dynamics investigated in this study, only the fast variant covers the relevant time scales and was thus used for the experiments described below.

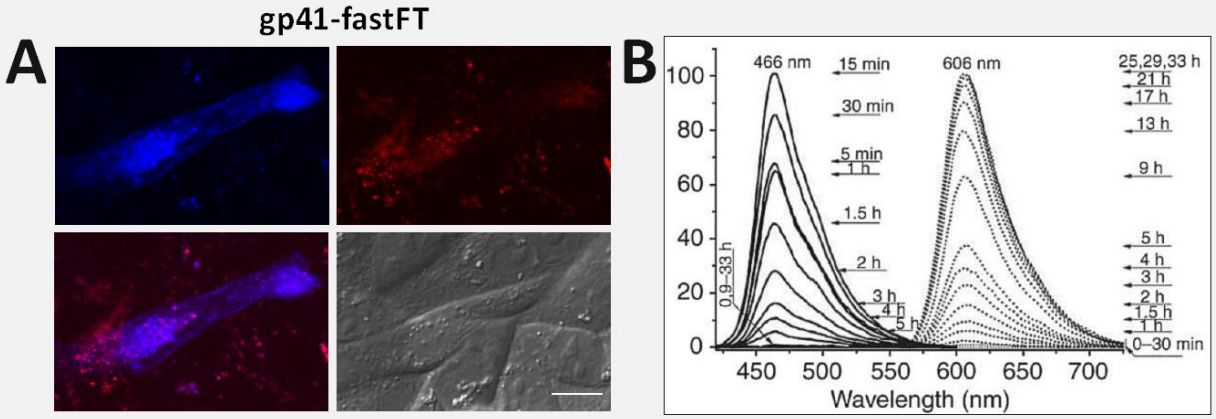

Figure 4-9: Confocal images of timer fluorophore-labeled gp41. (A) The quickly maturating timer fluorophore fastFT was used to replace YFP from gp41-YFP. Gp41-fastFT was expressed in CHO-K1 cells and imaged using confocal microscopy. (B) Spectrometric characterization of the fastFT emission in dependence of the maturation time (from Subach et al.[170]). Scale bar, 10µm.

The gp41-FT proteins remains intracellularly localized after reinternalization. Upon expression of gp41-fastFT in CHO-K1 cells, both protein forms (blue and red) were found distributed over most of the cell body. But, significant differences were found in the cell periphery and perinuclear region (Figure 4-9A). Whereas red fluorescence was found to be concentrated in the perinuclear region, the blue form of the protein was easily visible in the plasma membrane and Golgi apparatus. Interestingly, this observation indicates that only younger proteins are localized at the plasma membrane. If gp41 would be reinternalized and then recycled to the plasma membrane, older proteins (red fluorescence) should be detectable at the surface as well. It appears promising to conduct further experiments to characterize the gp41 succession in the cell in more details. A fluorescent timer pulse chase approach using inducible promotors as described in Subach et al. for LAMP-2A[170] most likely will allow a precise elucidation of the trafficking steps of the protein.

4.5 Chasing the molecular basis of gp41 raft partitioning

In the preceding part the FLIM-FRET based raft partitioning assay was established and verified by conducting different negative and positive controls. Moreover, the chimeric protein gp41-YFP was demonstrated to still exhibit many important features of its physiological counterpart, the native gp160 protein. Intracellular distribution and trafficking, but also incorporation in virus-like particles were indicated to be undisturbed by the fluorescent labeling. Next, to elucidate the intrinsic domains, motifs or amino acids responsible for the properties of the protein, truncation and mutation variants had to be generated.

4.5.1 Construction of gp41-truncation and mutation variants

Numerous variants of the original, membranotropic wild type gp41-YFP were produced. Substantial protein section or complete domains were removed to unravel the role and significance of gp41 motifs for raft partitioning, trafficking and other assembly related properties (Figure 4-10).

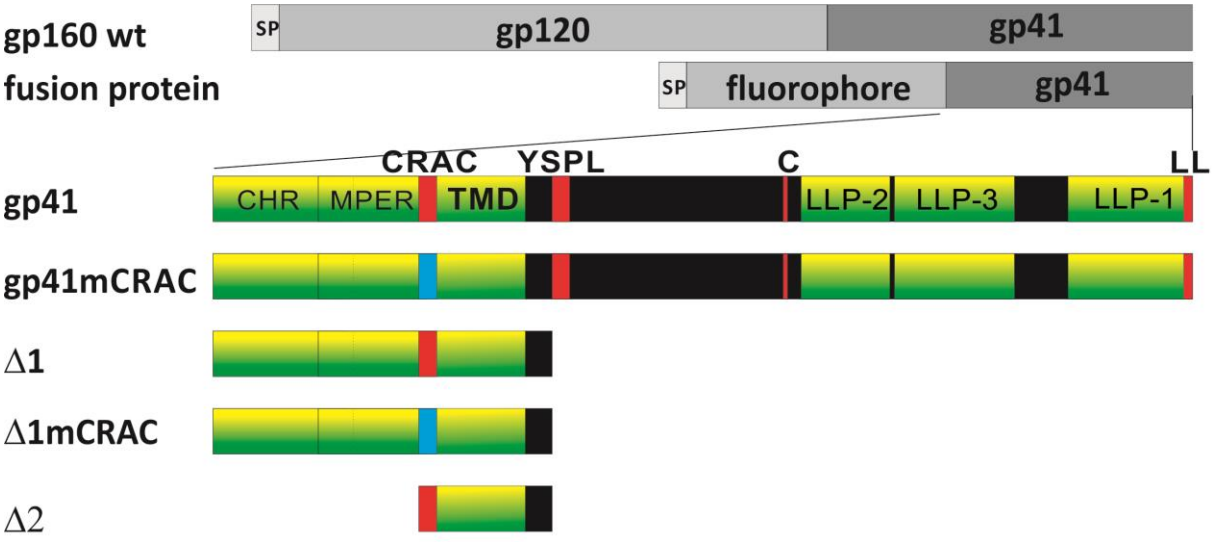

Figure 4-10: Gp41 fusion protein variants. Schematic representation of different fluorescently labeled gp41 variants. Important sequences, such as CRAC, YSPL internalization signal, palmitoylated cysteine and the C-terminal dileucine motif are highlighted in red whereas the mutated CRAC is displayed in blue. The α-helical sections of the protein are shown in green and yellow. SP=Signal peptide.

Two truncation variants are of particular importance in the following investigations. The protein Δ1 was generated by removing most of the cytoplasmic domain (truncation at amino acid 703) of the wild type-like gp41-YFP. An additional removal of the external MPER (amino acid 670), but retaining the CRAC domain was performed to generate the Δ2 variant. Moreover, a leucine to isoleucin exchange in the gp41 CRAC domain, yielding gp41mCRAC and Δ1mCRAC, was conducted. Since cholesterol is highly enriched in lipid rafts, the functionality of this cholesterol binding motif should have a significant impact on the protein's raft partitioning.

4.5.2 Characterization of gp41 fusion proteins

The cytosolic region of gp41 contains three known amino acid sequences mediating interaction with different cellular adaptor proteins that are involved in directed vesicle transport (see 1.2.2.3). To study the influence of those motifs and other parts of the cytoplasmic domain in that context, the truncations and mutations were investigated to characterize their role for gp41 localization and trafficking.

The variant Δ1 shows physiological intracellular trafficking. Colocalization studies as described before (4.2.1) were performed to reveal the role of the gp41 cytoplasmic tail in the context of endocytosis. The CT truncation variant Δ1 was co-transfected with rab5, rab7 and rab11 or stained with ER-tracker and lysotracker after transfection. Negligibly colocalization was found again with ER and lysosomal marker indicating a physiologic synthesis and folding (Figure 4-11). Compared to the wild type-like gp41-YFP (Figure 4-5), slightly less spatial correlation was found with rab5, rab7 and rab11 reflecting a significantly reduced endocytosis of that truncated variant lacking all 3 known internal, endocytosis-related interaction motifs (Figure 4-11).

The gp41 cytosolic domain restricts gp41 surface exposure. Total internal reflection fluorescence microscopy can be used to exclusively image fluorescent molecules close to the surface of the microscopic slide. Therefore, it is an ideal tool to study fluorescent proteins at or adjacent to the surface of an expressing cell. Gp41-YFP was detected using conventional epifluorescence microscopy yielding the already described distribution of fluorescence with a bright spot in the Golgi apparatus and no clearly visible staining of the plasma membrane. Upon TIRFM illumination, the fluorescence signal from perinuclear compartments was

considerably reduced and the fine structure of the plasma membrane emerged. This finding is indicative of a surface exposure of the protein under study and supports the assumption that the fluorescently tagged gp41-YFP construct is expressed physiologically. Nevertheless, the protein variant Δ1 showed significantly more plasma membrane exposure due to the removal of the cytoplasmic internalization motifs.

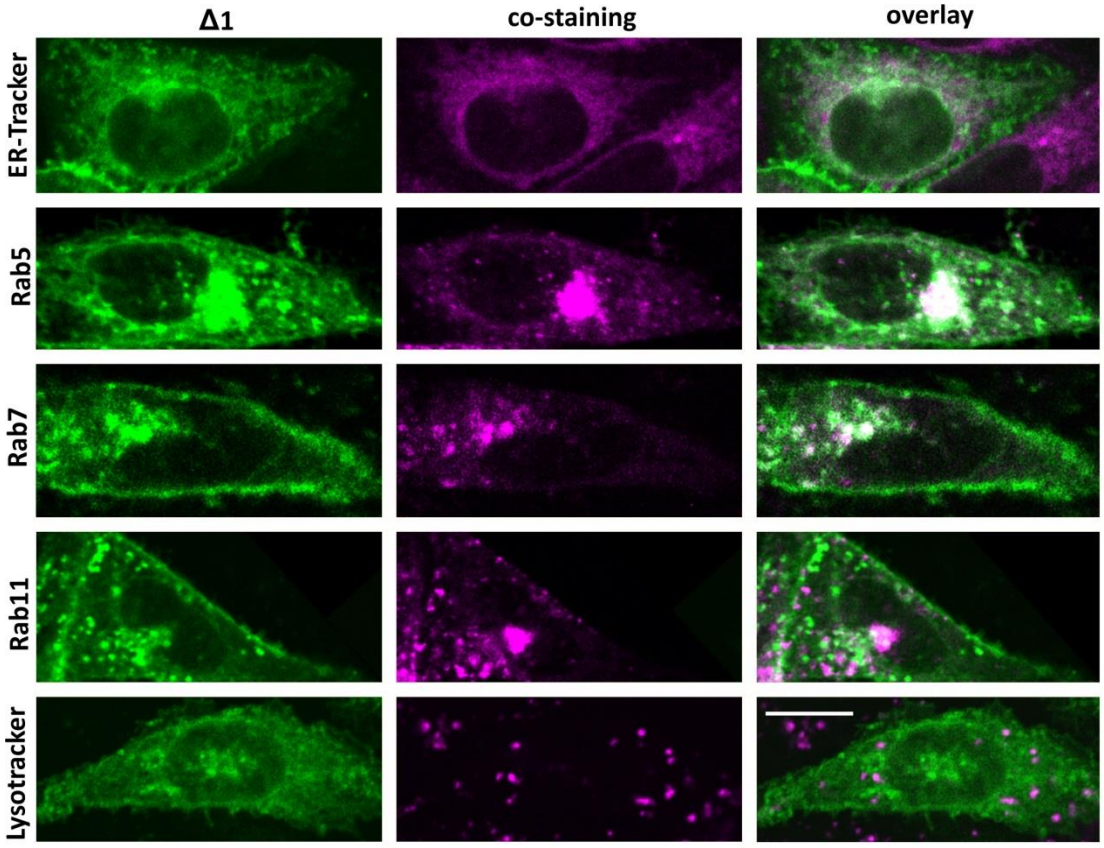

Figure 4-11: Intracellular distribution of the Δ1 variant. Colocalization study of Δ1 with lysosomal and ER-specific markers and different fluorescently labeled rab proteins as reporter of early endosomes and clathrin-coated vesicles (rab5), late-endosomes and lysosomes (rab7) and early and recycling endosomes (rab11). Scale bar, 10µm.

The localization of different gp41 variants was furthermore investigated utilizing confocal microscopy. Obtained fluorescent images from equatorial slices of transfected cells were analyzed regarding plasma membrane fluorescence. Cells were co-transfected with GPI-CFP and gp41 variants since the CFP fluorescence allows an easy identification of the plasma membrane on confocal images. After selecting the plasma membrane in CFP images, the YFP fluorescence in the same region of interest was assumed to report plasma membrane expression of the YFP-labeled protein under study. As expected, gp41-YFP was significantly

depleted at the plasma membrane compared to the cytoplasmic truncation variant Δ1 (Figure 4-12B). Nevertheless, for both variants (gp41-YFP and Δ1) the surface exposure was found to be unaffected by the introduction of a CRAC-mutation, demonstrating that differences in the raft related FRET between mutant and respective wild type (gp41mCRAC and gp41-YFP, Δ1mCRAC and Δ1) are not a side effect of a changes in the plasma membrane expression (Figure 4-12). Surprisingly, the Δ2 variant showed a decrease in the surface exposure compared to the Δ1 variant. It is unlikely that this is a result of a recovery of the gp41-internalization since Δ2, as Δ1 lacks all intrinsic endocytosis motifs. Probably, it is rather consequence of an in general lower expression level of the Δ2 construct.

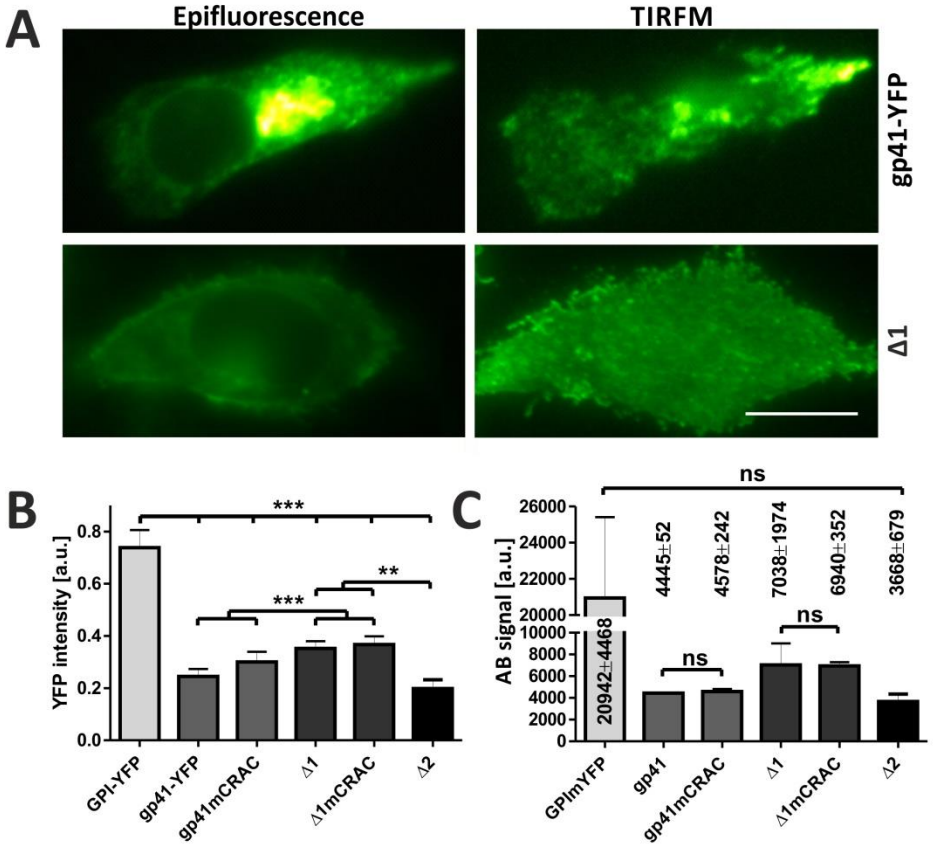

Figure 4-12: Plasma membrane exposure of gp41 fusion proteins. (A) Epifluorescence and TIRFM images of CHO-K1 cells expressing gp41-YFP or Δ1. Scale bar, 10µm. (B) The average YFP intensity at the plasma membrane of transfected CHO-K1 cells was obtained by analyzing background corrected confocal images. Each bar represents 20-50 cells from at least 2 independent experiments. (C) The anti-GFP fluorescence signal was detected as a measure of YFP plasma membrane expression in flow cytometer experiments. Individual bars represent at least two independent experiments. Individual bars represent two independent experiments. In all graphs the error bars display SEM. *** $p<0.001$, ** $p=0.001$-0.01, ns $p>0.05$.

Both aforementioned methods have their intrinsic limitations. Since in the image analysis assay only equatorial slices of the cells were analyzed, it can be argued that the results might only report the protein distribution in a distinct, potentially not representative region of the cells. TIRFM on the other hand gives only an impression of the surface exposure whereas quantification is difficult. Moreover, both described assays do not allow distinguishing between surface expression and intracellular fluorophores close to the plasma membrane. Even TIRFM, although it offers a minimal penetration depth of around 50-100 nm achieved with our instruments, still illuminates not only the plasma membrane but also adjacent cytoplasmic compartments. Therefore, flow cytometric, live cell immunofluorescence experiments were conducted. Anti-GFP fluorescent antibodies were used to specifically label those fusion proteins that are localized at plasma membrane, since only this population exposes its YFP to the extracellular environment. Then, the fluorescence emission of both reporters, YFP and the fluorescent moiety of the antibody was assessed in the flow cytometer experiments. Expressing cells were selected with respect to their YFP signals and the fluorescence intensity of the antibody was quantified as a measure of the fusion protein surface exposure. The results strongly resemble the observations described before (Figure 4-12). Both mutants displayed no significant differences to their respective wild type forms and again the Δ1 plasma membrane exposure was increased compared to the gp41-YFP construct and Δ2. The findings demonstrate that the microscopic assays described above, although only considering equatorial slices and based on image analysis of conventional confocal images, can be used to obtain quantitative data about plasma membrane localization. For comparison, GPI-YFP was analyzed with both approaches as well and the raft marker protein was found to be in three to five fold higher concentrations at the plasma membrane than the virus protein variants.

The gp41 cytoplasmic tail exclusively controls reinternalization. We hypothesized that the finding of a relatively low plasma membrane signal of Δ2 compared to Δ1 is a result of an in general lower expression level than the other fusion protein variants. This observation illustrates that the overall expression of the different labeled proteins cannot be expected to be identical and the cellular distribution has to be studied in more detail to obtain meaningful data regarding trafficking and reinternalization. To this aim, the flow cytometric live cell assay described before was expanded (Figure 4-12). Again, cells transfected with fluorescently labeled proteins were stained with anti-GFP fluorescent antibodies to quantify

the amount of surface exposed proteins. In addition, the ratio of antibody to YFP signal was assessed as a measure of plasma membrane to overall expression (Figure 4-13).

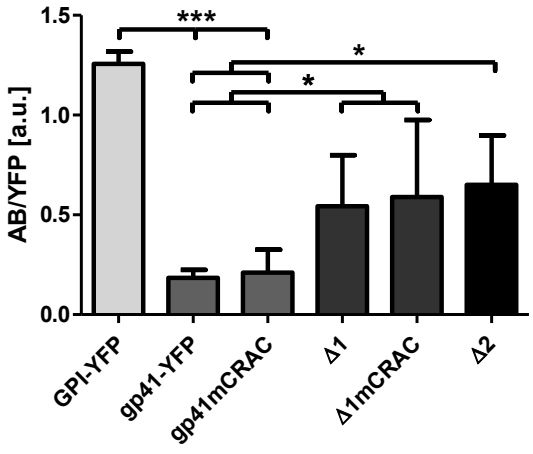

Figure 4-13: Plasma membrane versus overall expression ratio of gp41 fusion proteins. The anti-GFP fluorescence signal was detected as a measure of fusion protein plasma membrane expression in flow cytometer experiments. The ratio of antibody fluorescence versus overall YFP fluorescence is displayed to qualitatively investigate the proportion of protein expression in general to plasma membrane expression. Individual bars represent at least two independent experiments. In all graphs the error bars display SEM. *** $p<0.001$ and * $p=0.01$-0.05, ns $p>0.05$.

In this assay, all variants with a truncated cytoplasmic tail, namely Δ1, Δ1mCRAC and Δ2 displayed similar ratios whereas a significantly lower ratio was found for gp41-YFP and gp41mCRAC (Figure 4-13). Since the truncation variants (Δ1, Δ1mCRAC and Δ2) are all deficient in the interactions with cellular adaptor proteins this observations underline the relevance of the cytoplasmic tail for gp41 re-internalization. Moreover, it is indicated that the cellular distribution and in particular the gp41 reinternalization, is mainly controlled by the cytoplasmic tail whereas the external region that was removed from the variant Δ1 to obtain Δ2, did not contribute to this property. In agreement with the microscopic assay, both CRAC mutants displayed an intracellular distribution that resembles their respective wild type forms (Figure 4-13).

4.5.3 Plasma membrane raft partitioning of gp41 variants

The extracellular CRAC motif is the major factor of the gp41 plasma membrane raft association. In confocal microscopy, all gp41 variants proteins showed accumulations in the

perinuclear region but their plasma membrane exposure significantly differed. Gp41-YFP and gp41mCRAC were always found to be very weakly expressed at the surface, whereas significantly higher concentrations were usually found for all variants lacking the cytoplasmic domain (Figure 4-10). As rationalized before (4.5.3), the truncation variants were found to be enriched at the plasma membrane compared to the wild type gp41-YFP due to the removal of the protein's cytosolic domain that comprises all protein inherent endocytosis motifs[46,94] (compare also the section 4.5.2). Nevertheless, co-transfection of wild type protein gp41-YFP or the truncation variants Δ1 and Δ2 with the raft marker GPI-CFP caused comparable decreases of donor lifetimes, reproducibly yielding average FRET efficiencies of around 5 percent (Figure 4-14, Table 23).

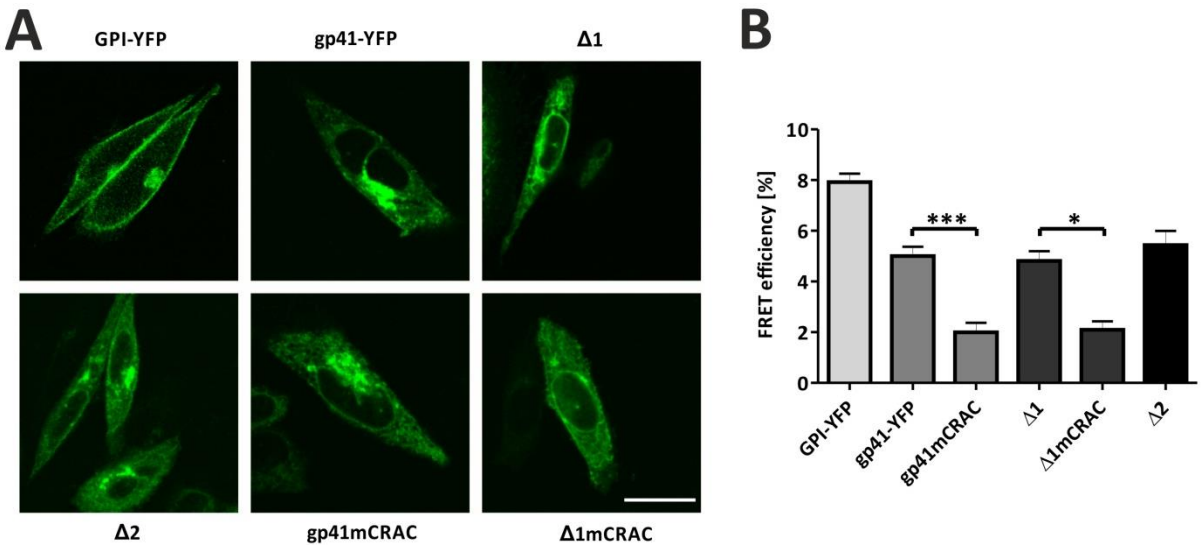

Figure 4-14: Confocal images and obtained FRET efficiencies of fluorescent gp41 variants. (A) Typical confocal images of GPI-YFP and various YFP-tagged gp41 variants expressed in CHO-K1 cells. Scale bar, 15µm. (B) Average FRET efficiencies with SEM calculated from measuring the lifetimes in the plasma membrane of at least 3 independent experiments each with 10-20 cells analyzed for each protein under study. The asterisks denote *** $p<0.001$, ** $p<0.01$, * $p<0.05$, ns $p>0.05$ by Student's test for unpaired data.

To investigate the role of cholesterol in the gp41 lateral organization, CRAC mutants of the wild type and the variant Δ1 were scrutinized. Upon co-transfection with GPI-CFP lower FRET efficiencies were found for both, gp41mCRAC and Δ1mCRAC (Figure 4-14, Table 23) reproducibly. Since intracellular distribution and expression levels were comparable to their respective wild type proteins (compare 4.5.2) this finding substantiates a specific function of the CRAC motif in lateral plasma membrane sorting to microdomains that contain GPI-

anchored proteins. For the sake of completeness, the different aforementioned positive and negative controls (4.3) were repeated several times to obtain significant data from independent experiments for all proteins investigated. All obtained fluorescence lifetimes are stated in Table 23. It is of note that the absolute lifetime values from the individual experiment reported in Figure 4-7 strikingly differ from the average values reported here. This is indicative of the high variability of CFP-lifetimes between different experiments. Low standard deviations could be achieved only by several repetitions of the measurements.

Table 23: Fluorescence lifetimes of GPI-CFP in presence and absence of different FRET-acceptor proteins. Average CFP lifetimes with SEM of at least 3 independent experiments each with 10-20 cells analyzed for each protein under study.

sample	GPI-CFP	GPI-CFP & GPI-YFP	GPI-CFP-YFP	GPI-CFP & gp41-YFP	GPI-CFP & gp41 mCRAC	GPI-CFP & gp41 Cherry	GPI-CFP & Δ1	GPI-CFP & Δ1 mCRAC	GPI-CFP & Δ2
τ_{av} ***[ns]***	**2.53** ±0.01	**2.38** ±0.01	**1.94** ±0.01	**2.42** ±0.01	**2.52** ±0.01	**2.52** ±0.01	**2.40** ±0.02	**2.46** ±0.01	**2.4** 0±0.02

4.6 Verifying plasma membrane raft clustering

To verify the reliability of the FRET-based assay an analysis approach was used which was initially introduced by Zacharias et al[144]. According to that reference, FRET efficiencies are independent of acceptor concentrations, if energy transfer does not originate from random fluorophore interactions. We applied this model by plotting the acceptor intensity, which is proportional to the fluorophore concentration, versus the FRET efficiency for at least 20 cells per protein studied (Figure 4-15). The FRET efficiencies of cells expressing the CRAC-comprising variants gp41-YFP, Δ1 and Δ2 showed saturation at low expression levels, which indicates a non-random organization (Figure 4-15, black plots). Importantly, the distribution of our experimental values in the three plots suggests an additional complexity of the system under study. As every dot represents an individual FRET value of one single cell, the plots indicate different populations of cells, at least two, with different, raft-related properties. To take this into account, the two populations were divided in groups of cells with FRET efficiencies of below and above 10 %. Both populations were then used for additional fits yielding significantly better statistics (Figure 4-15, light and dark grey). An interesting result

was obtained for the cherry-labeled variant of gp41. As described before, this chimeric protein was generated by replacing YFP with Cherry, yielding a construct that can be assumed to possess the same raft association as gp41-YFP but, due to the low spectral overlap of the fluorophore's excitation with the FRET-donor emission, should show a significantly reduced energy transfer. Of course, dissociation constants and acceptor intensity values from experiments with cherry cannot be directly related to the respective YFP results. Differences in molecular brightness of the fluorophores, excitation laser and emission wavelength impede a direct comparison.

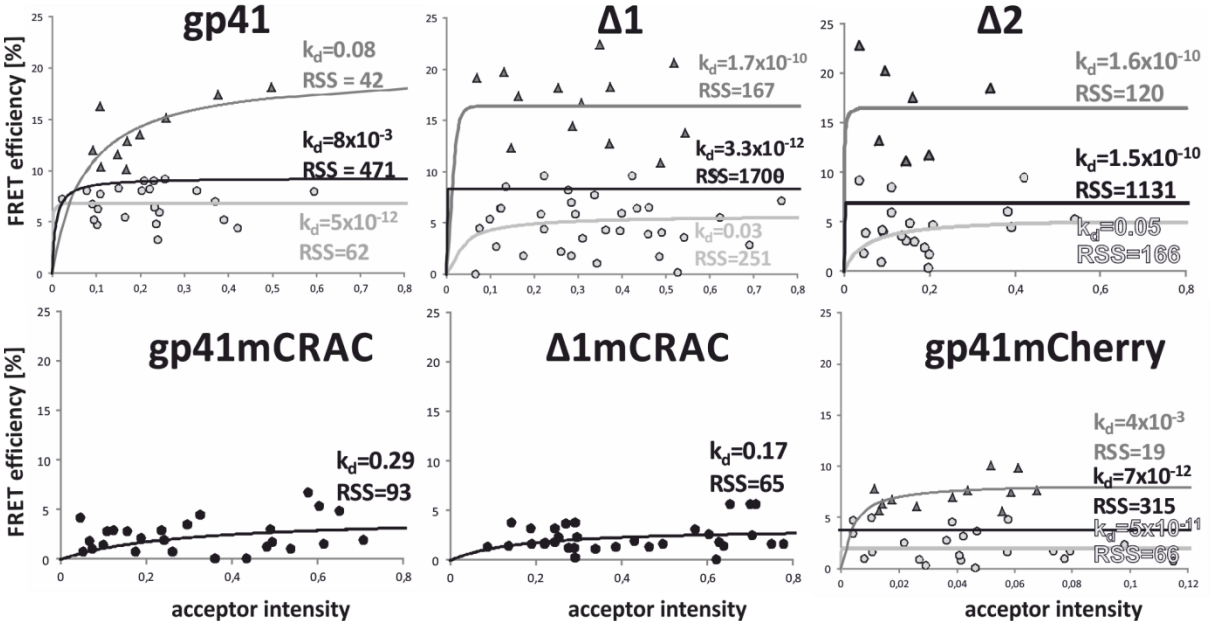

Figure 4-15: Raft clustering analysis of gp41 chimeric proteins. At least 20 cells of each fusion protein species were plotted and considered for overall binding kinetic fits (black). Two different subpopulations with FRET efficiencies of below (light grey, empty dots) and above 10 % (dark grey, filled triangles), respectively, were separately fitted for all proteins supposed to partition into lipid rafts. Dissociation constant K_d and residual sum of squares Rss are stated for every individual plot in the respective color.

However, although overall FRET efficiencies were, as expected found to be significantly reduced compared to gp41-YFP, again the fitting indicates saturation at low acceptor concentrations and two populations of cells resulting in different mean FRET values are suggested by the distribution of the data points. In contrast to that, obtained FRET efficiencies from the CRAC mutants, gp41mCRAC and Δ1mCRAC (Figure 4-15) turned out to be rather proportional to the surface density of the protein, reflecting that the FRET acceptor is randomly distributed in the plasma membrane and the slight decrease in the donor lifetime is a result of random collisions. Since local concentration and intracellular localization of both

proteins are very similar to their respective wild type forms (see 4.5.3), this observation demonstrates a CRAC dependent clustering of the glycoprotein gp41. We surmise that the FRET values assessed for the proteins gp41-YFP, Δ1 and Δ2 can be considered as reliable reporter of their accumulation in cholesterol enriched microdomains and are not an artifact of concentration dependent random interactions within the lipid bilayer or unwanted side effects of the fusion protein overexpression.

4.7 Insertion: Investigating population heterogeneities in membrane organization

As described before, unexpectedly our FRET data revealed considerable heterogeneities in the populations of transfected cells. At least two subpopulations with different microdomain properties were indicated. Taking into account that all gp41 constructs containing a functional CRAC domain showed virtually identical affinities to lipid domains, they should sense and report membrane organization comparably. Indicative of that assumption, we found a similar distribution of FRET values for all three constructs in the clustering analysis (Figure 4-15). Therefore, to shed further light on cell-to-cell differences in the lipid raft properties, FRET data of gp41-YFP, Δ1 and Δ2 joined in a common clustering analyses and histograms (Figure 4-16) yielding a more accurate analysis due to the higher number of observations considered. For comparison, the same procedure was conducted with the proteins that were found to be excluded from lipid rafts, namely gp41mCRAC and Δ1mCRAC. Merging all data from cells comprising a functional CRAC domain supports the previously suggested model. FRET versus intensity plots (Figure 4-16A) and even more strikingly the FRET histogram (Figure 4-16B) point to distinct and distinguishable populations of cells with a significant difference in the plasma membrane lipid rafts. Again, the assumption of a high and a low FRET population improved the curve fitting significantly, but furthermore, we found a clear bimodal distribution in the histogram with peaks at 6 and 18 % FRET efficiency, comprising about 80 and 20 %, respectively, of all cells considered. This observation indicates significant deviations of the plasma membrane organization between individual cells of a cell line and thus is in agreement with previous observations of a heterogeneity in the exposure of the raft related sphingolipid GM1 at the surface of monoclonal cells [190]. Conceivably, it reports a cell-to-cell variability in lipid rafts that could originate from differences in the lipid composition and physical properties of the domains, from their size and from their total fraction. Unexpectedly, a similar observation was made upon combining of all data of non-raft proteins

(gp41mCRAC and Δ1mCRAC). Single FRET efficiencies and saturation values were decreased compared to the non-mutants, but again the clustering analysis suggests two independent saturation plots and separate populations with peaks at 2 and 6 % were found in FRET histograms. Since the population of cells displaying FRET higher than 5 % just comprise 4 cells it is not useful to develop a model to explain this finding.

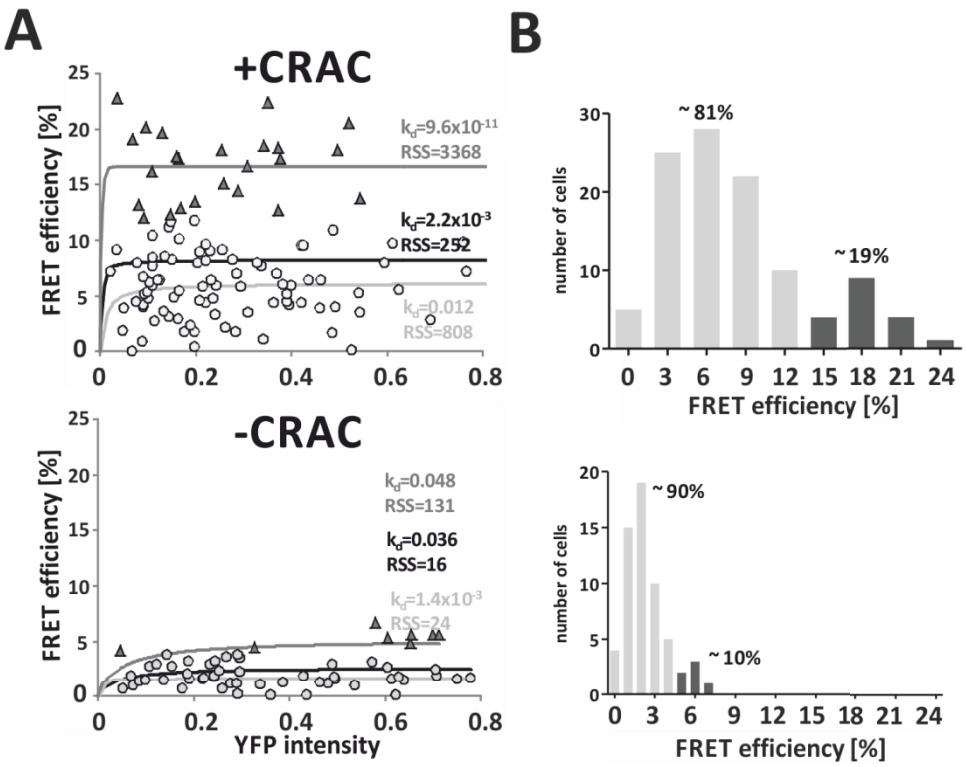

Figure 4-16: Microdomain heterogeneity. The FRET efficiencies of all proteins showing raft related FRET (gp41-YFP, Δ1, Δ2) and all proteins supposed not to partition into lipid rafts (gp41mCRAC, Δ1mCRAC) were combined in common FRET saturation analyses (A) and in FRET efficiency histograms (B). (A) Overall binding kinetic fits (black) are plotted together with two different fittings (light and dark grey) based on the two distinct subpopulations revealed in the respective histograms (B). According to the histograms, 12 % and 5 %, respectively were used as threshold to assign cells to the low FRET or high FRET population for the CRAC containing and lacking proteins. The fraction of the obtained populations is indicated in % in the histograms. Dissociation constant K_d and residual sum of squares Rss are stated for every individual plot in the respective color.

The objection might be raised that the populations found reflect differences between the proteins joined in the plots rather than differences of raft properties between cells. To face this question, the contributions of every of the single gp41 variants on the histogram was plotted in Figure 4-17.

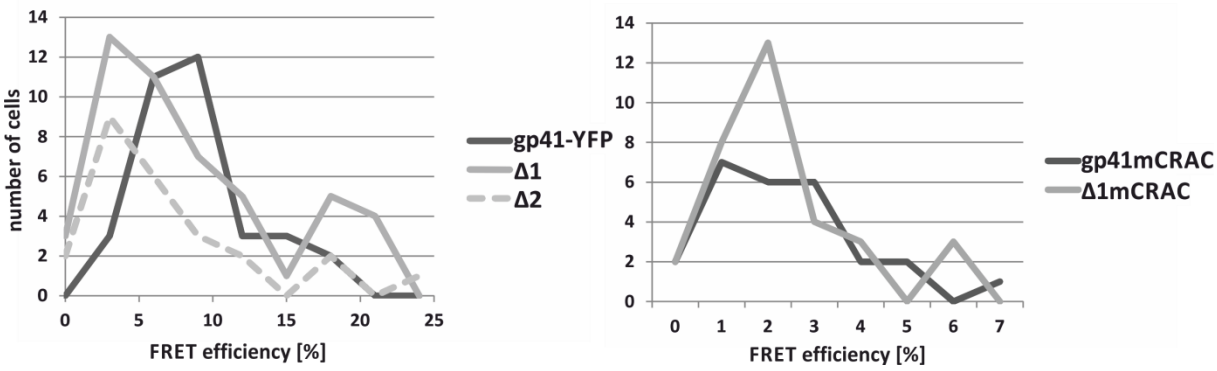

Figure 4-17: Individual protein contribution to raft populations. The FRET efficiency histograms of all individual CRAC-containing (gp41-YFP, Δ1, Δ2) and all individual CRAC-lacking proteins are plotted together to facilitate comparison.

An obvious conclusion from that plot is that the two individual Gaussian peaks observed in Figure 4-16 do not exclusively represent differences in the expressed protein. Nevertheless, although the overall number of single observations is, in particular for the CRAC-mutants, too low to deduce reliable conclusions, the distribution of the values from different proteins might contain additional information. Strikingly, Δ1 and Δ2, both lacking cytoplasmic domain and palmitoylation site, showed two completely separate peaks. Whereas those two truncation variants display distinct peaks at a low and at a high FRET efficiency, the wildtype is shifted towards medium values. Considering that FRET efficiency is a direct reporter of raft partitioning a careful examination of this observation might suggest lower maximum but also higher minimal raft partitioning of gp41-YFP compared to Δ1 and Δ2. This might point to a slightly more stable association of gp41-YFP with lipid rafts (indicated by the increase of the lower FRET efficiency). The decrease of the higher FRET efficiency of gp41-YFP might be a result of the in general lower plasma membrane expression compared to the truncation variant that is not sufficient anymore to completely saturate the is bigger lipid rafts of this population of cells.

4.7.1 Perspective: Cell-to-Cell variability in plasma membrane order

In the FLIM-FRET experiments described before, an unexpected observation was made. Systematic variations were found in the raft-related FRET efficiency of many different cells expressing fluorescently labeled proteins. We hypothesized that this heterogeneity is indicative of differences in the plasma membrane organization of the observed cells and thus rather reflects cellular properties than deviations in the expressed virus protein.

Cell-to-cell variability in membrane organization is an intrinsic property of homogeneous cell populations. CHO-K1 cells were seeded in low concentrations to study intra-population variations in the context of local density and position of individual cells in a colony (at the border or surrounded by other cells). At the next day, the cells were labeled with C6-NBD-PC, serving as a reporter of general membrane order. C6-NBD-PC shows fluorescence lifetimes that strongly depend on the organization of the membrane it is embedded in[112,191] and thus, ordered membrane environments are displayed by long lifetimes whereas disordered membranes cause a decrease of the stability of the excited state and thus a reduction of the fluorescence lifetime (Figure 4-18A).

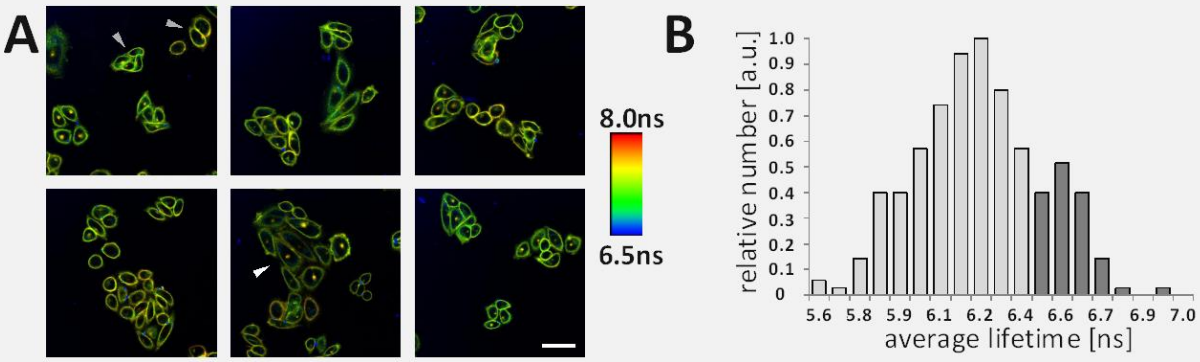

Figure 4-18: C6-NBD-PC fluorescence lifetime variations upon incorporation in cellular membranes. (A) CHO-K1 cells were labeled with C6-NBD-PC as a reporter of the membrane order. Amplitude-weighted average fluorescent lifetimes are displayed in pseudocolors in the range between 6.5 and 8 ns. Significant differences were found between single cells even within the same colonies (white arrow) or between cells in a similar local context (grey arrow). (B) Lifetime histogram of around 250 analyzed cells. Two populations were indicated by the plot, displayed in bright and dark grey, comprising around 80 and 20 % respectively. Scale bar, 40µm.

Again, a combination of all data in a histogram revealed two major populations, comprising 80 and 20 % of the cells (Figure 4-18B) which is in remarkable agreement with the previous experiments (see 4.7). CHO-K1 cells were investigated in different positions of a petri-dish and single colonies of variable size were selected to cover a wide spectrum of individuals with a differing local context. Although clear differences between single cells were found in this experiment, no obvious correlation between membrane order and position in the colony, position of the colony in the dish or cell shape were found. Contrary, significant differences were occasionally found between cells of a single colony or cells with the same size (Figure 4-18A, indicated by arrows). This observation points to another origin of the systematic differences obtained. We surmise that the cell cycle might be the underlying

process, since its progression requires extensive adaption of cellular structures and compartments.

Cell cycle progression is a possible source of the cell-to-cell heterogeneity in plasma membrane organization. To support this hypothesis we performed a well-established cell cycle experiment. To this aim cells were seeded in a low concentration to allow population cycling without any influence of contact inhibition. After one day of growth, cells were trypsinized and fixed with ethanol. Prior to the flow cytometer experiment, the sample was treated with PI allowing a quantitative staining of cellular DNA (Figure 4-19).

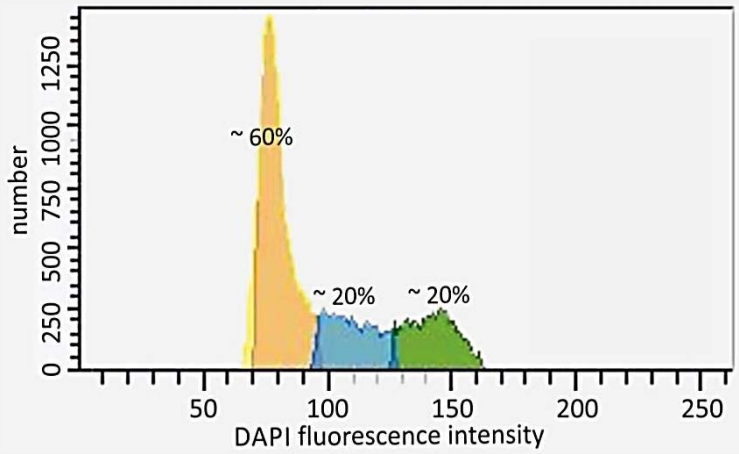

Figure 4-19: Flow cytometric cell cycle analysis. CHO-K1 cells were fixed, permeabilized and stained with PI to stain cellular DNA. Two clear peaks were found at 75 and 150 (a.u.) of PI intensity reporting a doubling of the DNA. The peaks comprised 60 and 20 %, respectively and the remaining events, representing cells in the S phase comprised again around 20 %.

Since the PI fluorescence of a single cell is proportional to the available amount of DNA cell cycle progression can be studied very precisely with this approach[192]. Fractions of around 20 % were found for cells either being in the G2/M phase or in the S phase. Thus, 60 % of CHO-K1 cells remain in the G1/G0 phase. Careful examination of images from FLIM-FRET and C6-NBD-PC experiments, showing that often smaller cells possessed high FRET values or C6-NBD-PC lifetimes (not shown), respectively, might indicate that indeed the condensing of DNA and cell body during division of the cell is accompanied by an increase of plasma membrane order.

4.8 Elucidating raft partitioning of gp41 variants in the Golgi apparatus

For all fusion proteins used in this study, including the GPI-anchored fluorescent proteins, accumulations in the perinuclear regions were found in at least some of the investigated cells. To clearly identify this cellular site, antibody stainings were conducted. GP41-YFP was expressed in CHO-K1 cells and the Golgi apparatus was targeted with anti-58K or anti-Giantin antibodies. Both cellular proteins clearly co-localized with the gp41-YFP accumulation in the perinuclear region (Figure 4-3) demonstrating that this intracellular protein accumulation site indeed constitutes this cellular compartment.

CRAC-dependent raft association of gp41 already occurs in the Golgi apparatus. It has been hypothesized that lipid rafts, which are generally supposed to be a feature of plasma membranes, already emerge in Golgi apparatus and exocytic vesicles [118,145,193,194]. Therefore, FLIM images were now analyzed in the perinuclear region. Due to the experimental setup, FRET values of the individual cells are assessed by measuring the fluorescent lifetime of the FRET-donor GPI-CFP. As mentioned before, only a minor fraction of the GPI-CFP expressing cells showed a signal in the Golgi apparatus. Nevertheless, individual cells with all variants could be analyzed and significant FRET efficiencies were found. Again, all CRAC comprising gp41-chimeras caused FRET efficiencies of at about 6 percent (Figure 4-20).

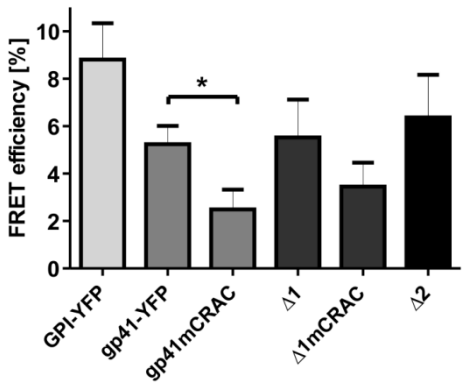

Figure 4-20: Golgi apparatus raft partitioning experiments using FLIM-FRET. FRET efficiencies in the Golgi apparatus from lifetime measurements of at least 2 independent experiments and 10 or more cells analyzed. All bars display FRET efficiencies in percent with SEM. The asterisk denotes * $p<0.05$ by Student's test for unpaired data.

Lower FRET efficiencies on the other hand were found again for both CRAC mutants (Figure 4-20). This finding supports the previous observation of a CRAC dependent raft partitioning.

Moreover, the observation of similar FRET efficiencies in the Golgi apparatus as at the plasma membrane is indicative of the lateral segregation already existing in the Golgi apparatus. Statistical relevance of the difference between wildtype and CRAC mutant was only found for gp41-YFP but not for Δ1 (Figure 4-20). This is a result of the high variance of the values that is typical for this kind of FRET-approach and also a result of the relatively low number of analyzed cells due to the small fraction of GPI-CFP expressing individuals with a perinuclear accumulation.

4.9 Detecting palmitoylation of gp41 variants

The gp41 fusion proteins are palmitoylated in CHO-K1 cells. Since recent experimental data from other cellular and viral glycoproteins[97,98] suggest a more important role of gp41 lipidations for the raft partitioning of the protein, a biochemical assay was performed to verify palmitoylation of the non-truncated constructs. Both variants comprising cysteine 764, gp41-YFP and gp41mCRAC but not the truncated construct Δ1 were clearly found to be palmitoylated (Figure 4-21). Considering the wild type-like raft partitioning of the Δ1 variant (Figure 4-14), this finding is in support of the previous conclusion that gp41 lipidation at position 764 play a minor or no role in the protein's raft partitioning.

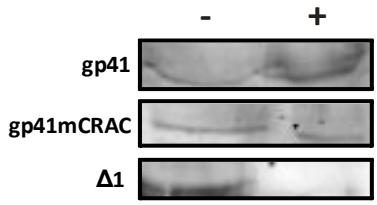

Figure 4-21: Acyl-biotinyl exchanged pull-down of gp41 fusion proteins. Isolated, palmitoylated proteins (+) and the non-palmitoylated fraction (-) were detected on Western blots using anti-GFP antibodies.

4.10 Analyzing lipid raft partitioning using giant plasma membrane vesicles

A growing number of methods have been applied in recent years to study membrane organization and lipid rafts. Fundamental work in the field focused on artificial membrane systems like large unilamellar vesicles (LUVs) and giant unilamellar vesicles which allow studying membrane behavior in the context of a distinct bilayer composition and under clearly

defined conditions. In particular GUVs offer the advantage to show phase separation and domain formation in a micrometer scale and thus allow a microscopic investigation of that lateral segregation. However, although they are a valuable model system, GUVs and LUVs significantly differ in many characteristics from cellular membranes. They should be rather considered as a system to study general thermodynamic and physical properties of membrane assemblies than as an actual model of naturally occurring bilayers. Therefore, vesicles derived from cellular membranes, the so called giant plasma membrane vesicles[195], plasma membrane spheres (PMSs)[196] or blebs were often utilized to study lipids, proteins and peptides in a context that resembles physiological conditions more closely. GPMVs can be used to report a potential intrinsic preference for a certain bilayer environment since they are known to undergo μm-scale phase separation upon cooling. Thus, compared to living cells, GPMVs offer the advantage to allow a microscopic observation of a protein's or a lipid's distribution.

Depending on the cell line, a spontaneous formation of plasma membrane vesicles can be induced by different treatments. Whereas some cell lines shed the so called PMS already upon incubation in hypotonic medium[196], other cells have to be treated with different chemicals to induce GPMV formation[175]. In the present study, two different preparation protocols were followed. Blebbing was either triggered by utilizing paraformaldehyde and dithiothreitol (PFA/DTT) or N-ethylmaleimide (NEM) since both reagents were reported to generate vesicles with significantly different properties. It has been shown, that proteins associated with the disordered phase of PFA/DTT blebs localize to the ordered phase in NEM-blebs[97].

The protocols of these methods are based on a published workflow by Levental[97] (Figure 3-2). Prepared vesicles were cooled down to induce macroscopic phase separation, microscopically imaged and subsequently analyzed. Partitioning of the protein under study in ld and lo domain is quantified and considered as reporter of its intrinsic membrane domain preference.

4.10.1 GPMV preparation types

When the GPMV preparation protocol was published first[197], several different preparation methods have been described and tested. The most reliable and easy approach bases on a mixture of paraformaldehyde and dithioreitherol. However, in recent years it was shown in several studies, that this preparation method produces vesicles with significantly different

properties compared to the native plasma membrane[97,175]. Therefore, different protocols were utilized to circumvent or at least minimize preparation induced artifacts (Figure 4-22).

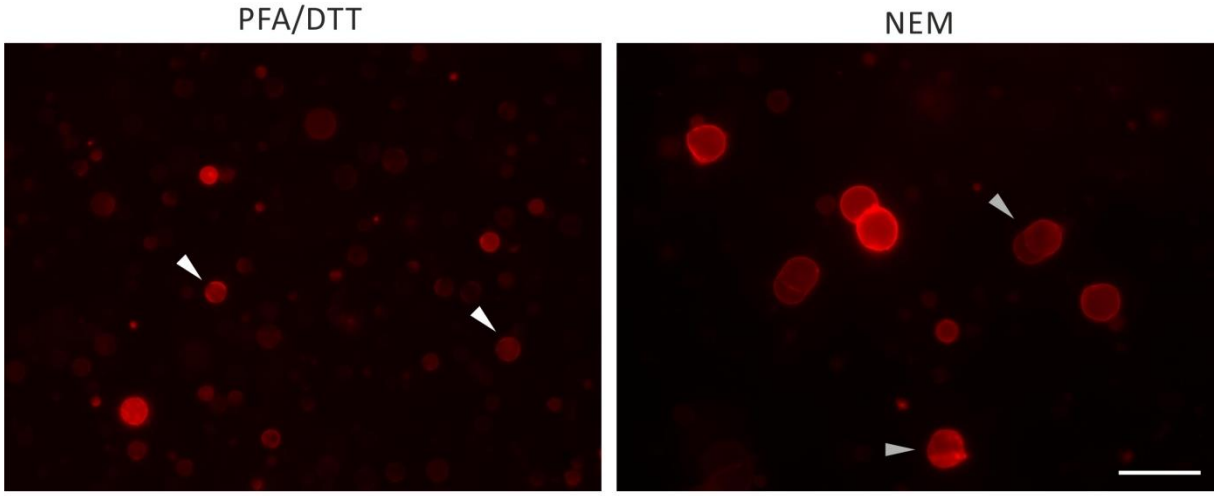

Figure 4-22: Comparison of GPMV preparation methods. RBL cells were labeled with R18 and subjected to blebbing for one hour. After sedimentation for another 30 minutes, suspensions were observed using epifluorescence microscopy. PFA/DTT preparations turned out to produce considerably more blebs, less contamination (grey arrows) and more often phase separation (white arrows). Scale bar, 30µm.

NEM was often applied as alternative since it could be shown that the lateral segregation of plasma membrane proteins in NEM-induced vesicles resembles much better their behavior under physiological condition[175]. Moreover it was found, that GPMVs produced with this method require very low temperatures to undergo microscopic phase separation whereas PFA/DTT blebs are known to spontaneously form ordered and disordered domains already close to room temperature. On one hand this might indicate a physiological and more relevant behavior of those particles but on the other hand it also renders the investigation more laborious since temperatures below 4°C are hard to achieve on a microscopic stage and produce further problems like condense water and freezing of the sample. Another huge drawback of the NEM preparation protocol is the low efficiency of that procedure.

PFA/DTT preparations produce high concentrations of clean GPMVs. To investigate the differences between the two aforementioned preparation methods, we tested both with rat basophile leukemia cells (RBL) which are supposed to be a well suited GPMV-preparation cell line (see 4.10.2). Compared to the PFA/DTT assay the absolute number and the percentage of phase separating GPMVs produced upon NEM-treatment was found to be

significantly lower and the samples were often highly contaminated with cell debris and irregularly shaped membranous particles (Figure 4-22).

4.10.2 Cell type dependence of GPMV preparation

Different cells lines show significant differences in their sensitivity to bleb induction. Whereas some of them already start blebbing upon cooling or treatment with hypotonic PBS, for most of the standard laboratory culture cells the treatment has to be more invasive. Usually, PFA/DTT reliably stimulates the production of GPMVs from many different cell lines[97,197]. Nevertheless, the quality and quantity of the obtained vesicles remarkably differ. In many publication RBL cells are used[113,175,191,195,198–200] since they seem to yield high amounts of vesicles and solutions that are relatively free of cell debris and other impurities.

GPMV preparations from RBL cells yield the highest amount and quality of plasma membrane vesicles. We tested six different standard cell lines regarding their sensitivity to the blebbing procedure (Figure 4-23). The dog-derived cell line MDCK (Madin-Darby canine kidney), the human cell lines HEK293T (human embryonal kidney) and HeLa (Henrietta Lacks, cervical cancer), the rodent cell lines CHO-K1 (chinese hamster ovary) and RBL and the african green monkey cell line Cos7 (Cercopethecus aethiops origin-defective SV-40) were used to cover a wide spectrum of different species and tissues. GPMVs were produced from all cell lines and observed using epifluorescence microscopopy. Obtained images were then judged with respect to the number and purity (contamination with cell debris) of GPMV, heterogeneity and occurring phase separation. In our experiments, in particular the cell lines MDCK and HeLa produced very low numbers of clean membrane vesicles and thus are not suitable for blebbing assays. Cos7 and even more CHO-K1 cells yielded better preparations. The absolute number of vesicles was still very low, but they turned out to be pure and relatively free of attached cell debris. HEK293T cells are only weakly adherent compared to the other cell lines considered. As a result of that, the GPMV supernatants of HEK293T cells always contain many floating cells or even huge cell aggregates that entered the solution due to the harsh blebbing procedure. Since the protocol includes cell labeling prior to the blebbing, high numbers of cells in the samples tend to outshine the small vesicles and preclude reasonable microscopic investigations. RBL preparations on the other hand, yielded very high amounts of phase separating vesicles that are widely free of other artifacts and pollutions.

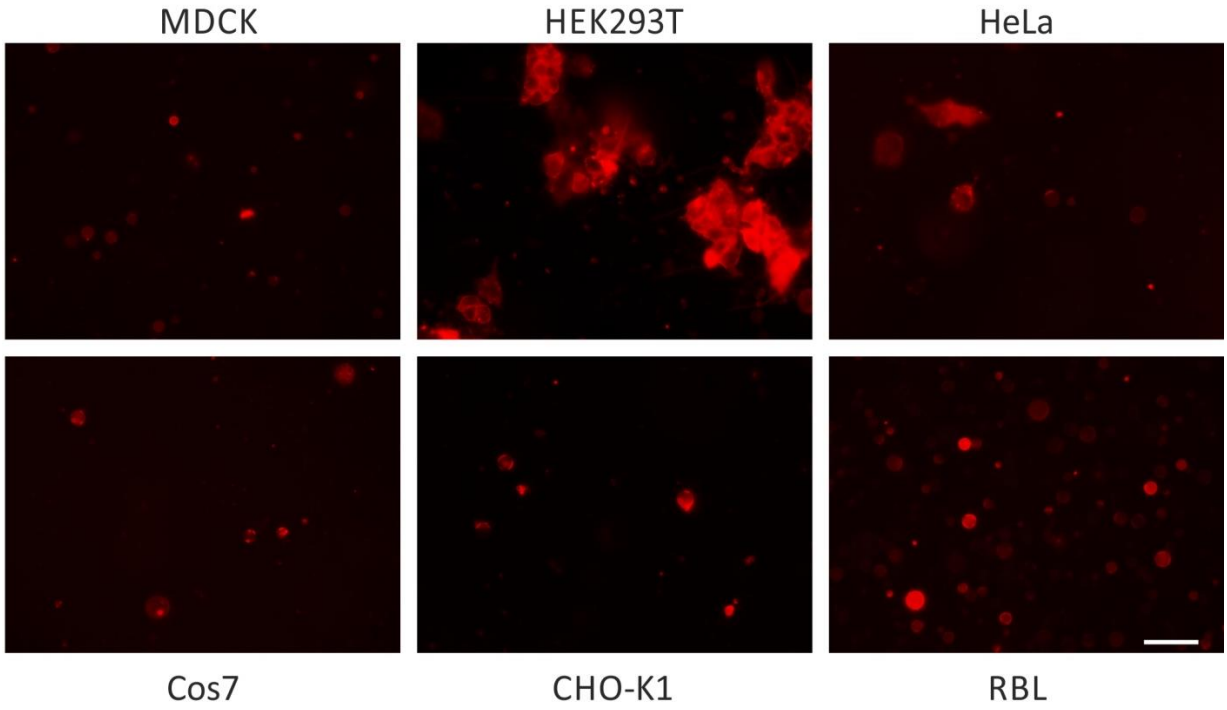

Figure 4-23: Comparison of different cell lines for GPMV preparation. Six cell lines were seeded in petri dishes and after overnight culture; blebbing was induced by PFA/DTT treatment. After sedimentation for another 30 minutes, suspensions were observed using epifluorescence microscopy. Typical images are displayed above. Scale bar, 30µm.

4.10.3 Domain partitioning of fluorescent proteins in GPMVs

To study bilayer phase preference of the proteins under study directly, RBL cells were transfected with fluorescently labeled fusion proteins and investigated with the GPMV assay described before.

GPI-YFP and Δ1 segregate to different phases in PFA/DTT blebs. GPI-YFP and the gp41 variant Δ1 were tested first since both proteins were found to possess a high surface expression. Although RBL cells are better suited for bleb formation (4.10.2), transfection was conducted in CHO-K1 cells since plasmid delivery in RBL cells is not possible with conventional lipofection methods and requires expensive nucleofection. Nevertheless, following transfection, the proteins were expressed for 24 hours and PFA/DTT blebbing was performed for 1h. DiD was used as a marker for the disordered domain and as expected, GPI-YFP as a known ordered phase protein was found in the DID-negative regions of the vesicles (Figure 4-24A).

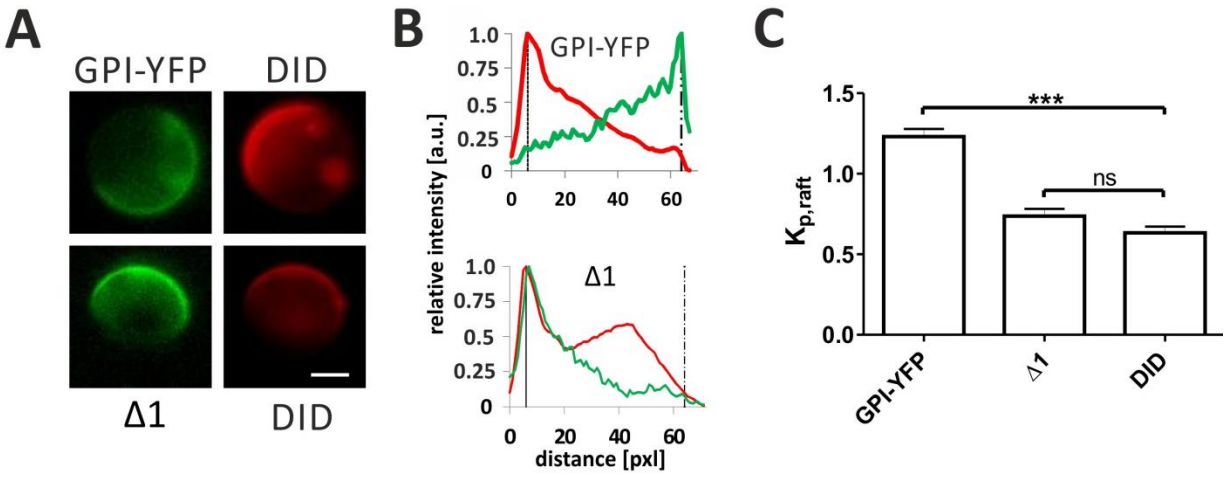

Figure 4-24: Phase partitioning of fusion proteins in GPMVs prepared according to PFA/DTT protocol from CHO-K1 cells transfected with GPI-YFP or Δ1. (A) Typical epifluorescence images of YFP-labeled fusion proteins (green) and DiD (red) in exemplary GPMVs. Scale bar, 5µm. (B) Intensity line plots of fluorescence in the YFP (green), displaying GPI-YFP and Δ1 respectively, and DiD (red) channel. Black lines indicate the position of the membrane in the plot and thus the position considered for the calculation of the partitioning coefficient. (C) Partitioning coefficient in the ordered domain of phase separating GPMVs from 10 different vesicles containing GPI-YFP or Δ1 and DiD. The asterisks denote *** $p<0.001$, ns $p>0.05$ by Student's test for unpaired data.

Line plots of those vesicles showed maxima of YFP and DiD at the respective minimum of the other fluorophore demonstrating that GPI-YFP preferentially partitions in the ordered domains of blebs from CHO-K1 cells (Figure 4-24B). On the other hand the protein Δ1, that has been shown before to colocalize with GPI-anchored proteins in nm-size domains of the plasma membrane (Figure 4-14) was found to be highly enriched in the DiD-positive phase. Moreover, the protein was not only observed to colocalize with the ld marker but it turned out to be excluded from the lo phase. This indicates a strong association of the fusion protein with the disordered domain of PFA/DTT blebs. Partitioning coefficients were calculated to further quantify this observation. Comparable values were found for DiD and Δ1 and a significantly increased raft partitioning was obtained for GPI-YFP. This finding is in agreement with previous publications reporting that PFA/DTT causes an unphysiological lateral sorting behavior of many raft but not GPI-anchored proteins[97].

The NEM vesicle preparation protocol produces vesicles with negligible protein concentrations. To circumvent the issue of an unphysiological phase partitioning behavior of raft proteins due to the treatment with PFA/DTT, and alternative, less harsh protocol was proposed[198]. Since the NEM-based vesicle preparation turned out to be less efficient in

general (Figure 4-22), the better suited RBL cells were utilized to obtain sufficient amounts of GPMVs. Thus, GPI-YFP or the viral proteins Δ1 and gp41-YFP were nucleofected in RBL cells and after an expression of 24 h subjected to NEM-vesicle preparation. The supernatant of those cells contained only small fractions of pure, sufficiently sized and phase separating vesicles due to the low efficiency of the NEM protocol. Although the overexpression was verified to cause normal protein concentrations using confocal microscopy (data not shown), unexpectedly, all NEM induced GPMVs showed, if any only an extremely dim, virtually undetectable fluorescence of the virus derived fusion proteins. GPI-YFP signals on the other hand were detectable in many vesicles and even phase segregation occurred occasionally (not shown).

Anti-GFP antibody labeling does not increase the detectable fusion protein fluorescence. Conceivably, both aforementioned viral fusion proteins are incorporated in NEM-GPMVs at very low concentrations. A labeling with fluorescent antibodies was performed in order to amplify the fluorescent signal and to allow detection of low concentrated proteins. Two different labeling protocols were tested. Either the antibody staining was conducted on adherent cells before the blebbing procedure or preformed blebs were immunofluorescently labeled in the collected cell supernatant. Unfortunately, both procedures have some serious inherent drawbacks.

Firstly, we tested an antibody labeling of preformed vesicles. To verify the binding of the antibody, an Alexa568 anti-GFP was utilized in combinations with YFP-labeled fusion proteins. Indeed, we could obtain GPMVs with both fluorescent signals demonstrating the feasibility of the assay. Upon labeling with FITC-labeled antibodies we achieved a slight amplification of the overall green fluorescent signal. Unfortunately, this improvement of the detectable fluorescence was accompanied by a strong increase of the background fluorescent due to unbound antibody in the vesicle environment. Since a washing of the fragile vesicles is not possible, this inevitable side-effect lowers the signal-to-noise ratio to an extent that completely outweighs the slight signal increase by the treatment (not shown).

In contrast to that, antibody-labeling of expressing cells clearly increased their fluorescence signals without increasing the background. Surprisingly, this amplification effect was not seen in the blebs produced by those cells. Whether antibodies are somehow excluded from

blebbing plasma membrane fractions or the signal amplification was too weak to be sensed cannot be concluded from those experiments (not shown).

4.11 Inquiring oligomerization of chimeric proteins

An early and important step of virus maturation is the assembly of newly synthesized protein monomers to functional oligomeric complexes. Although initial oligomerization of gp160 is known to occur in the Endoplasmic reticulum[201–203] posttranslationally, oligomer stability was reported to be significantly impaired by the cleavage in the Golgi apparatus[203]. The localization and timing of an enduring and stable gp41 oligomer formation is hard to study and might be coupled to protein maturation level and cell type. Possibly, depending on circumstances and cellular context an efficient and stable oligomerization demands specific plasma membrane components or even the tight packing in the virus envelope.

4.11.1 FAIM as a tool to study gp41 oligomerization

Fluorescence anisotropy is a physical property that allows investigating homo-FRET, energy migration between chromophores of the same species. Therefore, it is often used to report oligomerization of labeled proteins without any previous purification in the context of living cells. Moreover, FAIM even enables the localization of this intermolecular assembly event.

Env derived fusion proteins show low fluorescence anisotropies. First of all, transfections were conducted either with the fluorescently labeled Δ1 variant, possessing high plasma membrane expression rates or with GPI-YFP as a monomeric negative control and expressing cells were investigated with respect to fluorescence polarization. As expected[98], a homogeneous and localization independent fluorescence anisotropy of about 0.3 was found for GPI-YFP (Figure 4-25 and Figure 4-26). These anisotropy values obtained for GPI-YFP are in agreement with previous results for GPI-anchored fluorescent protein[98,139] and, according to Sharma et al.[139] indicate GPI-YFP monomers clustered in plasma membrane lipid rafts of less than 5nm in diameter. While the Δ1 variant showed a comparable fluorescence polarization in intracellular compartments, mainly Golgi apparatus and endoplasmic reticulum, a significantly reduced anisotropy of around 0.1 was found at the plasma membrane (Figure 4-25 and Figure 4-26).

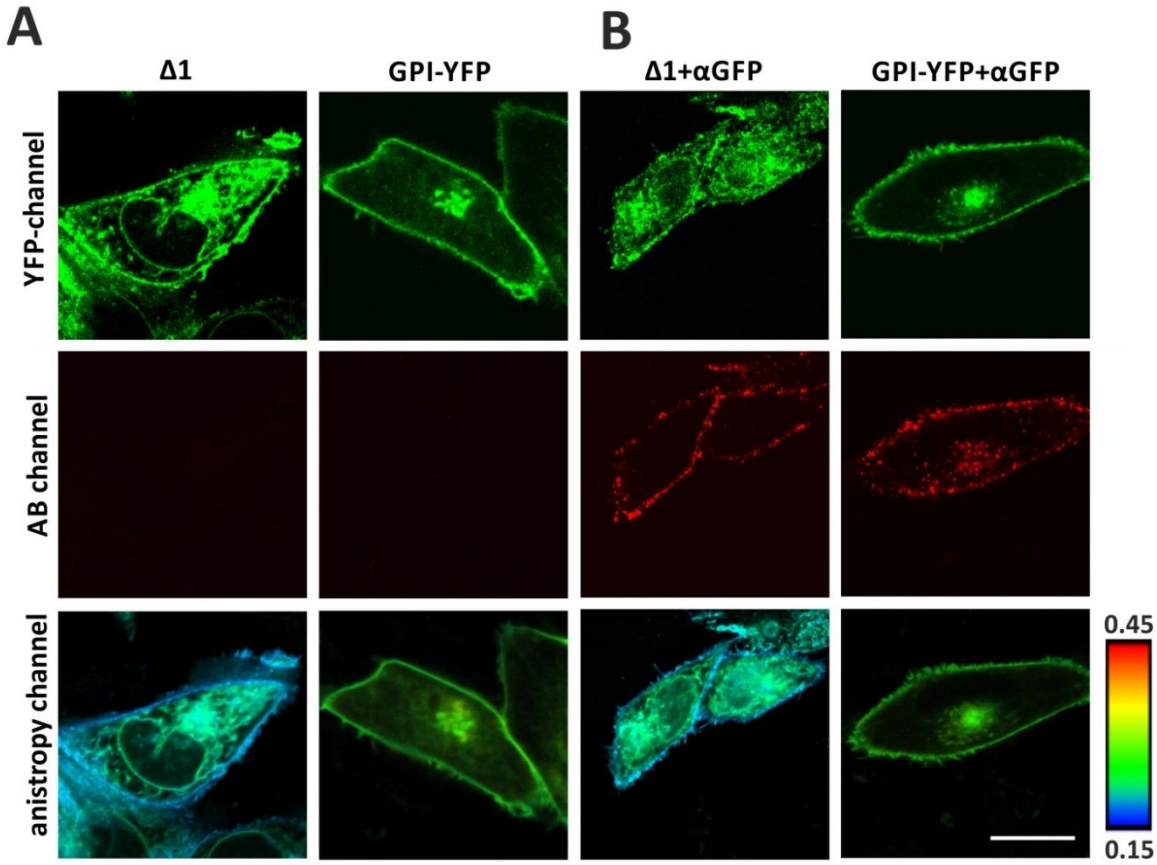

Figure 4-25: FAIM in presence and absence of GFP-antibodies. (A) Fluorescence anisotropy of YFP labeled proteins. Confocal and fluorescence polarization images of CHO-K1 cells transfected with the raft marker GPI-YFP and the Δ1 fusion protein. (B) Fluorescent labeled protein expressing cells were tagged with a red fluorescent anti-GFP (αGFP) antibody in order to study the influence of fluorophore motility and rotational motion on the fluorescence anisotropy. Scale bar, 15µm.

Low fluorescence anisotropy reports oligomerization. In this context, either an increased rotational mobility or homo-FRET can cause low anisotropy values. Since depending on the fluorophores, homo-FRET requires often even shorter distances to occur (<4nm)[150] than hetero-FRET, this energy migration is usually considered as a reporter of direct interactions or in case of one labeled protein species of oligomerization. To exclude that the reduced anisotropy at the plasma membrane is a result of a facilitated rotational motility, live cell anti-GFP fluorescent antibody staining experiments were performed (Figure 4-25). If indeed an accelerated motion of the fluorescent protein at the plasma membrane would cause the anisotropy decrease observed, it should be significantly increased by the direct binding of a bulky antibody. However, the anisotropy of both proteins, GPI-YFP and Δ1 were found to be unaffected by the antibody treatment, indicating that low anisotropy values, in fact reflect appearing homo-FRET. It might be objected, that this homo-FRET might be another

consequence of the clustering of the proteins under study in plasma membrane lipid rafts as described before[98]. But, in disagreement with that hypothesis, the putative, non-oligomeric raft marker protein GPI-YFP, although being highly enriched in lipid rafts (Figure 4-14), displayed a higher and homogenous anisotropy over the whole cells.

Gp41-YFP oligomers are stabilized at the plasma membrane. The observation of an oligomerization of the Δ1 variant at the plasma membrane suggest that their assembly largely occurs here and not already, subsequent to the protein synthesis, in the Endoplasmic reticulum. Since an important characteristic of this variant is the absence of the well characterized gp41 endocytosis signals, the protein is transported to the plasma membrane and if any, only a small subset of the Δ1 population is reinternalized into cytoplasmic compartments. The wild type protein gp41-YFP on the other hand, still comprising internal domain and hence the interaction sites for the cellular endocytosis machinery is endocytosed efficiently. Accordingly, gp41-YFP was not only found to be non-monomeric at the plasma membrane but also in intracellular membrane compartments (Figure 4-25 and Figure 4-26A). This finding either suggests that gp41-YFP oligomers found in intracellular membranes represent already assembled multiprotein complexes reinternalized from the cell surface or it reports that the gp41 cytosolic domain contains factors that cause intracellular oligomerization.

Gp41 oligomerization is CRAC dependent. Different protein inherent determinants of the HIV-1 envelope glycoprotein oligomerization have been reported in the last decades. Most of all, the transmembrane domain[84,204] and extracellular region[69,205–209] were shown to be involved in the assembly of functional trimers. The fusion proteins used in this study lack a considerable portion of the external region of gp41 and the complete gp120 interaction partner. To elucidate which of the remaining protein domains are relevant for oligomerization, several truncation and mutation variants were compared applying the anisotropy approach (Figure 4-26). As expected, on average low anisotropy values of around 0.2 were found for cells expressing gp41-YFP and Δ1 (Figure 4-26E), reporting that the maintained gp41 domains comprise all intrinsic factors sufficient to ensure efficient oligomerization of both proteins. In contrast, anisotropy values comparable to the putative monomer control GPI-YFP were obtained for both CRAC-mutants, gp41mCRAC and Δ1mCRAC and the truncation variant Δ2 indicating an important function of CRAC domain and external region for oligomer assembly (Figure 4-26).

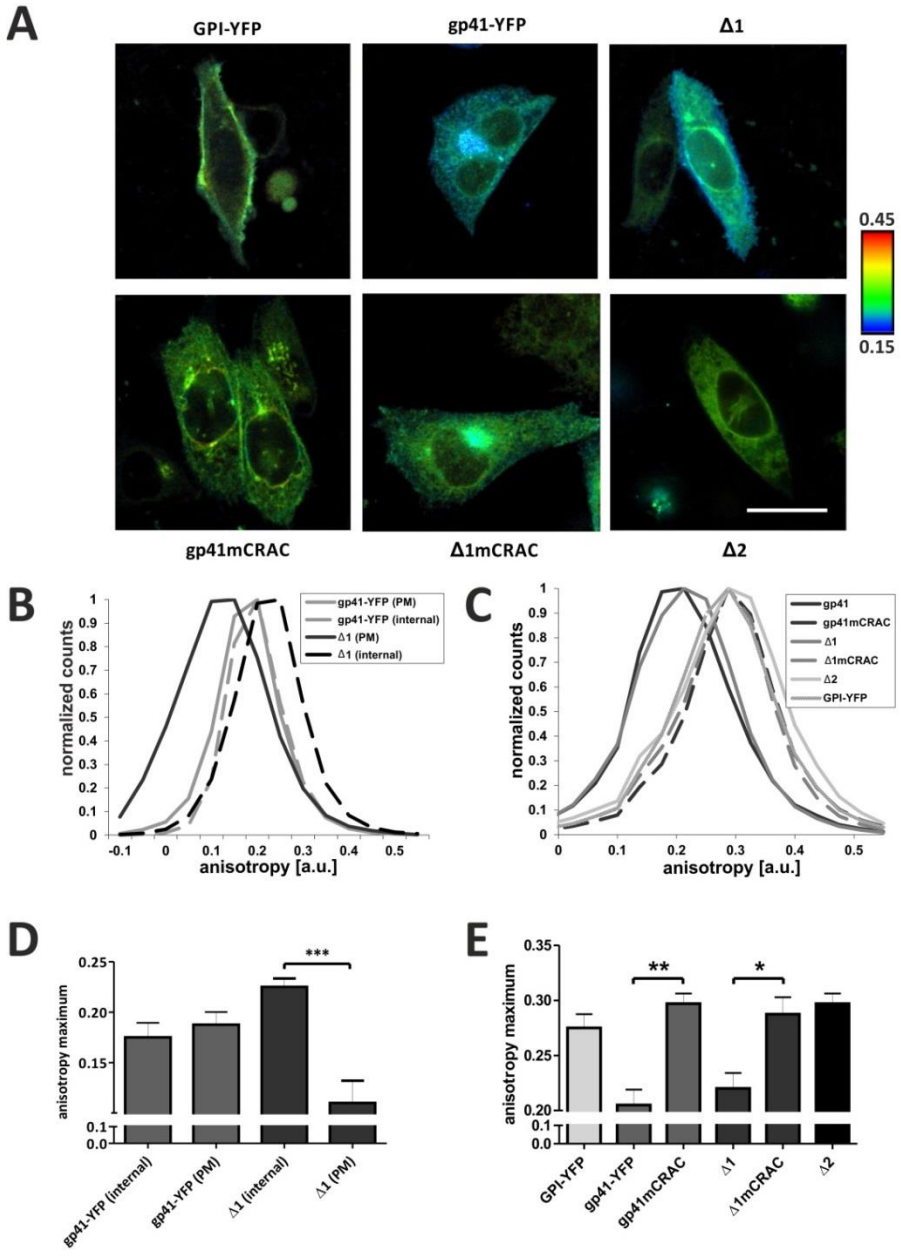

Figure 4-26: Oligomerization analysis using fluorescence a microscopy. (A) Fluorescence anisotropy images of CHO-K1 cells transfected with the raft marker GPI-YFP or gp41 fusion proteins. Pseudocolors refer to absolute anisotropy values. Scale bar, 15µm. (B and C) Anisotropy histogram plots allow appraising the oligomeric diversity of the protein under study. (D and E) Bar charts of average anisotropy maxima to compare the overall oligomerization state. Only the protein variant Δ1 and as a reference gp41-YFP were analyzed with respect to the localization dependence of occurring oligomerization (B and D) since only in Δ1-expressing cells differences were found. 5-10 different cells from at least two independent experiments were analyzed for the localization analysis and 5-15 from at least three different experiments for the different protein variants. The asterisks denote *** $p<0.001$, ** $p<0.01$, * $p<0.05$, ns $p>0.05$ by Student's test for unpaired data. Bars display average values with SEM.

Considering the truncation variants scrutinized, it is evident that whereas an external region including a functional CRAC motif is sufficient (Δ1) to drive gp41 oligomerization in the plasma membrane of expressing cells, the transmembrane domain alone is not (Δ2). It is of note that in the context of two protein backbones (gp41-YFP and Δ1) the mutation of the CRAC motif abolished oligomerization completely, although both proteins still comprise TMD, MPER and the majority of the CHR.

4.12 Analyzing membrane perturbation caused by the MPER of gp41

4.12.1 Flow cytometric study of gp41 membrane perturbation

In 2010 Apellaniz et al. reported, that peptides derived from the membrane-proximal external region (MPER) of gp41 possess membrane-disturbing properties[210]. It was shown, that the MPER causes membrane perturbation resulting in a pore-formation and leakage of large and giant unilamellar vesicles. It is reasonable to assume, that a comparable disturbance of the membrane integrity in a living cell is significantly affecting its condition even up to the viability. We performed flow cytometer experiments to investigate this hypothesis. As a parameter for the plasma membrane integrity we measured the cellular uptake of propidium iodide (PI). Precisely, cells expressing different fusion proteins were treated with PI and analyzed using a FACS (Figure 4-27).

The gp41-YFP fusion protein possesses membrane perturbation properties. As a proof of principle, three different samples were investigated. Cell transfected with gp41-YFP, Gag-GFP as membrane lytic negative control and mock-transfected cells were analyzed using the PI uptake assay. Untransfected cells revealed a PI-positive population of small particles (Figure 4-27, blue arrows) and a PI-negative population of bigger objects, most likely representing intact cells (Figure 4-27, red yellow). A very similar distribution was found for cells transfected with Gag-GFP. The population of dead cells was slightly elevated, most likely due to the overexpression of the viral protein (Figure 4-27, blue arrows). In case of cells transfected with gp41-YFP the plots remarkably changed. The population of dead cells increased significantly, probably as a result of the membrane lytic influence of gp41. Moreover, a new population of cells with the size of an intact cell but with a significantly higher PI intensity appeared (Figure 4-27, yellow arrows). These events might represent

living cells possessing an elevated PI uptake caused by a gp41-induced plasma membrane perturbation.

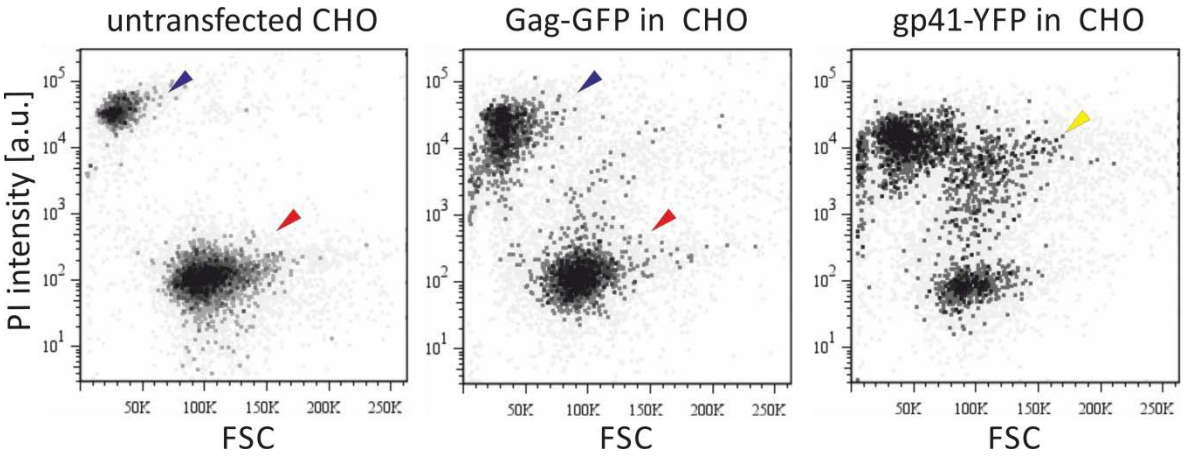

Figure 4-27: Flow cytometric membrane integrity assay. Cell transfected with gp41-YFP, Gag-GFP as negative control and mock-transfected cells were analyzed. The dot plots display the PI intensity versus the forward scatter. Typically, two populations were found for instance in case of mock-transfected cells and negative control, one representing small, dead cells with a high PI fluorescence (blue arrows) and the other one representing larger, living cells with a low PI signal (red arrows). Another new population emerged upon expression of gp41-YFP (yellow arrow). Cells appeared having high PI signals although still remaining relatively high forward scatter signals and thus most likely represent living cells.

The extracellular MPER is the crucial region for the gp41 induced membrane perturbation. Three different gp41 variants were investigated, the wild type gp41-YFP, the cytosolic domain truncation form Δ1 and the minimal variant Δ2 lacking intra and extracellular α-helices. Compared to the non-perturbing negative control GPI-YFP, the protein gp41-YFP showed significantly elevated PI signals in all experiments (Figure 4-28A and B). Expression of the variant Δ1 often caused a further increase of the plasma membrane violation and of the amount of PI positive cells up to twice the number found in the negative control (Figure 4-28B). As mentioned above, this variant is lacking the protein intrinsic endocytosis signal and hence displays a higher plasma membrane concentration. As a result of that, plasma membrane perturbation is expectedly increased and PI uptake is facilitated. The further truncation of the extracellular MPER of the Δ1 variant, leading to the fusion protein Δ2, completely abolished its toxicity and a viability comparable to the negative control was achieved (Figure 4-28B). This finding confirms the crucial role of the MPER for the protein's membrane lytic properties. Taken together, the results clearly demonstrate that the gp41 plasma membrane perturbation is primarily governed by two factors, the presence of the

intracellular endocytosis signals that control PM localization and retention, and the external MPER as the actual molecular factor of pore forming and bilayer disturbance.

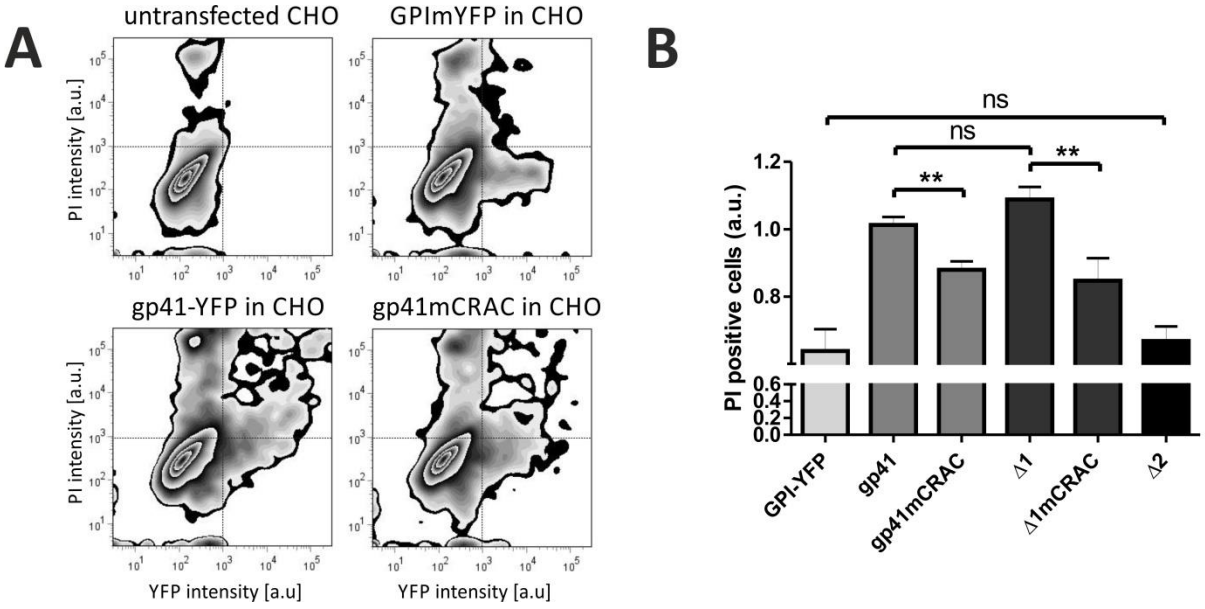

Figure 4-28: Plasma membrane perturbation of gp41 variants. CHO-K1 cells transfected with different fluorescent proteins were treated with PI as a reporter of plasma membrane and cell integrity. (A) Density plots of typical flow cytometer experiment. The propidium iodide channel is displayed in the y-axis, fluorescent protein signal in x-direction. In order to quantify the impact of the proteins on the cell viability and membrane integrity, the upper right quadrant populations, representing dead amongst fluorescent were related to the total fluorescent populations in both right quadrants. The obtained ratio was then plotted in bar charts as a reporter of membrane integrity. (B) Membrane perturbation results from at least three independent experiments per protein. To balance protein independent cell variations between different experiments, all samples of one experiment were normalized to the wild type gp41 fusion protein and obtained PI uptake values were then averaged over all experiments. The asterisks denote ** p=0.001-0.01, ns p>0.05, p < 0.005 by Student's test for unpaired data.

The CRAC domain is responsible for the MPER mediated membrane perturbation. FLIM-FRET experiments revealed an explicit influence of the CRAC domain on the gp41 properties (Figure 4-14). Since the cell toxicity of gp41 fusion proteins seems to depend on a direct membrane interaction of the bilayer adjacent MPER (Figure 4-28B) it is conceivable to surmise a CRAC related membrane perturbation. To test this hypothesis, CRAC mutants were expressed and compared regarding plasma membrane perturbation with their respective wild type forms. Indeed, both variants, gp41mCRAC and Δ1mCRAC, showed a significantly reduced membrane perturbation (Figure 4-28A and B) pointing to an important function of the CRAC motif in the membrane perturbation caused by the MPER.

4.12.2 Perspective: Patch clamp to sense gp41 plasma membrane perturbation.

We and others reported a significant membrane perturbation exerted by the HIV-1 glycoprotein gp41[38,92] (compare also 4.12). It was suggested, that lentivirus lytic peptides are the crucial factor of that influence[40] and thus it was hypothesized they might even form α-helix based pores through the membrane[92]. Other publications assign a membrane disturbance to the proteins MPER due to a partial embedding of the amphipathic, α -helical structure of this domain[38,210]. This observation was confirmed by the results of our propidium iodide-based flow cytometer experiments with expressed gp41 variants (compare 4.12). However, although this approach clearly demonstrated an influence of gp41-derived fusion proteins on the propidium iodide uptake it does not allow to study this process in more details. It cannot be concludingly decided from the data, if the increase of the PI-fluorescent upon expression of gp41 reports a higher permeability of the plasma membranes or rather a higher level of necrotic cells as a result of a gp41-induced membrane leakage. To learn more about the molecular background of the membrane disturbing influence of gp41, patch clamp experiments were performed by Matthias Prigge and Jonas Wietek (Humboldt University, Department of Biology, Group of Experimental Biophysics). Cells were used expressing the protein Δ1 since this protein showed the strongest influence on the propidium iodide-uptake in our flow-cytometer experiments and in addition, as a membrane perturbation negative-control, GPI-YFP. Mock transfected and cells expressing the two proteins were then studied in cell-attached patch clamp experiments (Figure 4-29A, B).

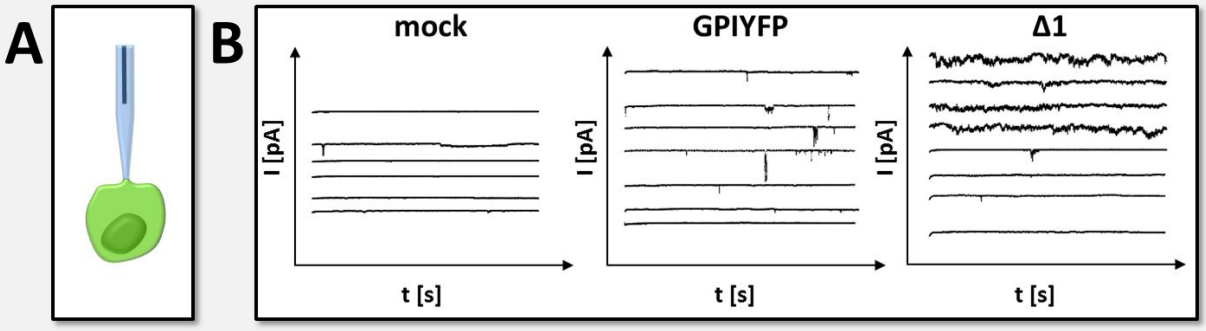

Figure 4-29: Electrophysiology measurements of gp41 mediated membrane perturbation. (A) Schematic representation of a cell-attached patch clamp experiment. (B) Current traces of CHO-K1 cells expressing GPI-YFP, Δ1 or mock-transfected cells were investigated in the cell-attached mode to study the plasma membrane permeability.

In this assay, cells are sucked until the patching pipette is sealed with the plasma membrane, then an electrical field is applied and the current is measured over time. Considerable differences of the current traces were found between both negative controls and Δ1 (Figure 4-30). Whereas the curves were smooth and regular for the mock and GPI-YFP transfected cells, Δ1 expression caused often noisy and irregular traces that are typical for membrane lytic proteins[8]. In electrophysiology measurements, often the integral of the current over time is used to quantify the ion transport capacity of the membrane under study. Although this approach didn't produce statistical significant differences in our investigation, again remarkable deviations were found (Figure 4-30).

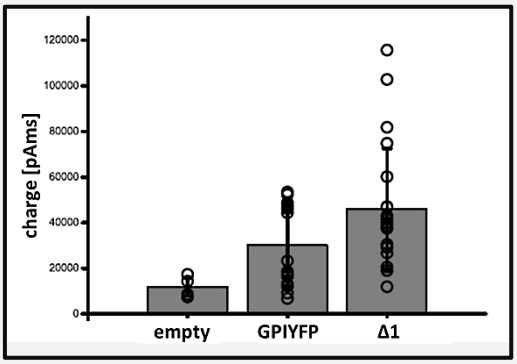

Figure 4-30: Quantification of membrane permeability. Integrals of the transported charge over time as a measure of the overall membrane perturbation efficiency of mock-transfected cells and cells expressing GPI-YFP or Δ1.

High integrals, up to 6 times higher than the negative control were only found for Δ1. The integral was already clearly increased in case of GPI-YFP compared to the mock-transfection which might simply reflect overexpression stress that the cell is suffering from and that is weakening the membrane. Nevertheless, it is striking, that very high values of around 120000 pA were only found for the glycoprotein Δ1, whereas even GPI-YFP only produced values around 60000 pA in maximum.

5. Discussion

The goal of the present study was to investigate inherent properties of the HIV-1 transmembrane protein gp41. Several biophysical and biochemical methods were utilized to elucidate raft partitioning, oligomerization, localization and trafficking of a YFP labeled, membranotropic wild type form and several truncation and mutation variants of the viral glycoprotein.

We used FLIM-FRET to examine whether gp41 partitions into lateral domains of the plasma membrane. To our knowledge, this is the first experimental approach to determine a preferential lipid raft sorting of a relevant portion of the viral envelope complex in living cells. Constructs were produced containing all parts of the wild type protein that are able to interact with cellular membranes in the assembly context, namely transmembrane domain, external membrane proximal region, C-terminal heptad repeat and most importantly, cytoplasmic tail. An N-terminal labeling approach was favored over cytoplasmatic tagging to avoid interference of the fluorescent protein with the predominantly membrane associated C-terminal domain. We could show that expressed *gp41 variants cluster with the raft marker* protein GPI-CFP in cellular plasma membrane microdomains and by comparing the different fusion protein variants we were able to identify the intrinsic cholesterol binding motif, the *CRAC domain as the main factor* of this property.

5.1 Raft partitioning of the glycoprotein gp41

5.1.1 Critical evaluation of FLIM-FRET data

We found a low, but reproducible FRET efficiency for the membranotropic wild type gp41-YFP that indicates a significant raft partitioning of the glycoprotein (Figure 4-14). Neither abolishing of the protein's cytosolic domain, including one palmitoylation site and three amphipathic α-helices, nor an additional removal of the membrane proximal external region did significantly impair this behavior (Figure 4-14). On the other hand, a single amino acid change in the cholesterol recognition amino acid consensus decreased the FRET efficiencies decisively (Figure 4-14). Considering the unimpaired raft partitioning of the minimal variant (Δ2) our results suggest, that the CRAC is a sufficient determinant of the protein's raft

association. Since other motifs like palmitoylated cysteines or amphipathic α-helices, suspected to cause a lateral plasma membrane sorting[74,90,97,98,113,144,211] are abolished in this variant they do not or at least to a minor extend, contribute to this property of gp41.

5.1.1.1 Validity of the CFP lifetime data

To judge the reliability of our results it is important to understand the meaning and validity of FLIM-FRET data in general and in this approach in particular. In general, absorption, excitation and fluorescence spectra depend on the specific electron configuration of a fluorophore (Figure 5-1).

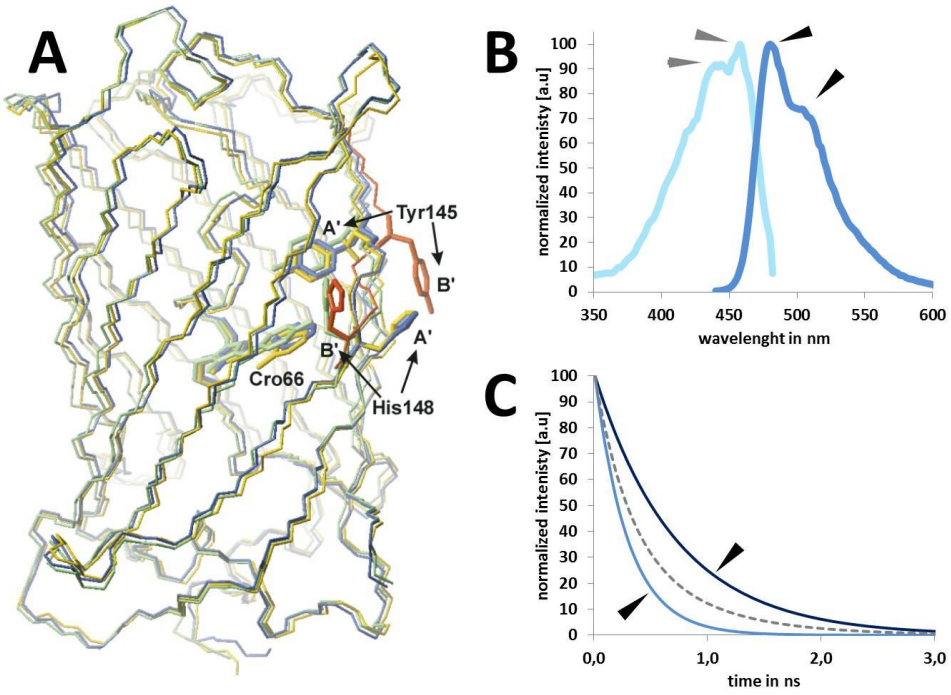

Figure 5-1: Conformational states of CFP. (A) In this representation C_α traces of the CFP, GFP and YFP β-barrel are displayed in blue and green and yellow. The two CFP chromophore conformations are highlighted in blue, A' and red, B'. Adapted from [176] (B) and (C) The two conformational states of CFP (labeled with black and grey arrows) are reflected in (B) excitation (in light blue) and emission (dark blue) spectrum and in (C) the biexponential (grey dashed line) fluorescent lifetime decay that is indicative of two independent components (dark and bright blue)[176]. It is yet unknown, what spectral peak and which of the lifetime decay curves is representative of what molecular conformation.

Thus, the shape and position of the spectra is characteristic for certain fluorophores and represent some kind of a spectral fingerprint. The same holds true for the stability of the excited state of the fluorophore. Fluorescent molecules often show typical fluorescence

lifetime decays that are representative of distinct molecule conformation and electronic arrangements. CFP for instance shows a complex biexponential lifetime decay that is supposed to originate from different conformational states of the chromophore in the β-barrel of the fluorescent protein[176]. This has to be taken into account when CFP-lifetimes are utilized for the calculation of FRET efficiencies to derive meaningful and reliable conclusions form the data obtained.

Although FLIM-FRET measuring equipment is highly sensitive[185], the accuracy of TCSPC experiments is typically limited by several practical aspects. Different sample parameters such as photostability and molecular brightness of the fluorophore under study or a high background fluorescence and thus low signal-to-noise often significantly restricts the precision of assessed data. As a result of that, from their lifetime decays it is usually not possible to distinguish between both CFP conformational states and therefore amplitude-weighted lifetimes are used to describe and quantify the CFP fluorescence. Although in our experiments the fluorescent lifetime values were highly deviating between single cells and single experiments, due to many repetition low standard errors were achieved and the overall fluorescent lifetimes of the donor-construct and the positive controls are supported by published data (Table 24).

Table 24: Amplitude-weighted average fluorescence lifetimes of GPI-CFP in presence and absence of FRET-acceptor proteins. Experimental data from this study are displayed together with relevant published data.

	GPI-CFP	GPI-CFP & GPI-YFP	GPI-CFP-YFP
Thesis	**2.53** ± 0.01 ns	**2.38** ± 0.01 ns	**1.94** ± 0.01 ns
Millington[212]	**2.4 ns**	----	**1,88 ns**
Scolari[98]	**2.3 - 2.6 ns**	**2.13 - 2.39 ns**	----

It is important to keep in mind that fluorescence in general and fluorescent lifetimes in particular depend on different contextual factors. FRET experiments aim on detecting the aftermath of energy transfer that is a lowering of the fluorescent intensity and a shortening of the fluorescent lifetime. But temperature, pH, presence of other energy transfer partners and quencher molecules can influence both properties as well and have to be considered to

reliably judge results of FRET experiments. In this work, mainly the fluorophores localized on the cell surfaces were analyzed. The environmental conditions were thus predetermined by the composition of the used media and therefore, they can be assumed to be more or less identical in all experiments.

5.1.1.2 Significance of obtained FRET efficiencies

In general, FRET is used to report a high proximity between the molecules under study. Due to the strict distance requirements of this energy transfer it is indicative of direct protein interactions or enrichment in spatially highly constricted environments. Nevertheless, FRET experiments involve a high risk of an overestimation of random collisions between the FRET-partners due to high concentrations that might contribute to the probability of energy transfer as well. To take this into account, the concentration dependence of FRET saturation has to be considered (Figure 5-2).

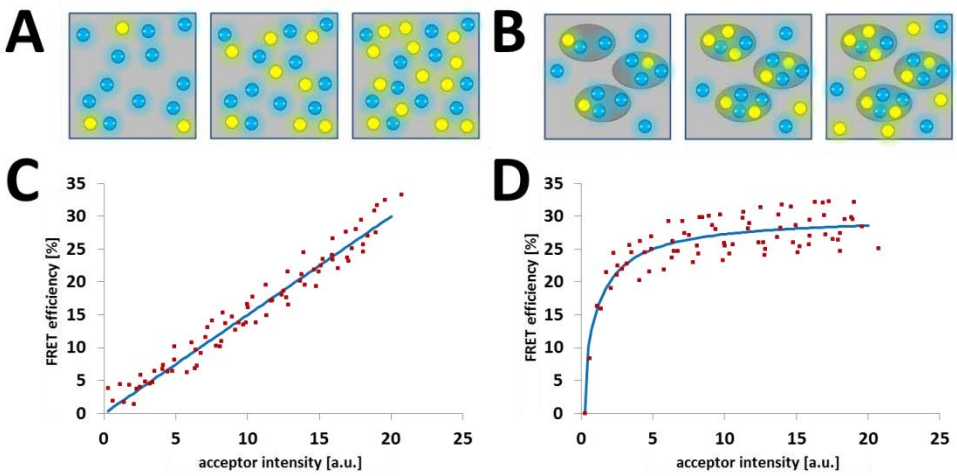

Figure 5-2: Principle of FRET saturation analysis. Schematic representation and theoretical expectations for unclustered (A and C) versus raft clustered (B and D) donors and acceptors (cyan and yellow circles representing CFP and YFP). A constant number of available donor fluorophores was assumed in both cases.

The idea of that analytic approach is that FRET as a result of random interactions between the participation molecules should be directly and linearly proportional to the concentration of the acceptor[144] (Figure 5-2 A and C). Saturation should be only reached at very high concentrations when the system is completely crowded with fluorescent molecules. In contrast to that, for specific interactions a saturation at low concentrations would be

expected[144] (Figure 5-2 B and D). This contemplation is very important to avoid false-positive results and judge obtained values qualitatively. Since all CRAC containing gp41 variants elucidated in this studied showed FRET saturation at low concentrations and no further concentration dependent increase of the FRET efficiency, we surmise that obtained *FRET values indeed reflect raft enrichment* (Figure 4-15). It is noteworthy that both CRAC-mutants, gp41mCRAC and Δ1mCRAC did not shown saturation in the concentration range investigated in this study.

Although this analysis allows a reliable and qualitative interpretation of the FRET values, a quantitative analysis can be quite sophisticated. FLIM-FRET values usually represent bulk-data of numerous fluorophores at the same time. For a stoichiometric molecular binding with a distinct distance of the interaction, obtained data basically depend on two factors, the relative fraction of the donors undergoing energy transfer and the distance between the participating FRET-partners. Depending on the analytic precision either information can be separated or if not, an efficient, average distance can be surmised. However, the situation is much more complex if FRET is used to study raft partitioning. A qualitative conclusion can often be drawn easily, but it is quite difficult to get accurate distance information. Obtained values depend on the individual size of the lipid rafts, the relative fraction of the FRET donors and acceptors that are partitioning in lipid rafts and the non-stoichiometric proportion between donor and acceptor. This complexity of the system and the resulting high number of variables impedes a quantitative interpretation of the data. Nevertheless, under the following conditions and assumption it is possible to assess some rough estimation and develop a plausible model.

(1) The relationship between the FRET efficiency and the inter-fluorophore distance is given by the equation (from [150])

$$\boldsymbol{F = \frac{{R_0}^6}{{R_0}^6 + r^6}}$$

(2) The FRET radius R_0 of the pair CFP-YFP is roughly 5nm (from [213]).
(3) The average distance of homogeneously distributed membrane anchored fluorescent proteins is too high for FRET to occur (based on [139]), only raft enriched proteins undergo energy transfer.
(4) The overall number of FRET donor molecules (GPI-CFP) in the plasma membrane and in lipid rafts is constant in all experiments.
(5) ~20 % of all GPI-anchored fluorescent proteins are clustered in plasma membrane lipid rafts of CHO-K1 cells (based on [139]) .

(6) Since a further increase of the acceptor amount in the concentrational saturation region does not increase the FRET efficiency, lipid rafts are in that range crowded with fluorescent proteins.

The fourth and fifth points are of course only simplifications of the real situation. Considering that saturation of the FRET efficiency is a result of a crowding of the microdomains, the number of competing raft proteins (gp41 variants, GPI-YFP) will directly influence the absolute number and ratio of raft residing donor molecules and GPI anchored proteins in general. Nevertheless, if this is objection is neglected, quantitative information can be estimated.

In the previously described flow cytometric approach (see Figure 4-12), the fluorescence of surface bound anti-GFP antibodies was detected as a measure of the surface localization of the antigen. GPI-YFP was found to be in much higher concentrations at the plasma membrane than the virus protein variants (Figure 4-12). The surface exposure of GPI-YFP was indicated to be between 3 to 6 times higher compared to the different gp41-construct. Nevertheless, for all non-mutated gp41 chimeras a FRET-saturation was found already at low concentration level. If with the high plasma membrane concentration of GPI-YFP already around 20 % of those proteins are sufficient to completely crowd the lipid rafts (point 5), the fraction of raft localized gp41 protein variants needs to be correspondingly higher to cause saturation of the plasma membrane microdomains (Figure 5-3). This conclusion would be indicative of 60 % (for the Δ1 variant) to 100 % (for the gp41-YFP variant) of the virus derived proteins partitioning in GPI-enriched plasma membrane microdomains. This high affinity of gp41 for plasma membrane lipid rafts is also indicated by the small k_d values, below 10^{-3} of the FRET saturation plots (Figure 4-15).

What does that mean for the CRAC-mutants? Considering, that their surface expression resemble the respective wild type proteins, the low FRET efficiencies obtained indicate a significantly lower fraction of fluorescent proteins partitioning in the lipid rafts. Interestingly, both CRAC mutants were never, even at very high concentrations found to reach the FRET-saturation level of the non-mutant proteins (Figure 4-15). *We surmise that no, or only a very low percentage of the mutant proteins partition into lipid raft whereas all CRAC-wildtype variants*, gp41-YFP, Δ1 and Δ2 *are preferentially localized in GPI-enriched plasma membrane microdomains*.

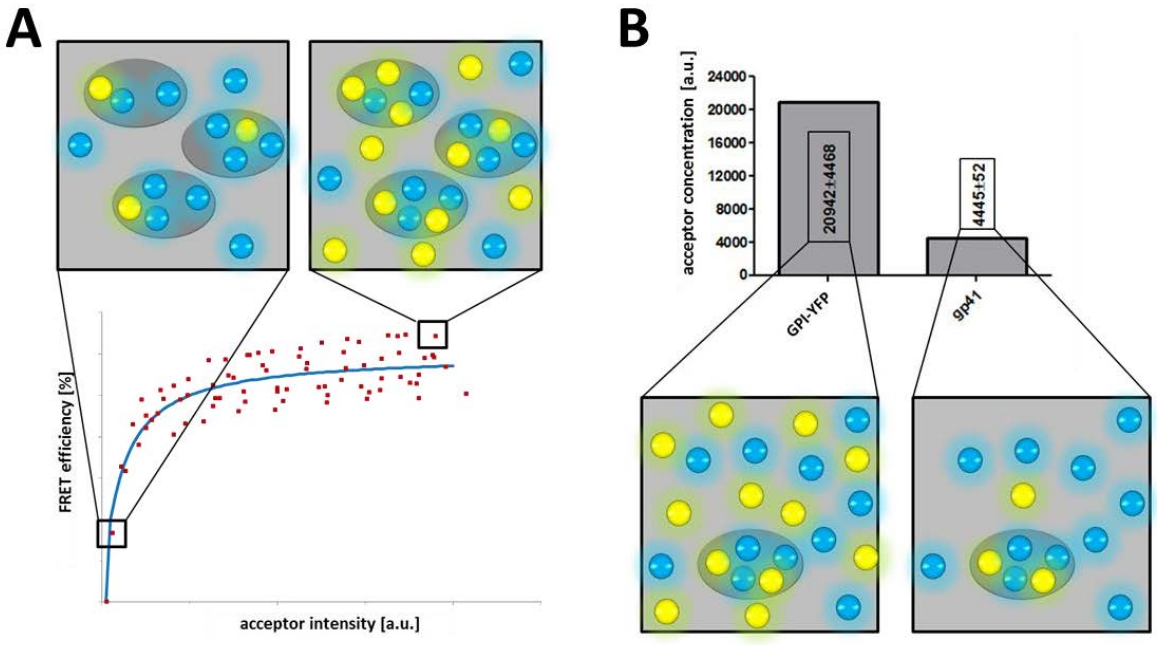

Figure 5-3: Interpretation of FLIM-FRET results. (A) Based on the model proposed by Zacharias et al.[144] it was assumed that FRET saturation is reached at low protein concentrations due to the preferential sorting in plasma membrane microdomains. If the protein concentration is elevated above a certain level, the lipid rafts are already crowded with proteins, all additional proteins are excluded, and thus distribute homogenously in the plasma membrane. Here, they are highly diluted and do not cause energy transfer anymore. (B) It was reported that around 20 % of the GPI-anchored proteins are required to crowd plasma membrane lipid rafts completely. Considering, that the plasma membrane concentration of gp41 is in average five times lower than the GPI-YFP concentration and still already produces FRET saturation at low concentrations, the fraction of raft residing gp41 proteins has to be roughly 5 times higher meaning that gp41 should be almost completely incorporated in plasma membrane lipid rafts.

The question remains, what is the background of deviations in the average FRET efficiency between different proteins supposed to reside in lipid rafts. *The dissimilarity in the saturation FRET efficiency between the acceptor molecule GPI-YFP and the fluorescently labeled gp41 variants, for example, can be, as a consequence of (6) exclusively explained by deviating distances due to different heights of the fluorophores above the membrane or by orientational differences*. It does not reflect variances in the raft partitioning.

By exerting the simplifications points described before, the height difference can be estimated as well. For the quantification of FRET between GPI-CFP and GPI-YFP all donor moieties at the plasma membrane were considered to calculate the average FRET efficiency of 8 % (Figure 4-14). If the respective, overall lowering of the CFP-fluorescence lifetime is caused

by only 20 % of the GPI-anchored CFPs whereas 80 % remained unchanged (according to point 5), the energy transfer of the lipid raft localized GPI-CFP molecules is around 5 times higher than the calculated 8 % and thus reports average distances between GPI-anchored fluorescent proteins of 5.3 nm in the lipid rafts (according to point 1 and 2). It should be underlined that this consideration is apriori independent of the actual fraction of raft residing acceptor molecules since it is assumed that in the FRET saturation region as many acceptors as possible are localized in the microdomains (that means the same number for all different proteins causing FRET saturation). Therefore, the same calculation can be conducted for gp41 constructs. Again, a fivefold higher FRET efficiency is assumed (based on point 5). Since all raft residing gp41 variants showed a FRET efficiency of around 5 percent, a final *average distance of 8.5 nm between GPI-CFP and gp41 derived chimeras is obtained*.

5.1.2 Giant plasma membrane vesicles as a tool to study raft partitioning

As a complementary method to study a preferential association of proteins with ordered membrane domains, a GPMV approach was conducted. It has been shown previously that proteins supposed to partition into lipid rafts colocalize with markers of the ordered but not of the disordered domain of phase separating GPMVs[97]. However, the most common preparation method based on PFA/DTT is supposed to produce artificial results and not to be reflective of native conditions since DTT is a strong depalmitoylation agent[97]. Therefore, a DTT-independent preparation technique was established utilizing NEM instead of PFA/DTT to circumvent this effect[97]. Unfortunately, this preparation method is in general less efficient than the unphysiological PFA/DTT approach (see 4.10.1) and in our experiments viral fusion chimeras were always barely detectable in the NEM-GPMV membranes (see 4.5.3). Even an additional amplification of the fluorescence signal using fluorescent anti-GFP antibodies was not sufficient to increase the signals significantly (see 4.5.3). This observation of only weak expression of the fluorescent proteins in NEM-induced GPMVs was quite unexpected and the fact that clearly higher amounts of the viral chimera were found in PFA/DTT-GPMVs suggests an underlying sorting mechanism during the vesicle formation or in other words a selective exclusion of the proteins from forming NEM-induced GPMVs. *Therefore, an investigation of the gp41 phase preference in plasma membrane-derived vesicles was impossible in our hands*.

5.1.3 Biological relevance of the gp41 raft partitioning

The biological role of lipid rafts in general and their significance in the context of virus assembly is still under debate[136]. In case of the HIV-1 glycoprotein gp41 the intrinsic cholesterol binding motif was suspected to cause microdomain partitioning but foregoing studies on this topic reported partly inconsistent findings. Whereas the gp41 CRAC domain was clearly shown to specifically bind cholesterol[76], *in other publications CRAC mutations turned out not to cause sequestering of gp41 from detergent resistant membrane fractions*[81]. The role of the gp41 lipidation in this context is even more ambiguous. DRM partitioning was described to be palmitoylation independent in one study[101] and dependent in others[90,99,100]. The different methodical approaches used in those studies might be one explanation for the discrepancies, partly also with the results at hand. As mentioned before, *most of the investigations of gp41 raft association are based on DRM assays*, which are in general believed to be prone to artifacts and misinterpretation and have to be scrutinized carefully[119]. Furthermore, results from other publications cannot be compared directly with the data of the present study since *different virus isolates, typically the isolates HXB2 and NL4-3 (in this study: JRFL), with important deviations in the amino acid sequence were repeatedly used*. In particular, the palmitoylated cysteine at position 837, lacking in the envelope complex used in this study, was described to be vital for raft association of HXB2 gp41[90]. Possibly, CRAC mutations introduced in those HXB2 derived glycoproteins[81] might have been counterbalanced by the raft driving properties of that lipidation. Another hypothesis is implied by observations suggesting that different population of lipid rafts exist in plasma membranes[90,99,214]. Light and heavy rafts, possessing different densities in sucrose gradients, were found to be enriched in different proteins. Conceivably, CRAC domain and palmitoylation trigger association of the protein with different raft species. *Palmitoylation mutants found to be excluded from one subpopulation of lipid rafts in DRM assays might still be sorted into another kind of microdomains due to the raft driving properties of the CRAC domain and, as a result of that, are still able to co-cluster with the raft marker GPI-CFP*. This hypothesis is supported by the work of Nebl et al.[214] who reported GPI anchored proteins in both fractions, light and heavy rafts. Of course GPI anchoring is a very abundant protein modification and it is not known in which of the fractions GPI-YFP and GPI-CFP would be enriched in. Interestingly, it was reported that the introduction of serines at both palmitoylation sites of gp41 completely abolished incorporation of Env in light and heavy rafts[99] in the context of a non-truncated protein backbone. However, it could be shown that

bulky, hydrophobic amino acids could replace palmitoylated cysteines without eliminating the raft association of the protein[99]. This observation again points to a minor role of the lipidation for the microdomain partitioning. The phenomenon of light and heavy raft will be discussed again in the population heterogeneities section of the discussion.

Another interesting hypothesis is implied by recent *in silico* experiments[215]. The membrane organization of the Influenza transmembrane protein hemagglutinin (HA) was simulated in phase separating bilayers. In summary it was proposed that HA localizes at the periphery of microdomains as a result of an exclusion of the irregular and bulky transmembrane domain in combination with a preferential lipid raft incorporation of the protein's cytoplasmic palmitoylation in the intracellular leaflet. In addition, *palmitoylations have already been identified as the crucial factor of HA lateral membrane organization* by using the same FLIM-FRET approach as applied in this study[98]. In this light, our finding of a palmitoylation independence of the gp41 raft partitioning is even more surprising.

What could be the background of those differences between gp41 and HA? In contrast to HA, gp41 comprises both, intracellular and extracellular elements assumed to have raft targeting properties, the internal palmitoylation and the external CRAC motif. Consequently, gp41-YFP should equally interact with lipid rafts on both leaflets and thus might have a higher affinity for microdomains in general. In our experiments, a solely mutation of the CRAC domain significantly reduced raft partitioning (Figure 4-14**:** gp41-YFP vs. gp41mCRAC), whereas a removal of the cytoplasmic tail and thus palmitoylation site did not (Figure 4-14: gp41-YFP vs. Δ1). Moreover, an annihilation of both did not result in a further decrease of the microdomain association (Figure 4-14: gp41mCRAC vs. Δ1mCRAC). This might indicate, that only the interaction with external leaflet lipid rafts results in energy transfer from the extracellular GPI-CFP to gp41-YFP but not a potential association of the cytoplasmic palmitoylation with lipid rafts at the internal leaflet. The presumption is conceivable that the results would be different if an internal labeling approach (as published by Engel et al. [124]) would have been applied. However, in the aforementioned FLIM approach on HA, FRET was found between the same raft marker of the extracellular leaflet (GPI-CFP) and the only internally raft coupled HA. Therefore, this hypothesis appears not very likely.

It is also conceivable that CRAC-mutants that comprise the palmitoylation are pushed to the interface of raft and disordered phase as suggested for HA from the simulations for

palmitoylated Influenza HA[215]. As a result of that the average distance to the raft residing GPI-anchored reporter proteins would increase resulting in a significantly reduced FRET. This hypothesis would also explain the low, but different from zero level of remaining FRET for the CRAC-mutant gp41mCRAC (Figure 4-14). But in disagreement with that speculation, this basal level remains also for the Δ1mCRAC variant that does not contain the palmitoylated cysteine and thus should be completely excluded from lipid rafts. Moreover, FRET was found to be proportional to the acceptor intensity for both CRAC-mutants pointing to an energy transfer that is induced solely by random interaction and therefore reports complete absence of any preferred clustering or local enrichment.

5.2 Population heterogeneity in plasma membrane lipid rafts

To date, lateral membrane organization is often schematized in a very simplified way. Bilayers are typically pictured as a homogeneous surface of a disordered "sea" with some floating, raft domains having a higher degree of packaging and order. Although supposed to be highly dynamic, the size, number and composition of the lipid rafts are assumed to be similar amongst different cells within a cell population and temporally stable in individual cells. However, careful examination of our FLIM-FRET results implies an additional complexity of plasma membrane organization (Figure 4-16). By obtaining data on a single cell level we were able to distinguish two separate populations of cells displaying significantly differing raft-related FRET efficiencies. *Most likely, those systematic differences of the obtained FRET efficiencies reflect variations in the average size or composition of plasma membrane lipid rafts between individual cells*. It is noteworthy that comparable results were obtained utilizing C6-NBD-PC as a reporter of overall membrane order (Figure 4-18). Again two populations were found with significant differences in the plasma membrane organization and *factors like position in a cell colony or local cell density could be ruled out to be source of this heterogeneity*. A flow cytometric cell cycle analysis revealed the average fractions of individual cells being in G1/G0, S or G2/M-phase (Figure 4-19) and allowed to hypothesize that the populations of high FRET and high C6-NBD-PC lifetime might be identical with cells being in G2/M phase, whereas the low FRET and low C6-NBD-PC population represents the remaining cells in G1/G0 and S phase. We want to point out, that potentially the finding of systematic variations of single cell lipid rafts described in this work might indicate the same phenomenon as the light and heavy lipid rafts

described before (5.1.3). It is conceivable, that the two classes of lipid rafts observed in biochemical bulk experiments indeed do not reflect different kind of lipid rafts in every single cell, as proposed in the publication of Nebl et al.[214], but rather the same two populations of cells that caused the significant differences in the energy transfer from raft marker to gp41-chimeras found in our experiments.

It has to be discussed what could be the molecular background of the two observed populations. What are the different average FRET efficiencies indicative of? In the approach applied in this study, differences in the energy transfer can originate from four causations: differences in

(I) the association of the fluorescently labeled protein's with rafts,

(II) the orientation of the fluorescence dipoles,

(III) the distance of the participating fluorophores and most importantly

(IV) the overall number of fluorescent proteins residing in plasma membrane lipid rafts.

Considering the crowding of the lipid rafts with fluorescent proteins that has been discussed before, (IV) should reflect overall ratio of microdomains vs. plasma membrane area. Since it can be assumed that the protein properties do not systematically differ between individual cells, (I), (II) and (III) can be neglected and variations in the plasma membrane organization are the only explanation left. Considering that, in addition the overall order of the plasma membrane could be demonstrated to vary from cell-to-cell, *we surmise that the individual size of the lipid rafts or their absolute number is significantly higher in the small cell population* since this hypothesis is suited to explain both, increased FRET efficiency and reduced NBD-lifetime.

5.3 Oligomerization of gp41 variants

The question remains open, what exactly the biological role of the gp41 preference for plasma membrane microdomains is. And closely related to that question: Why is a conservation of a cholesterol binding motif evolutionary beneficial for human immunodeficiency viruses? It has often been hypothesized that an enrichment of the virus components in cholesterol enriched lipid rafts facilitates the virus assembly processes. However, direct experimental evidences for this hypothesis are missing. In this study, fluorescent polarization microscopy was used to address gp41 oligomer assembly in living cells. Firstly, GPI-YFP was used as a

multimerization negative control and the obtained values are in agreement with previously published data (Table 25). *Then, it could be shown that gp41-YFP exist as oligomer at the plasma membrane and in intracellular compartments*, demonstrating that gp41 alone, even in absence of gp120, has the propensity to form stable protein oligomers (Figure 4-26). In contrast to gp41-YFP, the variant Δ1 was found to be oligomerized exclusively at the surface of the cells (Figure 4-26). Obviously, for the multimerization of this variant, conditions are required that are only provided by the plasma membrane environment. The difference between Δ1 and gp41-YFP is the truncation of the cytoplasmic tail. Therefore, the difference in the oligomerization behavior of those variants can be explained by two models:

(I) The oligomerization of both variants occurs at the plasma membrane, but whereas the internalization-deficient variant Δ1 remains at the plasma membrane, gp41-YFP is endocytosed efficiently after oligomerization at the surface. Thus, only this variant can be found in its oligomeric form in internal compartments.
(II) The cytoplasmic domain causes intracellular oligomerization of gp41-YFP.

Model (II) is supported by the work of Lee[216] who reported spontaneous multimerization of the gp41 cytoplasmic domain. However, from our data it is impossible to distinguish between both models. A pulse chase oligomerization analysis or the introduction of mutations in the internalization motifs of gp41-YFP could shed further light on that question. In contrast to previous, indirect studies on gp41[84,204] we could clearly show, that *the transmembrane domain of gp41 is not sufficient to cause an efficient oligomer assembly of gp41-YFP* (Figure 4-26, Δ2 variant). This finding also indicates that MPER and the adjacent heptad region are the main factor of gp41 oligomerization and is therefore in line with several publications[69,205–209]. However it is contradictory to two studies reporting that the gp41 transmembrane domain causes di- and trimerization of reconstituted proteins in *in vitro*-cross linking experiments[204] and that it maintains a trimeric structure in a molecular dynamics simulation. However, both experimental approaches are highly artificial and might not reflect the native protein behavior. On the other hand, it has to be taken into account as well, that the Δ2 variant used in this study only comprises a short linker between transmembrane domain and the bulky, fluorescent protein. Therefore, it is also plausible, that the membrane spanning domain indeed contains motifs able to cause intermolecular interactions but the oligomerization is impeded by the sterical hindrance through the label. Interestingly, we also demonstrated that the *oligomerization of the gp41-YFP fusion proteins is diminished for variants with CRAC*

mutations (Figure 4-26). This observation may implicate a function of the CRAC domain for an efficient assembly or stabilization of protein oligomers and has not been reported before.

Table 25: Anisotropies of chimeric fusion proteins. Experimental data are displayed together with relevant published data.

	Protein	Anisotropy
Thesis	GPI-YFP	**0.28** ±0.01
	Gp41-YFP	**0.21** ±0.01
	Gp41-YFP (intracellular)	**0.18** ±0.01
	Gp41-YFP(plasma membrane)	**0.19** ±0.01
	Gp41-mCRAC	**0.30** ±0.01
	Δ1	**0.22** ±0.01
	Δ1 (intracellular)	**0.25** ±0.01
	Δ1 (plasma membrane)	**0.11** ±0.02
	Δ1mCRAC	**0.29** ±0.02
	Δ2	**0.30** ±0.01
Sharma et al.[139]	GPI-YFP (lipid rafts)	**0.29** ±0.01
	GPI-YFP (∞ dilution)	**0.31**
Bader et al.[143]	GFP (monomer)	**0,29**
	GFP (dimer)	**0,25**
	GFP (trimer)	**0,21**

Whereas the importance of the external region of gp41 for formation of functional trimers has already been described extensively[69,205–209], the discovered role of the CRAC motif needs to be further deliberated. What could be the molecular background and biological relevance of this CRAC dependent oligomerization observed for the gp41 constructs? We surmise that the lateral sorting of gp41 in plasma membrane lipid rafts is the crucial point in this context. *We suppose that, as a result of the CRAC dependent protein accumulation in microdomains, the probability of oligomer assembly events was significantly enhanced* and that this resulted in a higher fraction of oligomers in case of a raft partitioning fusion proteins gp41-YFP and Δ1.

However, we want to point out, that the observed trafficking and oligomerization behavior of our constructs does only partly reflect the native progression of the HIV-1 envelope complex. Trimerization was previously reported to be influenced by different parts of gp41[69,203,205–209,216] but also by the surface subunit gp120[203]. It is likely that gp120 or some of the external parts of gp41 that have been removed in this study could provoke an intracellular and raft independent oligomer assembly. Under physiological condition, the precursor gp160 (gp41/gp120) already trimerizes in the ER [27,203] and subsequently, after cleavage in the Golgi apparatus the two individual subunits remain associated by weak, non-covalent interactions[69], while the stability of this mature hetero-oligomer has been reported to be significantly impaired[203] by the processing. However, stable trimers are a prerequisite for an efficient virus progression since virus-cell-fusion requires formation of the coiled-coil motif and, finally, the six-helix-bundle of the gp41 ectodomains. Hypothetically, the conformational change of the ectodomain that accompanies the membrane fusion may temporarily destabilize the external region and thus influence its role of in the preservation of functional trimers. The CRAC motif dependent oligomerization of gp41 in raft domains could be important to keep the stability during the conformational change. This is in support of a model suggesting lipid rafts not only as protein enrichment platforms but also as a subcompartments that stabilize protein complexes and facilitate protein interactions.

Without any doubts, our data demonstrate, that *gp41 transmembrane domain and external domain alone (Δ1 variant) have the potential to form stable oligomers at the plasma membrane* of expressing cells and furthermore, that the *oligomerization is significantly enhanced by the gp41 cholesterol binding domain*.

5.4 Membrane perturbation by gp41

It seems reasonable to assume that either, raft association and oligomerization state of gp41 influence other properties and functions of this protein. To address this question, as an example, the membrane destabilization potential of the different protein variants was studied in live cell cytometer experiments. The propidium iodide-uptake of transfected cells was used as an indicator of gp41 toxicity and pore-forming properties in the plasma membrane. *The protein gp41-YFP was demonstrated to cause a significantly decrease of the membrane integrity compared to the negative controls* (Figure 4-28). Supporting recent results of vesicle

leakage experiments[9] primarily *the MPER was found to cause gp41-mediated membrane disturbance* (Figure 4-28) as seen by the negative control-like result for the Δ2 variant. A truncation of the cytosolic protein domain produced a further slight increase of PI uptake compared to gp41-YFP as a result of higher plasma membrane concentrations caused by the concomitant removal of the gp41 internalization motifs. It is of note that the cytoplasmic domain also comprises the three lentivirus lytic peptides (1.2.2.3.1) and could thus be expected to cause membrane perturbation as well. From our experiments it can be deduced that this function of the cytoplasmic tail is not of relevance in the assembly context. Instead it might be constricted to entry processes and is supposably mediated by interaction with other components within the virion. However, as before the *CRAC mutation of wild type and truncated gp41 influenced the protein behavior significantly*. A reduced number of PI positive cells was found, pointing to an important function of this motif in the MPER induced membrane perturbation (Figure 4-28). *Most likely, the gp41 lyticity is strongly influenced by the CRAC dependent lateral sorting in lipid rafts*. The MPER might depend on the microdomain environment that significantly deviates from other parts of the bilayer, to cause membrane perturbation. At first glance this seems to be implausible since lipid rafts are, due to their compositional differences, supposed to be more ordered and more rigid than other parts of the plasma membrane, which should impede a disturbance of the bilayer integrity. However, recent experimental data demonstrated an amplified membrane perturbation of MPER peptides in vesicles containing cholesterol[38].

In recent years, different conformations have been suggested for gp41 with the MPER oriented perpendicular or parallel to the plasma membrane[69] allowing to suggest an expanded, conceivable model of the observations described before. We propose a mechanism based on a cholesterol dependent conformational change in the gp41 membrane adjacent, external region. The interaction of the CRAC domain with cholesterol might cause a recruitment of the MPER α-helix towards the membrane which in turn exerts pore-forming and membrane leakage (Figure 5-4). This mechanism might be evolutionary beneficial since protein conformation and function are in this way directly regulated by the lipid composition of the surrounding membrane. Since cholesterol is enriched in viral, plasma and endosomal membranes but less in Golgi apparatus and endoplasmic reticulum[163,217] an unfavorable disruption of intracellular protein synthesis compartments might be prevented. Consequently, the mechanism could permit longer survival of infected cells and as a result of that, higher yields of virus particles.

Of course, other explanations of the phenomenons observed are conceivable as well. Considering obtained results from oligomerization experiments it is also reasonable to assume, that the gp41 membrane perturbation property depends on assembled oligomers. Hence, the obtained CRAC-dependence of the bilayer destabilization/pore-formation[81,210] would be an indirect result of the gp41 oligomerization, which in turn is constrained to a lateral sorting into lipid rafts and by that to a functional CRAC domain. Further experiments are necessary to achieve a complete and conclusive understanding of the interplay between raft partitioning, protein complex formation and membrane perturbation of the HIV-1 envelope protein.

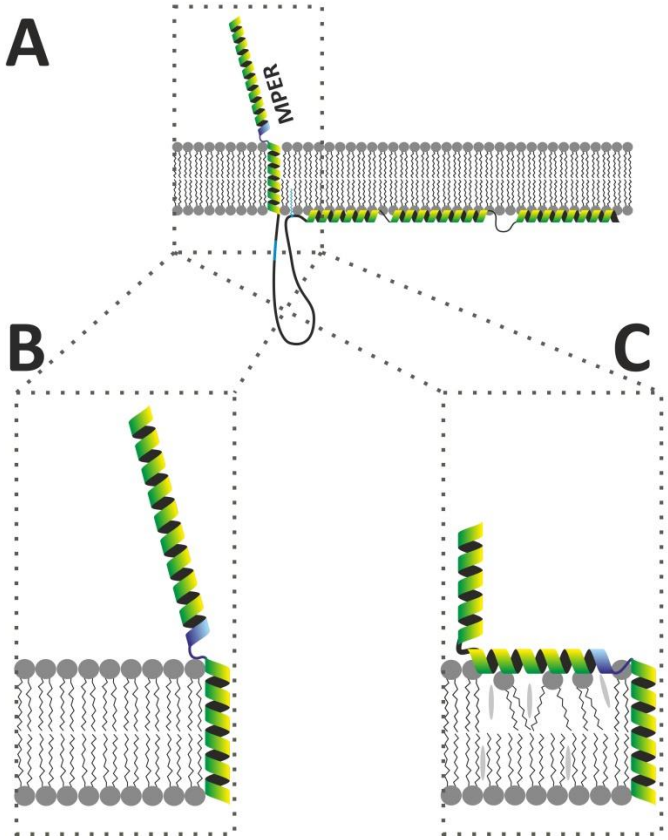

Figure 5-4: Hypothetical mechanism of CRAC dependent membrane perturbation. (A) Gp41 structure in absence of membrane cholesterol. (B and C) Magnification of the relevant portion of gp41. (B) Possibly, in absence of cholesterol, the gp41 CRAC domain does not bind to the membrane resulting in a protein conformation with the MPER oriented rather perpendicular to the bilayer. (C) As a consequence of an interaction between the CRAC domain and cholesterol in the membrane the MPER might be recruited towards the plasma membrane, thereby penetrating the bilayer surface and disturbing the membrane integrity.

5.5 Integration of the results into the prevailing understanding of gp41

In this study several properties of the HIV-1 glycoprotein gp41 were investigated in a live cell context. Data were obtained that report intracellular trafficking, oligomerization, plasma membrane lipid raft partitioning, protein-cytotoxicity, membrane perturbation, palmitoylation and virus particle incorporation. Although many of those properties appear completely independent of each other, in particular in case of gp41 they might be highly interconnected. Lipid raft partitioning for instance, might be of relevance for oligomerization and virus particle incorporation of gp41. Oligomerization is a conceivable factor of protein-induced membrane perturbation and pore-formation. Thus, a comprehensive view on all observation is of high importance. For a better understanding, all variants used in this study are displayed in Figure 5-5.

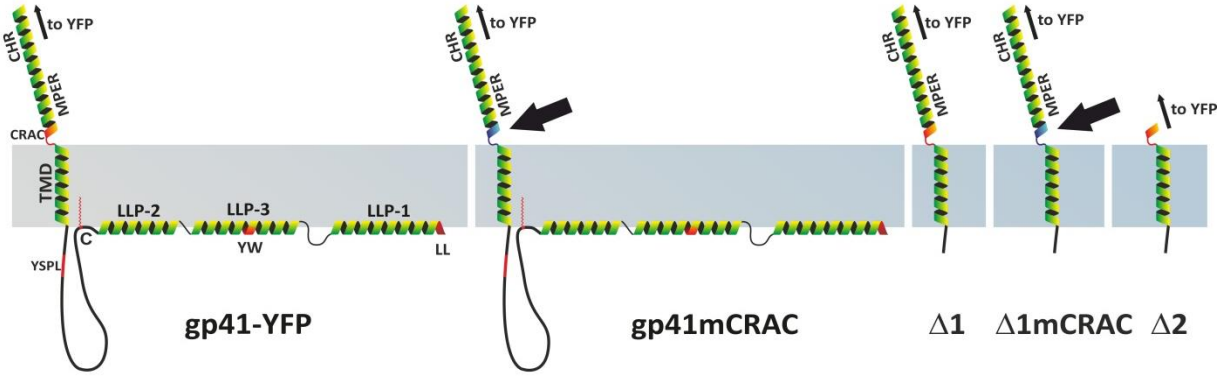

Figure 5-5: Supposed schematic structures of gp41 constructs. Important motifs are highlighted in red and. From YFP tagged N-terminus to the C-terminus are CRAC domain, YXXL endocytosis motif and palmitoylation displayed. In the mCRAC variants, the cholesterol binding motif (blue) is labeled with a black arrow.

The most prominent result from all experiments is that the mutation that has been introduced in the protein's cholesterol binding motif strongly influences most of the studied properties. Mutants showed significantly reduced raft partitioning, membrane perturbation and even oligomerization (summarized in Table 26). It should be underlined again, that the introduced mutation only comprised one single amino acid exchange from a leucin to an isoleucine and thus should only have a minor influence on the domains overall properties, such as folding, hydrophobicity or charge. Since the very same mutation was found to hamper the cholesterol binding potential of the CRAC domain[78,79] it is very likely that this function is the crucial factor causing all observed mutation-induced changes. A specific binding of proteins to lipid

raft components is a well-known mechanism of raft partitioning control (Reviewed in [74]). *We surmise that cholesterol binding of the gp41 CRAC domain causes the protein's sequestering in plasma membrane microdomains. Moreover, we suggest that this local enrichment significantly stabilizes gp41 oligomers* (also discussed in 6).

Table 26: Summarized results of major experiments. FRET efficiencies, anisotropies and PI-uptake rates are shown for GPI-YFP and different gp41 variants. GPI-YFP should be considered as a raft partitioning positive control, whereas it serves as a negative control regarding oligomerization and membrane perturbance.

Protein	GPI-YFP	Gp41-YFP	Gp41mCRAC	Δ1	Δ1mCRAC	Δ2
FRET efficiency [ns]	**7.93** ±0.33	**5.00** ±0.37	**2.00** ±0.37	**4.81** ±0.38	**2.10** ±0.34	**5.43** ±0.56
anisotropy [a.u]	**0.28** ±0.01	**0.21** ±0.01	**0.30** ±0.01	**0.22** ±0.01	**0.29** ±0.02	**0.30** ±0.01
PI-uptake$_{norm}$ [a.u.]	**0.64** ±0.06	**1.01** ±0.02	**0.88** ±0.03	**1.09** ±0.04	**0.85** ±0.07	**0.67** ±0.04

Since Env oligomerization is a non-covalent, reversible association of laterally diffusing proteins it is subjected to the laws of mass action. In a steady-state the overall number of oligomers is concentration dependent and high local concentrations in lipid rafts should therefore increase the probability of the formation of functional oligomers. Interestingly, *the CRAC-mutation was found to influence gp41 membrane perturbation* as well. We suggest that cholesterol binding again is the basis of that behavior. Two different models can be proposed. (1) Cholesterol binding causes an enrichment of gp41-YFP in plasma membrane lipid rafts and thus facilitates or stabilizes oligomerization. Since oligomerization is often assumed to be prerequisite of poreformation[92] in this way cholesterol binding might be linked with membrane perturbation via raft partitioning dependent oligomerization. (2) In the presence of cholesterol, the MPER membrane binding affinity is significantly increased. The region is recruited towards the bilayer, partly penetrates it and thus disturbs the membrane integrity causing leakage.

It is reasonable to guess, that other protein functions are related to lipid raft partitioning as well. It has been proposed that gp41 adopts different conformations with structural consequences for the accessibility of endocytosis motifs[92,102]. Conceivably, this refolding process is related to microdomain incorporation as well. Therefore, even counterintuitive

properties like trafficking might be related to lipid raft partitioning. However, this hypothesis is not supported by our surface exposure data (4.5.2).

6. Summary and conclusions

In the framework of this study we used several methods to study different properties of the HIV-1 glycoprotein gp41. Aim and purpose was to shed further light on membrane-related phenomena and intrinsic properties of the protein in the context of expressing cells without the influence of other viral components. The surface subunit of the envelope complex, the glycoprotein gp120 and some external parts of the transmembrane subunit, gp41 were replaced by a yellow fluorescent protein to allow different fluorescence-based experiments. Fusion proteins were produced containing all membrane proximal regions and domains supposed to interact with cellular membranes in the synthesis and assembly phases of the virus lifecycle. This approach offers several advantages. The fluorescent tag allows a microscopical visualization of the intracellular localization but moreover also direct interaction studies based on FLIM-FRET and anisotropy measurements that enabled us to assess information in a length-scale below the detection limit of light microscopy. By replacing only external and membrane-distanced parts of the envelope complex with the fluorophore it was ensured that direct membrane-interactions and in particular the function of the cytoplasmic tail are unaffected by the tagging. However, conclusions about properties of the envelope complex that might be related to the removed parts, such as for example about the oligomerization[43,207,209] cannot be definitely judged from our results.

Although HIV and its components have been extensively studied and thus this virus is in general one of the best characterized pathogens, still many questions remain open. The cytoplasmic tail of the envelope complex is a typical example. Although the unusually length of this domain is highly conserved in lentiviruses, it does not exist in that form in other retroviruses[91]. The role of the cytoplasmic tail in the virus lifecycle and its specific function is not fully understood[91]. Moreover, other already identified domains and motifs, in particular in the membrane adjacent, intracellular but also external region of gp41 have not been concludingly elucidated yet and their relevance is often still under debate[91]. Known and supposed interactions of virus components with host cell proteins, compartments and structural elements need to be further investigated to achieve a complete understanding of the virus biology and allow an efficient control of the HIV pandemic and individual infections. For example, it has been proposed that many viruses and in particular HIV might use the lateral subcompartmentation of cellular membrane systems to facilitate their highly regulated assembly (reviewed in [218]). Many, strong indications have been already found pointing to an

important function of cholesterol-enriched lipid rafts. Most importantly, it has been demonstrated that virus envelope strongly resembles host cell microdomains[163,164], and thus significantly differs from the overall plasma membrane, with respect to lipid and protein composition. Moreover, it was shown that virus assembly shifts away from the plasma membrane to the Golgi apparatus in cells harboring a non-sense mutation in proteins involved in the cholesterol-trafficking that causes a respective dislocation of the cellular cholesterol[219]. On the other hand, in some studies lipid raft partitioning of the virus envelope complex was observed not to be important for different protein functions such as Env incorporation and virus progression in general. Furthermore, contradictory and inconsistent results were obtained regarding gp41 intrinsic factors of a potential microdomain preference.

The outstanding question that we aimed to address with this study was, what is the role of lipid rafts in the HI virus assembly. The obtained results allow drawing the following conclusion in that context.

1. The majority of overexpressed HIV-1 gp41 glycoproteins do efficiently partition into GPI-enriched plasma membrane microdomains in CHO-K1 cells.
2. The proteins intrinsic cholesterol binding motif (CRAC) is the sufficient and necessary determinant of this property. Other parts of the protein from the virus isolate JR-FL such as palmitoylation or membrane interacting amphipathic α-helices do not contribute to the raft affinity.
3. CRAC mutations do not influence protein expression and surface exposure.
4. The glycoprotein's C-terminal heptad repeat, membrane proximal external region (MPER) and transmembrane domain alone are sufficient to drive oligomerization of gp41 even in absence of other parts of the Env gene product.
5. The external region is crucial for the oligomerization of the chimera. Upon removal, this property is abolished.
6. The external region-induced oligomerization is CRAC dependent which might point to an oligomer stabilizing function of the protein's lipid raft partitioning.
7. Gp41 possesses membrane perturbing properties that are CRAC and external region dependent.
8. The plasma membrane organization significantly differs between individuals of a cell line. At least two populations exist with systematic differences in the lipid rafts.

Taken together those findings confirm the hypothesis that gp41 is a lipid raft residing protein. Moreover, the highly conserved CRAC domain was found to be an indispensible prerequisite of the lateral sorting. Surprisingly, we found that other properties such as oligomer stability and membrane perturbation also depend on a functional CRAC domain. Whether this is a

direct consequence of CRAC interactions in the respective contexts or results from CRAC induced lipid raft partitioning remains open.

Since the removal of the gp41 external domain and gp120 significantly interferes with the oligomerization properties of the glycoproteins, conclusions from the results at hand about the native situation are highly hypothetical. Nevertheless, a model is suggested that integrates our observations with previous results (Figure 6-1).

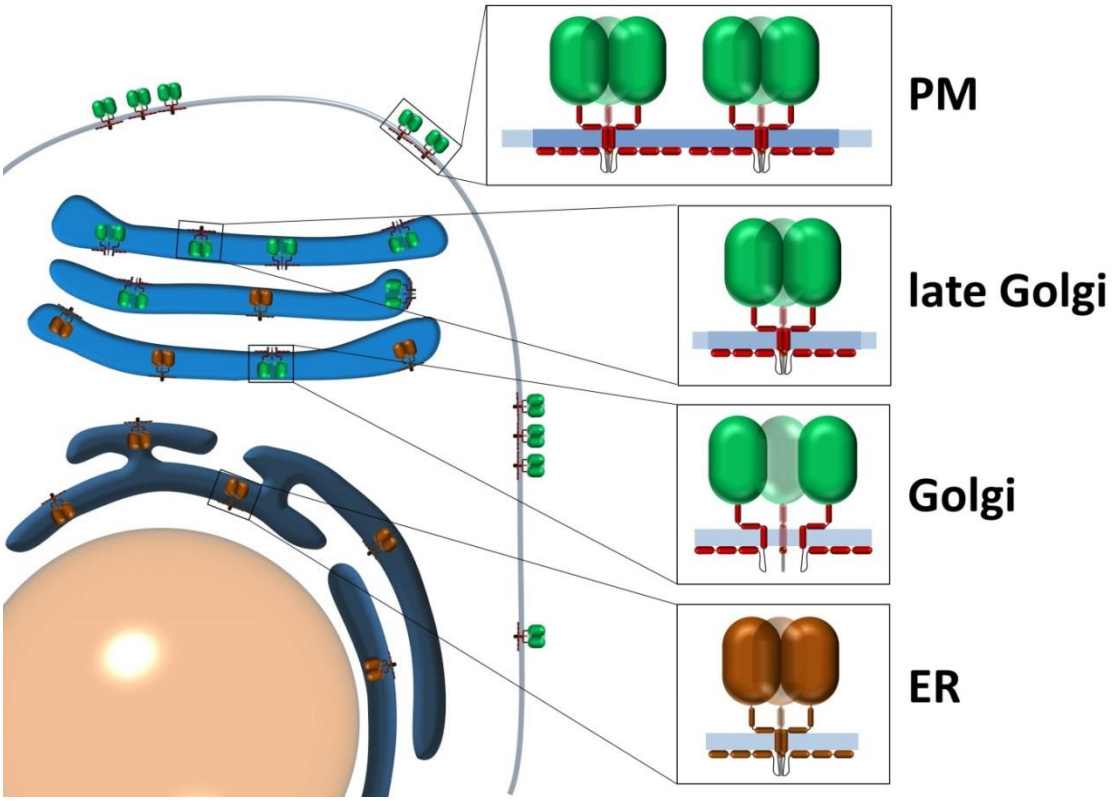

Figure 6-1: Model of HIV-1 Env progression from synthesis site to the plasma membrane. The Env glycoprotein is synthesized as a polyprotein precursor in the rough endoplasmic reticulum. Here, monomers of gp160 also oligomerize into predominantly trimers. Upon proteolytical cleavage by cellular proteases in the Golgi apparatus the surface subunit gp120 and the transmembrane subunit gp41 are generated. Although, gp120 and gp41 remain associated by non-covalent interaction, forming a heterotrimeric glycoprotein spike, this process reduces the oligomer stability significantly. In the late Golgi apparatus and in the plasma membrane the complex partitions into microdomains, causing a local enrichment and therefore effective stabilization of the oligomeric structure.

From biochemical experiments it is known, that the precursor protein of the envelope complex, the protein gp160 is synthesized in the rough endoplasmic reticulum[27]. The

precursor oligomerizes and is transferred to the Golgi apparatus where proteolytic cleavage into gp41 and gp120 occurs[27]. This cleavage decreases the oligomer stability[203] but the complex remains assembled as a trimer of heterodimers that is finally transported to the plasma membrane. We surmise, that indeed factors within gp120 are important for the early trimerization of Env in the endoplasmic reticulum. Upon enzymatic cleavage in the Golgi apparatus and due to the instable, non-covalent linkage connection between the two subunits, the oligomerization influence of gp120 might be only weakly transferred to gp41 and thus the complete complex is destabilized. But, the emerging local enrichment of the glycoproteins in lipid rafts of the Golgi apparatus and later in the plasma membrane might compensate for this destabilization. As a result of the high concentrations that are induced in the lipid rafts, the monomer to oligomer equilibrium is pushed towards the oligomerization state. This hypothesis would be in agreement with the previously published biochemical results and the findings of this work.

However, this study also raised some completely new issues. Is there any influence of the CRAC domain on the investigated properties even in physiological environments (i.e. macrophages)? Although lipid raft partitioning can be expected to be unaffected by the truncations introduced in the protein gp41-YFP, oligomerization and membrane perturbation might be different compared to the wild type situation. The relevance of CRAC mutations here would be an interesting topic to elucidate. Undoubtedly, the most prominent question that was raised by this work is what is the biological meaning of the observed inhomogeneity of the membrane organization? What are the cell-to-cell differences related to? Do they follow cellular adaptions while the cell is progressing through the cell cycle or do they reflect differences in the microenvironment of individual cells? What is the molecular background of the deviating lipid raft size and overall membrane order? Some of the hypothesis made before, are based on assumptions that need further verification. The uncertainties and the open questions have to be studied in complementary and perpetuating approaches. For this purpose, some of the produced constructs may be used in the future to study their behavior especially upon coexpression with Gag-constructs. Moreover, the finding that the cytoplasmic tail of gp41 is not involved in the proteins raft partitioning should be considered for further raft partitioning experiments and suggests an intracellular gp41 labeling approach as conducted by Engel et. al[124].

Addendum

Bibliography

1. Brennan, R. O. & Durack, D. T. Gay compromise syndrome. *Lancet* **2,** 1338–9 (1981).

2. Hymes, K. B. *et al.* Kaposi's sarcoma in homosexual men-a report of eight cases. *Lancet* **2,** 598–600 (1981).

3. Kaposi's sarcoma and Pneumocystis pneumonia among homosexual men--New York City and California. *MMWR. Morb. Mortal. Wkly. Rep.* **30,** 305–8 (1981).

4. CDC. Pneumocystis Pneumonia --- Los Angeles. *CDC Wkly. news* **30,** 1–2 (1981).

5. U.S. Department of Health & Human Services. www.aids.gov.

6. Avert.org. (2012). at <www.avert.org>

7. Osmanov, S. & Pattou, C. Estimated global distribution and regional spread of HIV-1 genetic subtypes in the year 2000. *JAIDS J. ...* (2002). at <http://journals.lww.com/jaids/Abstract/2002/02010/Estimated_Global_Distribution_and_Regional_Spread.13.aspx>

8. Martinac, B. *et al.* Yeast K1 killer toxin forms ion channels in sensitive yeast spheroplasts and in artificial liposomes. *Proc. Natl. Acad. Sci. U. S. A.* **87,** 6228–32 (1990).

9. Worobey, M. *et al.* Direct evidence of extensive diversity of HIV-1 in Kinshasa by 1960. *Nature* **455,** 661–4 (2008).

10. Reeves, J. D. & Doms, R. W. Human immunodeficiency virus type 2. *J. Gen. Virol.* **83,** 1253–65 (2002).

11. Fischer, H. E. & Reuben, J. M. Human Immunodeficiency Virus Type 2: Implications for Blood Donors. *Curr. Issues Transfus. Med.* **2,** (1993).

12. Martin-Serrano, J. & Neil, S. J. D. Host factors involved in retroviral budding and release. *Nat. Rev. Microbiol.* **9,** 519–31 (2011).

13. Aids, U. W. *World AIDS day Report 2011 Faster. Smarter. Better.* (2011).

14. Buonaguro, L., Tagliamonte, M., Tornesello, M. L. & Buonaguro, F. M. Genetic and phylogenetic evolution of HIV-1 in a low subtype heterogeneity epidemic: the Italian example. *Retrovirology* **4,** 34 (2007).

15. Gao, F. *et al.* Origin of HIV-1 in the chimpanzee Pan troglodytes troglodytes. *Nature* **397,** 436–41 (1999).

16. Bhardwaj, N., Hladik, F. & Moir, S. The immune response to HIV. **5,** (2012).

17. Fauci, a S., Pantaleo, G., Stanley, S. & Weissman, D. Immunopathogenic mechanisms of HIV infection. *Ann. Intern. Med.* **124,** 654–63 (1996).

18. Prof Dr Luc Kestens, P. & Institute of Tropical Medicine, A. Virology and Immunology of HIV. at <http://www.itg.be/internet/e-learning/written_lecture_eng/6_immune_responses_to_hiv_infection.html>

19. McMichael, A. J., Borrow, P., Tomaras, G. D., Goonetilleke, N. & Haynes, B. F. The immune response during acute HIV-1 infection: clues for vaccine development. *Nat. Rev. Immunol.* **10,** 11–23 (2010).

20. Clapham, P. R. HIV-1 receptors and cell tropism. *Br. Med. Bull.* **58,** 43–59 (2001).

21. Connor, R. I., Sheridan, K. E., Ceradini, D., Choe, S. & Landau, N. R. Change in coreceptor use correlates with disease progression in HIV-1--infected individuals. *J. Exp. Med.* **185,** 621–8 (1997).

22. McGraw-Hill. How the HIV Infection Cycle Works. at <http://highered.mcgraw-hill.com/sites/0072495855/student_view0/chapter24/animation__how_the_hiv_infection_cycle_works.html>

23. Briggs, J. a G. & Kräusslich, H.-G. The molecular architecture of HIV. *J. Mol. Biol.* **410,** 491–500 (2011).

24. Protein Data Bank. at <http://www.pdb.org/pdb/home/home.do>

25. Swanson, C. M. & Malim, M. H. SnapShot: HIV-1 proteins. *Cell* **133,** 742, 742.e1 (2008).

26. Zhao, G. *et al.* Mature HIV-1 capsid structure by cryo-electron microscopy and all-atom molecular dynamics. *Nature* **497,** 643–646 (2013).

27. Checkley, M. A., Luttge, B. G. & Freed, E. O. HIV-1 envelope glycoprotein biosynthesis, trafficking, and incorporation. *J. Mol. Biol.* **410,** 582–608 (2011).

28. Markosyan, R. M., Cohen, F. S. & Melikyan, G. B. Time-resolved Imaging of HIV-1 Env-mediated Lipid and Content Mixing between a Single Virion and Cell Membrane. **16,** 5502–5513 (2005).

29. Fassati, A. Multiple roles of the capsid protein in the early steps of HIV-1 infection. *Virus Res.* **170,** 15–24 (2012).

30. Chinen, J. & Shearer, W. T. Molecular virology and immunology of HIV infection. *J. Allergy Clin. Immunol.* **110,** 189–198 (2002).

31. Liu, J., Bartesaghi, A., Borgnia, M. J., Sapiro, G. & Subramaniam, S. Molecular architecture of native HIV-1 gp 120 trimers. **455,** 109–113 (2009).

32. Ashkenazi, A. & Shai, Y. Insights into the mechanism of HIV-1 envelope induced membrane fusion as revealed by its inhibitory peptides. *Eur. Biophys. J.* **40,** 349–57 (2011).

33. Wilen, C. B., Tilton, J. C. & Doms, R. W. HIV: Cell Binding and Entry. *Cold Spring Harb. Perspect. Med.* **2,** (2012).

34. Weiss, C. D. HIV-1 gp41 : Mediator of Fusion and Target for Inhibition © Permanyer Publications 2010. (2010).

35. Gallay, P. Syndecans and HIV-1 pathogenesis. *Microbes Infect.* **6,** 617–22 (2004).

36. Lehmann, M. J., Sherer, N. M., Marks, C. B., Pypaert, M. & Mothes, W. Actin- and myosin-driven movement of viruses along filopodia precedes their entry into cells. *J. Cell Biol.* **170,** 317–25 (2005).

37. Melikyan, G. B. Common principles and intermediates of viral protein-mediated fusion: the HIV-1 paradigm. *Retrovirology* **5,** 111 (2008).

38. Apellániz, B., Ivankin, A., Nir, S., Gidalevitz, D. & Nieva, J. L. Membrane-proximal external HIV-1 gp41 motif adapted for destabilizing the highly rigid viral envelope. *Biophys. J.* **101,** 2426–35 (2011).

39. Zhu, P. *et al.* Distribution and three-dimensional structure of AIDS virus envelope spikes. *Nature* **441,** 847–52 (2006).

40. Schibli, D. J., Montelaro, R. C. & Vogel, H. J. The membrane-proximal tryptophan-rich region of the HIV glycoprotein, gp41, forms a well-defined helix in dodecylphosphocholine micelles. *Biochemistry* **40,** 9570–8 (2001).

41. Reuven, E. M. *et al.* HIV-1 gp41 transmembrane domain interacts with the fusion peptide: implication in lipid mixing and inhibition of virus-cell fusion. *Biochemistry* **51,** 2867–78 (2012).

42. Liu, S. *et al.* Membrane topology analysis of HIV-1 envelope glycoprotein gp41. *Retrovirology* **7,** 100 (2010).

43. Faingold, O., Cohen, T. & Shai, Y. A GxxxG-like Motif within HIV-1 Fusion Peptide Is Critical to Its Immunosuppressant Activity, Structure, and Interaction with the Transmembrane Domain of the T-cell Receptor. *J. Biol. Chem.* **287,** 33503–11 (2012).

44. Jiang, J. & Aiken, C. Maturation-dependent human immunodeficiency virus type 1 particle fusion requires a carboxyl-terminal region of the gp41 cytoplasmic tail. *J. Virol.* **81,** 9999–10008 (2007).

45. Hollier, M. J. & Dimmock, N. J. The C-terminal tail of the gp41 transmembrane envelope glycoprotein of HIV-1 clades A, B, C, and D may exist in two conformations: an analysis of sequence, structure, and function. *Virology* **337,** 284–96 (2005).

46. Lopez-Vergès, S. *et al.* Tail-interacting protein TIP47 is a connector between Gag and Env and is required for Env incorporation into HIV-1 virions. *Proc. Natl. Acad. Sci. U. S. A.* **103,** 14947–52 (2006).

47. Doms, R. W. The plasma membrane as a combat zone in the HIV battlefield. *Genes Dev.* **14,** 2677–2688 (2000).

48. Eckert, D. M. & Kim, P. S. Mechanisms of viral membrane fusion and its inhibition. *Annu. Rev. Biochem.* **70,** 777–810 (2001).

49. Harrison, S. Viral membrane fusion. *Nat. Struct. Mol. Biol.* **15,** 690–698 (2008).

50. White, J. M., Delos, S. E., Brecher, M. & Schornberg, K. Structures and Mechanisms of Viral Membrane Fusion Proteins. **43,** 189–219 (2009).

51. Mobley, P. W., Lee, H., Curtain, C. C., Waring, A. J. & Gordon, M. The amino-terminal peptide of HIV-1 glycoprotein 41 fuses human erythrocytes. **1271,** 304–314 (1995).

52. Rafalski, M., Lear, J. D. & DeGrado, W. F. Phospholipid interactions of synthetic peptides representing the N-terminus of HIV gp41. *Biochemistry* **29,** 7917–22 (1990).

53. Gordon, L. M. *et al.* The amino-terminal peptide of HIV-1 glycoprotein 41 interacts with human erythrocyte membranes: peptide conformation, orientation and aggregation. *Biochim. Biophys. Acta - Mol. Basis Dis.* **1139,** 257–274 (1992).

54. Tristram-Nagle, S. & Nagle, J. F. HIV-1 fusion peptide decreases bending energy and promotes curved fusion intermediates. *Biophys. J.* **93,** 2048–55 (2007).

55. Tristram-Nagle, S. & Chan, R. HIV fusion peptide penetrates, disorders, and softens T-cell membrane mimics. *J. Mol. ...* **402,** 139–153 (2010).

56. Blacklow, S. C., Lu, M. & Kim, P. S. A trimeric subdomain of the simian immunodeficiency virus envelope glycoprotein. *Biochemistry* **34,** 14955–62 (1995).

57. Chan, D. C., Fass, D., Berger, J. M. & Kim, P. S. Core structure of gp41 from the HIV envelope glycoprotein. *Cell* **89,** 263–73 (1997).

58. Weissenhorn, W., Dessen, A. & Harrison, S. C. Atomic structure of the ectodomain from HIV-1 gp41. *Nature* **387,** 426–430 (1997).

59. Kilby, J. M. *et al.* Potent suppression of HIV-1 replication in humans by T-20, a peptide inhibitor of gp41-mediated virus entry. *Nat. Med.* **4,** 1302–7 (1998).

60. Berkhout, B., Eggink, D. & Sanders, R. W. Is there a future for antiviral fusion inhibitors? *Curr. Opin. Virol.* **2,** 50–9 (2012).

61. Jing, S., Zhao, Q. & Debnath, A. Peptide and Non-peptide HIV Fusion Inhibitors. *Curr. Pharm. Des.* **8,** 563–580 (2002).

62. Louis, J. M. *et al.* Revisiting monomeric HIV-1 protease. Characterization and redesign for improved properties. *J. Biol. Chem.* **278,** 6085–92 (2003).

63. Sen, J., Jacobs, A. M. Y., Jiang, H. & Rong, L. The disulfide loop of gp41 is critical to the furin recognition site of HIV gp160. 1236–1241 (2007). doi:10.1110/ps.072771407.furin

64. Ashkenazi, A., Merklinger, E. & Shai, Y. Intramolecular interactions within the human immunodeficiency virus-1 gp41 loop region and their involvement in lipid merging. *Biochemistry* **51,** 6981–9 (2012).

65. Sun, Z.-Y. J. *et al.* HIV-1 broadly neutralizing antibody extracts its epitope from a kinked gp41 ectodomain region on the viral membrane. *Immunity* **28,** 52–63 (2008).

66. Suárez, T., Gallaher, W. R., Agirre, a, Goñi, F. M. & Nieva, J. L. Membrane interface-interacting sequences within the ectodomain of the human immunodeficiency virus type 1 envelope glycoprotein: putative role during viral fusion. *J. Virol.* **74,** 8038–47 (2000).

67. Sáez-Cirión, A. *et al.* Structural and functional roles of HIV-1 gp41 pretransmembrane sequence segmentation. *Biophys. J.* **85,** 3769–80 (2003).

68. Sáez-Cirión, A. *et al.* Sphingomyelin and cholesterol promote HIV-1 gp41 pretransmembrane sequence surface aggregation and membrane restructuring. *J. Biol. Chem.* **277,** 21776–85 (2002).

69. Liu, J. & Lu, M. Structure of the HIV-1 gp41 Membrane-Proximal Ectodomain Region in a Putative Prefusion Conformation. *Structure* **48,** 2915–2923 (2010).

70. Jiang, S. B., Lin, K., Strick, N. & Neurath, A. R. Inhibition of HIV-1 Infection by a Fusion Domain Binding Peptide from the HIV-1 Envelope Glycoprotein GP41. *Biochem. Biophys. Res. Commun.* **195,** 533–538 (1993).

71. Alfsen, a, Iniguez, P., Bouguyon, E. & Bomsel, M. Secretory IgA specific for a conserved epitope on gp41 envelope glycoprotein inhibits epithelial transcytosis of HIV-1. *J. Immunol.* **166,** 6257–65 (2001).

72. Fantini, J., Cook, D. G., Nathanson, N., Spitalnik, S. L. & Gonzalez-Scarano, F. Infection of colonic epithelial cell lines by type 1 human immunodeficiency virus is associated with cell surface expression of galactosylceramide, a potential alternative gp120 receptor. *Proc. Natl. Acad. Sci. U. S. A.* **90,** 2700–4 (1993).

73. Li, H. & Papadopoulos, V. Peripheral-type benzodiazepine receptor function in cholesterol transport. Identification of a putative cholesterol recognition/interaction amino acid sequence and consensus pattern. *Endocrinology* **139,** 4991–7 (1998).

74. Epand, R. M. Proteins and cholesterol-rich domains. *Biochim. Biophys. Acta* **1778,** 1576–82 (2008).

75. Van Duyl, B. Y. *et al.* A synergistic effect between cholesterol and tryptophan-flanked transmembrane helices modulates membrane curvature. *Biochemistry* **44,** 4526–32 (2005).

76. Vincent, N., Genin, C. & Malvoisin, E. Identification of a conserved domain of the HIV-1 transmembrane protein gp41 which interacts with cholesteryl groups. *Biochim. Biophys. Acta* **1567,** 157–64 (2002).

77. Epand, R. M., Sayer, B. G. & Epand, R. F. Peptide-Induced Formation of Cholesterol-Rich Domains†. *Biochemistry* **42,** 14677–14689 (2003).

78. Epand, R. R. F. R. M., Thomas, A., Brasseur, R. & Vishwanathan, S. A. Juxtamembrane protein segments that contribute to recruitment of cholesterol into domains. *Biochemistry* **45,** 6105–6114 (2006).

79. Greenwood, A. I. *et al.* CRAC motif peptide of the HIV-1 gp41 protein thins SOPC membranes and interacts with cholesterol. *Biochim. Biophys. Acta* **1778,** 1120–30 (2008).

80. Lorizate, M., Huarte, N., Sáez-Cirión, A. & Nieva, J. L. Interfacial pre-transmembrane domains in viral proteins promoting membrane fusion and fission. *Biochim. Biophys. Acta* **1778,** 1624–39 (2008).

81. Chen, S. S.-L. *et al.* Identification of the LWYIK motif located in the human immunodeficiency virus type 1 transmembrane gp41 protein as a distinct determinant for viral infection. *J. Virol.* **83,** 870–83 (2009).

82. Salzwedel, K., West, J. T. & Hunter, E. A conserved tryptophan-rich motif in the membrane-proximal region of the human immunodeficiency virus type 1 gp41 ectodomain is important for Env-mediated fusion and virus infectivity. *J. Virol.* **73,** 2469–80 (1999).

83. Shang, L., Yue, L. & Hunter, E. Role of the membrane-spanning domain of human immunodeficiency virus type 1 envelope glycoprotein in cell-cell fusion and virus infection. *J. Virol.* **82,** 5417–28 (2008).

84. Kim, J., Hartley, T., Kim & Engelman. Molecular dynamics studies of the transmembrane domain of gp41 from HIV-1. *Biochim. Biophys. ...* **1788,** 1804–1812 (2009).

85. Yue, L., Shang, L. & Hunter, E. Truncation of the membrane-spanning domain of human immunodeficiency virus type 1 envelope glycoprotein defines elements required for fusion, incorporation, and infectivity. *J. Virol.* **83,** 11588–98 (2009).

86. Miyauchi, K., Komano, J., Yokomaku, Y., Sugiura, W. & Yamamoto, N. Role of the Specific Amino Acid Sequence of the Membrane-Spanning Domain of Human Immunodeficiency Virus Type 1 in Membrane Fusion. **79,** 4720–4729 (2005).

87. Hunter, E. & Swanstrom, R. Retrovirus envelope glycoproteins. *Curr. Top. Microbiol. Immunol.* **157,** 187–253 (1990).

88. Gao, F. *et al.* Molecular cloning and analysis of functional envelope genes from human immunodeficiency virus type 1 sequence subtypes A through G. The WHO and NIAID. *J. ...* **70,** 1651–1667 (1996).

89. Srinivas, S. K., Srinivas, R. V, Anantharamaiah, G. M., Segrest, J. P. & Compans, R. W. Membrane interactions of synthetic peptides corresponding to amphipathic helical segments of the human immunodeficiency virus type-1 envelope glycoprotein. *J. Biol. Chem.* **267,** 7121–7 (1992).

90. Yang, P. *et al.* The cytoplasmic domain of human immunodeficiency virus type 1 transmembrane protein gp41 harbors lipid raft association determinants. *J. Virol.* **84,** 59–75 (2010).

91. Da Silva, E. S., Mulinge, M. & Bercoff, D. P. The frantic play of the concealed HIV envelope cytoplasmic tail. *Retrovirology* **10,** 54 (2013).

92. Costin, J. M., Rausch, J. M., Garry, R. F. & Wimley, W. C. Viroporin potential of the lentivirus lytic peptide (LLP) domains of the HIV-1 gp41 protein. *Virol. J.* **4,** 123 (2007).

93. Affranchino, J. L. & González, S. a. Mutations at the C-terminus of the simian immunodeficiency virus envelope glycoprotein affect gp120-gp41 stability on virions. *Virology* **347,** 217–25 (2006).

94. Wyss, P., Berlioz-torrent, C., Boge, M. & Blot, G. The Highly Conserved C-Terminal Dileucine Motif in the Cytosolic Domain of the Human Immunodeficiency Virus Type 1 Envelope Glycoprotein Is Critical for Its Association with the AP-1 Clathrin Adapter. **75,** 2982–2992 (2001).

95. Murakami, T. Roles of the interactions between Env and Gag proteins in the HIV-1 replication cycle. *Microbiol. Immunol.* **52,** 287–95 (2008).

96. Berlioz-Torrent, C. *et al.* Interactions of the cytoplasmic domains of human and simian retroviral transmembrane proteins with components of the clathrin adaptor complexes modulate intracellular and cell surface expression of envelope glycoproteins. *J. Virol.* **73,** 1350–61 (1999).

97. Levental, I., Lingwood, D., Grzybek, M., Coskun, Ü. & Simons, K. Palmitoylation regulates raft affinity for the majority of integral raft proteins. *PNAS* **107,** 22050–22054 (2010).

98. Scolari, S. *et al.* Lateral distribution of the transmembrane domain of influenza virus hemagglutinin revealed by time-resolved fluorescence imaging. *J. Biol. Chem.* **284,** 15708–16 (2009).

99. Bhattacharya, J., Peters, P. & Clapham, P. immunodeficiency virus type 1 envelope glycoproteins that lack cytoplasmic domain cysteines: impact on association with membrane lipid rafts and incorporation onto. *J. Virol.* **78,** 5500–5506 (2004).

100. Rousso, I., Mixon, M. B., Chen, B. K. & Kim, P. S. Palmitoylation of the HIV-1 envelope glycoprotein is critical for viral infectivity. *Proc. Natl. Acad. Sci. U. S. A.* **97,** 13523–5 (2000).

101. Chan, W., Lin, H. & Chen, S. Wild-type-like viral replication potential of human immunodeficiency virus type 1 envelope mutants lacking palmitoylation signals. *J. Virol.* **79,** 8374–8387 (2005).

102. Buratti, E., McLain, L., Tisminetzky, S.G., Cleveland, S.M., Dimmock, N.J., Baralle, F. E. The neutralizing antibody response against a conserved region of HIV-1 gp41 (amino acid residues 731–752) is uniquely directed against a conformational epitope. *J. Gen. Virol.* (1998).

103. Land, A., Zonneveld, D. & Braakman, I. Folding of HIV-1 envelope glycoprotein involves extensive isomerization of disulfide bonds and conformation-dependent leader peptide cleavage. *FASEB J.* **17,** 1058–67 (2003).

104. Murakami, T. & Freed, E. O. The long cytoplasmic tail of gp41 is required in a cell type-dependent manner for HIV-1 envelope glycoprotein incorporation into virions. *Proc. Natl. Acad. Sci. U. S. A.* **97,** 343–8 (2000).

105. Saad, J. S. *et al.* Structural basis for targeting HIV-1 Gag proteins to the plasma membrane for virus assembly. *Proc. Natl. Acad. Sci. U. S. A.* **103,** 11364–9 (2006).

106. Bhattacharya, J., Repik, A. & Clapham, P. R. Gag regulates association of human immunodeficiency virus type 1 envelope with detergent-resistant membranes. *J. Virol.* **80,** 5292–300 (2006).

107. Egan, M. a, Carruth, L. M., Rowell, J. F., Yu, X. & Siliciano, R. F. Human immunodeficiency virus type 1 envelope protein endocytosis mediated by a highly conserved intrinsic internalization signal in the cytoplasmic domain of gp41 is suppressed in the presence of the Pr55gag precursor protein. *J. Virol.* **70,** 6547–56 (1996).

108. Meer, G. Van, Voelker, D. R. D., Feigenson, G. W. G. & van Meer, G. Membrane lipids: where they are and how they behave. *Nat. Rev. Mol. Cell Biol.* **9,** 112–24 (2008).

109. De Almeida, R. F. M., Fedorov, A. & Prieto, M. Sphingomyelin/phosphatidylcholine/cholesterol phase diagram: boundaries and composition of lipid rafts. *Biophys. J.* **85,** 2406–16 (2003).

110. Simons, K. & Ikonen, E. Functional rafts in cell membranes. *Nature* **387,** 569–72 (1997).

111. Haluska, C. K. *et al.* Combining fluorescence lifetime and polarization microscopy to discriminate phase separated domains in giant unilamellar vesicles. *Biophys. J.* **95,** 5737–47 (2008).

112. Stöckl, M. Giant vesicles – An ideal tool to study lateral phospholipid distribution and domain dependent protein membrane interactions Dissertation. (1980).

113. Levental, I., Grzybek, M. & Simons, K. Greasing their way: lipid modifications determine protein association with membrane rafts. *Biochemistry* **49,** 6305–16 (2010).

114. Wang, J. K., Kiyokawa, E., Verdin, E. & Trono, D. The Nef protein of HIV-1 associates with rafts and primes T cells for activation. *Proc. Natl. Acad. Sci. U. S. A.* **97,** 394–9 (2000).

115. Ono, a & Freed, E. O. Plasma membrane rafts play a critical role in HIV-1 assembly and release. *Proc. Natl. Acad. Sci. U. S. A.* **98,** 13925–30 (2001).

116. Mizuno, H. *et al.* Fluorescent probes for superresolution imaging of lipid domains on the plasma membrane. *Chem. Sci.* **2,** 1548 (2011).

117. Simons, K. & Gerl, M. J. Revitalizing membrane rafts: new tools and insights. *Nat. Rev. Mol. Cell Biol.* **11,** 688–99 (2010).

118. Simons, K. & Sampaio, J. L. Membrane organization and lipid rafts. *Cold Spring Harb. Perspect. Biol.* **3,** a004697 (2011).

119. Lichtenberg, D., Goñi, F. M. & Heerklotz, H. Detergent-resistant membranes should not be identified with membrane rafts. *Trends Biochem. Sci.* **30,** 430–6 (2005).

120. Leslie, M. Mysteries of the cell. Do lipid rafts exist? *Science* **334,** 1046–7 (2011).

121. Jermy, A. Bacterial lipid rafts discovered. *Nat. Rev. Microbiol.* **8,** 756 (2010).

122. Kolter, R. & Lo, D. Functional microdomains in bacterial membranes. 1893–1902 (2010). doi:10.1101/gad.1945010.1

123. Holm, K. & Weclewicz, K. Human immunodeficiency virus type 1 assembly and lipid rafts: Pr55gag associates with membrane domains that are largely resistant to Brij98 but sensitive to Triton X. *J. ...* **77,** 4805–4817 (2003).

124. Engel, S. *et al.* FLIM-FRET and FRAP reveal association of influenza virus haemagglutinin with membrane rafts. *Biochem. J.* **425,** 567–73 (2010).

125. Chang, T.-H., Segovia, J., Sabbah, A., Mgbemena, V. & Bose, S. Cholesterol-rich lipid rafts are required for release of infectious human respiratory syncytial virus particles. *Virology* **422,** 205–13 (2012).

126. Mañes, S., del Real, G. & Martínez-A, C. Pathogens: raft hijackers. *Nat. Rev. Immunol.* **3,** 557–68 (2003).

127. Van Hamme, E., Dewerchin, H. L., Cornelissen, E., Verhasselt, B. & Nauwynck, H. J. Clathrin- and caveolae-independent entry of feline infectious peritonitis virus in monocytes depends on dynamin. *J. Gen. Virol.* **89,** 2147–56 (2008).

128. Campbell, S. M., Crowe, S. M. & Mak, J. Virion-associated cholesterol is critical for the maintenance of HIV-1 structure and infectivity. *AIDS* **16,** 2253–61 (2002).

129. Campbell, S. M., Crowe, S. M. & Mak, J. Lipid rafts and HIV-1: from viral entry to assembly of progeny virions. *J. Clin. Virol.* **22,** 217–27 (2001).

130. Mañes, S. *et al.* Membrane raft microdomains mediate lateral assemblies required for HIV-1 infection. *EMBO Rep.* **1,** 190–6 (2000).

131. Kuhl, B. D., Cheng, V., Wainberg, M. a & Liang, C. Tetherin and its viral antagonists. *J. Neuroimmune Pharmacol.* **6,** 188–201 (2011).

132. Waheed, A. a *et al.* Inhibition of human immunodeficiency virus type 1 assembly and release by the cholesterol-binding compound amphotericin B methyl ester: evidence for Vpu dependence. *J. Virol.* **82,** 9776–81 (2008).

133. Kupzig, S. *et al.* Bst-2/HM1.24 is a raft-associated apical membrane protein with an unusual topology. *Traffic* **4,** 694–709 (2003).

134. Zheng, Y. H., Plemenitas, a, Linnemann, T., Fackler, O. T. & Peterlin, B. M. Nef increases infectivity of HIV via lipid rafts. *Curr. Biol.* **11,** 875–9 (2001).

135. Simons, K. & Toomre, D. Lipid rafts and signal transduction. *Nat. Rev. Mol. Cell Biol.* **1,** 31–9 (2000).

136. Munro, S. Lipid rafts: elusive or illusive? *Cell* **115,** 377–388 (2003).

137. Owen, D. M., Magenau, A., Williamson, D. & Gaus, K. The lipid raft hypothesis revisited--new insights on raft composition and function from super-resolution fluorescence microscopy. *Bioessays* **34,** 739–47 (2012).

138. Sengupta, P. L.-S. Probing protein heterogeneity in the plasma membrane using PALM and pair correlation analysis. **8,** 969–975 (2012).

139. Sharma, P. *et al.* Nanoscale organization of multiple GPI-anchored proteins in living cell membranes. *Cell* **116,** 577–89 (2004).

140. Brown, D. A. & Rose, J. K. Sorting of GPI-Anchored Proteins to Membrane Subdomains during Transport to the Apical Cell Surface. *Cell* **66,** 533–544 (1992).

141. Varma, R. & Mayor, S. GPI-anchored proteins are organized in submicron domains at the cell surface. *Nature* **394,** 798–801 (1998).

142. Bader, A. N., Hofman, E. G., van Bergen En Henegouwen, P. M. P. & Gerritsen, H. C. Imaging of protein cluster sizes by means of confocal time-gated fluorescence anisotropy microscopy. *Opt. Express* **15,** 6934–45 (2007).

143. Bader, A. N. *et al.* Homo-FRET imaging as a tool to quantify protein and lipid clustering. *Chemphyschem* **12,** 475–83 (2011).

144. Zacharias, D. a, Violin, J. D., Newton, A. C. & Tsien, R. Y. Partitioning of lipid-modified monomeric GFPs into membrane microdomains of live cells. *Science* **296,** 913–6 (2002).

145. Resh, M. D. Membrane targeting of lipid modified signal transduction proteins. *Subcell. Biochem. 37 217–232*

146. T. Houjou, J. Hayakawa, R.Watanabe, Y. Tashima, Y. Maeda, T. Kinoshita, R. T. Changes in molecular species profiles of glycosylphosphatidylinositol anchor precursors in early stages of biosynthesis. *J. Lipid Res. 48 1599–1606* (2007).

147. Nikolaus, J. *et al.* Hemagglutinin of influenza virus partitions into the nonraft domain of model membranes. *Biophys. J.* **99,** 489–98 (2010).

148. Zheng, Y.-H., Plemenitas, A., Fielding, C. J. & Peterlin, B. M. Nef increases the synthesis of and transports cholesterol to lipid rafts and HIV-1 progeny virions. *Proc. Natl. Acad. Sci. U. S. A.* **100,** 8460–5 (2003).

149. Kimura, H., Momiyama, M., Tomita, K., Tsuchiya, H. & Hoffman, R. M. Long-working-distance fluorescence microscope with high-numerical-aperture objectives for variable-magnification imaging in live mice from macro- to subcellular. *J. Biomed. Opt.* **15,** 066029 (2010).

150. Lakowicz, J. R. *Principles of Fluorescence Spectroscopy*. (2006).

151. Padilla-Parra, S. & Tramier, M. FRET microscopy in the living cell: Different approaches, strengths and weaknesses. *Bioessays* 369–376 (2012). doi:10.1002/bies.201100086

152. Gambin & Deniz. Multicolor Single-Molecule FRET to explore Protein Folding and Binding. **6,** 1540–1547 (2011).

153. Sisamakis, E., Valeri, A., Kalinin, S., Rothwell, P. J. & Seidel, C. A. M. in *Single Mol. Tools, Part BSuper-Resolution, Part. Tracking, Multiparameter, Force Based Methods* (Enzymology, N. G. W. B. T.-M. in) **Volume 475,** 455–514 (Academic Press, 2010).

154. Chan, F. T. S., Kaminski, C. F. & Kaminski Schierle, G. S. HomoFRET fluorescence anisotropy imaging as a tool to study molecular self-assembly in live cells. *Chemphyschem* **12,** 500–9 (2011).

155. Rizzo, M. a, Springer, G. H., Granada, B. & Piston, D. W. An improved cyan fluorescent protein variant useful for FRET. *Nat. Biotechnol.* **22,** 445–9 (2004).

156. Lakadamyali, M. Super-Resolution Microscopy: Going Live and Going Fast. *Chemphyschem* 1–8 (2013). doi:10.1002/cphc.201300720

157. Cox, S. & Jones, G. E. Imaging cells at the nanoscale. *Int. J. Biochem. Cell Biol.* **45,** 1669–78 (2013).

158. Nikon. Total Internal Reflection Fluorescence (TIRF) Microscopy. at <http://www.microscopyu.com/articles/fluorescence/tirf/tirfintro.html>

159. BDBiosciences. Flow Cytometry Web-Based Training. at <http://www.bdbiosciences.com/services/training/itf_launch.jsp>

160. Nguyen, D. H. & Hildreth, J. E. Evidence for budding of human immunodeficiency virus type 1 selectively from glycolipid-enriched membrane lipid rafts. *J. Virol.* **74,** 3264–72 (2000).

161. Pickl, W. F., Pimentel-mui, F. X. & Seed, B. Lipid Rafts and Pseudotyping. **75,** 7175–7183 (2001).

162. Lindwasser, O. W. & Resh, M. D. Multimerization of Human Immunodeficiency Virus Type 1 Gag Promotes Its Localization to Barges , Raft-Like Membrane Microdomains. **75,** 7913–7924 (2001).

163. Aloia, R. C., Tian, H. & Jensen, F. C. Lipid composition and fluidity of the human immunodeficiency virus envelope and host cell plasma membranes. *Proc. Natl. Acad. Sci. U. S. A.* **90,** 5181–5 (1993).

164. Chan, R. *et al.* Retroviruses human immunodeficiency virus and murine leukemia virus are enriched in phosphoinositides. *J. Virol.* **82,** 11228–38 (2008).

165. Fujii, K., Hurley, J. H. & Freed, E. O. Beyond Tsg101 : the role of Alix in.

166. Waheed, A. a & Freed, E. O. The Role of Lipids in Retrovirus Replication. *Viruses* **2,** 1146–1180 (2010).

167. Halwani, R., Khorchid, A., Cen, S. & Kleiman, L. Rapid Localization of Gag / GagPol Complexes to Detergent-Resistant Membrane during the Assembly of Human Immunodeficiency Virus Type 1. *Society* **77,** 3973–3984 (2003).

168. Hancock, J. F. Lipid rafts : contentious only from simplistic standpoints. **7,** 456–462 (2009).

169. Silvius, J. R. Partitioning of membrane molecules between raft and non-raft domains: insights from model-membrane studies. *Biochim. Biophys. Acta* **1746,** 193–202 (2005).

170. Subach, F. & Subach, O. Monomeric fluorescent timers that change color from blue to red report on cellular trafficking. *Nat. Chem. ...* **5,** 118–126 (2009).

171. Saiki, R. K. *et al.* Enzymatic amplification of beta-globin genomic sequences and restriction site analysis for diagnosis of sickle cell anemia. *Science* **230,** 1350–4 (1985).

172. Urban, a. A rapid and efficient method for site-directed mutagenesis using one- step overlap extension PCR. *Nucleic Acids Res.* **25,** 2227–2228 (1997).

173. Scolari, S. Lateral organization of the transmembrane domain and cytoplasmic tail of influenza virus hemagglutinin revealed by time resolved imaging. (1981). at <\url{urn:nbn:de:kobv:11-100102051}>

174. Kapp, K., Schrempf, S., Lemberg, M. K. & Dobberstein, B. Post-Targeting Functions of Signal Peptides. 1–16 (2009).

175. Levental, I., Grzybek, M. & Simons, K. Raft domains of variable properties and compositions in plasma membrane vesicles. *Proc. Natl. Acad. Sci. U. S. A.* **108,** 11411–6 (2011).

176. Hyun Bae, J. *et al.* Expansion of the Genetic Code Enables Design of a Novel "Gold" Class of Green Fluorescent Proteins. *J. Mol. Biol.* **328,** 1071–1081 (2003).

177. Seifert, M. H. J. *et al.* Slow exchange in the chromophore of a green fluorescent protein variant. *J. Am. Chem. Soc.* **124,** 7932–42 (2002).

178. Buschmann, V. *et al.* Polarization Extension Unit for LSM Upgrade Kits q q. *http://www.picoquant.com/technotes/technote_polarization_extension_lsm.pdf* 1–7

179. Olympus. Manual, TOTAL INTERNAL REFLECTION ILLUMINATION SYSTEM. at <http://www.olympus-europa.com/microscopy/en/microscopy/hidden_misd/download_jsp.jsp?link=/medical/rmt/media/content/content_misd/documents_2/manuals_2/IX2_RFAEVA2__instruction_manual_001_V1-en_20100101.pdf>

180. Wan, J., Roth, A. F., Bailey, A. O. & Davis, N. G. Palmitoylated proteins: purification and identification. *Nat. Protoc.* **2,** 1573–84 (2007).

181. Keller, P., Toomre, D., Díaz, E., White, J. & Simons, K. Multicolour imaging of post-Golgi sorting and trafficking in live cells. *Nat. Cell Biol.* **3,** 140–9 (2001).

182. Linstedt, a D. *et al.* A C-terminally-anchored Golgi protein is inserted into the endoplasmic reticulum and then transported to the Golgi apparatus. *Proc. Natl. Acad. Sci. U. S. A.* **92,** 5102–5 (1995).

183. 1998-2013 Abcam plc. Abcam - Manufacturer Website. at <http://www.abcam.com/Giantin-antibody-9B6-Golgi-Marker-ab37266.html>

184. Blot, G., Janvier, K., Panse, S. Le, Benarous, R. & Berlioz-torrent, C. Targeting of the Human Immunodeficiency Virus Type 1 Envelope to the trans-Golgi Network through Binding to TIP47 Is Required for Env Incorporation into Virions and Infectivity. **77,** 6931–6945 (2003).

185. PicoQuant. PicoQuant - TauSPAD product description. at <http://www.picoquant.com/products/tau_spad/tau_spad.htm>

186. Kreis, E. Views and Reviews Role of Microtubules in the Organisation of the Golgi Apparatus. **70,** 67–70 (1990).

187. Zerial, M. & McBride, H. Rab proteins as membrane organizers. *Nat. Rev. Mol. Cell Biol.* **2,** 107–17 (2001).

188. Diez, S., Helenius, J. & Howard, J. Biomolecular motors operating in engineered environments. *Protein Sci. Encycl.* 1–18 (2008). doi:10.1002/9783527610754.bt03

189. Schnapp, B. J. Trafficking of signaling modules by kinesin motors. *J. Cell Sci.* **116,** 2125–35 (2003).

190. Snijder, B. *et al.* Population context determines cell-to-cell variability in endocytosis and virus infection. *Nature* **461,** 520–3 (2009).

191. Nikolaus, J. Hemifusion and lateral lipid domain partition in lipid membranes of different complexity. (2011). at <http://scholar.google.com/scholar?hl=en&btnG=Search&q=intitle:Hemifusion+and+lateral+lipid+domain+partition+in+lipid+membranes+of+different+complexity#0>

192. Krishan, A. Rapid flow cytofluorometric analysis of mammalian cell cycle by propidium iodide staining. *J. Cell Biol.* **66,** 188–193 (1975).

193. Vetrivel, K. S. *et al.* Association of gamma-secretase with lipid rafts in post-Golgi and endosome membranes. *J. Biol. Chem.* **279,** 44945–54 (2004).

194. Surma, M. A., Klose, C. & Simons, K. Biochimica et Biophysica Acta Lipid-dependent protein sorting at the trans-Golgi network ☆. *BBA - Mol. Cell Biol. Lipids* (2012). doi:10.1016/j.bbalip.2011.12.008

195. Levental, I. J. Cholesterol-dependent phase separation in cell-derived giant plasma-membrane vesicles. **424,** 163–167 (2011).

196. Keller, H., Lorizate, M. & Schwille, P. PI(4,5)P2 degradation promotes the formation of cytoskeleton-free model membrane systems. *Chemphyschem* **10,** 2805–12 (2009).

197. Scott, R. E., Perkins, R. G., Zschunke, M. A., Hoerl, B. J. & Maercklein, P. B. Plasma membrane vesiculation in 3T3 and SV3T3 cells. I. Morphological and biochemical characterization. *J. Cell Sci.* **35,** 229–43 (1979).

198. Levental, I., Lingwood, D., Grzybek, M., Coskun, U. & Simons, K. SI- Palmitoylation regulates raft affinity for the majority of integral raft proteins. *Proc. Natl. Acad. Sci. U. S. A.* **107,** 22050–4 (2010).

199. Thaa, B. Assemblierung von Influenzaviren: Wechselwirkungen der Proteine M1 und M2 mit Membranen und Membrandomänen. (2011). at <http://scholar.google.com/scholar?hl=en&btnG=Search&q=intitle:Assemblierung+von+Influenzaviren+:+Wechselwirkungen+der+Proteine+M1+und+M2+mit+Membranen+und+Membrandomänen#0>

200. Miesenböck, G., Angelis, D. De & Rothman, J. Visualizing secretion and synaptic transmission with pH-sensitive green fluorescent proteins. *Nature* **394,** 192–195 (1998).

201. Earl, P. L., Moss, B. & Doms, R. W. Folding, interaction with GRP78-BiP, assembly, and transport of the human immunodeficiency virus type 1 envelope protein. *J. Virol.* **65,** 2047–55 (1991).

202. Schawaller, M., Slvlith, G. E., Skehel, J. J. & Wiley, D. C. Studies with Crosslinking Reagents on the Oligomeric Structure of the env Glycoprotein of HIV The product of the envgene of HIV , gpl60 , contains 861 amino acids and is processed proteolytically to generate gpl20 containing 488 amino acids and gp41 conta. *Methods* **369,** 367–369 (1989).

203. Earl, P. L., Doms, R. W. & Moss, B. Oligomeric structure of the human immunodeficiency virus type 1 envelope glycoprotein. *Proc. Natl. Acad. Sci. U. S. A.* **87,** 648–52 (1990).

204. Lenz, O. *et al.* Trimeric membrane-anchored gp41 inhibits HIV membrane fusion. *J. Biol. Chem.* **280,** 4095–101 (2005).

205. Liu, J. *et al.* Role of a putative gp41 dimerization domain in human immunodeficiency virus type 1 membrane fusion. *J. Virol.* **84,** 201–9 (2010).

206. Bernstein, H. B. *et al.* Oligomerization of the hydrophobic heptad repeat of gp41. *J. Virol.* **69,** 2745–50 (1995).

207. Center, R. J., Kemp, B. E. & Poumbourios, P. Human immunodeficiency virus type 1 and 2 envelope glycoproteins oligomerize through conserved sequences. *J. Virol.* **71,** 5706–11 (1997).

208. McInerney, T. L., El Ahmar, W., Kemp, B. E. & Poumbourios, P. Mutation-directed chemical cross-linking of human immunodeficiency virus type 1 gp41 oligomers. *J. Virol.* **72,** 1523–33 (1998).

209. Poumbourios, P., el Ahmar, W., McPhee, D. a & Kemp, B. E. Determinants of human immunodeficiency virus type 1 envelope glycoprotein oligomeric structure. *J. Virol.* **69,** 1209–18 (1995).

210. Apellániz, B., Nieva, J. L., Schwille, P. & García-Sáez, A. J. All-or-none versus graded: single-vesicle analysis reveals lipid composition effects on membrane permeabilization. *Biophys. J.* **99,** 3619–28 (2010).

211. Resh, M. D. Palmitoylation of ligands, receptors, and intracellular signaling molecules. *Sci. STKE* **2006,** re14 (2006).

212. Millington, M. *et al.* High-precision FLIM-FRET in fixed and living cells reveals heterogeneity in a simple CFP-YFP fusion protein. *Biophys. Chem.* **127,** 155–64 (2007).

213. He, L. *et al.* A flow cytometric method to detect protein-protein interaction in living cells by directly visualizing donor fluorophore quenching during CFP-->YFP fluorescence resonance energy transfer (FRET). *Cytometry. A* **55,** 71–85 (2003).

214. Nebl, T. *et al.* Proteomic analysis of a detergent-resistant membrane skeleton from neutrophil plasma membranes. *J. Biol. Chem.* **277,** 43399–409 (2002).

215. Parton, D. & Tek, A. Formation of Raft-Like Assemblies within Clusters of Influenza Hemagglutinin Observed by MD Simulations. *PLoS Comput. ...* (2013). at <http://dx.plos.org/10.1371/journal.pcbi.1003034>

216. Lee, S. F. *et al.* Multimerization potential of the cytoplasmic domain of the human immunodeficiency virus type 1 transmembrane glycoprotein gp41. *J. Biol. Chem.* **275,** 15809–19 (2000).

217. Ikonen, E. Cellular cholesterol trafficking and compartmentalization. *Nat. Rev. Mol. Cell Biol.* **9,** 125–38 (2008).

218. Takahashi, T. & Suzuki, T. Role of Membrane Rafts in Viral Infection. *Open Dermatology Journal,* **3,** 178–194 (2009).

219. Coleman, E. M., Walker, T. N. & Hildreth, J. E. K. Loss of Niemann Pick type C proteins 1 and 2 greatly enhances HIV infectivity and is associated with accumulation of HIV Gag and cholesterol in late endosomes/lysosomes. *Virol. J.* **9,** 31 (2012).

220. Jaroniec, C. P. *et al.* Structure and dynamics of micelle-associated human immunodeficiency virus gp41 fusion domain. *Biochemistry* **44,** 16167–80 (2005).

221. Montero, M. *et al.* Neutralizing epitopes in the membrane-proximal external region of HIV-1 gp41 are influenced by the transmembrane domain and the plasma membrane. *J. Virol.* **86,** 2930–41 (2012).

Acknowledgements

First and foremost I want to thank Prof. Andreas Herrmann for allowing me to work as a Diploma and PhD student in his group. As my supervisor he did not only have a decisive influence on my experimental work and my ongoing projects, but even more importantly he has always been a fundamental factor of my personal development as a scientist. It is the combination of independent working and his experience-based guidance that generates a creative and ambitious atmosphere in his laboratory which is perfectly suited to push the people working for him to tap their full potential. Moreover, he established a dense net of collaboration partners and acquaintances all over the world which he always generously shares with his colleagues and students.

Thanks belong to Dr. Peter Müller and Dr. Thomas Korte. Both of them provide an indispendsible knowledge pool not only regarding the methods and the projects of the group but also in terms of biophysics and virology in general. In spite of the fact that they, as Andreas Herrmann, are often involved in lectures, practical courses and student tutoring they are always open for scientific discussions.

In general I'd like to thank all the members of our lab for creating such a positive working environment. All of them, the permanent lab members Gudrun Habermann, Sabine Schiller and Silvia Kietzmann, but also the bacherlor and master students and most importantly the other PhD students and Postdocs, Caroline Mair, Aoufa Amoussouvi, Luisa Losensky, Joanna Ziomkowska, Gabriele Schreiber, Salvatore Chiantia, Lotte Teufel, Christian Sieben, Jörg Nikolaus, Chris Höfer, Matthias Schade and in particular Andrea Gramatica were inspiring scientifically but furthermore often also became close friends.

I am indebt with the "Veit laboratory", in particular with Bastian Thaa and of course Michael Veit for many discussions and I have to underline the sedoulus and helpful reviewing of many manuscripts, abstracts and parts of this work that Michael Veit was always ready to conduct.

I want to thank Ilya Levental for contributing to this work by performing and teaching me the palmitoylation assay and the GPMV approach that he improved in recent years significantly. His positive attidude and intoxicating enthusiasm in combination with his well-founded knowledge was always very inspiring for me.

Thanks also belong to the SPP1175: "Dynamics of cellular membranes and their exploitation by viruses" for funding work and travel within this PhD time.

Publications

Talks

"THE ROLE OF LIPID RAFTS IN VIRUS ASSEMBLY - The Cholesterol Recognition Amino Acid Consensus of the HIV-1 Glycoprotein gp41 is the Crucial Factor of the Protein's Lateral Plasma Membrane Sorting, Oligomerization and Membrane Perturbing Properties." Keystone Symposium X7 2012 (Whistler, British Columbia, Canada).26.03-31.03.2012

"THE ROLE OF LIPID RAFTS IN VIRUS ASSEMBLY - The cholesterol recognition amino acid consensus of the hiv-1 glycoprotein gp41 is AN Important mediator of different protein properties." Marie Curie ITN "Virus Entry" Network Meeting 2012 (Menorca, Spain). 08.05.2012-20.05.2012

"Cell-to-cell variability in plasma membrane lipid rafts – relevance for virus progression". Marie Curie ITN "Virus Entry" Network Meeting 2012 (Greifensee, Switzerland). 13.-15.02.2013

"Cell-to-cell variability in plasma membrane lipid rafts„. Biophysical Society 57th Annual Meeting (Philadelphia, PA , USA). 02.-06.02.2013

"Fluorescent Particle Tracking and Total Internal Reflection Fluorescence Microscopy". Young scientist workshop - Methods to study influenza virus. (Berlin, Germany). 20.09.-22.09.2011

Posters

"Raft association and intracellular localization of the human immunodeficiency virus-1 glycoprotein 41 investigated by fluorescence lifetime imaging microscopy". 4th European Congress of Virology 2010 (Cernobbio, Italy). 07.04.-11.04.2010

"Chasing raft localisation signals: FLIM-FRET reveals CRAC mediated microdomain association of the Human immunodeficiency virus glycoprotein gp41." 55th Biophysical Meeting annual meeting 2011 (Baltimore, MD, USA). 05.03.-09.03.2011

"THE ROLE OF LIPID RAFTS IN VIRUS ASSEMBLY – Identification and characterization of microdomain partitioning factors of the HIV-1 glycoprotein gp41 using FLIM-FRET and fluorescence anisotropy microscopy ".56th Biophysical Meeting annual meeting 2012 (San Diego, CA, USA). 25.02.-29.02.2012

"FLIM-FRET as a tool to study protein partitioning in plasma membrane microdomains of living cells. Identifying raft localisations signal of the HIV glycoprotein gp41." 12th Methods and Applications of Fluorescence 2012 (Strasbourg, France). 11.09.-14.09.2011

Manuscripts

Milles, S., Meyer, T. Scheidt, Holger A.,**Schwarzer, R**.,Thomas, L., Marek, M., Szente, L., Bittman, R., Herrmann, A.,Pomorski, T., Huster, D., Müller, P. (2013) "*Organization of fluorescent cholesterol analogs in lipid bilayers — Lessons from cyclodextrin extraction."* Biochimica et Biophysica Acta (BBA) - Biomembranes 1828, 1822–1828.

Heek, T., Nikolaus, J., **Schwarzer, R**., Fasting, C., Welker, P., Licha, K., Herrmann, A., et al. (2013). *"An amphiphilic perylene imido diester for selective cellular imaging"*. Bioconjugate chemistry, 24(2), 153–8. doi:10.1021/bc3005655

Wawrzinek, R., Wessig, P., Möllnitz, K., Nikolaus, J., **Schwarzer, R**., Müller, P., & Herrmann, A. (2012). *"DBD dyes as fluorescent probes for sensing lipophilic environments."* Bioorganic & medicinal chemistry letters, 22(17), 5367–71. doi:10.1016/j.bmcl.2012.07.056

Schwarzer, R., Scloari, S., Levental, I., Buschmann, V., Veit, M., Herrmann, A. *"Motifs of the HIV-1 Glycoprotein gp41 controlling lateral sorting and oligomerization."* In Preparation.

Buschmann, V., Bleckmann, A., Bülter, A., Krämer, B., Nikolaus, J., **Schwarzer, R**., Korte, T., et al. *Polarization Extension Unit for LSM Upgrade Kits*. http://www.picoquant.com/technotes/technote_polarization_extension_lsm.pdf, 1–7.

Collaborations

Partner	Project
Dr. Ilya Levental	Protein palmitoylation assay and investigation of GPMV phase separation
Dr. Bert Nitsche	Structured illumination microscopy og fluorescently labeled gp41 (not shown)
Dr. Volker Buschmann	Establishment of fluorescence anisotropy imaging microscopy

Curriculum vitae

Eidesstattliche Erklärung

Hiermit erkläre ich, die vorliegende Arbeit selbständig und nur unter Verwendung der angegebenen Hilfsmittel angefertigt habe. Alle Stellen, die dem Wortlaut oder dem Sinn nach anderen Werken entnommen sind, sind nach bestem Wissen und Gewissen durch Angabe der Quellen als Entlehnung kenntlich gemacht worden.

Ein Teil der beschriebenen Ergebnisse wurde in Zusammenarbeit mit anderen Mitarbeitern der Arbeitsgruppe Molekulare Biophysik erzielt und sind entsprechend gekennzeichnet.

Ich besitze keinen entsprechenden Doktorgrad und habe mich anderwärts nicht um einen Doktorgrad beworben.

Die dem Promotionsverfahren zugrunde liegende Promotionsordnung ist mir bekannt.

Roland Schwarzer

Berlin,